Aus dem

Institut für Kardiovaskuläre Physiologie und Pathophysiologie im Walter-Brendel-Zentrum für Experimentelle Medizin

Ludwig-Maximilians-Universität München

The anti-tumorigenic role of CARD9 signaling cascade in conventional dendritic cells in colitis-associated colon cancer

Dissertation
zum Erwerb des Doctor of Philosophy (Ph.D.)
an der Medizinischen Fakultät der
Ludwig-Maximilians-Universität München

vorgelegt von
Vanessa Franziska Küntzel

aus
Mainz, Deutschland

Jahr
2024

Mit Genehmigung der Medizinischen Fakultät der
Ludwig-Maximilians-Universität München

Erstes Gutachten:	Prof. Dr. Barbara Schraml-Schotta
Zweites Gutachten:	Prof. Dr. Anne Krug
Drittes Gutachten:	Priv. Doz. Dr. Daniel Kotlarz
Viertes Gutachten:	Priv. Doz,. Dr. Christian Schulz

Dekan: Prof. Dr. med. Thomas Gudermann

Tag der mündlichen Prüfung: 18.04.2024

Abstract (English):

Colorectal cancer (CRC) is the third most common type of cancer worldwide, with around 2 million new cases yearly, and the second most common cause of overall cancer mortality. A common risk factor for developing CRC is inflammatory bowel disease (IBD), marked by a chronic inflammatory process within the intestinal compartment. Genome-wide association studies (GWAS) identified *Card9* polymorphisms associated with an increased risk of colon cancer development. CARD9 acts in a complex with BCL10-MALT1 and is exclusively expressed in myeloid cells, like macrophages, dendritic cells (DCs), and Neutrophils. Previous studies on the role of CARD9 in tumor development have shown contradicting results regarding tumor development and identified signaling mechanisms for CARD9 independently of BCL10 and MALT1. This study aimed to characterize the role of CARD9-BCL10-MALT1 signaling in DCs under homeostatic conditions, acute inflammation, and colitis-associated cancer. DCs belong to the innate immune system and play a crucial role in antigen uptake, processing, and presentation to T cells. DCs can be split into two main subsets, conventional DC1 (cDC1) and cDC2, each specialized for the induction of cytotoxic CD8 T cells or CD4 T helper cells, respectively.

CARD9 signaling was abrogated in cDCs by deleting its interaction partner BCL10 or the deletion of upstream SYK kinase using the *Clec9a-cre* mouse model combined with floxed alleles of the targeted gene. Deletion of both proteins had no impact on the development of cDCs, particularly in the intestinal compartment. However, transcriptional profiling of BCL10 deficient intestinal cDCs revealed reduced mitochondrial biogenesis-related gene expression, specifically in OXPHOS. Presumably caused by decreased mTOR and Myc signaling, indicating that the deletion of BCL10 likely affects the early activation or maturation of cDCs. In contrast, the deletion of SYK in cDCs did not show differences in metabolic signaling. Further, cDC-specific deletion of BCL10, but not SYK, led to a reduced Th17 induction in the colon of these mice. However, lower Th17 presence and altered metabolism of BCL10 deficient cDCs had no impact on acute colitis. Similarly, the *Clec9a*$^{cre/+}$*Syk*$^{fl/fl}$ mice showed no alterations in acute colitis.

Nonetheless, increased tumor development could be observed in cDC-specific BCL10 deficient mice upon chronic colitis. This increased tumor development could be traced to a defect in anti-tumor immunity when BCL10 is deleted in cDCs. Tumor-infiltrating T cells showed a reduction of unconventional γδ T cells, increased tolerogenic CD4 T cells, and less cytotoxicity within the tumor environment. If this protective effect on BCL10 in cDCs is mediated via SYK signaling is part of future investigations.

Table of Content

List of Figures

List of Tables

List of Abbreviations

Abbreviation	Full name
AOM	AOM
APC	Antigen presenting cell
BCL10	B cell lymphoma 10
CAC	Colitis-associated cancer
CARD9	Caspase recruitment domain-containing protein 9
CBM complex	CARD9-BCL10-MALT1 complex
CD	Chron's disease
cDC	conventional Dendritic cell
cDC1	Conventional Dendritic cell type 1
cDC2	Conventional Dendritic cell type 2
CDP	Common dendritic cell precursor
cKO	Conditional knockout
CLR	C-type lectin receptors
CO	Colon
CRC	Colorectal cancer
DC	Dendritic cell
DDAMP	Damage-associated molecular pattern
DN DC	Double negative DCs
DP cDC2	Double positive cDC
dsDNA	Double-strand deoxyribonucleic acid
DSS	Dextran sulfate sodium
DTA	Diphtheria toxin subunit A
DTR	Diphtheria toxin receptor
ER	Endoplasmic reticulum
FAP	Familial adenomatous polyposis
GWAS	Genome-wide association studies
HGD	high-grade dysplasia
IBD	Inflammatory bowel disease
IEL	Intraepithelial lymphocytes
IFN	Interferon
Ig	Immunoglobulin
IKKβ	Inhibitor of NFκB kinase subunit 2
IL	Interleukin
IL6R	receptor for IL-6 (IL6R
ILC	Innate lymphoid cell
ITAM	Immunoreceptor tyrosine-based activation motif
JNK	c-Jun N-terminal Kinase
LN	Lymph node
LOH	Loss of heterogeneity
LP	Lamina propria
M cells	Microfold cells
MALT1	Mucosa-associated lymphoid tissue lymphoma translocation protein 1
MAPK	Mitogen-activated protein kinase
MHC	Major histocompatibility complex

mLN	mesenteric Lymph node
MoDCs	Monocytes derived dendritic cells
NK cell	Natural killer cell
NOD	Nucleotide-binding domain
NOS	Reactive nitrogen species
NSAID	Non-steroidal anti-inflammatory drug
PAMP	Pathogen-associated molecular pattern
PD-L1	Programmed-death ligand 1
PKCδ	Protein kinase C δ
PP	Peyer's patches
PRR	Pattern recognition receptor
RA	Retinoic acid
RIG I	Retinoic acid-inducible gene I
RNA	Ribonucleic acid
ROS	Reactive oxygen species
SI	Small intestine
SP cDC2	Single positive cDC
STAT	Signal transducer and activator of transcription
SYK	Src-homology 2 (SH2) domain-containing spleen tyrosine kinase
Th	T helper cell
TLR	Toll-like receptor
TNFR	TNF receptor
TNFα	Tumor necrosis factor α
Treg	Regulatory T cells

1. Introduction

1.1 Dendritic cells are essential inducers of T cell responses

The body's immune system is a complex network of cells, tissues, and organs, facilitating protection against harmful pathogens and damage. The immune response can be divided into an immediate (innate) or specialized (adaptive) immune response. The innate immune system has several cellular components, including granulocytes (Neutrophils, Eosinophils & Mast cells), monocytes, natural killer (NK) cells, innate lymphoid cells (ILCs), macrophages and dendritic cells (DCs). Further, the complement system contributes to innate immunity, and barrier organs such as the lung and intestines harbor a mucosal barrier containing antimicrobial peptides (Turvey and Broide 2010, Murphy, Travers and Walport 2014, Ignacio, Breda and Camara 2017). Innate immune cells are equipped with germline-encoded pattern recognition receptors (PRRs). These PRRs can be surface receptors, like Toll-like (TLRs) and C-type lectin receptors (CLRs), to recognize extracellular pathogens. In addition, PRRs such as Retinoic acid-inducible gene I (RIG I) -like receptors, AIM2-like receptors, and nucleotide-binding domain (NOD) or leucine-rich repeat-containing receptors are located in the cytoplasm to detect intracellular pathogens. Predominantly, these PRRs recognize pathogen-associated molecular patterns (PAMPs). However, some can recognize damage-associated molecular patterns (DAMPs) deriving from dead cells (Iwasaki and Medzhitov 2010, Medzhitov and Janeway Jr 2000, Kumar, Kawai and Akira 2011). So-called antigen-presenting cells (APC), especially dendritic cells, link the innate and adaptive immune systems (Cabeza-Cabrerizo et al. 2021). The adaptive immune system enables a pathogen-specific immune response and provides a long-lasting memory. However, the process of activation and expansion of specific B and T cell clones is slow, especially for pathogens encountered for the first time. Hence, the innate immune system builds the front line and drives the initial response toward invading pathogens (Murphy, Travers and Walport 2014, Alberts, Johnson, Lewis and al. 2002).

The primary function of DCs is to uptake, process, and present antigens to orchestrate an antigen-specific immune response. Upon antigen encounter, DCs undergo a maturation process marked by upregulating specific activation/co-stimulatory molecules, such as CD80, CD86, and CD40 (Pakalniškytė and Schraml 2017). Furthermore, DCs that encountered antigens in the peripheral tissues upregulate CCR7, facilitating their migration via the afferent lymphatic vessels into the lymph nodes (LN) for antigen presentation to T cells, driving T cell activation and polarization. (Paul 2011, Merad et al. 2013). This T cell induction usually requires three signals: (1) antigen presentation via major histocompatibility complex I (MHCI) or MHCII, (2) co-stimulatory molecules, and (3) secretion

of cytokines to drive the activation and polarization of T cells (Gerner, Casey and Mescher 2008). Besides this T cell induction, DCs secrete cytokines and chemokines to attract other immune cells to the side of infection/damage and induce the healing process by activating epithelial cell proliferation (Steinman, Gutchinov, Witmer and Nussenzweig 1983, Paul 2011).

1.1.1 Conventional dendritic cells (cDCs) derive from a Clec9a$^+$ progenitor

DCs were first described in the 1970s by Steinman and Cohn and termed 'dendritic' cells based on their morphological characteristics (Steinman and Cohn 1973). DCs were divided into two main subtypes, plasmacytoid DCs (pDCs) and cDCs, and were described to have a myeloid origin (Merad et al. 2013). However, recent findings question the ontogenetic relationship between pDCs and cDCs due to evidence of a lymphoid ontogeny of pDCs (Rodrigues et al. 2018, Herman and Grün 2018, Dress et al. 2019, Ziegler-Heitbrock et al. 2023).

Throughout different organs, cDCs are identified based on their expression of CD11c and MHCII (Schraml and e Sousa 2015) and have historically been separated into the two main subsets cDC type 1 (cDC1) and cDC2, identified by their expression of CD8a and CD4, respectively (Vremec et al. 2000, Edwards et al. 2003). Within the last decade, intense research on DC-poesies dissected the ontogeny and transcription factors driving cDC1 and cDC2 development.

Most immune cells, including cDCs, arise from hematopoietic stem cells, differentiated into multipotent progenitors. These progenitors subdivide into the common lymphoid progenitor and common myeloid progenitor. The latter further subdivides and leads, among other progenitors, to the development of the cDC committed progenitor that, in turn, gives rise to the pre-DCs, and both cell types are marked by the expression of CLEC9A/DNGR1 (Auffray et al. 2009, Schraml and e Sousa 2015, Cabeza-Cabrerizo et al. 2019, Schraml et al. 2013). At this stage of development, pre-DCs exit the bone marrow and migrate through the bloodstream to lymphoid and peripheral tissues, where they differentiate into cDC1 or cDC2 (Liu et al. 2009). This differentiation process has been described to be imprinted already when the pre-DCs leave the bone marrow (Grajales-Reyes et al. 2015, Schlitzer et al. 2015). As soon as cDC1 and cDC2 are fully differentiated, they are thought to be in a post-mitotic state with an average lifetime of 10-14 days. Therefore, most cDCs need to be replenished continuously by bone marrow-derived progenitors (Ginhoux et al. 2009). Only a tiny fraction of cDCs retain their potential to divide actively (Liu et al. 2007). However, pre-DCs can proliferate after tissue settling (Cabeza-Cabrerizo et al. 2019, Ugur et al. 2023).

The development of the cDC lineage depends on the FMS-like tyrosine kinase 3 (FLT3) receptor and its ligand FLT3L (Waskow et al. 2008, Maraskovsky et al. 1996) and only partially dependents on GM-CSF (Kingston et al. 2009, Greter et al. 2012). Development of cDC1s is further based on the transcription factors IRF8, BATF3, NFIL3, and ID2 (Hildner et al. 2008, Hacker et al. 2003, Edelson et al. 2011, Aliberti et al. 2003).

In contrast to the identified necessities for cDC1 development, transcription factors that drive cDC2 differentiation must be better defined. The fact that cDC2s are a heterogeneous population might contribute to this situation (Cabeza-Cabrerizo et al. 2019). However, it has been shown that IRF4 and RelB contribute to cDC2 phenotype and function (Caton, Smith-Raska and Reizis 2007, Persson et al. 2013, Schlitzer et al. 2013, Murphy et al. 2016). An additional transcription factor involved in the development of cDC2s is ZEB2, expressed in pre-cDC2s and cDC2s (Schlitzer et al. 2015, Miller et al. 2012). It is downregulated in pre-cDC1s and cDC1s as ZEB2 suppresses ID2 and thereby commits development towards cDC2 (Scott et al. 2016). Furthermore, two subpopulations of cDC2s can be defined based on their requirement of either NOTCH2 and RBP-J or KLF4 expression, revealing a heterogeneity within the cDC2s (Lewis et al. 2011, Tussiwand et al. 2015). This heterogeneity has undergone intense research, leading to the finding that some cells with cDC2-characteristics originate from a non-DNRG1 expressing progenitor with a potential lymphoid origin (Salvermoser et al. 2018, Sulczewski et al. 2023, Rodrigues et al. 2023)

1.1.2 The intestinal compartment harbors four intestine-characteristic cDC subsets

cDCs can be found throughout the intestinal compartment, consisting of the small intestine (SI), the colon, organized lymphoid tissues, like Peyer's patches (PP), and draining lymph nodes (Stagg 2018). Within the connective tissue beneath the intestinal epithelium, so-called lamina propria (LP), and gut-draining lymphoid tissues, four subsets of cDCs can be defined. XCR1 and CD103 expression marks the cDC1s, whereas two cDC2 subsets can express both CD103 and CD11b or only CD11b (Cerovic, Bain, Mowat and Milling 2014). Including the classification by transcriptions factors, $CD103^-$ cDC2s express lower levels of IRF4 than their CD103 expressing counter partners. Further, intestinal $CD103^+$ cDC2s resemble the NOTCH2-depended cDC2 subset from lymphoid tissues (Lewis et al. 2011). Nevertheless, differentiation into CD103 negative cDC2s appears not to seem definitive, as these cells can transform into $CD103^+$ cDC2 in the presence of Transforming growth factor β (TGFβ) (Bain et al. 2017). Additionally, within $CD103^-CD11b^+$ cDC2s, further subsets can be identified through the expression of CCR2, indicating even more heterogeneity in the cDC2 compartment (Scott et al. 2015).

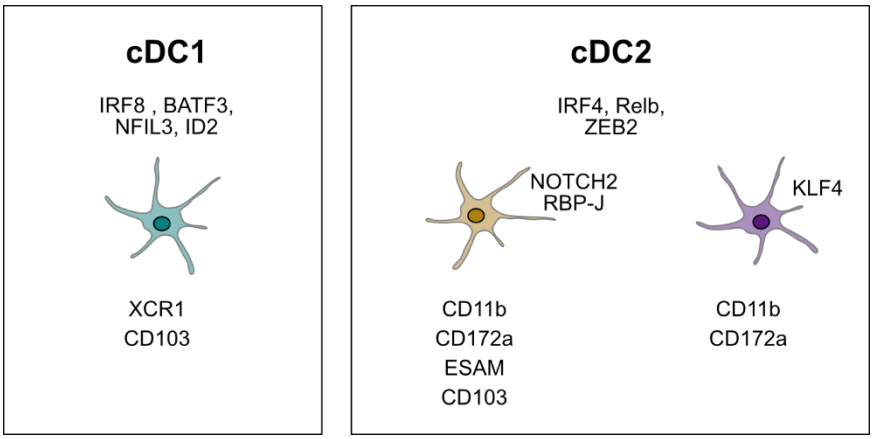

Figure 1 Commonly associated phenotypic markers of intestinal cDC subsets.
On a genetic basis, the development of cDC1 is dependent on IRF8, BATF3, NFIL3, and ID2. The expression of XCR1 and CD103 marks differentiated cDC1s. Expression of IRF4, RelB, and ZEB2 contribute to cDC2 development and function. NOTCH2 and RBP-J-dependent cDC2s resemble the $CD103^{+}CD11b^{+}$ cDC2s in the intestine and express CD172a and ESAM. Another cDC2 type relies on KLF4 expression and expresses CD11b and CD172a.

Within the intestinal cDCs, a fourth population can be identified, lacking both CD103 and CD11b expression. These double negative DCs (DN DCs) cells are absent in *Rorγt*$^{-/-}$ knockout mice, leading to the hypothesis that these cells derive from gut-associated lymphoid tissue (GALT) (Cerovic et al. 2013). More recently, expression of XCR1 or CD172α has been detected in a fraction of this double negative population. However, the function of this minor population is still unknown, and their ontogeny is debated (Joeris, Müller-Luda, Agace and Mowat 2017).

Like other LN, mesenteric LNs (mLN) draining the intestines harbor similar cDC populations as SI and colon, respectively. cDCs differentiated from pre-DCs in the LN remain there and are termed resident cDCs and classically subdivided by XCR1 and CD172α expression. They can be distinguished from so-called migratory cDCs by their lower MHCII but higher CD11c expression. Migratory cDCs differentiate in the peripheral organs and travel via afferent lymph vessels into the respective LN (Merad et al. 2013).

The diversity of cDC subsets throughout the intestinal axis changes in a segment-specific manner and is presumably imprinted by luminal-derived signals and antigens (Mowat and Agace 2014). In contrast to the high frequency of $CD103^{+}$ cDC2 in the SI LP, the colon is dominated by cDC1, and the cDC2 compartment shifts towards CD103 negative population (Esterházy et al. 2019, Cerovic et al. 2014). Along with the change in cDC composition, the overall frequency of APCs, including cDCs and macrophages, decreases from the duodenum, the upper part of the SI, towards the colon (Moreira et al. 2021).

A challenging factor in identifying cDCs in the intestine without the cDC-specific fate-mapping model Clec9a^{Cre} was that CD11c and MHCII expression can also be found on intestinal macrophages. In contrast to other organs, intestinal macrophages only partially express F4/80 and are constantly replenished by monocytes in the adult intestine (Shaw et al. 2018, Bain et al. 2014, dos Anjos Cassado 2017). Under steady-state conditions, segregation between cDCs and macrophages can be drawn by the expression of CD64/FcγR1, CD11b, and high levels of CX3CR1 (Tamoutounour et al. 2012). Nevertheless, CD64 usage requires caution as CD64 expressing cDCs could be identified in the kidney and under inflammatory conditions in the lung by fate-mapping (Schraml et al. 2013, Bosteels et al. 2020). In addition, CX3CR1 is expressed in low (CD103^{+}) and intermediate (CD103^{-}) levels by intestinal cDC2 populations (Cerovic et al. 2014). However, only the intestinal cDC1s and cDC2 subsets, not macrophages migrate, upon antigen encountering into the mLN to facilitate T cell priming (Cerovic et al. 2014).

1.1.3 cDCs contribute to intestinal homeostasis by controlling T cell activation

Under basal conditions, intestinal antigens acquired by cDCs require immune tolerance to prevent the immune system from reacting against itself (Hawiger et al. 2001). Particularly in the intestine, cDCs must mediate tolerance to food-derived antigens (Esterházy et al. 2016). This tolerogenic capacity is underlined by the high Aldehyde dehydrogenase levels in intestinal cDCs, metabolizing vitamin A into retinoic acid (RA) (Guilliams et al. 2010). RA contributes to the induction of regulatory T cells (Treg) and induces the expression of gut-homing factors on activated T cells (Coombes et al. 2007, Sun et al. 2007, Worthington, Czajkowska, Melton and Travis 2011, Jaensson-Gyllenbäck et al. 2011). Beyond the intestinal cDC subsets, cDC1s have the highest tolerogenic signature, and the deletion of cDC1 in *CD11c^{cre}Irf8^{flox}* mice leads to a minor reduction of regulatory T cells in the intestine (Luda et al. 2016). However, overall oral tolerance is not affected as CD103^{+} cDC2s contribute to Treg induction and compensate for the loss of cDC1. Equivalently, targeting cDC2 does not affect the Treg population, and only the ablation of total cDCs causes a deficiency in intestinal Tregs (Welty et al. 2013, Esterházy et al. 2016). Interestingly, monocyte-macrophage-derived APCs are redundant for oral tolerance, underlining the essential role of cDCs in tolerance induction (Esterházy et al. 2016).

In conjunction with their role in tolerance induction, cDC1s contribute to intestinal T-cell homeostasis. The lack of cDC1 in *XCR1^{DTA}* or *CD11c^{cre}Irf8^{flox}* mice leads to decreased T cell numbers in the LP and the intraepithelial lymphocytes (IEL). Especially the cytotoxic CD4^{+}CD8αα^{+} TCRαβ IEL subset is absent, whereas other conventional (CD4^{+} /

CD8αβ⁺ TCRαβ) and unconventional (CD8αα⁺ TCRαβ / TCRγδ) IELs are not affected. Nonetheless, this only occurs in the small intestine and not the colon. T cell populations appear in regular numbers and frequencies in lymphoid organs (Moreira et al. 2021, Ohta et al. 2016, Luda et al. 2016).

Besides their shared capacity to induce tolerogenic T cells, cDC1 and cDC2 have distinct functions within the intestine. Marked by their expression of XCR1, cDC1s are the population responsible for cross-presenting exogenous antigens via MHCI to CD8 T cells, inducing cytotoxicity (Bachem et al. 2012). Upon pathogenic infection, *Batf3* deficient mice fail to induce CD8 T cell response due to lacking cDC1 (Hildner et al. 2008). Besides the induction of cytotoxic CD8 T cells, cDC1s mediate with the help of programmed-death ligand 1 (PD-L1), RA, and TGFβ the differentiation into tolerogenic FOXP3 expressing CD8 T cells (Joeris et al. 2021). Furthermore, cDC1s produce high amounts of IL12, thereby driving the differentiation of CD4 T helper cell type 1 (Th1) (Everts et al. 2016). CD103⁻ cDC2s contribute to this development of INFγ producing Th1 cells (Scott et al. 2015, Cerovic et al. 2013).

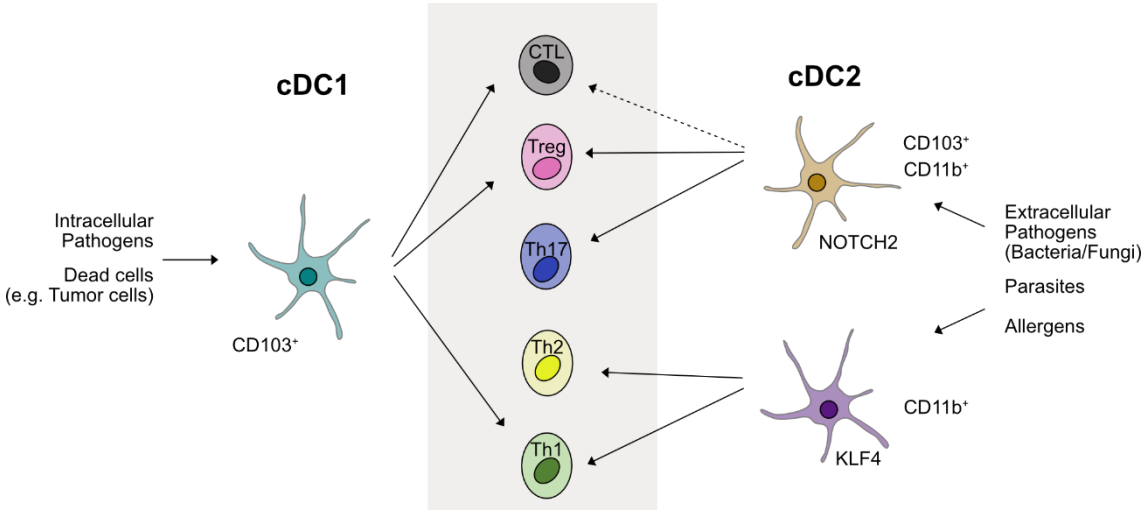

Figure 2 Proposed functions of intestinal cDCs.
Differentiated cDC1s drive immune responses against intracellular pathogens and recognize dead cells. CD103⁺ cDC1s prime CD8 T cells via cross-presentation and mediate tolerance through the induction of Tregs. cDC1s can also activate CD4 T cells and polarize towards the Th1 phenotype. The cDC2s respond to extracellular pathogens, parasites, and allergens. NOTCH2-dependent cDC2s express CD103 and CD11b in the intestine, contribute to Treg induction, and further polarize Th17 response. Under certain conditions, these cDC2s activate CD8 T cells through cross-dressing with MHCI. Another cDC2 type relies on KLF4 expression and activates CD4 T cells polarizing them towards Th2 phenotype and contributes to Th1 polarization. Adapted from (Murphy and Murphy 2022)

Under inflammatory conditions, it has been shown that monocytes can give rise to DC-like cells (MoDCs), partially migrating to the mLN and contributing to the T cell induction usually mediated by cDCs (Menezes et al. 2016, Rivollier et al. 2012). Hereby, MoDCs

and cDC2 may contribute to CD8 T cell responses induction via MHCI-cross-dressing. Thereby, APCs encounter pre-loaded MHCI from dead cells, transport them to their surface, and acquire the capacity to activate CD8 T cells in the presence of different costimulatory molecules and cytokines (Theisen et al. 2018, Duong et al. 2022, MacNabb et al. 2022, Dolan, Gibbs and Ostrand-Rosenberg 2006).

Whereas cDC1s are described to be necessary for the recognition of intracellular pathogens and dead cells, cDC2 facilitate the defense against extracellular pathogens and exceed the induction of CD4 T cell response (Pakalniškytė and Schraml 2017, Satpathy et al. 2013). The $CD103^+$ cDC2 subset is the primary driver of Th17 polarization, facilitated by producing IL-6, IL-23, and TGFβ (Persson et al. 2013, Schlitzer et al. 2013, Satpathy et al. 2013). That $CD103^-$ cDC2 do not contribute to Th17 induction could be shown by a normal intestinal Th17 formation in mice that lack *Klf4* in CD11c-expressing cells. However, these mice have an impaired Th2 response toward *Schistosoma mansoni,* revealing the critical function of KLF4-dependent cDC2 in Th2 polarization and the downstream recruitment of eosinophils and production of antibodies driving the allergic reactions (Tussiwand et al. 2015, Mayer et al. 2017).

Thus, their joint function is to activate T cells; the respective cDC subsets have specific characteristics in how they contribute to intestinal homeostasis. Both subtypes are necessary for tolerance induction; cDC1s are the main inducers of CD8 T cells, and cDC2s excel in the polarization of CD4 T cells towards Th17 and Th2.

1.2 DCs in Inflammation and Cancer

1.2.1 Controversial roles of cDC subsets during colon inflammation

Within the last few years, the role of cDCs in colitis underwent extensive research. However, it is still unclear whether cDCs have a pro- or anti-inflammatory role. Total ablation of cDCs in *CD11c-DTR/GFP* mice reduced the inflammation in acute colitis initiated by the chemical dextran sulfate sodium (DSS) (Abe et al. 2007). Similar effects were observed in TRUC mice, where the deletion of *Tbet* on a Rag1 deficient background leads to spontaneous colitis driven by tumor necrosis factor α (TNFα), followed by tumor development. Depletion of CD11c-expressing cells in these mice abrogated colitis and, therefore, tumor development (Garrett et al. 2009). Increasing the number of total DCs in mice via adoptive transfer of Bone-marrow-derived-DCs (BMDCs) before inducing the colitis led to a more severe course of colitis (Berndt et al. 2007). All three studies point toward a pro-inflammatory role of CD11c-positive cells. However, in these studies, different cell populations have been involved, as intestinal macrophages express CD11c,

and BMDCs were generated by GM-CSF culture, recently shown to generate a combination of macrophages and DC-like cells (Helft et al. 2015).

Batf3$^{-/-}$ knockout mice lack intestinal CD103^{+} cDC1 and resident and migratory cDC1 in the mLN. These mice showed no spontaneous intestinal inflammation and had no altered disease severity upon chemical-induced colitis (Edelson et al. 2010). Nevertheless, aged *Batf3* deficient mice show increased intestinal permeability, allowing commensal microbes to breach the epithelial barrier (Hamade et al. 2022). Another study aimed to deplete cDC1s in the *Clec9a-DTR* model by repetitive DT injections before and throughout DSS treatment. DT-treated Clec9a-DTR mice showed exacerbated colitis, attributed to decreased INFγ producing CD4 and CD8 T cells, further leading to lower anti-inflammatory IDO1 and IL-18bp levels in intestinal epithelial cells (Muzaki et al. 2016). Even though the study aimed to deplete differentiated cDC1 as they express CLEC9A/DNGR1 again, it must be considered that the *Clec9a-DTR* targets cDC committed precursors. Those will be depleted as well, leading to an overall reduction of cDCs whereby cDC1s are more affected than cDC2s, and cells derived from a non-DNGR1 expressing cell may fill the open niche of cDC2s (Salvermoser et al. 2018).

Within the last years, the research used the cDC1-restricted expression of XCR1. Specific deletion of cDC1 in *XCR1-DTA* mice leads to severe colitis, a drastic decrease of Tregs, and a shift towards Th17 (Moreira et al. 2021). Even though *Batf3* depletion leads to an absence of cDC1, it has been shown that under inflammatory conditions, cDC1s reappear in *Batf3*$^{-/-}$ knockout mice due to a compensatory effect of *Batf* and *Batf2* (Tussiwand et al. 2012). This fact plausibly explains the different outcomes in colitis studies with cDC1-depleting mouse models. Additional causes could be the gut microbiota, the mouse's genetic background, and the DSS's source and dose.

Research on intestinal cDC2 in colitis identified a potential pro-inflammatory role of this cDC subtype. The deletion of cDC2s via the *Clec4a4-DTR* mouse model protected mice from severe colitis induced by DSS supplementation of the drinking water (Muzaki et al. 2016). In another DSS colitis study, deletion of cDC2 from the intestinal system had no impact on disease outcome, even though mice showed decreased Th17 cells at the basal level (Welty et al. 2013). Other labs used a T cell-mediated colitis system induced via T cell transfer into Rag1 knockout mice, which lack mature B and T cells. Deletion of IRF4-dependent cDC2s ameliorated colitis severity, accompanied by decreased immune cell influx, leading to a less disrupted epithelial barrier. A reduced level of Th17 cells mediated this effect; therefore, lower levels of IL-17A and IL-17F cytokines were previously shown to correlate positively with colitis severity (Buchele et al. 2021, Pool 2018, Wedebye Schmidt et al. 2013).

Although deletion of cDC subsets influences acute colitis by acting in an anti- or proinflammatory manner, other studies suggest that the pathogenesis of acute colitis is mediated predominantly by monocyte-derived cells (Tamoutounour et al. 2012, Mildner, Yona and Jung 2013, Bain and Mowat 2014). This hypothesis is favored because the pathology of DSS-induced acute colitis does not require LP T cells, and the primary function of cDCs is the induction of T cell response (Dieleman et al. 1994, Kühl et al. 2007, Tsuchiya et al. 2003).

1.2.2 The cDC function is influenced by their metabolism

Within the last years, increasing research in immunometabolism suggests different metabolic pathways mediating the pro- and anti-inflammatory function of cDCs. For instance, recent studies placed PI3K/AKT/mTOR and p38a MAPK signaling pathways in context with the pro-inflammatory role of cDCs. The depletion of p38a MAPK in cDCs protected mice from severe acute colitis and colitis-driven cancer formation (Zheng et al. 2018). Moreover, cDC-specific deletion of PTEN, the primary negative regulator of the PI3K/AKT/mTOR pathway, aggravates chemical-induced colitis due to increased Th1 response (Kuttke et al. 2022). Nevertheless, it has to be considered that another study showed that *CD11c^{cre}Pten^{flox}* mice have a 5 to 6-fold increase of cDC1 in lymphoid and peripheral organs (Sathaliyawala et al. 2010). This effect of increased mTOR signaling leading to cDC1 expansion might be explained by the activation of the PI3K pathway upon Flt3L binding to its receptor, driving cDC development (McKenna et al. 2000). The fact that cDC2 are not increased upon overactivation of PI3K signaling points towards different metabolic requirements skewing cDC differentiation towards a specific subset. This is further underlined by the increased mitochondrial membrane potential and higher oxidative phosphorylation (OXPHOS) in splenic cDC1 compared to cDC2s (Møller, Wang and Ho 2022). Despite their distinct metabolic requirements for development and homeostasis, a common feature of cDCs is the rearrangement of their metabolism upon activation. This reprogramming is marked by a switch from a more catabolic (OXPHOS) towards anabolic metabolism, predominantly glycolysis. This so-called glycolytic burst has been attributed to be a conserved response upon PRR activation and further maturation of immunogenic cDCs (Everts et al. 2014, Thwe et al. 2019). In contrast, there is evidence that tolerogenic cDCs maintain high levels of OXPHOS in parallel to the upregulation of glycolysis (Wculek et al. 2019b). Leading to the assumption that cDC function is marked and influenced by their metabolism.

1.2.3 The cDC1s are essential for an effective anti-tumor response

Several other non-tumor cells can be found within a tumor, forming the tumor microenvironment (TME). Besides stromal cells, blood vessels, and extracellular matrix, immune cells are localized to different extents within the TME (Hanahan and Weinberg 2011). Within most solid tumors, monocytes and macrophages constitute the most significant fraction of immune cells, and DCs, especially cDCs, are rare (Gentles et al. 2015, Broz et al. 2014). Several cell subsets ingest tumor-derived antigens, although macrophages are the most potent. However, the significant population transporting those tumor-derived antigens into the tumor-draining LN (TDLN) are migratory cDC1. In the TDLN, cDC1s can transfer antigens to the resident cDC population, although studies showed that these resident cells could not stimulate naïve CD8 T cells ex vivo (Salmon et al. 2016, Roberts et al. 2016). Some studies demonstrated that a small fraction of migratory cDC2s contribute to the transport (Ruhland et al. 2020). The TDLN is the leading site of T cell priming, and only a tiny fraction of naïve T cells get primed in the TME (Thompson, Enriquez, Fu and Engelhard 2010). The overall hypothesis is that an insufficient cytotoxic CD8 T cell response is the leading cause of cancer immunosurveillance failure (Gerner, Casey and Mescher 2008), and the proportion of cDCs and CD8 T cells within the tumor and TDLN correlate with better prognosis (Gentles et al. 2015).

Throughout the last years, research on the role of cDCs in cancer development and cancer regression has increased, driven by the intense focus on immune therapies as alternatives to conventional treatments (Ferlay et al. 2020). Most research studies on the role of cDCs in cancer used transplantable tumor models, like cancer cell lines injected subcutaneously into mice, leading to constantly growing tumors. So-called rejection models use cancer cell lines forming an immunogenic TME, leading to tumor regression or rejection under standard conditions (Lai et al. 2020, Iwanowycz et al. 2021). Implementing these models to mice with a *Batf3*$^{-/-}$ background identified a non-redundant role of cDC1 in the immunogenic tumor regression and rejection process. However, cDC1 deficiency did not impact tumor growth if the tumor escaped from the immune response (Hildner et al. 2008, Maier et al. 2020, Salmon et al. 2016).

Additionally, cDC1s have been implicated as essential for T cell-based immunotherapies' effectiveness. For instance, the anti-tumor potency of adoptive T cell transfer or anti-PD1 treatment is lost in the absence of cDC1s (Sánchez-Paulete et al. 2016, Garris et al. 2018). In line with these findings, the transfer of cDC1s, pre-loaded with tumor antigens, reduces tumor growth (Wculek et al. 2019a). Utilization of this vaccination strategy induces a cytotoxic CD8 T cell response and leads to the induction of γδ T cells (Van Acker, Anguille, Van Tendeloo and Lion 2015). Latter ones kill tumor cells in a cytotoxic manner via the secretion of granzymes and perforins, similar to CD8 T cells (Niu et al. 2015).

The critical role of cDC1s during an anti-tumor immune response is further underlined by studies that expanded the cDC1 population within the tumor through intratumoral FLT3L injection, FLT3L expressing tumors or the transfer of FLT3L expressing T cells. This cDC1 expansion reduces tumor growth or even leads to tumor rejection (Salmon et al. 2016, Lai et al. 2020). Combination of FLT3L treatment with a PRR adjuvant, like polyI:C targeting TLR-3, induces an anti-tumor memory, whereby the formation of tissue-resident CD8 memory cells relies on cDC1 (Iborra et al. 2016, Salmon et al. 2016). This FLT3L-induced expansion of cDC1 is elevated in *Clec9a* knockout mice. However, under homeostatic conditions, ablation of DNGR1 does not affect tumor growth (Cueto et al. 2021).
Besides transplantable tumor models, a recent study showed a similar effect of reduced tumor growth after vaccinating mice with BMDCs mixed with tumor antigen in chemical-induced inflammation-driven carcinogenesis (Murwanti et al. 2023).

cDC2s are essential for CD4 T cell responses and likely mediate CD4 T cell anti-tumor immune responses. However, TME promotes their tolerogenic phenotype, favoring pro-tumorigenic Treg induction, indicated by the positive correlation of cDC2 and Treg frequency within the tumor (Binnewies et al. 2019). *CD11c^{cre}Irf4^{flox}* mice underline this pro-tumorigenic phenotype of cDC2s, as these mice show reduced tumor growth ascribed to elevated levels of Th1 cells infiltrating the tumor (Zhang et al. 2020). However, the depletion of Tregs increases co-stimulatory molecules and pro-inflammatory cytokines in tumor-associated cDC2s and expands the migratory cDC2 population (Binnewies et al. 2019).

The direct effect of CD4 T cells on tumor cells is low; they instead contribute to CD8 T cell responses, promoting cDC1 maturation through CD40 ligation. CD40 signaling increases the survival of cDCs stabilizes the MHCI:Antigen complex, and raises the expression of co-stimulatory molecules and IL-12 (Gerner, Casey and Mescher 2008). The contribution of CD40 licensing is highlighted by the success of anti-CD40 combined with anti-PD1 treatment, generating an anti-tumor immunity for immunogenic tumor types. It reduces tumor growth in tumors that usually do not respond to anti-PD-1 therapy (Garris et al. 2018). The induction of those cDC1-licensing CD4 T cells is driven by cDC1 themselves. This is most likely due to their capacity to present cell-associated antigens on MHCI and MHCII (Ferris et al. 2020, Wu et al. 2022).

Besides directly activating CD8 T cells, cDC1s secrete CXC-chemokine ligand (CXCL) 9 and CXCL10, recruiting CXCR3 expressing cells into the tumor, especially cytotoxic CD8 T cells, ILC1s, and NK cells. This property of cDC1s might explain their essential role in the effectiveness of adoptive T-cell therapies (Spranger, Dai, Horton and Gajewski 2017, Wendel, Galani, Suri-Payer and Cerwenka 2008). In addition to the recruitment of

T cells, CXCL9/10 secretion contributes to the positioning of T cells close to cDC1s, facilitating their local re-stimulation (Mikucki et al. 2015). Production of both chemokines is induced by type I interferons (IFNα & IFNβ) and IFNγ, indicating a feedback loop between cDCs and the recruited cell type (Mikucki et al. 2015).

Furthermore, IFNγ detected by cDCs induces their production of IL-12, leading together with co-stimulation to further activation and expansion of the CD8 T cells (Garris et al. 2018). However, the co-stimulatory interaction between cDCs and T cells is often disturbed within cancer. For instance, typical co-stimulatory interaction of either CD80 or CD86 with CD28 is outpaced by CTLA4, possessing increased affinity compared to CD28. CTLA4 expression inhibits co-stimulatory signaling and reduces T cell activation (Rowshanravan, Halliday and Sansom 2018). Another route of limiting T cell activation occurs via PD-L1 / PD-L2, expressed by APCs and several other cells in the TME, e.g., tumor cells. Both ligands bind PD-1 on T cells, inhibiting their proliferation and cytokine production (Rowshanravan, Halliday and Sansom 2018). Throughout the population of CD8 T cells localized in the tumor, the fraction of PD-1-expressing cells increases within a more immunosuppressive TME (Garris et al. 2018).

Beyond their recruitment via CXCL9/10, NK cells, in turn, attract cDC1s into TME through secreting CCL5 and XCL1. In addition, NK cells can produce FLT3L, contributing to cDC1 survival and maintenance (Barry et al. 2018, Böttcher et al. 2018). Further on, it has been shown that cDC1-derived IL-12 is required for NK cell-mediated suppression of tumor metastasis (Mittal et al. 2017). Ultimately, the cytotoxic activity of NK cells can be induced or further promoted by γδ T cells through 4-1BB/CD137 signaling (Maniar et al. 2010). Moreover, high NK and γδ T cell levels correlate with a better prognosis (Gentles et al. 2015). Along with their function within a tumor, NK cells can enter the LN and promote T cell priming under inflammatory and tumorigenic conditions (Chiossone, Dumas, Vienne and Vivier 2018).

In conclusion, cDC1s are essential for an effective anti-tumor response, mediating cytotoxic CD8 T cell and NK cell responses if tumors do not escape the immune response. In contrast, studies on cDC2s suggested that this cell type possesses a more pro-tumorigenic role. However, the function of cDCs is imprinted by the TME and, therefore, can differ depending on the tumor, as cancer is a rather heterogeneous disease. Further on, most of the studies used transplantable, subcutaneous tumors. Even though they used a colorectal cancer cell line, the actual role of cDCs might differ in tumors located in the colonic environment. Furthermore, the overall anti- or pro-tumorigenic function of the cDC subsets might be altered if only a specific signaling pathway is disrupted within these cells.

1.3 Sensing of pathogens through SYK and CARD9 by myeloid cells as an important mechanism in colorectal cancer

1.3.1 Chronic inflammation as a major risk factor of Colorectal Cancer

Colorectal cancer (CRC) is the third most common type of cancer worldwide, with around 2 million new cases yearly, and the second most common cause of overall cancer mortality (Ferlay et al. 2020). Besides age, environmental factors are major risk factors for developing CRC, including several lifestyle habits like smoking, consumption of alcohol, physical inactivity, and a Western diet (Johnson et al. 2013). And only 15 – 20 % of CRC patients have inherited the predisposition of CRC development (Rustgi 2007).

Additionally, inflammatory bowel disease (IBD) is a significant risk factor for developing CRC. IBD is a condition marked by a chronic inflammatory process within the intestinal compartment (Jess, Frisch and Simonsen 2013, Mattar, Lough, Pishvaian and Charabaty 2011). Two common types of IBD are ulcerative colitis (UC) and Chron's disease (CD) (Abraham and Cho 2009). UC is restricted to the colon, affecting the mucosa and submucosa pre-dominantly, whereas CD can affect the whole gastro-intestinal compartment, involving all layers. (Abraham and Cho 2009). IBD-related CRC, termed colitis-associated cancer (CAC), is responsible for approximately 2 % of the annual mortality from CRC overall and makes up to 15 % of yearly deaths of IBD patients (Keller, Windsor, Cohen and Chand 2019). The influence of the chronic inflammatory process in tumorigeneses is further highlighted by the fact that CD patients only have an increased risk of CAC development if they have inflammation sites in the colon (Gatenby et al. 2021).

In the case of chronic inflammation in UC and CD, epithelial cells have a high turnover to replace the tissue destroyed during inflammation. This recurring replenishment of damaged tissue requires high cell division rates, which provide opportunities for mutations and aberrant chromosome separations (Foster et al. 2018). However, epithelial cell restitution alone does not drive cancer development. In addition, the repetitive inflammatory processes lead to an oxidative environment caused by the release of reactive oxygen and nitrogen species by innate immune cells, representing a key feature of chronic inflammation. These reactive oxygen and nitrogen species interact with the DNA of surrounding epithelial cells, inducing DNA damage (Waldner and Neurath 2015). Both factors can lead to mutations in tumor suppressor genes or oncogenes (Beaugerie and Itzkowitz 2015).

Immune cells also secrete a wide range of cytokines and chemokines, harboring pro- and anti-inflammatory functions. For instance, a key cytokine during acute inflammation

is the pro-inflammatory TNFα and mice deficient for TNFα, or its receptors are less susceptible to CAC due to reduced inflammation (Szlosarek and Balkwill 2003), underlying the critical role of the inflammation during tumorigenesis. Further on, IL10 knockout mice, a standard mouse model to study colitis, develop spontaneous colitis when mice are kept under normal but not germ-free conditions. The inflammation-driven tumorigenesis is emphasized in this model because the additional treatment of these mice with the mutagenic chemical Azoxymethane (AOM) leads to tumor formation only in those suffering from colitis (Uronis et al. 2009).

The immune response during colitis can be influenced by the invasion of pathogens and microbial products from the intestinal lumen into the epithelial layers, further activating the immune system. However, the effect of the microbiota breaching the intestinal barrier during acute inflammation on tumor progression depends on the involved PRR and its downstream signaling cascade (Waldner and Neurath 2015). For instance, the TLR-2 and TLR-4 show contradicting outcomes when studied in AOM-DSS, a mouse model of CAC. TLR-4 deficient mice are protected from cancer development, whereas TLR-2 deficient mice have increased tumor development (Lowe et al. 2010, Fukata and Abreu 2007).

Further PRRs implicated in IBD and tumor development belong to the NLR family. Common mutations found in IBD patients affect NOD2, an intracellular receptor for mycobacteria (Boyle, Parkhouse and Monie 2014). The loss of function of NOD2 has been implicated in causing dysbiosis and increased intestinal inflammation (Waldner and Neurath 2015). In-depth GWAS studies identified NOD2 interaction partners, including Autophagy related 16 like 1 (ATG16L1) and Caspase recruitment domain-containing protein 9 (CARD9) as additional risk loci in IBD. As a result, *Card9* polymorphisms have been found in both forms of IBD, UC, and CD (Zhernakova et al. 2008). In the last decade, CARD9 was implicated in playing a crucial role in the process from chronic inflammation to tumor formation and progression.

1.3.2 CARD9 is important for sensing of fungi by myeloid cells

CARD9 is a protein exclusively expressed in myeloid cells, especially in macrophages, DCs, and Neutrophils. CARD9 is located in the cytoplasm and consists of an N-terminal CARD domain and a coiled-coil region at the C-terminus. The CARD domain is responsible for protein-protein interaction and can bind other CARD domains in a homophilic manner (Roth and Ruland 2013).

Within the last decade, the CARD9 function was described downstream of several PRRs, *e.g.,* the intracellular receptors for virus or bacteria-derived nucleic acids RIG-I or MDA5 or the dsDNA damage sensor Rad50 (Roth and Ruland 2013). However, its role below

the CLRs Dectin-1, Dectin-2, and Mincle, major PRRs in anti-fungal immunity, is the best characterized (Gross et al. 2006). Dectin-1 recognizes β-glucan carbohydrates derived from fungal cell walls, and Dectin-2 is known to bind fungal-derived α-mannans. In contrast, the repertoire of potential Mincle ligands is quite broad. Besides fungi, Mincle can bind the dead cell-derived ribonucleoprotein SAP130 and the glycolipid trehalose-6,6-dimycolate (TDM) expressed in mycobacteria. Subsequently, additional PAMPs and DAMPS were identified to activate Dectin-1, Dectin-2, and Mincle (Brown, Willment and Whitehead 2018).

Dectin-1 owns an intracellularly located immunoreceptor tyrosine-based activation motif (ITAM), which gets phosphorylated by Src family kinases upon ligand binding to the receptor. The receptor proximal recruitment of SYK requires two YxxxL motifs. As Dectin-1 bound ITAM has only one of these motifs, Dectin-1 forms a homodimer upon ligand binding, leading to a hemiITAM. Dectin-2 and Mincle recruit the adaptor proteins FcRγ or DAP12, which contain an ITAM domain, as the receptors lack this domain (Hartjes and Ruland 2019).

The binding of the SH2-domain of SYK to phosphorylated ITAM induces its activation, which is required for downstream initiation of phagocytosis, ROS production, and the induction of gene expression of pro-inflammatory cytokines and chemokines. Additional research has implicated SYK in the proximal activation of the NLR family, pyrin domain-containing 3 (NLRP3) inflammasome, which is required to cleave pro-IL-1β into its active form (Mócsai, Ruland and Tybulewicz 2010). SYK activation further induces the recruitment of protein kinase C δ (PKCδ), mediating the phosphorylation of CARD9, a critical step for the assembly of CARD9 with its direct interaction partner B cell lymphoma 10 (BCL10) via the CARD domain. BCL10 is constitutively bound to multifunctional protein mucosa-associated lymphoid tissue lymphoma translocation protein 1 (MALT1) (Strasser et al. 2012). The interaction of CARD9 with BCL10 and MALT1 forms a signaling complex called the CBM complex, leading to the activation of the canonical NFκB pathway and p38 MAPK and JNK signaling (Roth and Ruland 2013).
CBM complex assembly triggers the activation of IKKβ, thereby inducing the phosphorylation and proteasomal degradation of the inhibitor of NFκB (IκBα) (Vornholz and Ruland 2020). This further leads to the release of NFκB subunits RelA and c-Rel for their translocation to the nucleus to induce transcription of pro-inflammatory cytokines like pro-IL-1β, IL-6, IL-10, IL-23, and TNFα. MALT1 uses its catalytic caspase-like domain to cleave the NFκB subunit RelB, which acts in the noncanonical NFκB pathway, leading to IL-5 production and thereby driving Th2 immunity (Hartjes and Ruland 2019). This cytokine composition has consequences for further T-cell differentiation. Compared to TLR stim-

ulation, CLR activation and receptor proximal signaling via SYK and CBM-complex favors a polarization of CD4 T cells towards the Th17 phenotype (Ruland 2008). However, blocking of Dectin-2 in Dectin-1 deficient mice revealed that SYK-mediated Th17 induction is driven by Dectin-2 and not Dectin-1 (Drummond, Saijo, Iwakura and Brown 2011).

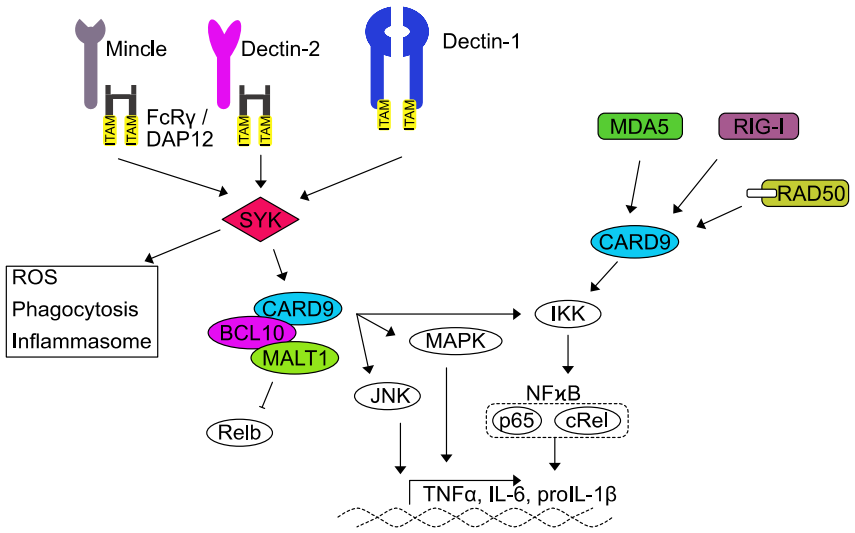

Figure 3 CARD9 Signaling Cascade

Upon detection of PAMPs/DAMPs, the CLR Dectin-1 dimerizes and activates SYK via coupled ITAM domains. Dectin-2 and Mincle recruit upon pathogen detection FcRγ or DAP12, harboring an ITAM domain and thereby inducing SYK activation. SYK mediates the assembly and activation of the CARD9-BCL10-MALT1 complex, which induces p38 MAPK and JNK signaling. CBM complex induces via the activation of IKK and inhibition of RelB the canonical NFκB pathway. CARD9 is also activated by the intracellular nucleic acid sensing PRRs MDA5, RIG-I, and RAD50. Promoting NFκB signaling that leads to the production of pro-inflammatory cytokines.

1.3.3 The role of CARD9 in cDCs during IBD is unclear

Under homeostatic conditions, CARD9 deletion induces an altered microbiome, so-called dysbiosis, with an increased fungal burden. Nonetheless, *Card9*$^{-/-}$ knockout mice show regular intestinal immune cell composition and epithelial barrier integrity and do not develop spontaneous colitis (Sokol et al. 2013). Even though *Card9*$^{-/-}$ mice exhibit an intact intestinal barrier in the colon, the deletion of its upstream receptor Mincle induced a defect in barrier function in the small intestine marked by a reduction in antimicrobial peptides like RegIIIγ and reduced IgA production (Martinez-Lopez et al. 2019).

Several groups have demonstrated that upon DSS-induced acute colitis, *Card9*$^{-/-}$ mice show increased loss of body weight and disease severity, marked by shortened colon length (Lamas et al. 2016, Malik et al. 2018, Sokol et al. 2013, Wang et al. 2018). However, during CAC, results have been contradicting, most likely because the loss of CARD9 leads to alterations of the intestinal microbiome, and different housing strategies have been used across studies. Altered microbiota causes differences in the production

of microbial metabolites between *Card9*$^{-/-}$ and control mice. Especially aryl-hydrocarbon receptor (AHR) ligands tryptophan-derived indole derivates are affected, leading to increased susceptibility of *Card9*$^{-/-}$ mice to colitis (Lamas et al. 2016).

In one CAC study, *Card9*$^{-/-}$ mice develop smaller and less dysplastic tumors in the colon (Bergmann et al. 2017), whereas other studies show increased tumor incidence (Malik et al. 2018, Wang et al. 2018). Bergman *et al.,* who co-housed knockout and control mice, showed that the smaller tumors in the colon of *Card9*$^{-/-}$ mice result from decreased IL-1β levels. The decreased IL-1β leads to diminished activation of ILC3 and results in reduced IL-22 production and less activation of cell proliferation via STAT3 in epithelial cells (Bergmann et al. 2017).

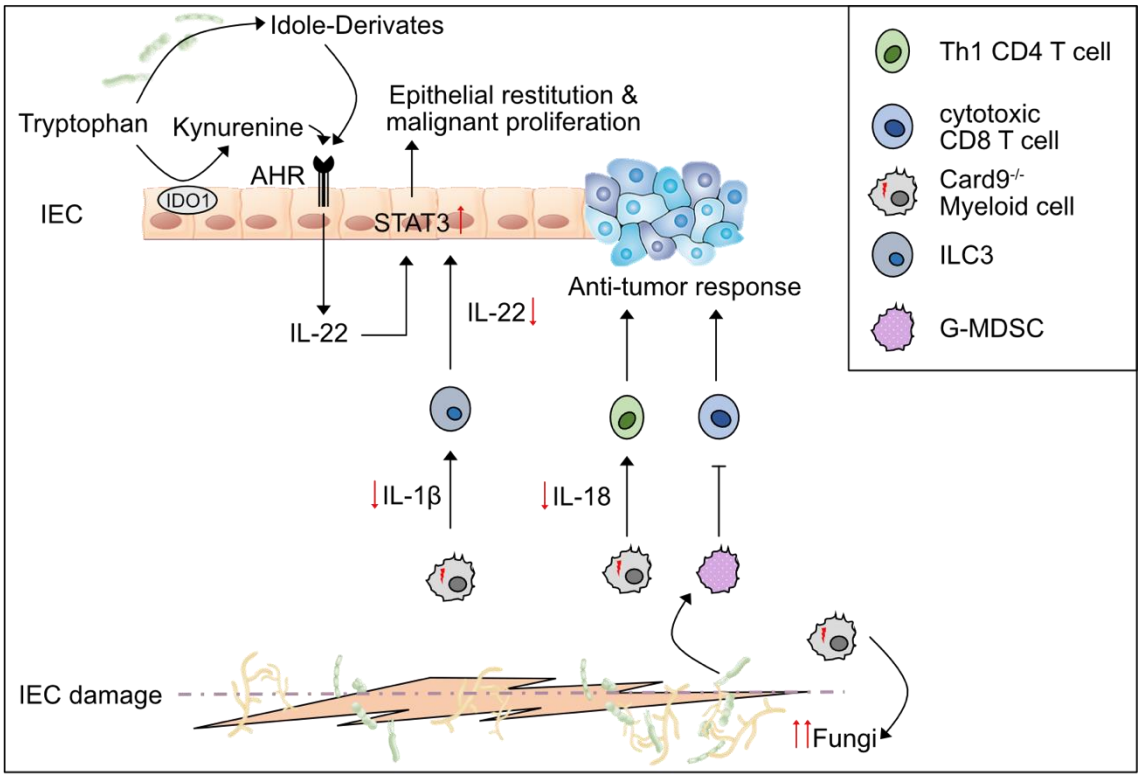

Figure 4 Signaling mechanism of CARD9 in CAC depicted by several studies.

CARD9 contributes to microbial homeostasis, and the deletion of CARD9 induces an expansion of fungi. On the one hand, this dysbiosis affects the tryptophan metabolism that mediates epithelial restitution via AHR signaling and Il-22 secretion. In addition, the heightened fungal burden induces accumulation of MDSCs, suppressing anti-tumor immune response by cytotoxic CD8 T cells. Further, SYK-CARD9 signaling induces the secretion of IL-18, leading to a Th1-driven antitumor response. In addition, CARD9 mediates the secretion of IL-1β that activates ILC3. In turn, ILC3s produce IL-22 driving epithelial restitution and malignant proliferation.

Besides the increased tumor load in single-housed *Card9*$^{-/-}$ mice, Malik *et al.* identified a role of CARD9 in the release of IL-18 and downstream activation of Th1 response (Malik et al. 2018). IL-18 is a cytokine transcribed into its pro-active form and requires cleavage

by Caspase-1 (Dinarello, Novick, Kim and Kaplanski 2013). Utilization of the *LysM*^{cre}-*Syk*^{flox} mice identified a SYK-CARD9-mediated activation of the inflammasome in myeloid cell lineage (monocytes, macrophages, and granulocytes) induced by alterations in the microbiota. In addition, they reversed the phenotype of increased tumor number by co-housing *Card9*$^{-/-}$ with control mice (Malik et al. 2018). A fecal transfer study further highlighted the role of CARD9-deletion-altered microbiota. Wildtype germ-free mice were colonized with the microbiota of *Card9*$^{-/-}$ mice and showed increased disease severity in subsequent DSS-induced colitis (Lamas et al. 2016).

Along with the increased tumor load in *Card9*$^{-/-}$ mice (mono-housed), Wang *et al.* showed that the increased fungal burden in the gut promotes the accumulation of myeloid-derived-suppressor cells (MDSCs) (Wang et al. 2018). These MDSCs have an immunosuppressive activity and can promote tumor development by suppressing cytotoxic T cells (Gabrilovich and Nagaraj 2009). It was shown that, in fungal infections of the central nervous system, neutrophils, which can fall under MDSCs gating, are recruited via the IL-1β axis (Drummond et al. 2019). Actual IL-1β mRNA levels were increased in the studies from Wang *et al.* but decreased in the contradictory publication from Bergmann *et al.*, suggesting that CARD9 mediates IL-1β production and secretion in a microbiota dependent manner.

Besides the studies focusing on the role of CARD9 in colitis and CAC, it has been shown that Dectin-1-SYK-CARD9 mediated maturation of DCs induces a potent expansion of antigen-specific CD8 T cells in vitro and in vivo. This increased frequency of cytotoxic CD8 T cells facilitates an anti-tumor immunity if mice were subcutaneously vaccinated with ovalbumin (OVA) and curdlan, a Dectin-1 specific antagonist, and later on challenged with OVA-expressing tumor cells (LeibundGut-Landmann, Osorio, Brown and Reis e Sousa 2008, Haas et al. 2017).

Further, a recent study dissected the role of CARD9 during acute colitis in different myeloid cell types and epithelial cells. Deleting CARD9 in epithelial cells (Villin^{cre}) or CD11c expressing cells (CD11c^{cre}), including DCs and macrophages, did not affect disease severity. However, since CD11c^{cre} models are not cell-type specific, the role of CARD9 in cDCs during acute colitis is still unclear. Thus far, it has been shown that CARD9 plays an essential role in colitis and oncogenesis. However, the myeloid cell type in which CARD9 mediates the inflammatory signals and regulates the homeostasis of the colon has yet to be defined. As cDCs have been shown to play an essential role in colitis, especially cDC1s are critical for the anti-tumor response, this thesis aimed to go one step further and study the signaling pathway around CARD9 in cDCs. In particular, the function of CARD9 with its interaction partners BCL10 and MALT1.

1.4 Aim of the Thesis

By crossing mice with a floxed *Bcl10* allele to *Clec9a*^{cre} mouse, the thesis aims to investigate the effect of loss of CBM signaling specifically in cDCs and thus define if CARD9 mediates a functional role in cDCs in CAC. To analyze the contribution of SYK-mediated activation, *Clec9a*^{cre}*Syk*^{flox} mice were used to abrogate CBM-complex activation via Dectin-1, Dectin-2, and Mincle, specifically in cDCs.

2. Material and Methods

2.1 Animal husbandry

Clec9a-cre (Schraml et al. 2013), *Bcl10-flox* (Rosenbaum et al. 2019), *Syk-flox* (Saijo et al. 2003), and C57BL/6J mice were bred at the Center for translational Cancer Research of the Technical University of Munich (TranslaTUM) and the Biomedical Center of the Ludwig-Maximilian's University in specific pathogen-free conditions. Mice over 8 weeks were considered adults and used for experiments until 14 weeks. Mice were bred so that conditional knockout (cKO) mice and controls were derived ideally from the same litter. Further on, cKO and control mice were cohoused at least 2 weeks before experimental use to minimize microbiota effects. All animal procedures were performed per national and institutional animal welfare guidelines and approved by the Regierung of Oberbayern.

2.2 Genotyping

Transgenic mice were genotyped through ear snips and taken by the animal caretakers in the animal facility. Tissues were digested in 200µl quick lysis buffer (10 mM Tris, 150 mM NaCl, 5 mM EDTA, 0.05 % NP40, pH 8,0) supplemented with 0.2 mg/ml ProteinaseK. Digestion occurred in a thermoshaker (Eppendorf) for 3 hours at 56 °C and 300 rpm. Heat inactivation of ProteinaseK was done at 90 °C for 10 min at 300 rpm. Undigested tissue was pelleted through centrifugation at max speed (~ 12700rpm) for 5 min at room temperature (RT). From the supernatant, 1µl was used for genotyping PCR. PCR

Table 1 Genotyping primers

PCR Primer - Locus	Sequence 5' – 3'	End concentration [µm]
Clec9a cre – BS49	AAA AGT TCC ACT TTC TGG ATG ATG A	0.5
Clec9a cre – BS47	GGC TCT CTC CCC AGC ATC CAC A	0.25
Clec9a cre – A65	TCA CTT ACT CCT CCA TGC TGA CG	0.25
Syk flox – Syk2 fwd	GCC CGT TCT GTG CCT ACT GG	0.5
Syk flox – Syk2 rev	TAG CTA ACC AAA CCC ACG GC	0.5
Bcl10 flox – fwd	CTA TCT GTA CCA ACA ACT GAA GAG	0.5
Bcl10 flox - rev	ATA CAG GAT TCT TAC ACA CTC GT	0.5

Table 2 PCR product size overview

PCR Product	Clec9a cre	Syk flox	Bcl10 flox
WT	597 bp	234 bp	130 bp
Mut	407 bp	349 bp	240 bp

Table 3 PCR Programs

Clec9a cre			**Syk flox**			**Bcl10 flox**		
95 °C	3 min		94 °C	5 min		98°C	30 sec	
95 °C	30 sec	35 cycles	94 °C	1 min	36 cycles	98°C	5 sec	30 cycles
60 °C	30 sec		63 °C	1 min		58°C	5 sec	
72 °C	40 sec		72 °C	1,5 min		72°C	15 sec	
72 °C	10 min		72 °C	10 min		72°C	1 min	
4 °C	hold		10 °C	hold		8°C	hold	

2.3 AOM/DSS – Colitis associated cancer model

Colitis-associated cancer experiments were performed in collaboration with the group of Prof. J Ruland at the TranslaTUM. Knockout mice and their controls were cohoused for at least 2 weeks before and throughout the experiments to minimize variations in the microbiota. Mice were injected intraperitoneally once on day 0 with 10 mg/kg AOM (Sigma) in PBS (Sigma), followed by three cycles of 2.5 – 1.5 % DSS (MP Biomedicals) dissolved in drinking water for five successive days at days 5, 26, and 47. Mice were monitored for weight loss and further colitis symptoms throughout each DSS cycle until mice recovered from acute colitis. Mice suffering from weight loss higher than 20 % of their initial weight or showing indication of severe illness were euthanized by cervical dislocation. Blood was collected from the submandibular vein (cheek punch) for systemic cytokine analysis on days 13, 34, and 55.

2.4 DSS – Acute colitis

Colitis experiments with *Clec9a*^{cre}*Bcl10*^{flox} mice were performed at the TranslaTUM in collaboration with the group of Prof. J Ruland. Colitis experiments with *Clec9a*^{cre}*Syk*^{flox} mice were performed at the BMC. Respectively, knockout mice and their controls were cohoused for at least 2 weeks before and throughout the experiments to minimize variations in the microbiota. 2.5 – 3.5 % DSS (MP Biomedicals) was dissolved in drinking water and administered to mice for 5 – 7 days, followed by 5 days of water only. Mice were monitored daily for weight loss and disease activity until the endpoint was reached. Disease activity index (DAI) score was calculated as a total score of body weight loss and clinical score (physical inactivity, bent posture, bristled fur, stool consistency, and rectal bleeding/prolaps). Mice suffering from weight loss higher than 20 % of their initial weight or showing indication of severe illness were euthanized by cervical dislocation.

2.5 Histological analysis of tissue sections

The AOM-DSS and DSS-treated mice colons were carefully cleaned from feces and mucus and prepared as a Swiss role. Tissues from AOM-DSS treated mice were fixed in 10% formalin for 48h, transferred to PBS, and handed over to the Institute of Pathology (Dr. K Steiger) for dehydration, paraffin embedding, Hematoxylin-eosin (H&E) staining, and histological scoring of tumor invasiveness.

Swiss roles from colitis mice were embedded in O.C.T.™ compound (Tissue -Tek®) and immediately placed on dry ice. After equilibration to -20 °C for 2 h, 10 µm sections were generated with the Leica CM3050 S Kryostat. For H&E staining, sections were equilibrated to RT and stained with 'Hemalum solution acid acc. to Mayer' (Roth) and 'Eosin Y solution 0.5% in water' (Roth) according to the instructions supplied with the chemicals.

H&E stained colon sections were analyzed with the bright field microscope Leica DM2500 and scored according to Siegmund et al., JPET, 2000 (Siegmund et al. 2001).

Table 4 Overview of scoring criteria (Siegmund et al. 2001)

Score	Inflammatory cell infiltrate	Epithelial damage
0	Rare inflammatory cells in lamina propria	Absence of damage
1	Increased numbers of inflammatory cells, including neutrophils in lamina propria	Discrete focal lymphoepithelial lesions
2	Confluence of inflammatory cells, extending into submucosa	Mucosal erosion/ulceration
3	Transmural extension of inflammatory cell infiltrate	Extensive mucosal damage and extension through deeper structures of the bowel wall

2.6 Serum Preparation

Collected blood was transferred into a 1.5 ml Eppendorf reaction tube and left for 1h at RT, allowing the blood to clot. The clot was removed through centrifugation at 10x g 10min at 4°C and collection of the supernatant. Collected serum was snap-frozen in liquid nitrogen and stored at freeze at -80°C. Serum cytokines were analyzed by LEGENDplexTM Mouse Inflammation (BioLegend) according to manufacturers' instructions.

2.7 Tissue explant cultures for cytokine detection

A 2 – 3 mm colon piece was collected from the desired location (e.g., middle of the colon) and transferred into a reaction tube containing 1 ml Gut medium to measure overall cytokines in intestinal tissue. Via vortexing for 30 sec, feces and mucus were removed. The tissue piece was weighed, transferred into 200 µl Gut medium, and incubated overnight at 37 °C, 5 % CO_2. The supernatant was collected, and cytokines were analyzed

by LEGENDplexTM Mouse Th Cytokine Panel and LEGENDplexTM Mouse Inflammation (both from BioLegend) according to manufactures instructions. The resulting cytokine values were normalized to tissue weight.

2.8 Immune cell Isolation from different tissues

2.8.1 Spleen and lymph nodes

Lymphatic organs, cleared from all fat, were cut into small pieces and digested for 30 min, shaking at 37 °C in a total volume of 1 ml RPMI (Thermo Fisher Scientific) using 0.2 mg/ml DNase I (Roche) and 200 U/ml CollagenaseIV (Worthington). Afterward, the cell suspension was passed through a 70 µm strainer and washed with FACS buffer (PBS (Sigma), 1 % FCS (Sigma), 2.5 mM EDTA (Invitrogen), 0.02 % sodium azide (Sigma)). If cells were prepared for sorting or culture, FACS Buffer without sodium azide (MACS buffer) was used. Red blood cells were lysed with Ammonium-Chloride-Potassium buffer (ACK buffer: 0.15 M NH_4Cl, 0.01 M $KHCO_3$, 0.1 mM EDTA, pH 7.25) for 2 min at RT, washed once, and resuspended in FACS buffer or complete RPMI (RPMI + 10 % FCS, 1 % Pen Strep (Gibco), 1 % L-Glutamine (Sigma), 1 % non-essential amino acids (Sigma), 1 % sodium pyruvate (Sigma), 0.05 mM ß-Mercaptoethanol (Gibco)) depending on further analysis.

2.8.2 Intestines

Colon was cut at Cecum and Rectum, all fat was removed, and the colon was flushed with ice-cold Gut wash solution (HBSS wo Ca/Mg (Gibco), 5 mM EDTA, 5 % FCS, 10 mM HEPES (Gibco)). The colon was placed in ice-cold PBS, cut open, and the remaining feces and mucus were removed by gently wiping the tissue. Colon was cut into 1 cm pieces, placed in 20 ml Gut wash solution containing 1 mM DTT, and incubated for 30 min at 37 °C while shaking. After 15-sec vortexing, colon pieces are transferred into fresh Gut Wash containing 1 mM DTT and incubated for 30 min, 37 °C, while shaking, followed by 15-sec vortexing. After DTT incubation, colon pieces are transferred into 20 ml Gut digestion solution (HBSS with Ca/Mg (Gibco), 5% FCS, 10mM HEPES) and washed for 15 min, rolling at 4 °C. Colon pieces are minced and digested in 3 ml Gut digestion solution with 400 U/ml CollagenaseIV and 0.4 mg/ml DNaseI for 30 min shaking at 37 °C. Cells and remaining tissue were meshed through a 100 µm strainer and washed once with Gut medium (RPMI + 10 % FCS, 1 % Pen Strep, 1 % L-Glutamine, 10 mM HEPES, 0.05 mM ß-Mercaptoethanol). Leukocytes were enriched over 70 % – 37 % – 30% Gradient, prepared from isotonic percoll solution (90% Percoll (Sigma), 10% 10x PBS (Gibco)).

Table 5 Preparation of Percoll solutions

Percoll dilution	Isotonic Percoll	Additive
70 %	28.0	12.0 HBSS (Sigma)
37 %	14.8	25.2 PBS
30 %	6.0	14.0 HBSS

Interphase between 70 % and 37 % was collected and washed once with Gut Medium and resuspended in FACS buffer or complete RPMI, depending on further analysis.

SI was cut at the stomach and cecum. After fat removal and flushing with the Gut wash, the small intestine was placed in ice-cold Gut Wash, Peyer's Patches were removed, and the intestine was cut open. SI was transferred to ice-cold PBS and treated in the following steps, likewise the colon. Due to the different organ structures, one DTT incubation is enough for the small intestine.

2.9 Ex vivo cytokine production of intestinal cells

To assess the cytokine production of T cells, leukocytes were isolated from the respective tissue as previously described. 1-2x10^6 leukocytes from lymphoid tissues were seeded in a 96-V bottom plate and restimulated with 10 ng/ml PMA (Calbiochem) and 1 µg/ml Ionomycin (Sigma-Aldrich) for a total of 4 hours. Half of the leukocytes isolated from the SI LP and total leukocytes isolated from CO LP were used for restimulation with 100 ng/ml PMA (Calbiochem) and 1 µg/ml Ionomycin (Sigma-Aldrich) for a total of 4 hours. For lymphoid tissue and LP-derived leukocytes, brefeldin A (5 µg/ml, Biolegend) was added after the first 2 hours of stimulation. Cytokines were detected by intracellular staining.

2.10 Flow Cytometry

Before surface staining, cells were incubated with Fc Block (anti-mouse purified CD16/32, 1:300 in FACS Buffer) for 10min at 4°C. Surface staining was performed in 100 µl for 20 min at 4 °C. Cells were washed twice with FACS buffer and resuspended in FACS buffer for direct analysis. Live/Dead staining was done by adding 0.25 µg DAPI (Sigma) 1 min before acquisition or for Zombie dyes (BioLegend) before Fc-Block. Therefore, cells were washed twice with PBS, resuspended in 100 µl PBs containing the respective Zombie dye (ZombieUV 1:500, Aqua Zombie 1:1000), and incubated for 15 min at 4 °C. Alternative Fixable Viability Dye efluor™ 780 (Thermo Fisher Scientific, 1:1000) was added with surface antibody master mix.

For the measurement of mitochondrial membrane potential, surface-stained cells were resuspended in Gut medium and incubated for 30 min, 37 °C, 5% CO_2 in the presence of 10 nM MitoProbe™ TMRM (Thermo Scientific™). Cells were washed once with FACS buffer and then directly acquired.

For intracellular and intranuclear staining, cells were first stained for surface epitopes and incubated with fixable live dead dyes. After the washing steps, the ebioscience Intracellular kit (Invitrogen) or ebioscience Foxp3 transcription factor staining kit (Invitrogen) was used according to the manufacturer's instructions. A general fixation with 2% paraformaldehyde for 15min at RT was performed after surface staining to preserve stained cells for up to 3 days.

Data was collected on an LSR Fortessa (BD Bioscience) or a Cytek® Aurora. Datasets were further analyzed in FlowJo™ 10 (Tree Stra, Inc.), and R. Aria III Fusion (BD Biosciences) or an Aria IIIu was used for cell sorting. CountBrightTM Absolute counting Beads (Thermo Fisher Scientific) were used for total cell quantification.

2.11 In vitro stimulation of cDCs

In vitro, cytokine-production splenocytes were isolated, as described before. After RBC lysis, the resulting pellet was resuspended in 90 µl MACS Buffer without sodium azide and 20 µl CD11c Microbeads (Miltenyi Biotech), incubated for 10 min at 4 °C in the dark. Cells were washed once with MACS buffer, followed by magnetic enrichment via LS columns according to the manufacturer's instructions. To increase the purity of CD11c cells, enrichment was performed over 2 consecutive columns.

10^5 CD11c enriched splenocytes were seeded per 96-well and stimulated overnight in 100 µl of complete RPMI substituted with the respective adjuvant.

Table 6 PRR Antagonist used for cDC stimulation.

Adjuvant	Company	Final concentration
Zymosan	Sigma	100 – 0.1 µg/ml
cPG (ODN 1826)	Invivogen	500 ng/ml
R848 (Resiquimod)	Sigma	2 µg/ml
LPS	Sigma	100 ng/ml

2.12 Real-Time PCR (qPCR)

Cells for Real-Time PCR were sorted directly in Extraction Butter using Aria Fusion (BD Biosciences). PicoPure™ RNA Isolation Kit (Thermo Fisher Scientific) was used to extract total RNA from the sorted cells according to the manufacturer's instructions. The quantity and quality of the isolated RNA were determined with the Nanodrop 2000

(Thermo Scientific). Next, cDNA was generated using the SuperScript™ III Reverse Transcriptase (Invitrogen) according to the manufacturer's instructions. Due to low amounts of isolated RNA, an optional supplementation of the reaction with RNaseOUTTM Recombinant RNase Inhibitor (Invitrogen) was performed.

PowerUP™ Syber™ Green Master Mix (Applied Biosystems) was used to perform the real-time PCR according to the manufacturer's instruction with a total reaction volume of 10 µl. 1 µl of transcript cDNA was used as input, and the final concentration for all primers was 500 nM. All primers were obtained from Sigma.

Table 7 Real-time PCR Primer pairs

Target gene	Primer	Sequence (5' -> 3')	Tm [°C]	Amplicon size
Polr2l	fwd	GGGAAGATCGTCGGCAACAAA	62.9	165
	rev	TAGGGGTGCATAGTTCAGCAG	61.3	
Cox7c	fwd	ATGTTGGGCCAGAGTATCCG	61.4	145
	rev	ACCCAGATCCAAAGTACACGG	61.5	
Cox6c	fwd	GCGTCTGCGGGTTCATATTG	61.5	102
	rev	TCTGCATACGCCTTCTTTCTTG	60.6	
Atp5e	fwd	CAGGCTGGACTCAGCTACATC	61.9	84
	rev	GTTCGCTTTGAACTCGGTCTT	60.8	
Atp5k	fwd	GTTCAGGTCTCTCCACTCATCA	60.8	95
	rev	CGGGGTTTTAGGTAACTGTAGC	60.4	
Ndufa3	fwd	ATGGCCGGGAGAATCTCTG	60.8	112
	rev	AGGGGCTAATCATGGGCATAAT	61.1	
Ndufa2	fwd	TTGCGTGAGATTCGCGTTCA	62.7	127
	rev	ATTCGCGGATCAGAATGGGC	62.7	
ß-Actin	fwd	GTT TGA GAC CTT CAA CAC CCC	57.3	318
	rev	GTG GCC ATC TCC TGC TCG AAG TC	57.3	

Real-time PCR runs were performed in the StepOnePlus Real Time PCR System (Applied Biosystems) and analyzed in the StepOne Software version 2.3.

Table 8 Real-time PCR Program

95 °C	20 sec	
95 °C	3 sec	40 cycles
60 °C	30 sec	
95 °C	15 sec	
60 °C	1 min	
95 °C	15 sec	+ 0.3°C / sec

2.13 Clean-up of genomic DNA

Cells were sorted directly in Wizard® SV Lysis buffer using Aria Fusion (BD Biosciences). Further extraction of the genomic DNA was performed with the Wizard® SV Genomic DNA Purification System according to manufactures instructions for isolation of genomic DNA from cells using a microcentrifuge.

2.14 Digital droplet PCR analysis

Bcl10 in different immune cells was quantified by a probe-based approach on the QX200 ddPCR system with automatic droplet generation (Bio-Rad Laboratories) by our collaborators in the lab of Prod J Ruland at the TranslaTUM. Reactions were run in duplicate (Bcl10WT/GT_cBCL10_del) or single (Cre/Tert) wells in a total reaction volume of 21 µl using the ddPCR Supermix for Probes (no UTP, Bio-Rad Laboratories). 10 ng of gDNA was used as an input for each reaction. An in-PCR-digestion was performed with MseI for Bcl10WT/GT_cBCL10_del and with BbsI for Cre/Tert reactions.

Table 9 Bcl10 assay Primers and ZEN™ double-quenched hydrolysis probes (IDT)

Target	**Type**	**Sequence 5' → 3'**
GT_cBCL10	del.for2	GAT TGC CAC AAG TTC AAG GC
GT_cBCL10	del.rev2	ACT GCT CTT CAG TTG TTG GT
GT_cBCL10	del.probe2	/56-FAM/TC CCA GGT C/ZEN/A GCC TGG TCT GTG GA/3IABkFQ/
Bcl10WT	for2	GCT CCT CTC TCA CTT GCA TC
Bcl10WT	rev2	GCA CCT AGA GAG GTT GTT GG
Bcl10WT	probe2	/5HEX/AG CCC TTT G/ZEN/C AGC CGG AGC CA/3IABkFQ/
BCL10WT	for3	GCT CCT CTC TCA CTT GCA TC
BCL10WT	rev3	GCA CCT AGA GAG GTT GTT GG
BCL10WT	probe3	/5HEX/AG CCC TTT G/ZEN/C AGC CGG AGC CA/3IABkFQ/

Final concentration of probes was 250 nM and primers were used at 900 nM. The gDNA samples derived from mice with known Bcl10/Cre genotypes were used as positive and negative controls, respectively. TaqMan ready-to-use 20x assays for Cre (Assay ID Mr00635245_cn) and Tert were purchased from ThermoFisher Scientific. The ddPCR data was analyzed using QuantaSoft Version 1.7.4.0917 using the auto-analyze function with manual correction and subsequently exported into a CSV file.

Table 10 PCR Program for the ddPCR

95 °C	5 min	
94 °C	30 sec	40 cycles
60 °C	1 min	
98 °C	10 min	
4 °C	hold	

2.15 In vitro T cell proliferation (CD4 and CD8)

DCs were sorted from colon LP Leukocytes as CD45.2$^+$ live, single, MHCII$^+$CD11c$^+$ cells, subdivided into the subsets by their expression of CD103 and CD11b. Sorted cells were transferred to V bottom 96-plate, resuspended in complete RPMI, serially diluted, and co-cultured with naïve CTV-labelled OT-I or OT-II cells at the indicated ratios in the presence of 20 µg/mL Ovalbumin (Hyglos).

For OT-I and OT-II naïve T cell isolation spleen was meshed through a 70 µm strainer and washed once with FACS buffer without sodium azide. For enrichment, the MojoSort™ Mouse CD8 Naive T Cell Isolation Kit (BioLegend) or MojoSort™ Mouse CD4 Naive T Cell Isolation Kit (BioLegend) was used according to the manufacturer's instructions.

For CTV (Thermo Fisher Scientific) labeling, enriched naïve T cells were resuspended at 20x10^6 cells/ml. The same volume of CTV working solution was added to a final concentration of 5 mM. Labeling occurred for 20 min at 37 °C in the dark and was stopped by adding pre-warmed PBS. Cells were washed once with PBS and resuspended in pre-warmed complete RPMI. CTV labelled naïve, transgenic T cells were analyzed for purity by Flow Cytometry prior to use. (Representative Purity checks: Figure 5 & Figure 6)

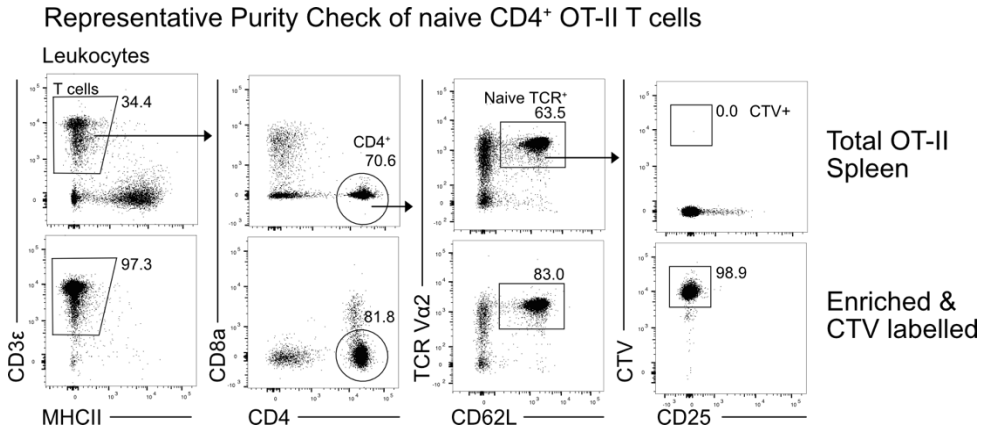

Figure 5 Purity check of enriched naïve CD4 T cells from OT-II spleen.
Representative purity check of naïve CD4 T cells isolated and enriched from OT-II spleen. T cells were identified as CD3ε positive (pre-gated on live Leukocytes). Next, CD4$^+$ T cells were gated and identified as naïve by the expression of CD62L. And the expression of the transgenic TCR Vα2 was confirmed. Last, even labeling with CTV was checked.

For Treg polarizing conditions, the cultures were supplemented with 5 ng/mL recombinant TGFβ, 10 µg/mL anti-IL-4, and 10µg/mL anti-IFN-γ (all Biolegend). For stimulation of the DCs, depleted Zymosan (Ivivogen) or Zymosan (Sigma) were added with or without 5 ng/ml TGFβ.

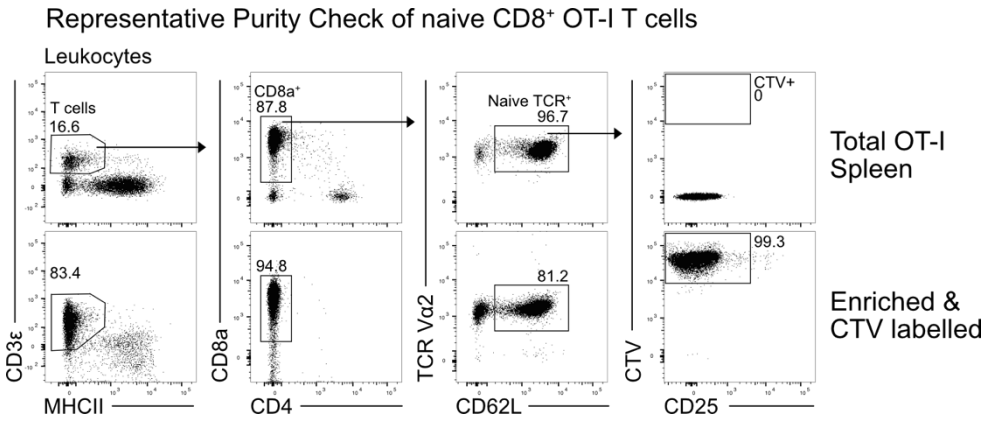

Figure 6 Purity check of enriched naïve CD8 T cells from OT-I spleen.
Representative purity check of naïve CD8 T cells isolated and enriched from OT-I spleen. T cells were identified as CD3ε positive (pre-gated on live Leukocytes). Next, CD8a$^+$ T cells were gated and identified as naïve by the expression of CD62L. And the expression of the transgenic TCR Vα2 was confirmed. Last, even labeling with CTV was checked.

Cultures were collected after 2.5 days for CD8 T cell assay and 3.5 days for CD4 T cell assays. Supernatants were collected for analysis of secreted cytokines by LEGENDplexTM Mouse Th Cytokine Panel according to the manufacturer's instructions. For intracellular cytokine detection, cells were restimulated with 10 ng/ml PMA (Calbiochem) and 1 µg/ml Ionomycin (Sigma-Aldrich) for a total of 5 hours. After the first 2 hours, brefeldin A (5 µg/ml, Biolegend) was added. Cytokines and transcription factors were detected by intracellular/intranuclear staining.

2.16 scRNA sequencing using 10x Genomics technique and Seurat algorithm

Leukocytes from the desired tissue were isolated as previously described and sorted according to the depicted gating strategy. For single sequencing of cells from steady-state mice, genotypes were run in separate reactions.

Table 11 Overview of generated single-cell sequencing Datasets. *Mice per Genotype

Sequencing Dataset	Genotypes	Mice*	Organ	Cell Type
C9A_BCL10_SS_DC	*Clec9a*$^{+/+}$*Bcl10*^{flox} *Clec9a*$^{cre/+}$*Bcl10*^{flox}	4	CO LP	MHCII$^+$CD11c$^+$
C9A_BCL10_SS_CD90	*Clec9a*$^{+/+}$*Bcl10*^{flox} *Clec9a*$^{cre/+}$*Bcl10*^{flox}	4	CO LP	CD90.2$^+$
C9A_SYK_SS_DC_CD90	*Clec9a*$^{+/+}$*Syk*^{flox} *Clec9a*$^{cre/+}$*Syk*^{flox}	2	SI LP	CD90.2$^+$ & cDCs
C9A_BCL10_AOMDSS_DC	*Clec9a*$^{+/+}$*Bcl10*^{flox} *Clec9a*$^{cre/+}$*Bcl10*^{flox}	4	Colonic Tumors	cDCs
C9A_BCL10_AOMDSS_CD90	*Clec9a*$^{+/+}$*Bcl10*^{flox} *Clec9a*$^{cre/+}$*Bcl10*^{flox}	4	Colonic Tumors	CD90.2$^+$

For single sequencing of leukocytes sorted from colonic tumors, cells originating from *Clec9a*$^{+/+}$*Bcl10*^{flox} or *Clec9a*$^{cre/+}$*Bcl10*^{flox} mice were stained with TotalSeq™-B0305 or TotalSeq™-B0310 (both BioLegend), respectively, during normal surface staining. After sorting CD90.2^{+} and cDCs of both genotypes were combined in equal ratios, respectively. To increase cell yield, two reactions were performed per cell type.

Cells were sorted into gut medium, counted, pelleted, and resuspended at 1x10^{3} cells/µL in PBS containing 0.04% BSA and loaded onto the Chromium Controller (10X Genomics). Samples were processed for single-cell encapsulation and cDNA library generation using the Chromium Single Cell 3' v3 Reagent Kits (10X Genomics) or the Chromium Next GEM Single Cell 3' Kit v3.1 combined with the 3' Feature Barcode Kit (10X Genomics). The constructed libraries were sequenced on an Illumina HiSeq2500 (Rapid Run) sequencer with 28 (read 1) + 91(read 2) base pair paired-end reads and a sequencing depth of 200 – 250 million reads per library. Sequencing data were processed using 10X Genomics Cell Ranger v6.0.0 pipeline. Sequencing reads were mapped to the mouse genome (mm10) using STAR {Dobin:2012ts} after spiking in the sequences of iCRE (GenBank iD: AY056050.1). Default parameters were selected for the Cell Ranger's count pipeline. The Cell Ranger's count pipeline gene matrix output was used as input for the Cell Ranger Aggregate pipeline. The latter was used to combine the samples of the different genotypes for the sequencing data from steady-state mice. And the multiple reactions of cells sorted from colonic tumors were combined with this pipeline.

Table 12 Gene matrix results after Cell Ranger Pipeline.

Sequencing Dataset	Number cells	Normalized Reads / Cell	Median Genes / Cell	Median UMI Counts / Cell
C9A_BCL10_SS_DC	9512	49520	2654	9371
C9A_BCL10_SS_CD90	8671	40019	1428	3728
C9A_SYK_SS_DC_CD90	19128	25205	1552	3288
C9A_BCL10_AOMDSS_DC	11796	26779	1081	2564
C9A_BCL10_AOMDSS_CD90	18696	74496	1898	5350

The respective matrixes were further analyzed with the R (Version 4.1.0) software package Seurat (Version 4) (Stuart et al. 2019, Hao et al. 2021). During quality control, cells expressing less than 200 genes or having more than 7.5% of mitochondrial genes and genes were removed from the dataset. Cells expressing both barcodes or no barcode were excluded from further analysis for datasets, including the barcode technology.
Further, cell cycle regression was performed to score cells according to their cell cycle and regressed differences between G2M and S phases. Datasets were normalized and

scaled using the SCTransform package (Hafemeister and Satija 2019). Determined variable features of the dataset were used for principal component (PC) analysis. Depending on the datasets, genes associated with the top 25 – 35 PCs were used for subsequent graph-based cluster identification with different resolutions and Uniform Manifold Approximation and Projection (UMAP) for dimensionality reduction. The Seurat package included FindAllMarkers and FindMarkers commands used to define cluster-specific markers and identify differentially expressed genes between the genotypes.

2.17 Statistical Analysis

The statistical significance was calculated using a two-tailed t-test in Prism 8 software (GraphPad). A p-value < 0.05 was considered significant.

2.18 Table of Antibodies

Antigen	Clone	Fluorochrome	Company
CD3ε	145-2C11	BV421, PE, PE/Cy5	BioLegend
CD4	RM4-5	PB, BUV395	BioLegend
CD4	GK1.5	APC, BUV737	BioLegend
CD8a	53-6.7	BV605, FITC	BioLegend
CD11b	M1/70	BV421, AF647, AF700, BUV737	BioLegend
CD11c	N418	BV421, BV785, PE, PB	BioLegend
CD16/CD32	2.4G2	purified	BD Biosciences
CD19	6D5	BV650, FITC, PE/Cy5	BioLegend
CD24	M1/69	FITC, BUV395	BioLegend
CD25	PC61	BV785	BioLegend
CD40	3/23	PE	BioLegend
CD44	IM7	APC/Cy7, BV650, PB	BioLegend
CD45.2	104	PB, FITC, PE/Cy7, PE/Dazzle594, BUV395	BioLegend
CD62L	MEL-14	PE/Cy7	Tonbo Bioscience
CD64 (FcɤRI)	X54-5/7.1	PE, PE/Cy7, APC	BioLegend
CD69	H1.2F3	PerCP/Cy5.5	BioLegend
CD80	16-10A1	FITC	BioLegend
CD86	GL-1	BV605	BioLegend
CD90.1	OX-7	AF700	BioLegend
CD90.2	30-H12	AF700, PE/Cy7	BioLegend
CD103	M290	BUV395	BD Biosciences
CD103	2E7	PE, BV605	BioLegend
CD152 (CTLA4)	UC10-4B9	PE/Cy7	ebioscience
CD161c (NK-1.1)	PK136	PE/Cy5, BV711	BioLegend
SiglecF	E50-2440	PerCP/Cy5.5	BD Bioscience
CD172a (SIRPα)	P84	PE/Cy7, PerCP/eFluor710	BioLegend
CD274 (PD-L1)	10F.9G2	BV421	BioLegend

CD274 (PD-L1)	MIH5	BUV737	ebioscience
CD279 (PD-1)	J43	BUV805	ebioscience
CD279 (PD-1)	29F.1A12	BV421	BioLegend
CD369 (Dectin-1)	bg1fpj	PerCP/eFluor710	ebioscience
CD369 (Dectin-1)		self-cojugated with PE	
F4/80	BM8	AF647	BioLegend
I-A/I-E (MHCII)	M5/114.15.2	APC/Cy7, AF700	BioLegend
MHC class I	28-8-6	FITC	BioLegend
Ly-6C	HK1.5	BV605, PB, FITC	BioLegend
LY-6G	1A8	FITC, PerCP/Cy5.5	BioLegend
V-alpha2 TCR	B20.1	FITC, BUV395	BD Biosciences
TCR γδ	GL3	BUV737	BD Biosciences
TCR ß chain	H57-597	BV785	BioLegend
XCR1	ZET	BV421, AF647, BV650	BioLegend
FOXp3	150D	AF647	BioLegend
FOXp3	FJK-16s	PE	ebioscience
IFN-γ	XMG1.2	APC, BV650	BioLegend
IL-10	JES5-16E3	PE	BioLegend
IL-17F	9D3.1C8	AF647	BioLegend
IL-17A	TC11-18H10.1	FITC	BioLegend
IL-22	Poly5164	PE	BioLegend
IL-22	1H8PWSR	PerCP/eFluor710	ebioscience
KI-67	SolA15	PerCP/eFluor710, PE	ebioscience
Rorγt	Q31-378	BV421	BD
TNF-alpha	MP6-XT22	PE, PerCP/Cy5.5, PE/Cy7, FITC, APC/Cy7	BioLegend
SYK	5F5	PE	Biolegend
Perforin	S16009A	APC	BioLegend
Granzyme B	QA16A02	PE/Dazzle594	BioLegend
Mouse IgG1, κ	MOPC-21	PE, AF647	BioLegend
Rat IgG1, κ	RTK2071	PE/Cy7, FITC, PE, APC, PerCP/Cy5.5	BioLegend
Rat IgG2a, κ	eBR2a	PerCP/eFluor710	BioLegend
Rat IgG2a, κ	RTK2758	APC, PE	BioLegend

3. Results

3.1 Flow Cytometric profiling of *Clec9a^{cre}Bcl10^{flox}* mice under steady-state conditions

3.1.1 Flow cytometric profiling of BCL10 deficient cDCs

Clec9a^{cre} mice were crossed with a mouse bearing a floxed *Bcl10* allele to obtain cDC-specific deletion of BCL10. Overall, *Clec9a$^{cre/+}$Bcl10$^{fl/fl}$* mice appeared healthy. To assess if the deletion of BCL10 in cDCs impacts cDC development, cDCs were analyzed by flow cytometry in multiple organs of *Clec9a$^{cre/+}$Bcl10$^{fl/fl}$* and control mice. In the spleen, auto-fluorescent F4/80^{hi} red pulp macrophages (RPMs) were excluded before the identification of cDCs through their expression of CD11c and MHCII. CD172a and CD24 further segregated this population, whereby the CD172a^{+} fraction resembles cDC2, and within the CD24^{+} gate, XCR1^{+} cDC1s could be identified (Figure 7). Quantification of total cDCs, RPMs, and the cDC subsets in the spleen showed similar frequencies and cell counts for *Clec9a$^{cre/+}$Bcl10$^{fl/fl}$* mice compared to the control mice.

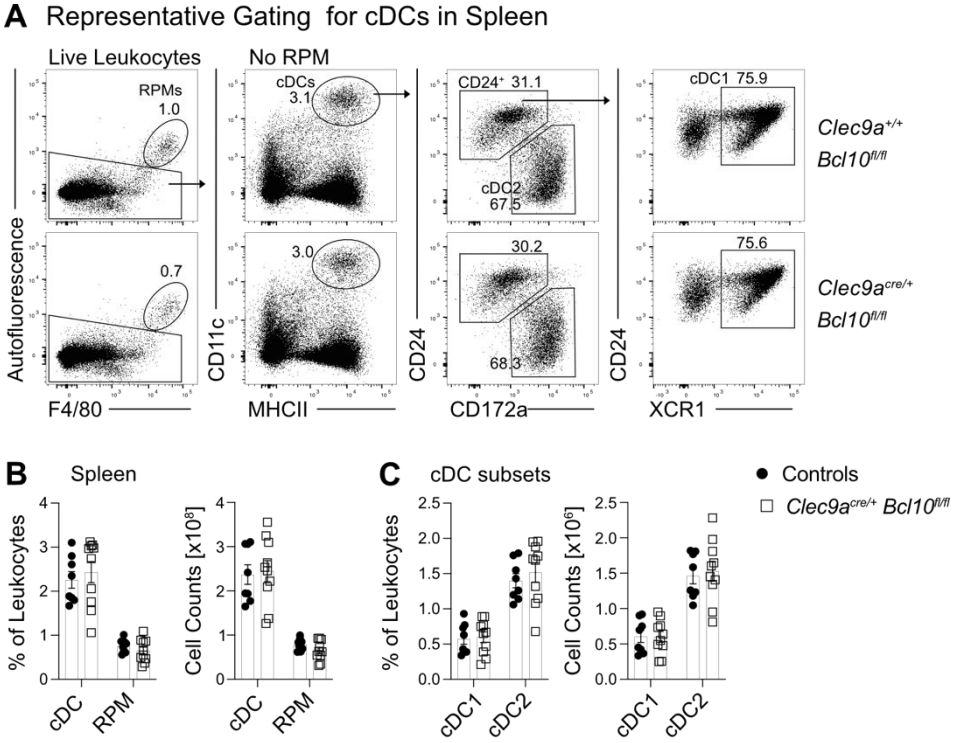

Figure 7 Quantification of cDCs in the Spleen of *Clec9a$^{cre/+}$Bcl10$^{fl/fl}$* mice.

A. Representative gating strategy of cDCs in the spleen from *Clec9a$^{+/+}$Bcl10$^{fl/fl}$* (top) and *Clec9a$^{cre/+}$Bcl10$^{fl/fl}$* (bottom) mouse. First, live leukocytes were gated, and auto-fluorescent F4/80^{hi} RPMs were excluded, and cDCs were gated as CD11c^{+} MHCII^{+}. Further, cDC2s were identified by CD172a, and cDC1s were gated in the CD24^{+} population as XCR1^{+}. **B.** Frequency and cell counts of cDCs, and RPMs and **C.** Frequency and cell counts of cDC1 and cDC2 in the spleen of *Clec9a$^{cre/+}$Bcl10$^{fl/fl}$* and control mice. Data from three independent experiments. Each dot represents one mouse. Bars indicate mean, and error bars indicate SEM. Statistical analyses were done by t-test.

In SI LP (Figure 8) leukocytes were identified and quantified as CD45.2$^+$ live cells. MHCII$^+$ were gated from CD19$^-$ cells, and Macrophages were separated from the cDCs by their expression of CD64. Within CD11c^{hi}CD64$^-$ cDCs, cDC1s (CD103$^+$CD11b$^-$), CD103 positive (DP) and CD103 negative (SP) cDC2 and double negative (DN DC) were gated. No difference in cell counts or frequency was observed for the indicated populations (Figure 8) between *Clec9a*$^{cre/+}$*Bcl10*$^{fl/fl}$ mice and their controls.

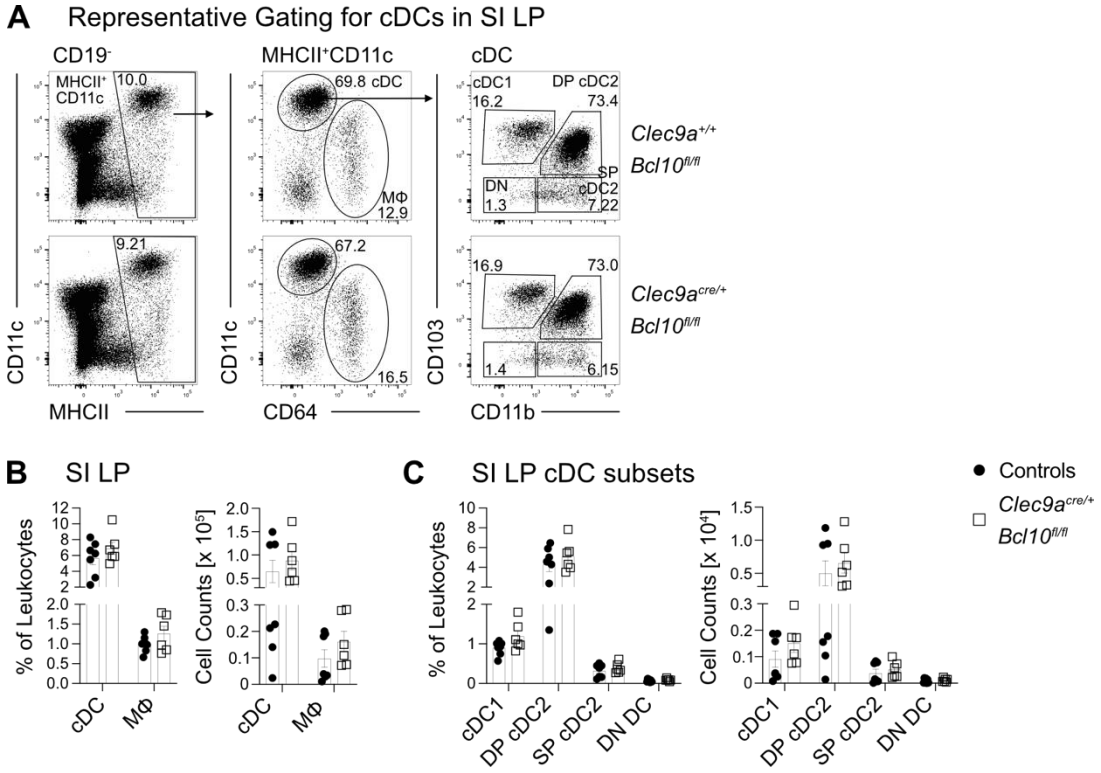

Figure 8 Occurrence of cDCs and Macrophages in the SI LP of *Clec9a*$^{cre/+}$*Bcl10*$^{fl/fl}$ mice.
A. Representative gating strategy of cDCs and macrophages in the SI LP from *Clec9a*$^{+/+}$*Bcl10*$^{fl/fl}$ (top) and *Clec9a*$^{cre/+}$*Bcl10*$^{fl/fl}$ (bottom) mouse. CD45.2$^+$, CD19 negative live leukocytes were gate and MHCII$^+$ cells were gated. Macrophages were separated from CD11c^{hi} cDCs by CD64. And cDCs were subdivided by their expression of CD103 and CD11b. **B.** Frequency and cell counts of cDCs, and Macrophages (MΦ) and **C.** Frequency and cell counts of cDC subsets in the SI LP of *Clec9a*$^{cre/+}$*Bcl10*$^{fl/fl}$ and control mice. Data from two independent experiments. Each dot represents one mouse. Bars indicate mean, and error bars indicate SEM. Statistical analyses were done by t-test.

In the PPs (Figure 9), MHCII$^+$CD11c^{hi} cells were designated as DCs, not cDCs, due to the lack of markers to exclude lysozyme expressing DCs derived from monocyte precursors. MHCII$^+$CD11c^{hi} were gated on CD45.2$^+$ leukocytes and subdivided through CD103 and CD11b into the four classical intestinal DC subsets. Frequency and total quantification of cell counts revealed no difference in total DC population nor in any subset upon BCL10 deletion in cDCs.

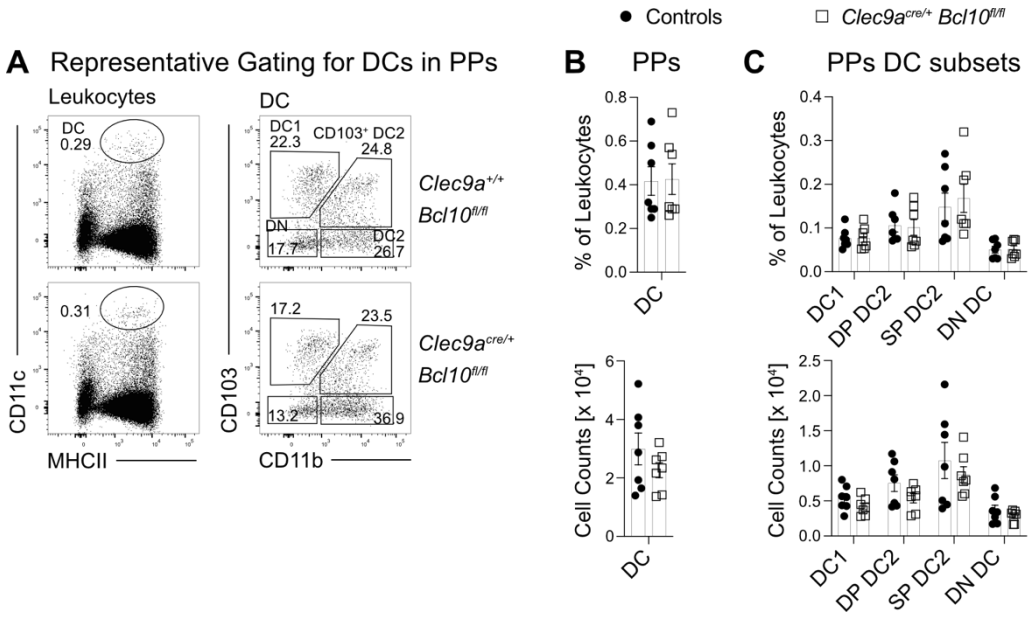

Figure 9 Identification and quantification of DCs in the PPs of *Clec9a$^{cre/+}$Bcl10$^{fl/fl}$* mice.
A. Representative gating strategy of DCs in the PPs from *Clec9a$^{+/+}$Bcl10$^{fl/fl}$* (top) and *Clec9a$^{cre/+}$Bcl10$^{fl/fl}$* (bottom) mouse. CD45.2^{+}, live cells were gated and MHCII^{+}CD11c^{hi} DCs were identified. DCs were subdivided into the four intestinal DC subsets by CD103 and CD11b. **B.** Frequency and cell counts of DCs, and **C.** Frequency and cell counts of DC subsets in the PPs of *Clec9a$^{cre/+}$Bcl10$^{fl/fl}$* and control mice. Data from two independent experiments. Each dot represents one mouse. Bars indicate mean, and error bars indicate SEM. Statistical analyses were done by t-test.

In parallel, the SI draining LN (SI LN) of *Clec9a$^{cre/+}$Bcl10$^{fl/fl}$* mice was analyzed for the distribution of the cDC subsets (Figure 10). T and B cells were excluded before cDC identification through gating on CD3ε^{-}CD19^{-} fraction. Migratory cDCs were separated from their resident counterparts by their increased expression level of MHCII and lower CD11c. Further, migratory cDCs were subdivided into CD103^{+}CD11b^{-} cDC1, CD103^{+}CD11b^{+} cDC2, CD103 negative counterparts, and the DN DC population. LN resident cDCs were separated into XCR1 expressing cDC1 and CD172a positive cDC2. Subsequent quantification of cell frequency and cell counts showed no difference in resident or migratory cDCs nor their respective subsets when BCL10 is deleted in cDCs.

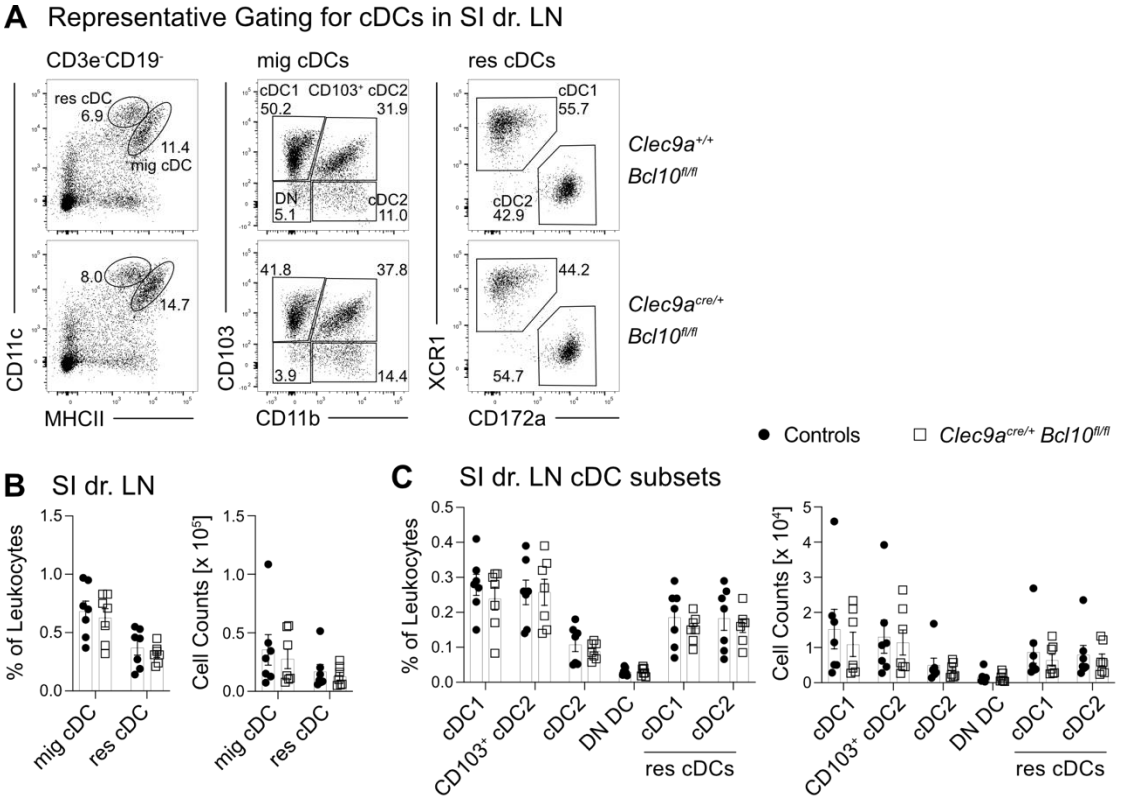

Figure 10 Quantification of resident and migratory cDCs in the SI LN of *Clec9a$^{cre/+}$Bcl10$^{fl/fl}$* mice.

A. Representative gating strategy of cDCs in the SI LN from *Clec9a$^{+/+}$Bcl10$^{fl/fl}$* (top) and *Clec9a$^{cre/+}$Bcl10$^{fl/fl}$* (bottom) mouse. Resident (res cDCs) and migratory (mig cDCs) cDCs were identified as CD11c^{hi}MHCII^{+} and CD11c^{+}MHCII^{hi}, respectively (Pre-gated on CD3ε^{-}CD19^{-} live leukocyte). Res cDCs were subdivided into cDC1 as XCR1^{+} and cDCs as CD172a^{+}. CD103 and CD11b segregated mig DCs into the four intestinal cDC subsets. **B.** Frequency and cell counts of res cDCs and mig cDCs and **C.** Frequency and cell counts of the respective cDC subsets in the SI LN of *Clec9a$^{cre/+}$Bcl10$^{fl/fl}$* and control mice. Data from two independent experiments. Each dot represents one mouse. Bars indicate mean, and error bars indicate SEM. Statistical analyses were done by t-test.

Next, CO LP leukocytes were identified, similar to the SI LP. MHCII^{+}CD11c^{+} were directly gated on CD45.2^{+} live cells, CD64^{+} Macrophages excluded, and the four intestinal cDC subsets were identified. As published, the overall frequency of APCs, including cDCs and Macrophages, decreased from SI LP (Figure 8) towards the colon (Figure 11). Further, as expected, the cDC compartment shifted towards cDC1s and CD103^{-} cDC2 dominated the cDC2s (Cerovic et al. 2014, Esterházy et al. 2019). Even though expected changes within the cDC compartment between SI LP and CO LP were found, no difference was observed between *Clec9a$^{cre/+}$Bcl10$^{fl/fl}$* mice and control mice regarding cell frequency and cell counts of total cDCs and macrophages or any cDC subset.

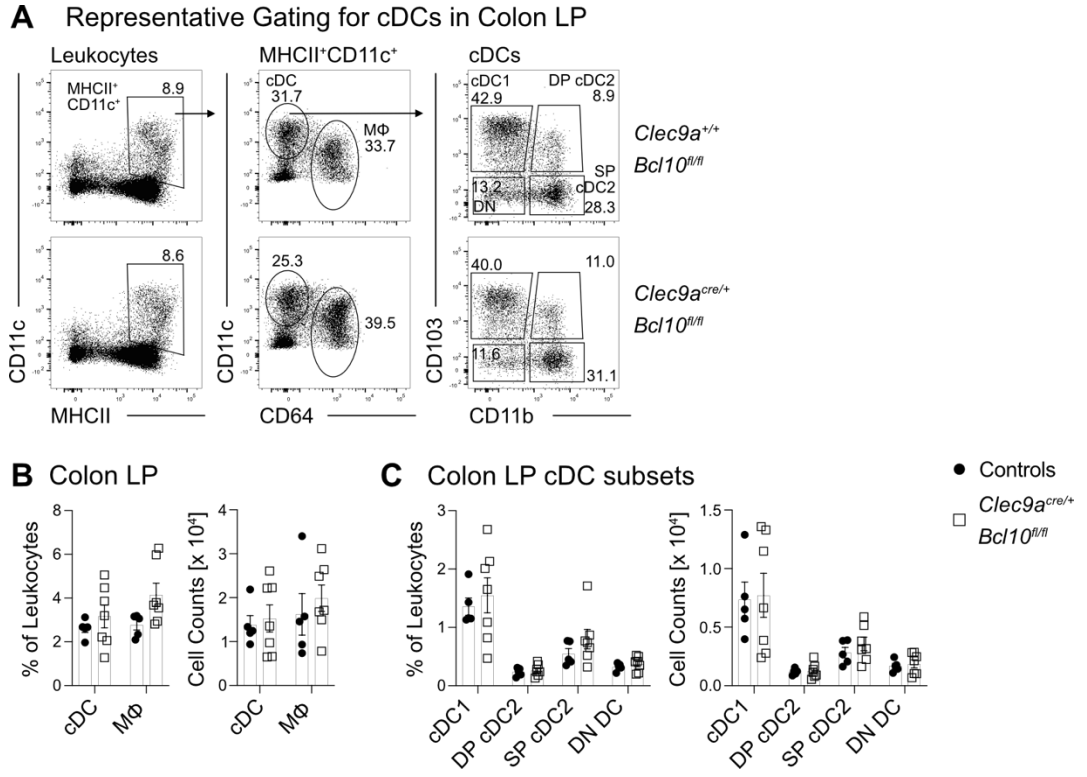

Figure 11 Quantification of cDCs and Macrophages in the CO LP of *Clec9a$^{cre/+}$Bcl10$^{fl/fl}$* mice. **A.** Representative gating strategy of cDCs and macrophages in the CO LP from *Clec9a$^{+/+}$Bcl10$^{fl/fl}$* (top) and *Clec9a$^{cre/+}$Bcl10$^{fl/fl}$* (bottom) mouse. CD45.2^{+}, live leukocytes were selected and MHCII^{+}CD11c^{+} cells were gated. Macrophages were separated from CD11c^{+} cDCs by CD64. And cDCs were subdivided by their expression of CD103 and CD11b. **B.** Frequency and cell counts of cDCs, and Macrophages (MΦ) and **C.** Frequency and cell counts of cDC subsets in the CO LP of *Clec9a$^{cre/+}$Bcl10$^{fl/fl}$* and control mice. Data from two independent experiments. Each dot represents one mouse. Bars indicate mean, and error bars indicate SEM. Statistical analyses was done by t-test.

In addition to CO LP, colon draining LN (CO LN) of *Clec9a$^{cre/+}$Bcl10$^{fl/fl}$* mice was dissected for cDC frequency and counts (Figure 12). As previously described, resident and migratory cDCs were separated based on their MHCII level and subdivided into cDC1 and cDC2 by XCR1 and CD172a or CD103 and CD11b. The analysis showed similar frequency and cell counts for total migratory and resident cDCs. However, migratory cDC1 subsets were significantly decreased in frequency but not in counts in the CO LN of *Clec9a$^{cre/+}$Bcl10$^{fl/fl}$* mice. A similar trend towards reduced frequency can be observed for the total population of migratory cDCs, presumably caused by the reduction of cDC1, the major subset within the migratory cDCs in the CO LN. No other differences were observed in the additional migratory cDC subsets, neither in resident cDC1 nor cDC2.

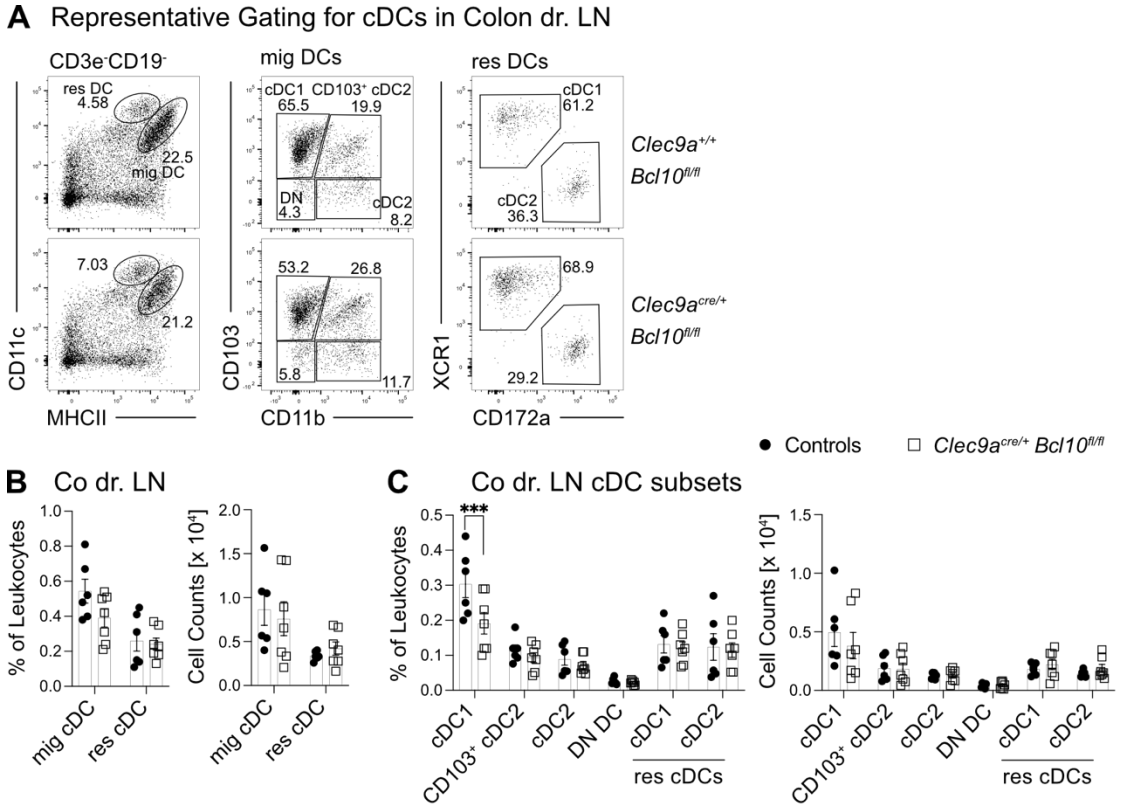

Figure 12 Distribution of resident and migratory cDCs in the CO LN of *Clec9a$^{cre/+}$Bcl10$^{fl/fl}$* mice.

A. Representative gating strategy of cDCs in the CO LN from *Clec9a$^{+/+}$Bcl10$^{fl/fl}$* (top) and *Clec9a$^{cre/+}$Bcl10$^{fl/fl}$* (bottom) mouse. Resident (res cDCs) and migratory (mig cDCs) cDCs were identified as CD11c^{hi}MHCII^{+} and CD11c^{+}MHCII^{hi}, respectively (Pre-gated on CD3ε^{-}CD19^{-} leukocyte). Res DCs were subdivided into cDC1 as XCR1^{+} and cDCs as CD172a^{+}. CD103 and CD11b segregated Mig DCs into the four intestinal cDC subsets. **B.** Frequency and cell counts of res cDCs and mig cDCs and **C.** Frequency and cell counts of the respective cDC subsets in the CO LN of *Clec9a$^{cre/+}$Bcl10$^{fl/fl}$* and control mice. Data from two independent experiments. Each dot represents one mouse. Bars indicate mean, and error bars indicate SEM. Statistical analyses was done by t-test. *** p-value < 0.001

In summary, the occurrence of total cDCs and the subdivision into organ-specific cDC1 and cDC2 subsets was not affected in the spleen and the intestinal tract when BCL10 was deleted in cDCs. However, within the CO LN, a significantly decreased frequency of migratory cDC1 was found.

3.1.2 Phenotypic profiling of the intestinal T cell compartment of *Clec9a$^{cre/+}$Bcl10$^{fl/fl}$* mice

The next step assessed the influence of BCL10 deletion in cDCs on intestinal T cell homeostasis. Therefore, the intestinal T cell compartment of *Clec9a$^{cre/+}$Bcl10$^{fl/fl}$* and control mice was investigated at steady state. T cells in the intestinal compartment were identified by expressing CD90.2 and CD3ε and subdivided into CD4 T cells, CD8 T cells,

and double-negative unconventional T cells (Figure 13). Whereas CD4 T cells were predominantly TCRαβ positive, a small fraction of CD8 T cells expressed TCRγδ. And unconventional T cells consisted of 50 % TCRαβ$^+$ and 50 % TCRγδ$^+$ cells (Data not shown).

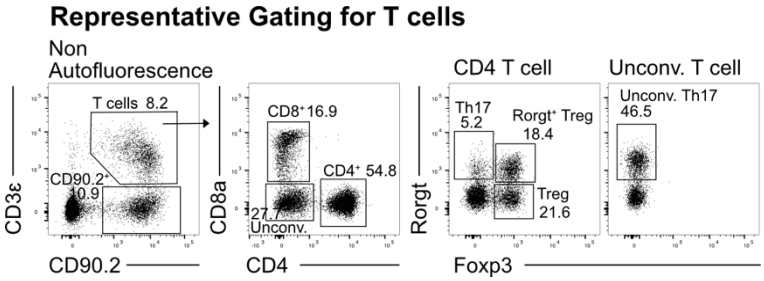

Figure 13 Gating strategy for intestinal T cells.
CD3ε$^+$ CD90.2$^+$ T cells were gated on non-autofluorescent CD45.2$^+$ leukocytes. T cells were subdivided into CD4, CD8, and double-negative unconventional (unconv.) T cells. CD4 T cells were segregated through Rorγt and Foxp3 into Th17, Rorγt$^+$ Tregs, and classical Tregs. In the double negative T cells, unconventional Th17 cells were identified as Rorγt-expressing cells.

Within the CD4 T cells, regulatory T cells (Tregs) were identified through their expression of Foxp3. In doing so, a gut specific Treg subset could be identified by the co-expression of Rorγt. Further, Rorγt single positive CD4 T cells were classified as Th17 cells. A similar Rorγt$^+$ population can be found within the CD4$^-$CD8$^-$ T cell population termed unconventional Th17 cells.

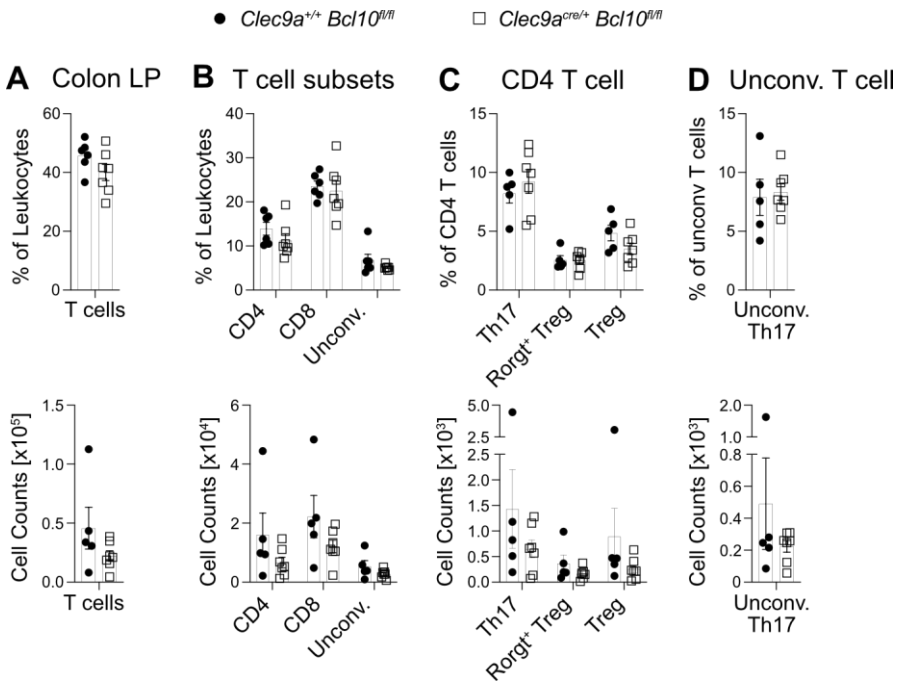

Figure 14 Equal quantification of T cells in the SI LP of *Clec9a$^{cre/+}$Bcl10$^{fl/fl}$* mice.
Frequency and cell count of **A.** Total T cells, **B.** CD4, CD8, and Unconv. T cell subsets, **C.** Th17, Rorγt$^+$ Treg and classical Treg, **D.** Unconv. Th17 cells. Data from two independent experiments. Each dot represents one mouse. Bars indicate mean, and error bars indicate SEM. Statistical analyses were done by t-test.

In the SI LP (Figure 14) of *Clec9a*$^{cre/+}$*Bcl10*$^{fl/fl}$ and control mice, similar frequencies and cell counts were found for the indicated T cell populations.

Further, cytokine production of CD4, CD8, and unconventional T cells was assessed for both genotypes after ex-vivo re-stimulation with PMA and Ionomycin (Figure 15).

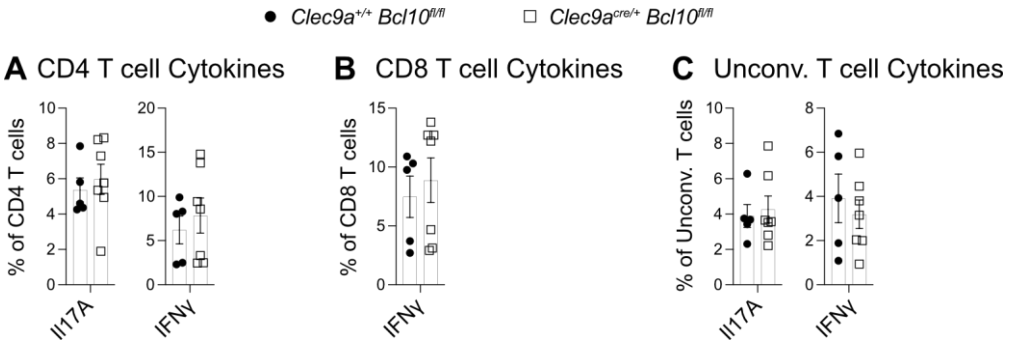

Figure 15 Equal cytokine production of SI LP T cells from *Clec9a*$^{cre/+}$*Bcl10*$^{fl/fl}$ mice.
Frequency of **A.** IL17A$^+$ and IFNγ$^+$ cells of CD4 T cells, **B.** IFNγ$^+$ cells of CD8 T cells, and **C.** IL17A$^+$ and IFNγ$^+$ cells of unconv. T cells after ex-vivo re-stimulation with PMA and Ionomycin. Data from two independent experiments. Each dot represents one mouse. Bars indicate mean, and error bars indicate SEM. Statistical analyses were done by t-test.

For CD4 T cells, similar frequencies of the Th17 cytokine IL-17A and Th1 characteristic cytokine IFNγ were detected in *Clec9a*$^{cre/+}$*Bcl10*$^{fl/fl}$ SI LP and their controls. Equal levels of IFNγ were measured in CD8 T cells from both groups. However, IFNγ levels spread between the two independent experiments. Also, cytokines secreted by unconventional T cells showed similar frequencies for *Clec9a*$^{cre/+}$*Bcl10*$^{fl/fl}$ and *Clec9a*$^{+/+}$*Bcl10*$^{fl/fl}$ mice. Taken together, the deletion of BCL10 in cDCs did not alter the T cell compartment in the SI LP.

Analysis of the T cells in the CO LP revealed similar frequencies and numbers for total T cells and the CD4, CD8, and DN subsets in *Clec9a*$^{cre/+}$*Bcl10*$^{fl/fl}$ mice compared to control mice (Figure 16). Further on, cDC-specific BCL10 deficient mice showed regular frequencies and numbers for classical and Rorγt$^+$ regulatory T cells. However, whereas the unconventional Th17 subset was detected in an equal frequency and cell count, *Clec9a*$^{cre/+}$*Bcl10*$^{fl/fl}$ mice showed a trend towards less CD4 Th17 cells.

Corresponding to the trend towards a decrease in Th17 cells, cytokine production of colonic CD4 T cells was significantly lower for IL-17A and IL-17F in *Clec9a*$^{cre/+}$*Bcl10*$^{fl/fl}$ mice (Figure 17). Additional cytokines (IL-10, IL-2, IFNγ, and TNFα) detected in CD4 T cells had a similar frequency in both groups. Further, no difference could be observed in the production of cytokines by CD8 and unconventional T cells in *Clec9a*$^{cre/+}$*Bcl10*$^{fl/fl}$ mice compared to control mice.

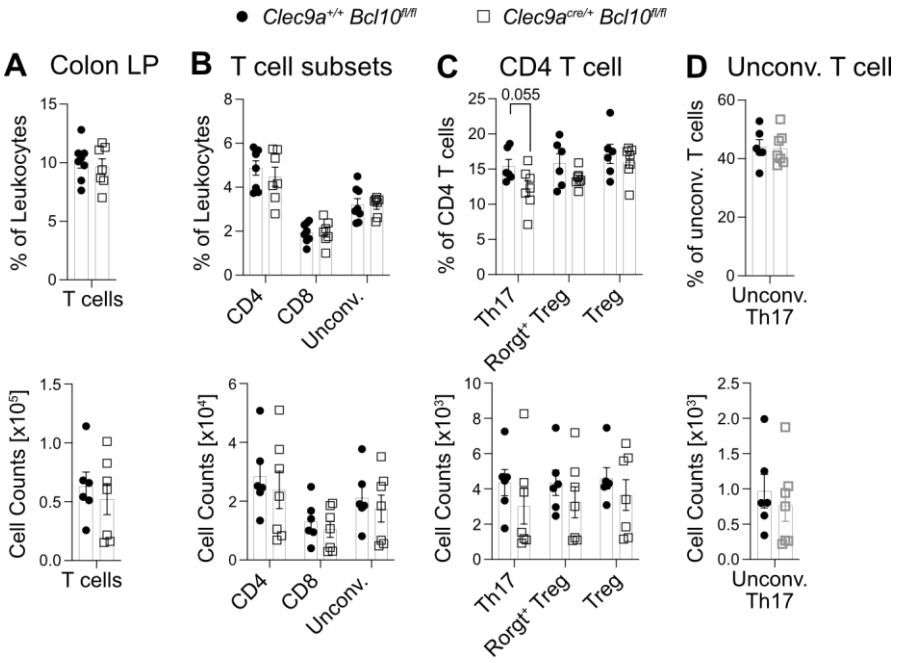

Figure 16 Equal quantification of T cells in the CO LP of *Clec9a$^{cre/+}$Bcl10$^{fl/fl}$* mice.
Frequency and cell numbers of **A.** Total T cells, **B.** CD4, CD8, and Unconv. T cell subsets, **C.** Th17, Rorγt^{+} Treg and classical Treg, **D.** Unconv. Th17 cells. Data from three independent experiments. Each dot represents one mouse. Bars indicate mean, and error bars indicate SEM. Statistical analyses were done by t-test.

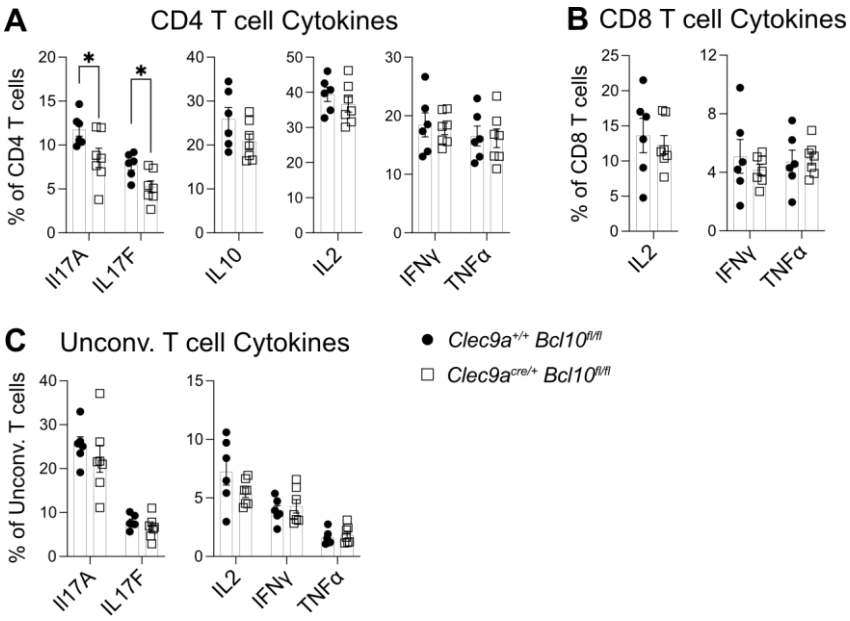

Figure 17 Decreased Th17 cytokines in the colon of *Clec9a$^{cre/+}$Bcl10$^{fl/fl}$* mice.
Cytokine production of CD4, CD8, and unconv. T cells after ex-vivo re-stimulation with PMA and Ionomycin. **A.** Frequency of IL17A^{+} and IL17F^{+}, IL10^{+}, IL2^{+}, IFNγ$^{+,}$ and TNFα^{+} cells of CD4 T cells, **B.** Frequency of IL2^{+}, IFNγ^{+} and TNFα^{+} cells of CD8 T cells, **C.** Frequency of IL17A^{+} and IL17F^{+}, IL2^{+}, IFNγ^{+} and TNFα^{+} cells of unconv. T cells. Data of 3 independent experiments. Each dot represents one mouse. Bars indicate mean, and error bars indicate SEM. Statistical analyses were done by t-test. * p-value < 0.05

Besides the analysis of T cell occurrence in the CO LP and their capacity to produce cytokines, the activation state of CD4, CD8, and unconventional T cells was determined (Figure 18). Effector T cells were identified by their CD44 expression and lack of CD62L. Memory T cells expressed CD44 and CD62L; naïve T cells were identified as CD62L positive and CD44 negative. Within the CD8 and unconventional T cell subsets, a small fraction of cells neither expressed CD44 nor CD62L. Comparison of the proportion of CD4 T cells, CD8 T cells, and unconventional T cells in these different activation states revealed no difference in T cell activation in *Clec9a*$^{cre/+}$*Bcl10*$^{fl/fl}$ mice and control mice.

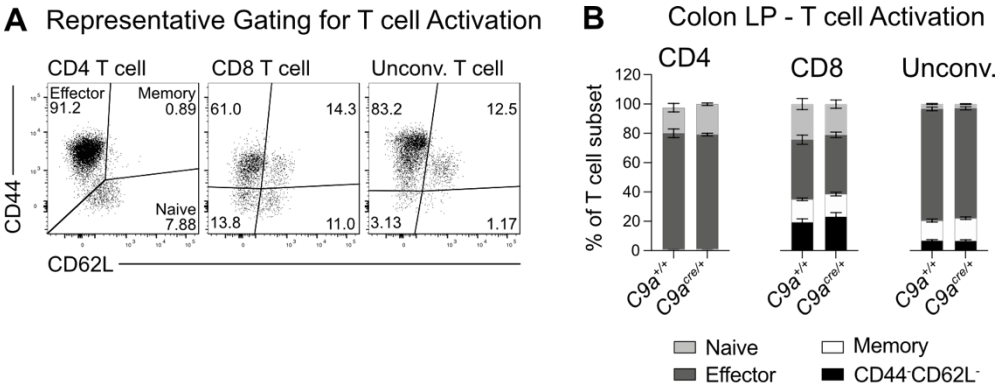

Figure 18 Similar activation of T cells in the CO LP of *Clec9a*$^{cre/+}$*Bcl10*$^{fl/fl}$ mice.
A. Representative gating strategy to identify effector (CD44$^+$), memory (CD44$^+$CD62L$^+$) and naïve (CD62L$^+$) T cells. For CD8 and unconv. T cells and an additional CD44$^-$CD62L$^-$ population was identified. **B.** Frequency of effector, memory, naïve, and CD44$^-$CD62L$^-$ T cells within CD4, CD8, and unconv. T cells, respectively. Data from three independent experiments. Bars indicate mean, and error bars indicate SEM (Control mice n = 6, *Clec9a*$^{cre/+}$*Bcl10*$^{fl/fl}$ n = 7). Statistical analyses were done by t-test.

Since cytokines secreted by cDCs can activate ILCs, NK cells, and IEL, which also contribute to intestinal homeostasis, colitis, and CAC pathology, the occurrence of those cell populations in the CO LP of *Clec9a*$^{cre/+}$*Bcl10*$^{fl/fl}$ was analyzed (Data not shown). This flow cytometric profiling revealed similar frequencies and cell numbers for the identified ILC1, ILC2, ILC3, lymphoid tissue inducer (LTi) cells, and NK cells in *Clec9a*$^{cre/+}$*Bcl10*$^{fl/fl}$ mice compared to their controls. Likewise, no differences were found in the IEL compartment of *Clec9a*$^{cre/+}$*Bcl10*$^{fl/fl}$ mice, neither for TCRαβ$^+$ or TCRγδ$^+$ IEL and their respective subsets.

In summary, deletion of BCL10 in cDCs has no effect on the proportion and activation of the primary T cell subsets in the CO LP, identified based on their expression of CD4 and CD8. Neither ILCs, NK cells, nor IEL showed any frequency or cell count alterations. Nonetheless, cDC-specific knockout of BCL10 altered the polarization of CD4 T cells, as *Clec9a*$^{cre/+}$*Bcl10*$^{fl/fl}$ mice showed decreased levels of Th17 cells and their characteristic cytokines.

3.2 Transcriptional profiling of intestinal cells from *Clec9a^{cre}Bcl10^{flox}* mice

The previous finding of an alteration in T cell polarization in the CO LP implicates a change in cDC function upon BCL10 deletion. To address the influence of BCL10 deletion on cDC function, a transcriptional profiling of cDCs from CO LP of *Clec9a$^{+/+}$Bcl10$^{fl/fl}$* and *Clec9a$^{cre/+}$Bcl10$^{fl/fl}$* mice was performed, utilizing a single-cell sequencing approach from 10x genomics.

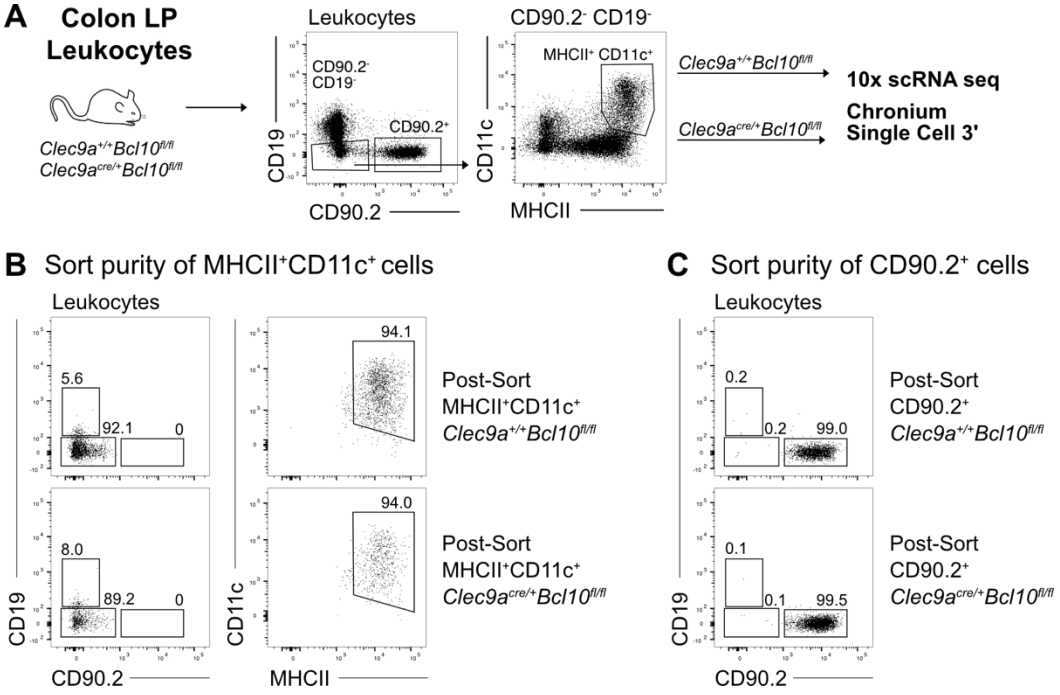

Figure 19 Workflow, sorting strategy, and sort purity of MHCII$^+$CD11c$^+$ cells and cD90.2$^+$ from CO LP for scRNA sequencing.

A. CO LP leukocytes were isolated from *Clec9a$^{+/+}$Bcl10$^{fl/fl}$* and *Clec9a$^{cre/+}$Bcl10$^{fl/fl}$* mice. CD90.2$^+$ cells were gated directly on CD45.2$^+$ live leukocytes. MHCII$^+$CD11c$^+$ cells were identified and sorted from CD19-CD90.2$^-$ gate. **B.** Purity check of MHCII$^+$CD11c$^+$ and **C.** Purity check of CD90.2$^+$ from CO LP of *Clec9a$^{+/+}$Bcl10$^{fl/fl}$* and *Clec9a$^{cre/+}$Bcl10$^{fl/fl}$* mice.

Therefore, MHCII$^+$CD11c$^+$ cells were sorted from four mice per genotype to achieve a sufficient number of cells (Figure 19). The sorted MHCII$^+$CD11c$^+$ population contained cDCs and macrophages. The latter was included as a control population since BCL10 should not be deleted in this cell type. In addition, CD90.2$^+$ cells were sorted from the CO LP of both groups to gain more insight into possible alterations within the T cell compartment. Both cell populations were processed in parallel, whereby cells of different genotypes were in separate reactions. Sequencing datasets of *Clec9a$^{+/+}$Bcl10$^{fl/fl}$* and *Clec9a$^{cre/+}$Bcl10$^{fl/fl}$* derived cDCs and CD90.2$^+$ cells were combined by cell type through the 10x genomics cell ranger aggregate platform.

3.2.1 Unbiased clustering of colonic DCs and macrophages

The combined dataset of sequenced MHCII^{+}CD11c^{+} cells from the CO LP of *Clec9a*$^{+/+}$*Bcl10*$^{fl/fl}$ and *Clec9a*$^{cre/+}$*Bcl10*$^{fl/fl}$ mice revealed 9492 cells with an average of 9372 reads and approximately 2500 detected genes per cell. UMAP approximation of the combined MHCII^{+}CD11c^{+} cells resulted in nine clusters (Figure 20). Expression of *Flt3l*, *Itgax,* and *Zbtb46* allowed the distinction of cDCs from macrophages (*Cxcr3*, *Mafb,* and *Cd63*) and a small fraction of monocytes (*Ccr2*). CDC1s were further identified through *Irf8*, *Xcr1,* and *Itgae*. Two cDC clusters shared the expression of *Irf4*, *Sirpa,* and *Itgam* and were separated through *Itage* into SP cDC2 and DP cDC2, respectively. A small cDC cluster was marked by a migratory signature (*Ccr7*, *Fscn1*, *Ccl22*) but lacked specific cDC1 or cDC2 markers and therefore was termed mig DCs. Small pDC (*Siglech*) and B cell (*Ly6c2*) contaminations were found and excluded from downstream analysis. Cell cycle regression identified the last cluster as highly proliferating cells.

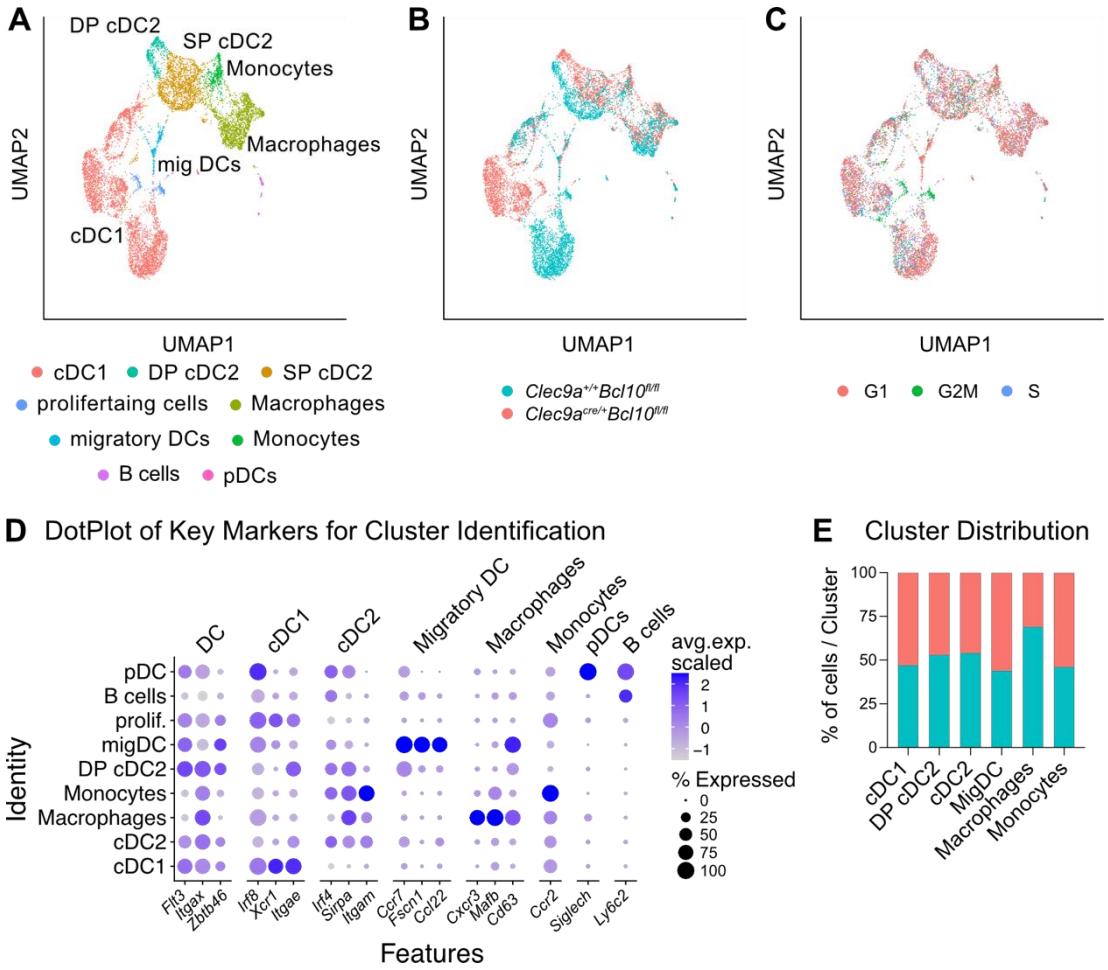

Figure 20 cDC1 from *Clec9a*$^{cre/+}$*Bcl10*$^{fl/fl}$ separate from their BCL10 sufficient counterparts. **A.** Unbiased clustering of colonic MHCII^{+}CD11c^{+} resulted in nine clusters. **B.** cDC clusters separate based on their genetic background. **C.** highly proliferating cells (G2M phase) form a separate cluster. **D.** Dot plot shows cluster identification based on cell-specific genes like transcription markers. **E.** Genotype distribution within every cDC, monocyte, and macrophage cluster.

Even though the distribution of cells derived from *Clec9a*$^{+/+}$*Bcl10*$^{fl/fl}$ and *Clec9a*$^{cre/+}$*Bcl10*$^{fl/fl}$ mice was equal within all clusters, the division of the clusters based on the genotype revealed a clear separation of the cDC1 cluster. This segregation was visible to a lesser extent in DP cDC2 and SP cDC2 clusters and was absent in monocyte and macrophage clusters. This separation of cDC clusters indicates a transcriptional difference within the cDC1s and cDC2 subsets from *Clec9a*$^{+/+}$*Bcl10*$^{fl/fl}$ and *Clec9a*$^{cre/+}$*Bcl10*$^{fl/fl}$ mice caused by the deletion of BCL10 in cDCs, but not monocytes and macrophages. That cDC1s show the most significant separation is expected, as they express *Clec9a* again in their differentiated state and, therefore, the Cre recombinase, both confirmed by the scRNA sequencing data (Figure 21). This Cre recombinase expression in the differentiated cDC1s presumably leads to a higher deletion of BCL10 compared to the deletion in cDC2 subsets. However, assessing the deletion of *Bcl10* in the scRNA dataset showed similar expression levels in cDC1, cDC2, and macrophage clusters separated by genotype. This can be explained as the sequencing occurs from the 5' end; transcripts of BCL10 could be detected even though floxed exon 2 was excised.

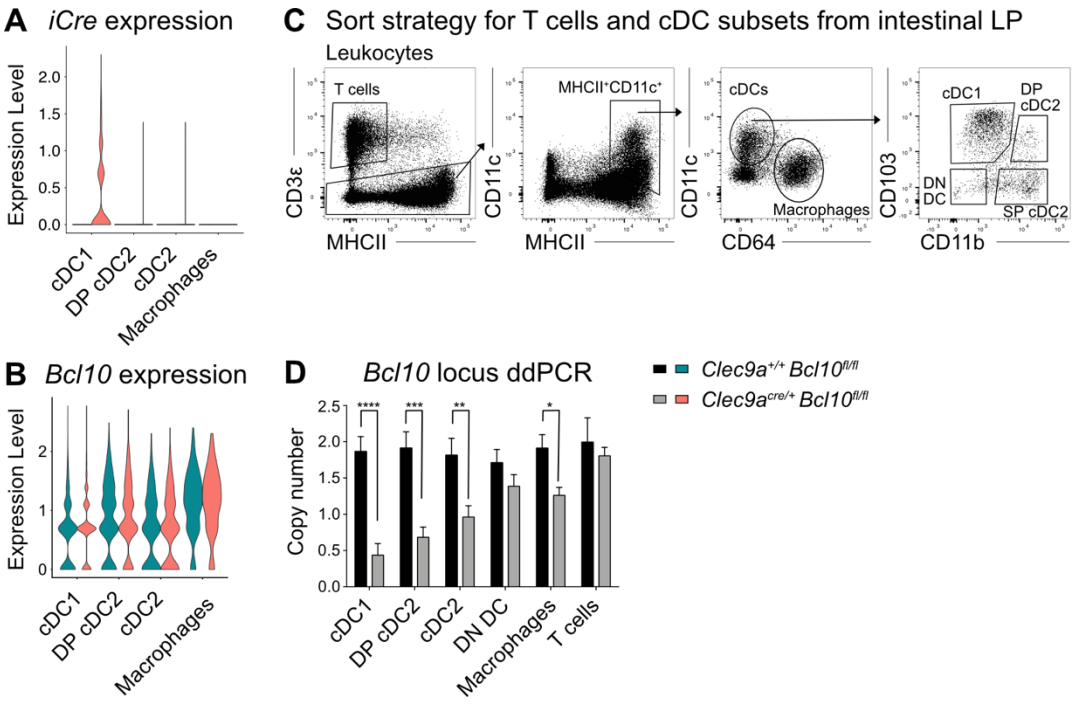

Figure 21 Colonic cDC1s have the highest Bcl10 deletion.

A. Transcriptional level of iCre in cDC subsets and macrophages. **B.** *Bcl10* expression in cDC subsets and macrophages. **C.** Representative gating strategy to sort T cells, macrophages, and the four cDC subsets in the intestinal LP for subsequent isolation of genomic DNA. **D.** Quantification of floxed Bcl10 locus in CO LP derived cDCs, macrophages, and T cells. (D) Data of 3 experiment; *Clec9a*$^{+/+}$*Bcl10*$^{fl/fl}$ n = 9, *Clec9a*$^{cre/+}$*Bcl10*$^{fl/fl}$ n = 8 (1 n = two pooled mice). Error bars indicate SEM. Statistical analyses were done by t-test. * p-value < 0.05, ** p-value < 0.01, *** p-value < 0.001, **** p-value < 0.0001

To analyze to what extent the floxed *Bcl10* allele is excised and if this correlates with the separation of the respective clusters, cDC subpopulations and macrophages were sorted from the intestinal LP, genomic DNA was extracted, and deletion efficiency of the floxed *Bcl10* allele was determined by digital droplet PCR. The ddPCR was performed by the collaborators' lab (Prof. Ruland's research group). In addition, T cells were sorted as a control population as they are not labeled in the *Clec9a*^{cre} Fate mapping models. As expected, the highest deletion rate was found in cDC1, followed by DP cDC2 and SP cDC2. No significant deletion of the floxed *Bcl10* locus was found in the DN DCs. However, macrophages showed a significant decrease in the copy number of floxed *Bcl10* locus, though the reduction was lower than in cDC subsets. Nonetheless, according to the sequencing data, this reduction did not lead to transcriptional alterations within this cell type. T cells from *Clec9a*$^{cre/+}$*Bcl10*$^{fl/fl}$ mice showed similar copy numbers of the floxed *Bcl10* locus compared to control mice (Figure 21).

3.2.2 DEG analysis of cDC clusters

A pairwise comparison of cDC clusters was performed to assess transcriptional differences between cDCs from *Clec9a*$^{+/+}$*Bcl10*$^{fl/fl}$ and *Clec9a*$^{cre/+}$*Bcl10*$^{fl/fl}$ mice. This analysis identified 1665, 421, 942, and 152 differentially expressed genes (DEGs) in cDC1, DP cDC2, SP cDC2, and migratory DCs, respectively. Within those genes in cDC1s, *Clec7a* was the gene with the highest positive $\log_2$foldchange. *Clec7a* encodes Dectin-1, the CLR upstream of the CARD9-BCL10-MALT1 signaling complex. Increased Dectin-1 was confirmed by flow cytometric analysis of cDC1 isolated from CO LP of *Clec9a*$^{cre/+}$*Bcl10*$^{fl/fl}$ and control mice (Figure 22), performed by the collaborators' lab (Prof. Ruland's research group).

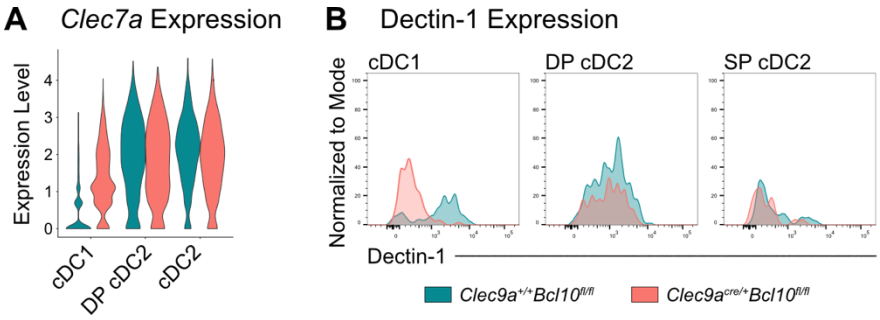

Figure 22 Clec7a/Dectin-1 expression increases in BCL10 deficient cDC1.
A. Transcriptional level of Clec7a in colonic cDC1, SP cDC2, and SP cDC2 from *Clec9a*$^{+/+}$*Bcl10*$^{fl/fl}$ and *Clec9a*$^{cre/+}$*Bcl10*$^{fl/fl}$ mice. **B.** Representative histograms of surface staining of *Clec7a* encoded protein Dectin-1 on cDC1, DP cDC2, and SP cDC2 isolated from CO LP of *Clec9a*$^{cre/+}$*Bcl10*$^{fl/fl}$ and their controls.

Having confirmed that the increased expression of the top differentially expressed gene *Clec7a* is also present in the protein level, gene set enrichment analysis (GSEA) was

performed based on total DEGs from the cDC1 cluster. This revealed a downregulation of genes involved in OXPHOS (Figure 23) and decreased levels of ribosomal genes (NES = -2.4931). A positive correlation between these two pathways is described in the literature (Argüello et al. 2020). In addition to reduced Rps and Rpl transcripts, genes mapped to the Cap-dependent translation (e.g., *Eif3j1* and *Eif2s2*) were expressed to a lesser extent in BCL10 deficient cDC1.

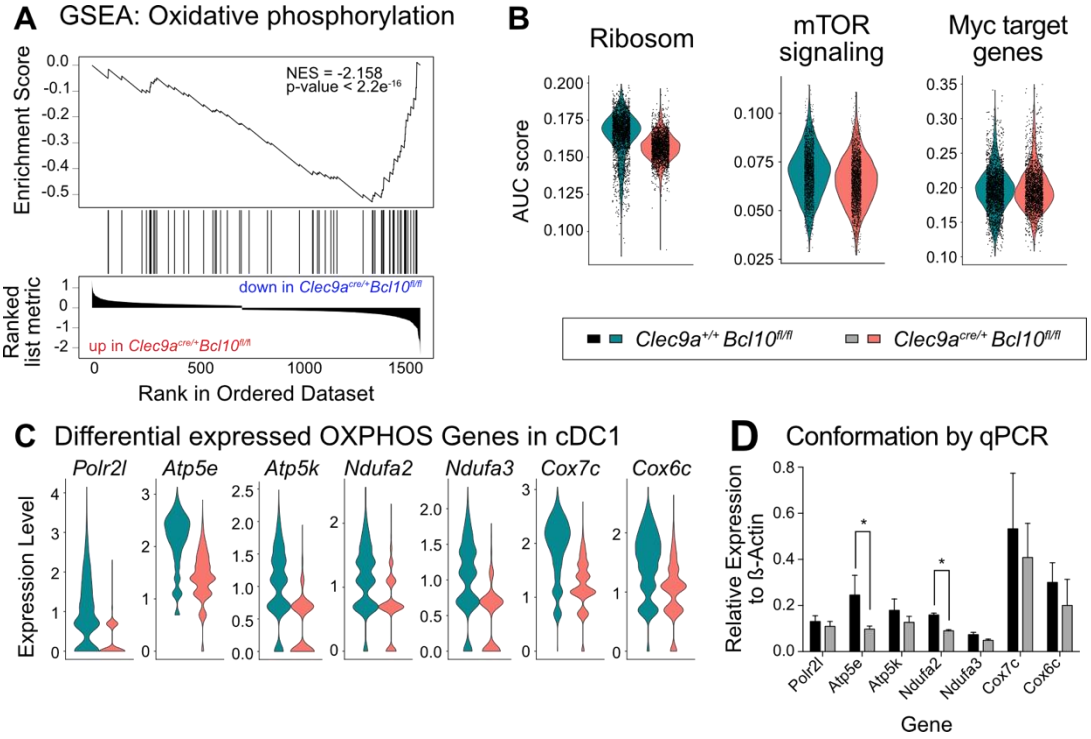

Figure 23 Downregulation of OXPHOS-related genes in BCL10 deficient cDC1.
A. Enrichment score of OXPHOS found in KEGG pathway GSEA of DEGs from cDC1. **B.** Area under the curve score of gene sets for the ribosome, mTOR signaling, and Myc target genes for cDC1 from *Clec9a*$^{+/+}$*Bcl10*$^{fl/fl}$ and *Clec9a*$^{cre/+}$*Bcl10*$^{fl/fl}$ origin. **C.** Gene expression of top seven differentially expressed OXPHOS gene in cDC1 cluster and **D.** Their expression level determined by qPCR in cDC1 sorted from CO LP of Clec*9a*$^{cre/+}$*Bcl10*$^{fl/fl}$ and their controls. (D) Data of 1 experiment; *Clec9a*$^{+/+}$*Bcl10*$^{fl/fl}$ n = 3, *Clec9a*$^{cre/+}$*Bcl10*$^{fl/fl}$ n = 3. Error bars indicate SEM. Statistical analyses were done by t-test. * p-value < 0.05

Utilization of different GSEA platforms identified several Myc target genes downregulated in cDC1 from *Clec9a*$^{cre/+}$*Bcl10*$^{fl/fl}$ mice. Induction of the Myc family through mTOR signaling is known to be involved in the metabolic reprogramming of the cDCs (Anderson III, Murphy, Eisenman and Murphy 2020). Therefore, the overall expression of genes involved in mTOR signaling was assessed by determining the area under the curve (AUC score) of the mTOR gene signature, revealing a decreased mTOR signaling BCL10 deficient cDC1. Differential expression of the top seven DEGs in cDC1, mapped to the OXPHOS pathway, was confirmed by qPCR.

Several differentially expressed genes involved in OXPHOS in BCL10 deficient cDC1 were found downregulated in DP cDC2, SP cDC2, and migratory DC, but in a smaller number and log_2foldchange. However, several genes upregulated upon *Bcl10* deletion excelled in cDC1. An over-representation analysis (ORA) mapped these genes to antigen processing and presentation pathways via MHCI and MHCII.

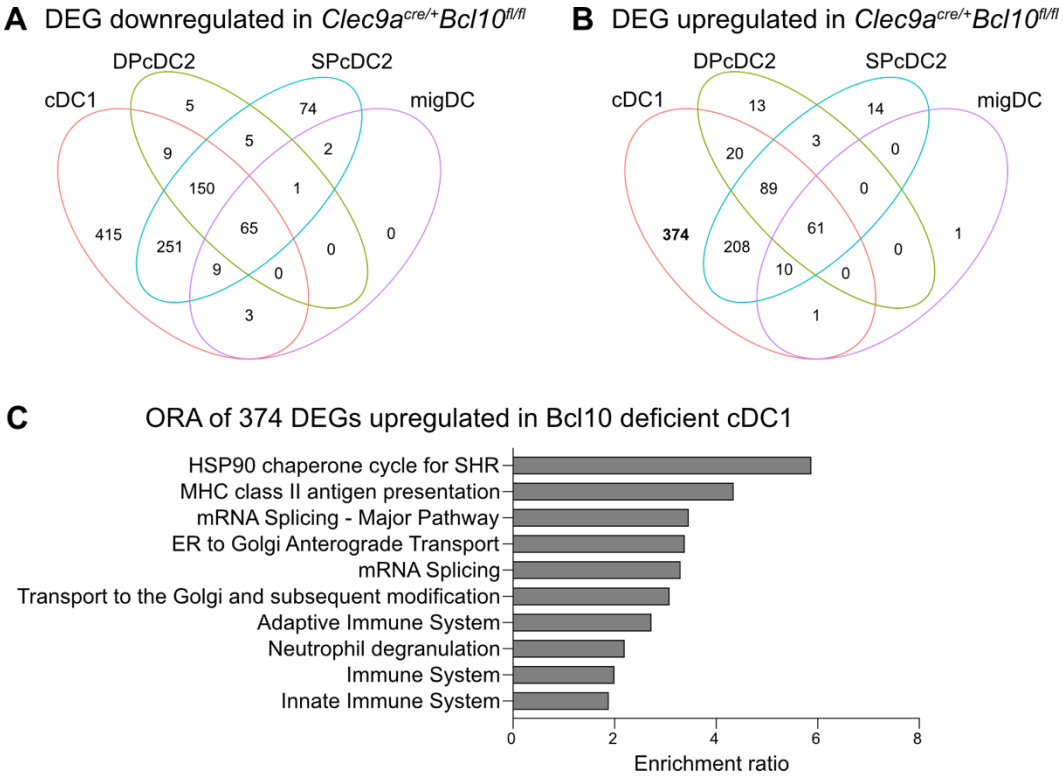

Figure 24 Colonic cDC subsets from *Clec9a*$^{cre/+}$*Bcl10*$^{fl/fl}$ mice share downregulated genes, and cDC1s have the highest number of upregulated DEGs.
Shared DEGs between different cDC clusters either **A.** downregulated, or **B.** upregulated in cDCs from *Clec9a*$^{cre/+}$*Bcl10*$^{fl/fl}$ mice. **C.** Over-representation analysis (ORA) of 374 genes only upregulated in *Bcl10* deficient cDC1.

Some of these upregulated genes were mapped to antigen processing and loading on MHCII (e.g., *Cd74* and *Ifi30*). Additional genes upregulated in BCL10 deficient cDC1 were depicted in cross-presentation pathways, including the heat shock protein 70 (HSP70), HSP90, and the transporter associated with antigen processing (TAP) machinery. Further on, this group of genes included genes directly encoding parts of the MHCI and MHCII complex. Flow cytometric analysis addressed whether this differential expression results in increased MHCI and MHCII levels (Figure 25).

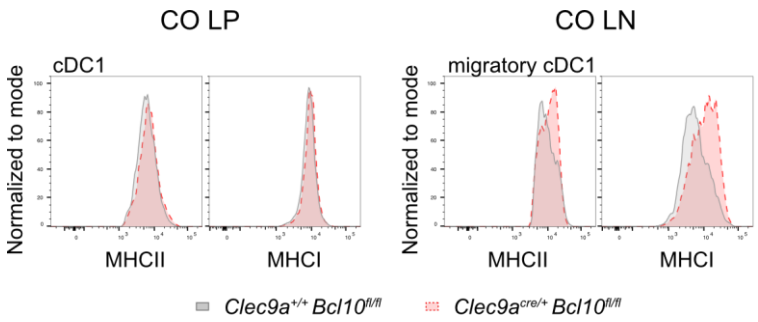

Figure 25 Increased MHCI and MHCII expression on migratory cDC1 in CO LN from *Clec9a$^{cre/+}$Bcl10$^{fl/fl}$* mice.

Representative histograms from flow cytometric analysis of MHCI and MHCII surface expression on MHCII^{+}CD11c^{+}CD64^{-}CD103^{+} cDC1 in CO LP (left) and MHCII^{hi}CD11c^{+}CD103^{+} migratory cDC1 in the CO LN (right) from *Clec9a$^{+/+}$Bcl10$^{fl/fl}$* (grey) and *Clec9a$^{cre/+}$Bcl10$^{fl/fl}$* (red) mice.

No difference in MHCI or MHCII complex expression was observed in cDCs isolated from CO LP between the genotypes even though cDC1 from *Clec9a$^{cre/+}$Bcl10$^{fl/fl}$* mice migrated from CO LP into the draining LN showed increased MHCI and MHCII, suggesting an increased activation of *Bcl10* deficient cDC1s.

3.2.3 In-depth investigation of the altered metabolism of cDCs from *Clec9a$^{cre/+}$Bcl10$^{fl/fl}$* CO LP and a possible cause

Upon activation and maturation, a metabolic switch from OXPHOS towards glycolysis occurs in DCs. Therefore, the possibility of an altered activation state in cDCs derived from CO LP of *Clec9a$^{cre/+}$Bcl10$^{fl/fl}$* mice was examined. Before this, the cell cycle phase was assessed to exclude that the altered metabolism of cDCs with *Clec9a$^{cre/+}$Bcl10$^{fl/fl}$* background is caused by a difference in the cell cycle (Figure 26). Cell cycle regression in the scRNA sequencing data set mice revealed equal cell phase distribution between the genotypes for all cDC and macrophage clusters. The latter were used as controls, showing no noticeable transcriptional differences in single-cell sequencing despite a slight reduction in BCL10. In addition to cell cycle regression based on the transcriptional profile of the respective cell type, the common proliferation marker Ki67 was stained in CO LP leukocytes and analyzed by flow cytometry. A previously described gating strategy was used to identify cDC subsets and macrophages in the CO LP. Equal staining intensities were observed for cDC1, both cDC2 subsets, the DN DC population, and macrophages. Therefore, the altered metabolism in colonic cDCs from *Clec9a$^{cre/+}$Bcl10$^{fl/fl}$* is not caused by a difference in the cell cycle.

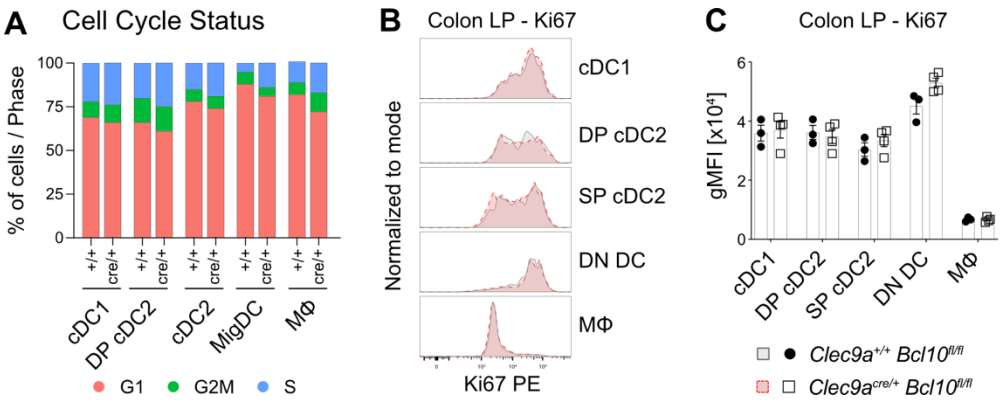

Figure 26 Deletion of *Bcl10* from cDCs does not affect their proliferation capacity.
A. Cell cycle regression grouped cDC subsets by their transcriptional expression profile into G1, G2M, and S Phase. **B.** Representative histogram of flow cytometric analysis of intracellular Ki67 and **C.** Geometric mean fluorescent intensity (gMFI) of the Ki67 signal in CD103$^+$ cDC1, CD103$^+$ CD11b$^+$ DP cDC, CD103$^-$ cDC2, DN DC and MHCII$^+$CD11c$^+$CD64$^+$ MΦ isolated from CO LP of *Clec9a*$^{+/+}$*Bcl10*$^{fl/fl}$ and *Clec9a*$^{cre/+}$*Bcl10*$^{fl/fl}$ mice. Data of 1 experiment. Each dot represents one mouse. Error bars indicate SEM. Statistical analyses were done by t-test.

Having excluded a difference in cell cycle as a cause for the altered metabolism, in the next step, classical activation markers CD40 and CD86, and PD-L1, as a marker for tolerogenic DCs, were selected to address the activation state of cDCs derived from CO LP of *Clec9a*$^{cre/+}$*Bcl10*$^{fl/fl}$ mice by flow cytometry (Figure 27).

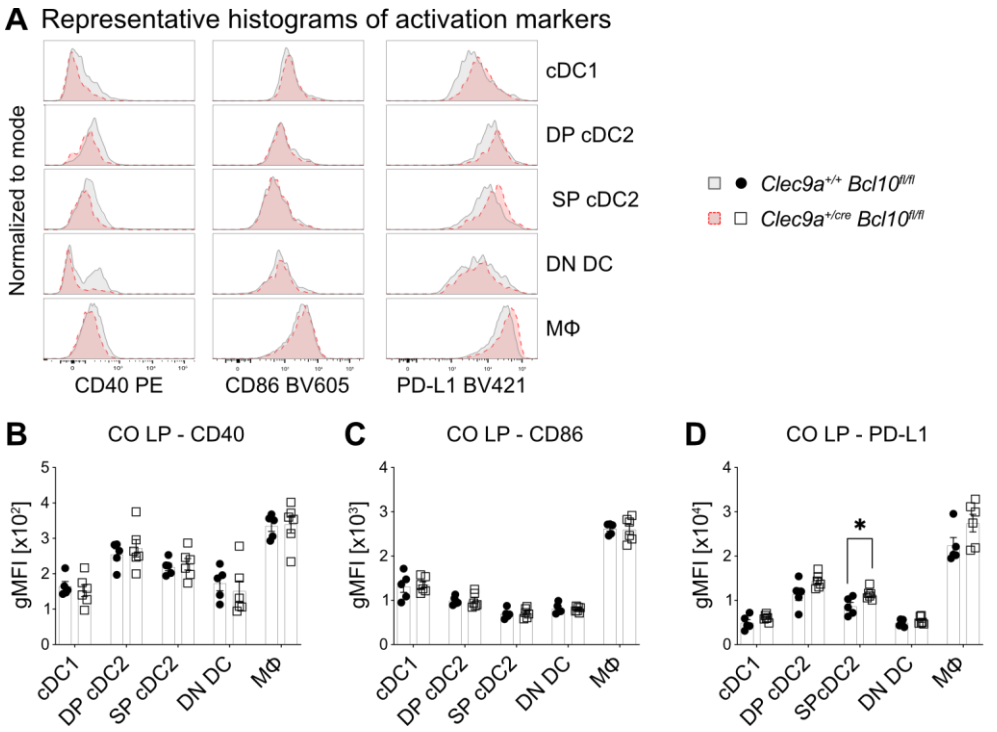

Figure 27 Expression of activation markers upon Bcl10 deletion in cDCs from CO LP.
A. Representative histogram of flow cytometric analysis of CD40, CD86, and PD-L1 and gMFI of **B.** CD40 **C.** CD86 and **D.** PD-L1 on CD103$^+$ cDC1, CD103$^+$ CD11b$^+$ DP cDC, CD103$^-$ cDC2, DN DC and MHCII$^+$CD11c$^+$CD64$^+$ MΦ isolated from CO LP of *Clec9a*$^{+/+}$*Bcl10*$^{fl/fl}$ and

Clec9a$^{cre/+}$*Bcl10*$^{fl/fl}$ mice. Data of 2 independent experiments. Each dot represents one mouse. Error bars indicate SEM. Statistical analyses were done by t-test. * p-value < 0.05

A similar gating strategy, as described in Figure 11, was applied to identify cDC1, CD103$^+$ cDC2 and their CD103 negative counterparts, DN DC fraction, and macrophages. Comparison of the histogram display of CD40 showed slight alterations towards decreased CD40 expression in cDCs and macrophages with *Clec9a*$^{cre/+}$*Bcl10*$^{fl/fl}$ background. However, total quantification of the fluorescent intensity revealed no difference in the expression level of CD40 in any of the identified cell populations. Further on, a similar expression pattern of CD86 was found on cDCs and macrophages from CO LP of *Clec9a*$^{cre/+}$*Bcl10*$^{fl/fl}$ mice compared to their controls. Histogram plots of PD-L1 displayed a shift of cDC1, both cDC2 subsets and macrophages, towards an increased signal intensity. Further analysis of the gMFI depicted a significant increase of PD-L1 on SP cDC2, and a similar trend was observed for DP cDC2 and macrophages but not for cDC1.

It should be considered that the increased transcriptional levels of genes encoding MHCI and MHCII complex in BCL10 deficient cDC1 were not found in protein level on cDC1 isolated from CO LP but on migratory cDC1 in the colon-draining LN. Therefore, a similar analysis of the activation state for CO LP cDCs was performed with cDCs isolated from CO LN of *Clec9a*$^{cre/+}$*Bcl10*$^{fl/fl}$ mice and their controls and identified according to the gating strategy described in chapter 3.1.1. Similar expression patterns of CD40 and CD86 were observed for migratory and resident cDC subsets, indicating an equal activation of BCL10 deficient cDCs compared to controls. Despite overlapping histograms of PD-L1 for all CO LN-derived cDC populations, the quantification of gMFI depicted a trend to increased PD-L1 expression in migratory cDC subsets.

In summary, no difference in activation was found in cDCs isolated from CO LP and CO LN of *Clec9a*$^{cre/+}$*Bcl10*$^{fl/fl}$ mice based on their expression level of CD40 and CD86. However, cDC2 in the CO LP and migratory cDCs in CO LN showed a slight, partially significant increase of PD-L1. Although no increased expression of the activation markers was found on cDCs, the increased expression of MHCI and MHCII and the altered expression of PD-L1 suggest an increased activation of cDCs leading to the decreased level of OXPHOS genes in cDCs from the colon of the *Clec9a*$^{cre/+}$*Bcl10*$^{fl/fl}$ mice.

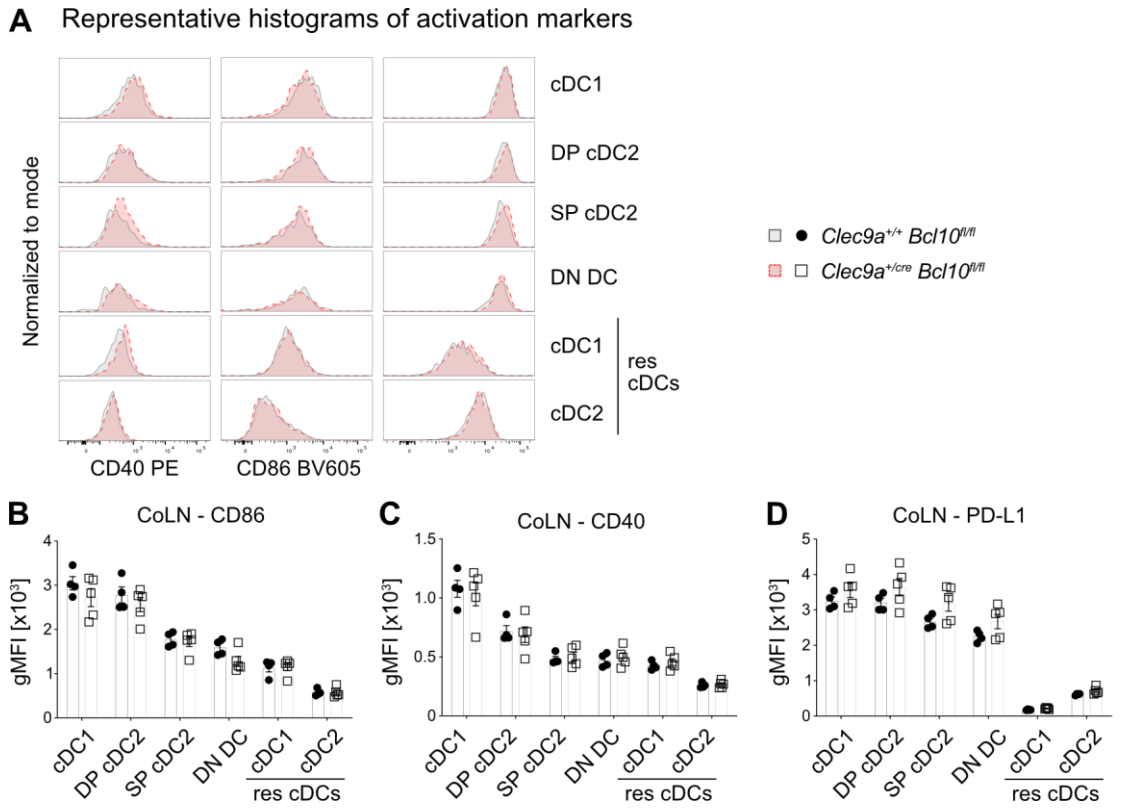

Figure 28 *Clec9a*$^{cre/+}$*Bcl10*$^{fl/fl}$ have comparable levels of activation markers in cDCs from CO LN.

A. Representative histogram of flow cytometric analysis of CD40, CD86 and PD-L1 and gMFI of **B.** CD40 **C.** CD86 and **D.** PD-L1 on migratory and resident cDC subsets isolated from CO LN of *Clec9a*$^{+/+}$*Bcl10*$^{fl/fl}$ and *Clec9a*$^{cre/+}$*Bcl10*$^{fl/fl}$ mice. Data of 2 independent experiments. Each dot represents one mouse. Error bars indicate SEM. Statistical analysis were done by t-test.

To evaluate if the decreased transcriptional level results in a lower OXPHOS rate, the mitochondrial function was compared between colonic cDCs from *Clec9a*$^{cre/+}$*Bcl10*$^{fl/fl}$ and control mice (Figure 29). In doing so, a flow cytometric approach was used to measure the mitochondrial membrane potential with the Mito Probe TMRM, allowing the investigation of mitochondrial function in a limited number of cells. Therefore, isolated leukocytes from either CO LP or CO LN were incubated at 37°C in the presence of TMRM, allowing the cells to restart their metabolism after being on ice during the tissue isolation procedure. cDC1 showed the highest TMRM signal intensity compared to cDC2s. However, no variation was found when each cDC subset was compared between genotype groups, and the lower expression of OXPHOS genes does not lead to a decrease in mitochondrial membrane potential, an indicator of OXPHOS.

After incubation at 37 °C, migratory and resident cDCs could no longer be segregated by their differential expression of MHCII; thus, an alternative gating had to be used to identify cDC subsets (Figure 29). Therefore, total MHCII^{+}CD11c^{+} cells were selected from live leukocytes. Next, the XCR1 expression allowed the separation of cDC1 from

cDC2. Within the XCR1$^+$ cDC1, migratory cDC1s were identified through their expression of CD103, and resident cDC1s were defined as XCR1$^+$CD103$^-$. XCR1 negative fraction of cDCs was subdivided by CD103 and CD11b. Migratory CO LP-derived DP cDC2 populations were uncovered by CD103 and CD11b expression and DN DC through their lack of both markers. A fourth detected CD103$^+$CD11b$^-$ population could not be assigned to a previously described cDC subset due to the lack of XCR1.

Quantification of the gMFI of TMRM revealed no significant changes in the mitochondrial membrane potential of cDCs in the CO LN of *Clec9a*$^{cre/+}$*Bcl10*$^{fl/fl}$ mice. Nevertheless, migratory cDC1s isolated from these mice tended to lower TMRM gMFI than migratory cDC1 isolated from CO LN of control mice. However, the latter group displayed a high spread.

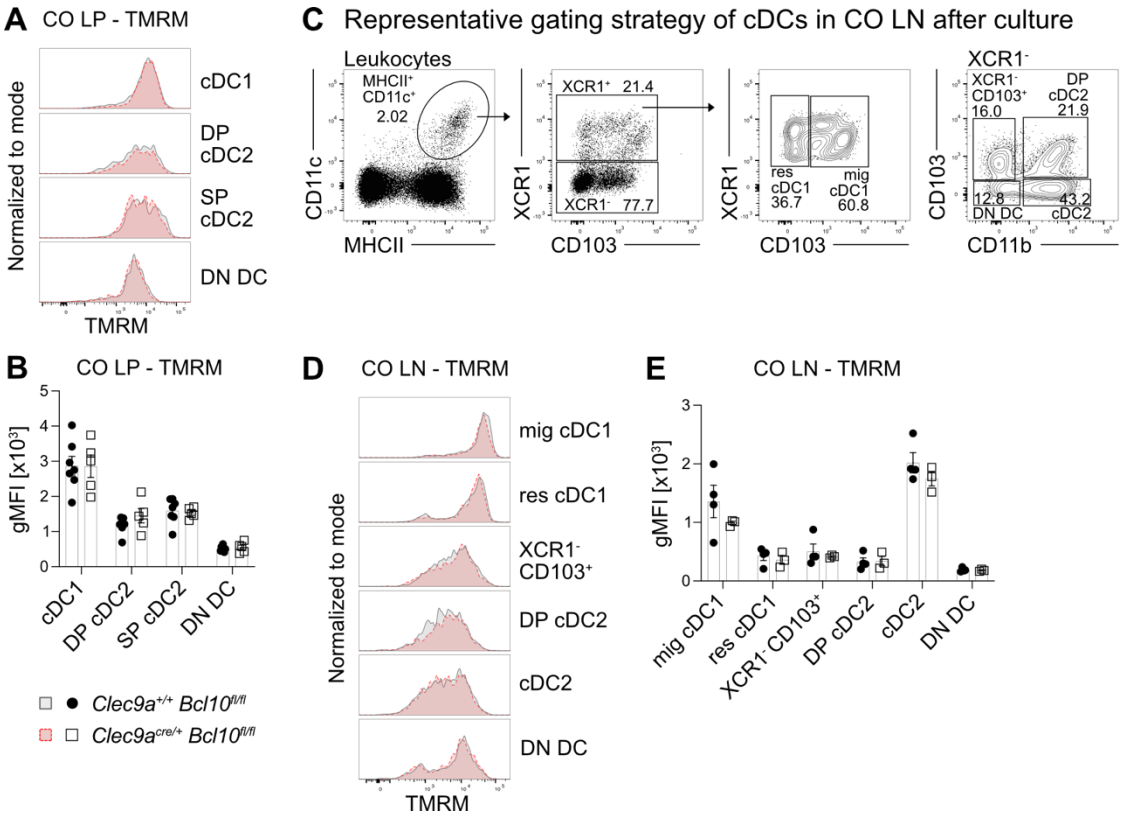

Figure 29 Similar mitochondrial membrane potential in intestinal cDCs from *Clec9a*$^{cre/+}$*Bcl10*$^{fl/fl}$ mice.

A. Representative histogram of flow cytometric analysis of TMRM and **B.** GMFI of TMRM in CD103$^+$ cDC1, CD103$^+$ CD11b$^+$ DP cDC, CD103$^-$ cDC2 and DN DC from CO LP of *Clec9a*$^{+/+}$*Bcl10*$^{fl/fl}$ and *Clec9a*$^{cre/+}$*Bcl10*$^{fl/fl}$ mice. **C.** Representative gating strategy to identify cDC subsets in CO LN after culture. Total MHCII$^+$CD11c$^+$ cells were gated on live leukocytes. XCR1 expression segregated cDC1 from cDC2. Migratory cDC1 were further identified as CD103$^+$ and resident cDC1 as CD103$^-$. XCR1 negative fraction was subdivided by CD103 and CD11b, leading to CD103$^+$CD11b$^+$ DP cDC2, CD11b$^+$ cDC2, DN DC, and CD103$^+$CD11b$^-$XCR1$^-$ population. **D.** Representative histogram of TMRM staining and **E.** GMFI of TMRM in cDC subsets in CO LN identified in (C.). Data of 2 independent experiments (CO LP) or 1 experiment (CO LN). Each dot represents one mouse. Error bars indicate SEM. Statistical analyses were done by t-test.

3.2.4 Transcriptional profiling of T cells and ILCs from CO LP of *Clec9a$^{cre/+}$Bcl10$^{fl/fl}$*

Next, CD90.2$^+$ cells from *Clec9a$^{+/+}$Bcl10$^{fl/fl}$* and *Clec9a$^{cre/+}$Bcl10$^{fl/fl}$* mice were analyzed by single cell sequencing. Aligned data files from both genotypes were combined using the Cell Ranger Aggregate platform. Subsequent quality control and cleanup led to 7892 cells with an approximate sequencing depth of 4406 reads and 1581 detected genes per cell. These cells were used as an input for unbiased clustering (Figure 30).

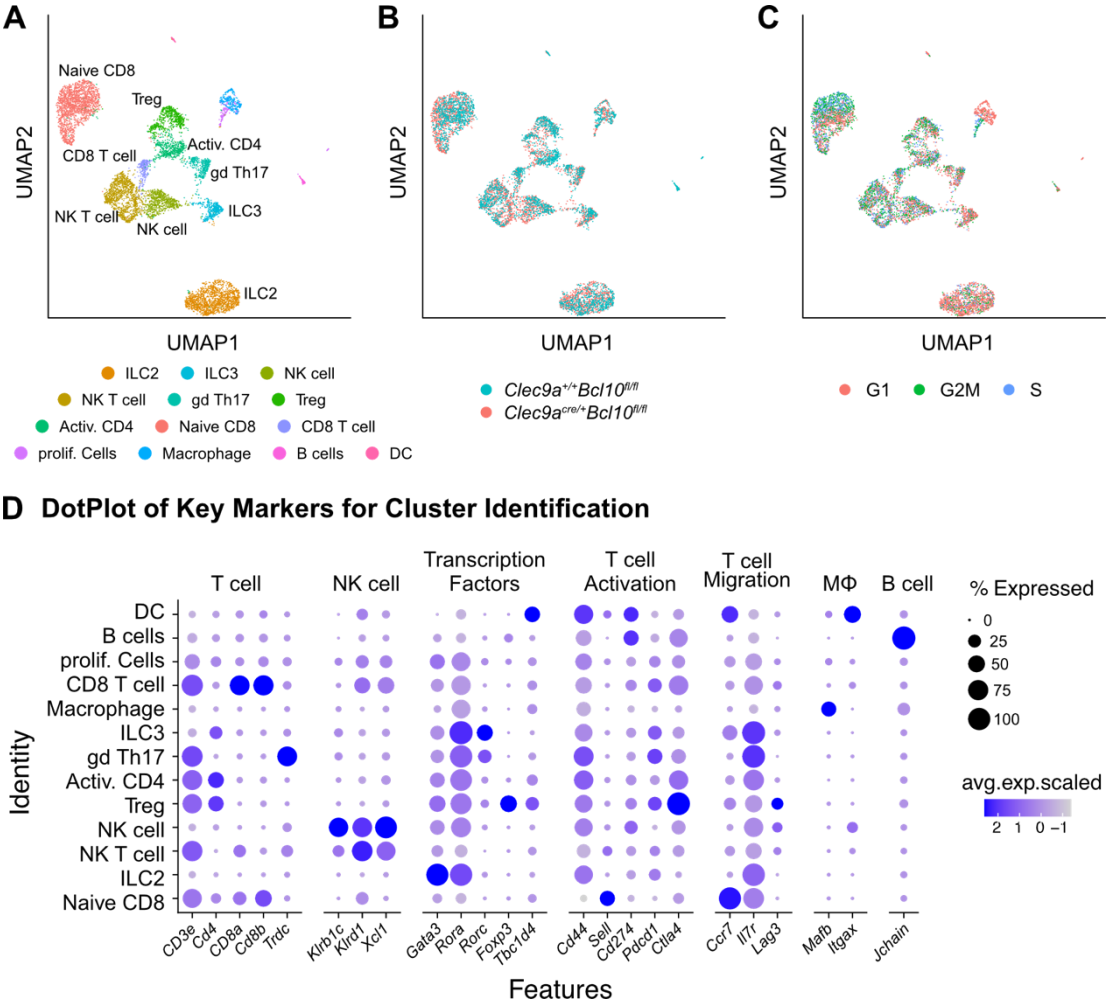

Figure 30 Comparable transcriptional profile of CD90.2$^+$ cells from CO LP of *Clec9a$^{cre/+}$Bcl10$^{fl/fl}$*.

A. Unbiased clustering of colonic CD90.2$^+$ cells resulted in 13 clusters. **B.** Cluster were separate based on their genetic background. **C.** Highly proliferating cells (G2M phase) form a separate cluster. **D.** Dot plot shows cluster identification based on cell-specific genes like *Cd3e* and TCR gene expression for T cells combined with transcription factor expression.

Unbiased clustering segregated 13 individual clusters, of which three clusters were composed of contaminations by B cells, macrophages, and DCs. In addition, cell cycle regression identified one cluster as highly proliferating cells. Expression of CD3ε and TCR encoding genes could identify six T cell clusters. Of those, only one cluster expressed

genes of the TCRγδ complex, together with *Rora* and *Rorc,* and therefore was determined as γδ Th17 cells. Another cluster of non-classical T cells was marked by high *Cd3e* but low TCR gene expression and was identified by *Klrd1* and *Xcl1* as NK T cells. Two CD8 T cell clusters were further segregated into naïve and activated through their *Cd44*, *Sell* (CD62L), *Pdcd1,* and *Ctla4* expression patterns. Residual T cells cluster included CD4 T cells, separated in activated CD4 T cells (*Cd4* & *Cd44*) and Tregs (*Foxp3* & *Ctla4*). The remaining non-T cell clusters were classified into NK cells (*Klrb1c, Klrd1, Xcl1*), ILC2 (*Rora, Gata3*), and ILC3 (*Rora, Rorc*).

A pairwise comparison of the two genotypes within each cluster revealed a low number of DEGs (30 – 154) with a log_2foldchage > 0.02. These DEGs were primarily shared between the clusters and belonged to a group of genes encoding parts of the ribosome, which may be due to a possible batch effect. Throughout all these DEGs, no hit candidates could be identified. However, the sequencing depth was too low to detect most cytokines.

3.3 BCL10 in cDCs has no severe impact on acute Colitis

3.3.1 DSS-induced acute colitis in *Clec9a$^{cre/+}$BCl10$^{fl/fl}$* mice

Having found that BCL10 deletion does not affect overall cDC development but alters some intrinsic metabolic pathways, the next step was investigating the role of BCL10 in cDCs during acute colitis. Challenging *Clec9a$^{cre/+}$BCl10$^{fl/fl}$* and control mice with the chemical DSS via the drinking water for seven days induced acute colitis marked by rapid weight loss without recovery (Figure 31). Acute colitis in *Clec9a$^{cre/+}$BCl10$^{fl/fl}$* mice was performed in collaboration with the Ruland lab (TUM). Mice were analyzed after ten days or when termination criteria were reached. Even though the disease activity score (DAI) revealed decreased severity in *Clec9a$^{cre/+}$BCl10$^{fl/fl}$* mice, a weight loss comparison showed no significant difference. In addition, endpoint analysis of colon length and colon length/bodyweight ratio were similar in both genotypes, and no significant difference was determined through histological evaluation of immune cell infiltration and epithelial damage. Serum cytokine analysis performed by the collaborators depicted lower levels of IL-23 and a trend toward a decrease in pro-inflammatory cytokines like IL-17A, IL-6, IFNγ, and TNFα. At the same time, the anti-inflammatory cytokine IL-10 was increased in the *Clec9a$^{cre/+}$BCl10$^{fl/fl}$* mice serum. Taken together, serum cytokine analysis points towards a decreased level of inflammation in *Clec9a$^{cre/+}$BCl10$^{fl/fl}$* mice, which, however, does not change the colitis's severity.

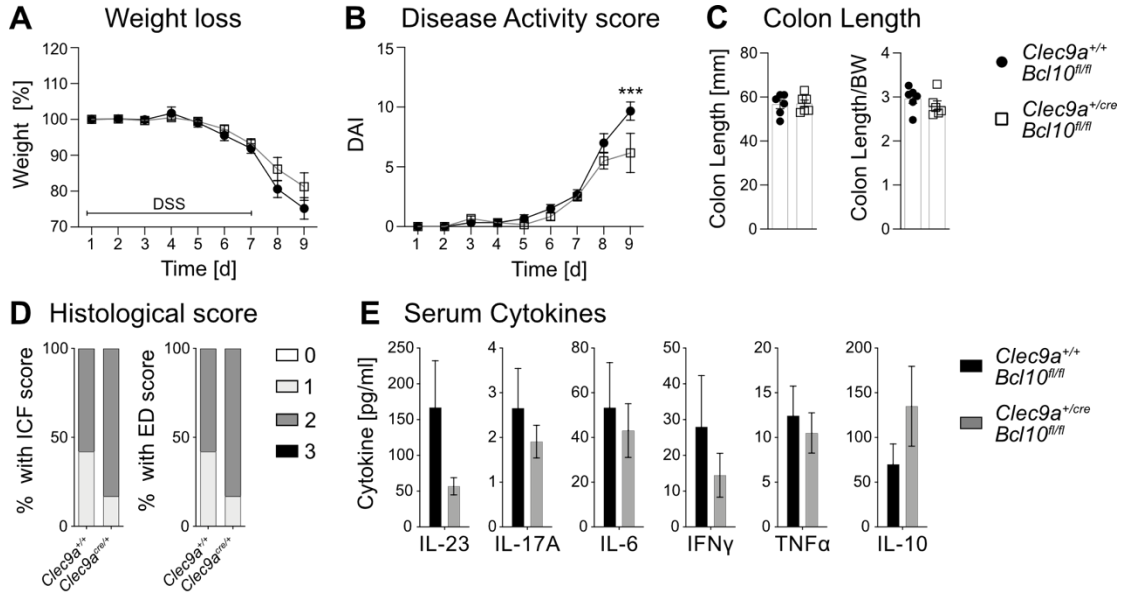

Figure 31 Potential attenuation of acute colitis severity in *Clec9a$^{cre/+}$BCl10$^{fl/fl}$* mice.
A. Weight loss, **B.** Disease activity index/score (DAI), **C.** Colon length and colon length vs. body-weight ratio at endpoint analysis and **D.** Histological score of immune cell infiltration (ICF) and epithelial damage determined in H&E stained cryo-sections of the colon from *Clec9a$^{cre/+}$BCl10$^{fl/fl}$* mice (n = 6) and their controls (n = 6) upon DSS induced acute colitis. **E.** Level of cytokines in the serum sampled on day 8 (n per group = 10), two pooled experiments. (A-D) Representative data of one experiment out of three independent repeats. Statistical analyses were done by t-test. *** p-value < 0.001

An influx of neutrophils usually accompanies colon inflammation, and the grade of inflammation correlates with the number of neutrophils. Therefore, neutrophil infiltration of the CO LP was assessed by flow cytometric analysis after DSS-induced acute colitis (Figure 32).

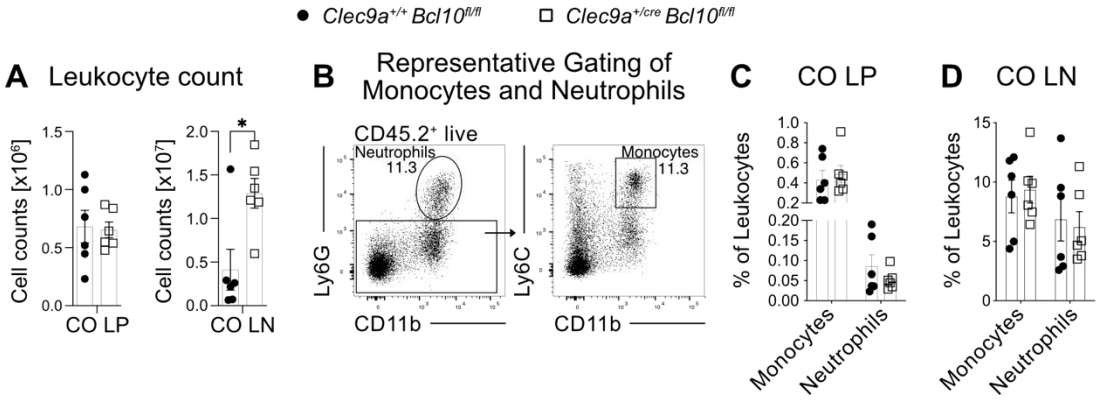

Figure 32 Increased cellularity of CO LN in *Clec9a$^{cre/+}$BCl10$^{fl/fl}$* mice in acute colitis.
A. Total leukocyte count isolated from CO LP (CD45.2$^+$) or CO LN of *Clec9a$^{cre/+}$BCl10$^{fl/fl}$* mice and their controls after acute colitis. **B.** Gating strategy to identify Neutrophils as Ly6G$^+$CD11b$^+$ and monocytes from Ly6G$^-$ fraction as Ly6C$^+$CD11b$^+$. **C.** Frequency of neutrophils and monocytes in CO LP and **D.** CO LN of *Clec9a$^{cre/+}$BCl10$^{fl/fl}$* mice and their controls after acute colitis. Representative data of one experiment out of three independent repeats. Each dot represents a mouse. Statistical analyses were done by t-test. * p-value < 0.05

Upon leukocyte gating, neutrophils were identified through their expression of Ly6G and CD11b. In addition, monocytes were gated within the Ly6G negative gate as the Ly6C^{+}CD11b^{+} population. The frequency of neutrophils and monocytes determined in CO LP and CO LN were similar between *Clec9a*$^{cre/+}$*BCl10*$^{fl/fl}$ and control mice. Even though neutrophil and monocyte numbers were increased in the CO LN of *Clec9a*$^{cre/+}$*BCl10*$^{fl/fl}$ mice, overall leukocyte count was significantly increased in these mice. This increase could not be traced back to a single immune cell population.

3.3.2 Flow cytometric profiling of cDCs and T cells in CO LP and CO LN *Clec9a*$^{cre/+}$*BCl10*$^{fl/fl}$ mice with acute colitis

Within the flow cytometric analysis of CO LP upon acute colitis induction (Figure 33), cDCs, and macrophages were identified in the CO LP as CD64 negative or positive CD11c^{+}MHCII^{+} cells, respectively, using the gating strategy described previously.

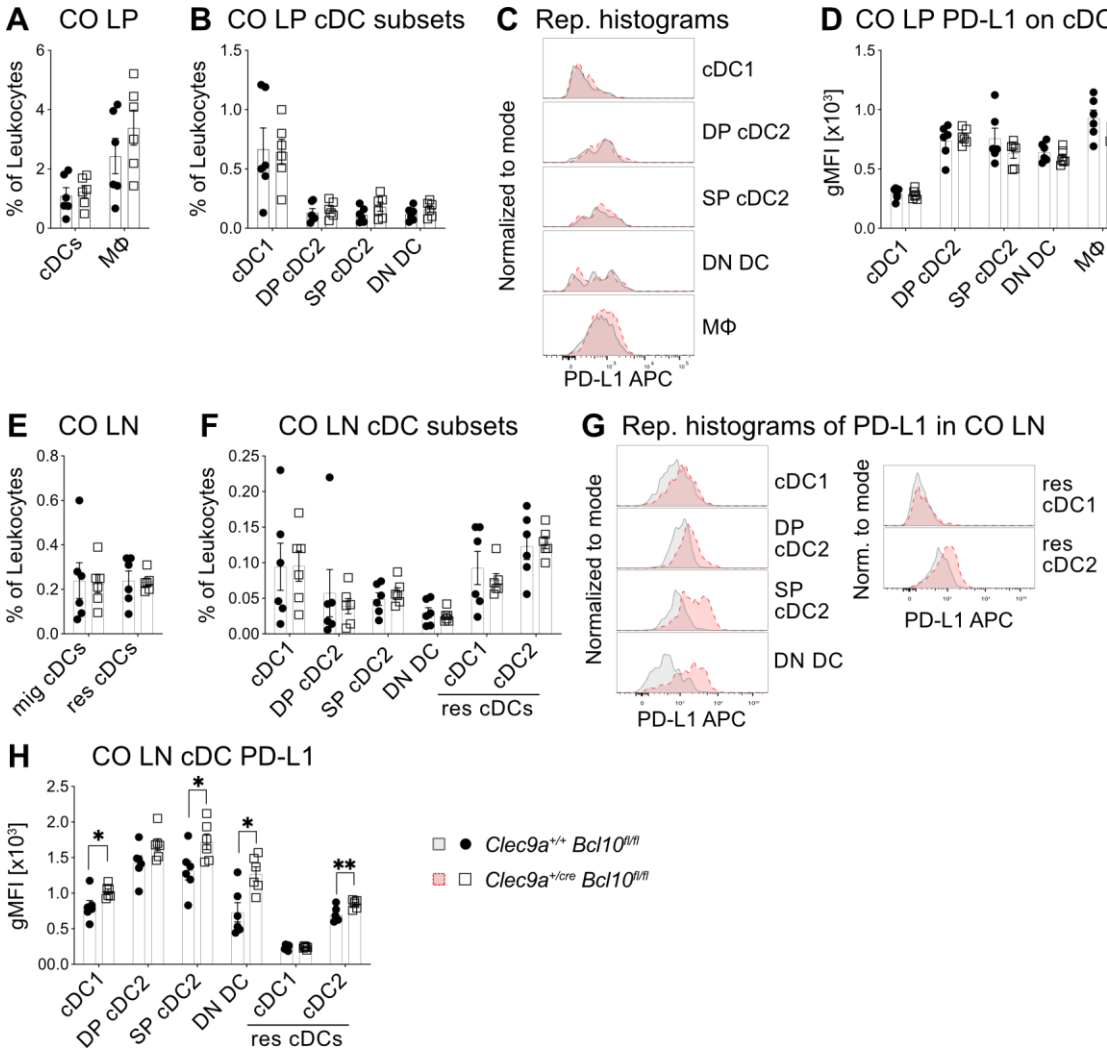

Figure 33 Increased PD-L1 on cDCs from CO LN of *Clec9a*$^{cre/+}$*BCl10*$^{fl/fl}$ mice during acute colitis.

Flow cytometric analysis of CO LP and CO LN of *Clec9a*$^{cre/+}$*BCl10*$^{fl/fl}$ mice and control mice on day 9 of DSS-induced acute colitis. **A.** Frequency of cDCs and macrophages and **B.** cDC1 and

cDC2 subsets in the CO LP. **C.** Representative histogram and **D.** Quantification of PD-L1 expression on cDC1, DP cDC2, SP cDC2, DN DC, and macrophages from CO LP. **E.** Frequency of total migratory and resident cDCs and **F.** cDC subsets in the CO LN**. G.** Representative histogram and **H.** Quantification of PD-L1 expression on migratory and resident cDC1 and cDC2 subsets from the CO LN. Representative data of one experiment out of three independent repeats. Each dot represents a mouse. Statistical analyses were done by t-test. * p-value < 0.05, ** p-value < 0.01

No difference could be observed between the genotypes regarding the frequency of total cDCs and macrophages, nor in the frequency of identified cDC subsets. The assessed expression level of PD-L1, which was slightly increased on cDC2 under homeostatic conditions, was similar when *Clec9a*$^{cre/+}$*BCl10*$^{fl/fl}$ mice were compared to control mice. Next, resident and migratory cDCs and their respective subsets in the CO LN were analyzed. However, no change in frequency in any population was detected. However, cell counts of all migratory and resident cDC1 and cDC2 subsets were increased in *Clec9a*$^{cre/+}$*BCl10*$^{fl/fl}$ mice due to the overall increase in cellularity of the CO LN. As in the CO LP, the expression of PD-L1 on cDCs in CO LN was evaluated. Visual comparison through overlaid histograms of cDCs derived from *Clec9a*$^{cre/+}$*BCl10*$^{fl/fl}$ mice with their controls revealed an increased expression level of PD-L1 in migratory and resident cDC subsets. This was confirmed when PD-L1 fluorescent intensity was quantified.

After the analysis of cDCs in the CO LP and CO LN of *Clec9a*$^{cre/+}$*BCl10*$^{fl/fl}$ mice with DSS-induced acute colitis, T cell compartment in both organs underwent in-depth phenotypic flow cytometric profiling (Figure 34 & Figure 35). Autofluorescent cells, predominantly macrophages, were excluded, and T cells were identified as the CD3ε^{+} population and subdivided by CD4 and CD8a. Within the CO LP of *Clec9a*$^{cre/+}$*BCl10*$^{fl/fl}$ mice and their controls, equal frequencies of total T cells and the CD4, CD8, and unconventional T cell subsets were determined. Further gating of Foxp3^{+} Tregs and identifying different activation states of the T cells based on CD44 and CD62L were described before. However, no difference was observed in the frequency of Tregs. Neither an alteration in the proportions of effector, memory, and naïve CD4, CD8, or unconventional T cells. Additional analysis of PD-1 expression by the three T cell subsets showed similar levels between *Clec9a*$^{cre/+}$*BCl10*$^{fl/fl}$ and control mice. However, according to decreased Th17 cytokines in steady state, colonic CD4 T cells from *Clec9a*$^{cre/+}$*BCl10*$^{fl/fl}$ mice with acute colitis secreted significantly less IL-17A upon ex-vivo re-stimulation. At the same time, unconventional T cells expressed similar amounts of IL-17A but increased levels of IL-22. No differences were detected between the two groups in IL10 expression by CD4 T cells or for IFNγ production by any of the three T cell subsets.

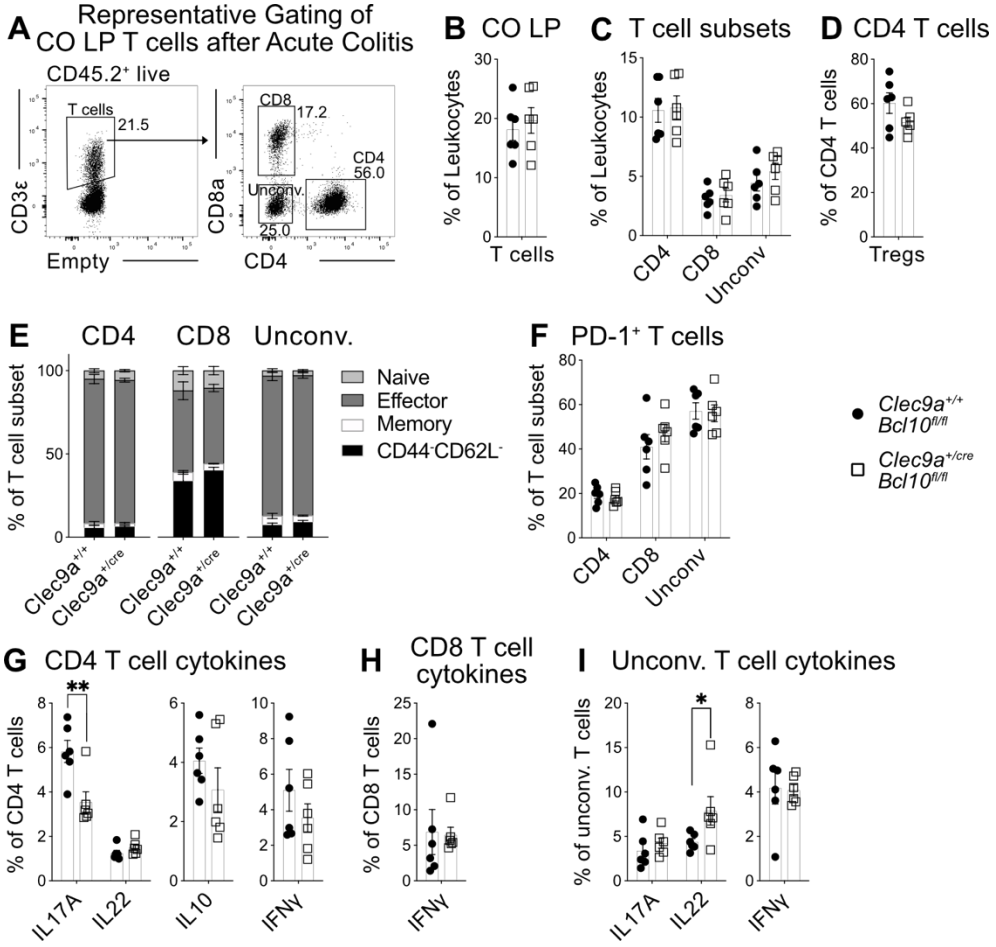

Figure 34 *Clec9a$^{cre/+}$Bcl10$^{fl/fl}$* mice with acute colitis have decreased IL-17A$^+$ CD4 T cells and increased IL-22$^+$ unconventional T cells in the CO LP.

Flow cytometric profiling of T cells in CO LP of *Clec9a$^{cre/+}$Bcl10$^{fl/fl}$* mice with acute colitis. **A.** Representative gating strategy to gate non-autofluorescent CD3ε$^+$ T cells out of CD45.2$^+$ live leukocytes. Further subdivision of T cells into CD4$^+$, CD8a$^+$, and DN (unconv.) T cells. **B.** Frequency of total T cells and **C.** the CD4, CD8, and unconventional T cell subsets in CO LP. **D.** Frequency of Tregs out of CD4 T cells. **E.** Frequency of naïve, effector, memory, and CD44$^-$CD62L$^-$ within the T cell subset. **F.** PD-1$^+$ cells of CD4, CD8, and unconventional T cells. Expression of **G**. IL-17A, IL-22, IL-10, and IFNγ by CD4 T cells, **H.** IFNγ by CD8 T cells, and **I.** IL-17A, IL-22, and IFNγ by unconventional T cells after re-stimulation with PMA/Ionomycin. Representative data of one experiment out of three independent repeats. Each dot represents a mouse. Statistical analyses were done by t-test. * p-value < 0.05, ** p-value < 0.01

A similar gating strategy for the CO LP was used to identify T cells and the respective subsets in the CO LN of *Clec9a$^{cre/+}$Bcl10$^{fl/fl}$* and control mice suffering from acute colitis. T cell frequency and the proportions of the CD4 and CD8 T cells showed similar values for *Clec9a$^{cre/+}$Bcl10$^{fl/fl}$* mice compared to control mice. Also, a small fraction of double-negative unconventional T cells was detected in equal frequencies. Within the CD4 T cells of *Clec9a$^{cre/+}$Bcl10$^{fl/fl}$* mice, the percentage of Tregs appeared partially decreased, even though this trend was not statistically significant. Assessment of the cytokine capacity of CD4 and CD8 T cells showed no changes in IL17-A, IL-22, IL10, and IFNγ.

However, like increased IL-22 production in the CO LP, unconventional T cells isolated from the CO LN of *Clec9a*$^{cre/+}$*BCl10*$^{fl/fl}$ mice produced more IL-22.

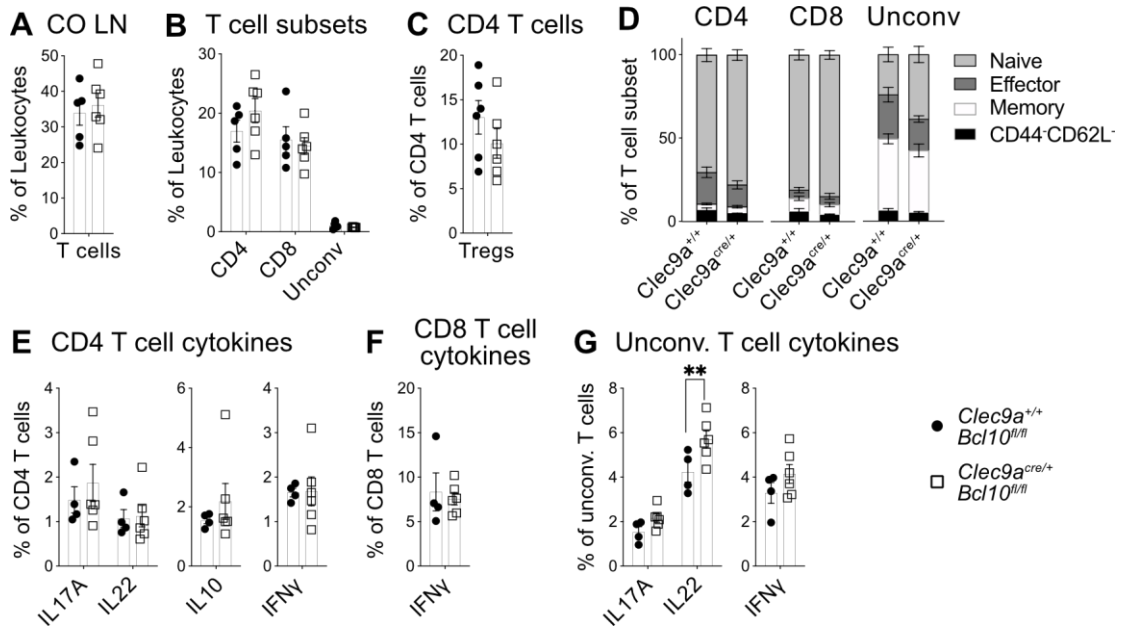

Figure 35 T cell compartment in the CO LN of *Clec9a*$^{cre/+}$*BCl10*$^{fl/fl}$ mice with acute colitis. Flow cytometric profiling of T cells in CO LN of *Clec9a*$^{cre/+}$*BCl10*$^{fl/fl}$ mice with acute colitis. **A.** Frequency of total T cells and **B.** the CD4, CD8, and unconventional T cell subsets in CO LN. **C.** Frequency of Tregs out of CD4 T cells. **D.** Frequency of naïve, effector, memory, and CD44^{-} CD62L^{-} within the T cell subset. Expression of **E**. IL-17A, IL-22, IL-10, and IFNγ by CD4 T cells, **F.** IFNγ by CD8 T cells, and **G.** IL-17A, IL-22, and IFNγ by unconventional T cells after re-stimulation with PMA/Ionomycin. Representative data of one experiment out of three independent repeats. Each dot represents a mouse. Statistical analyses were done by t-test. ** p-value < 0.01

In summary, *Clec9a*$^{cre/+}$*BCl10*$^{fl/fl}$ mice showed no alteration in disease severity upon DSS-induced acute colitis. And the cDC compartment within the CO LP, the site of inflammation, appeared unchanged. At the same time, cDCs in the CO LN showed increased levels of the tolerogenic marker PD-L1. Last, a decreased level of the pro-inflammatory cytokine IL-17A was detected in colonic CD4 T cells, and IL-22, known to support epithelial restitution, was increased in unconventional T cells in CO LP and CO LN of *Clec9a*$^{cre/+}$*BCl10*$^{fl/fl}$ mice.

3.4 Deletion of BCL10 in cDCs increases the susceptibility for colitis-associated-colon cancer

3.4.1 AOM- DSS induced CAC in *Clec9a$^{cre/+}$BCl10$^{fl/fl}$* mice

The next step after assessing the role of BCL10 in cDCs in acute colitis was the study of its role in colon cancer induced by chronic colitis. In collaboration with the Ruland lab (TUM), *Clec9a$^{cre/+}$BCl10$^{fl/fl}$* mice were challenged with three repetitive cycles of DSS treatment after one single injection of AOM (i.p.) (Figure 36). In doing so, mice commonly develop tumors, in the form of adenomas, throughout the colon within 2 – 3 weeks after the last DSS cycle.

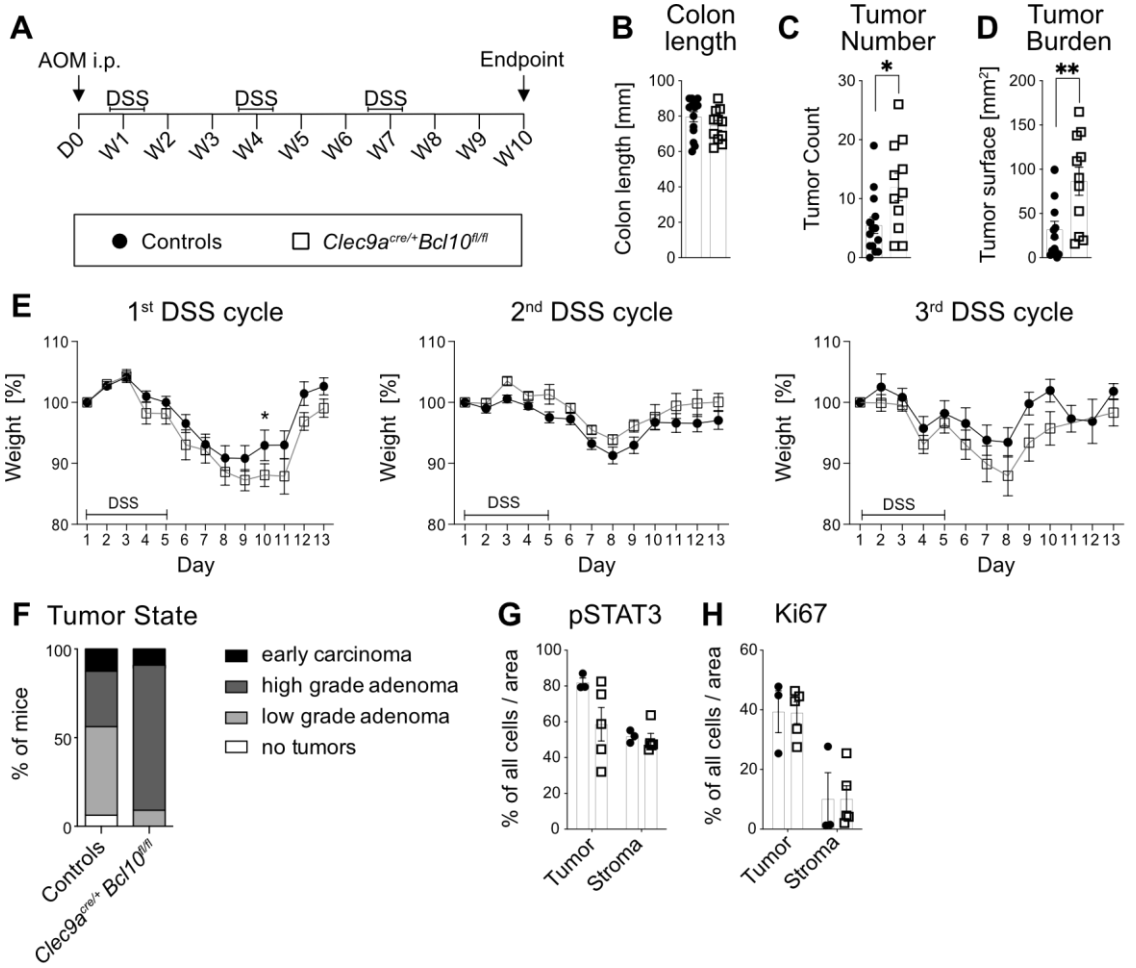

Figure 36 Deletion of BCL10 in cDCs aggravates tumor development in CAC.
A. Scheme of AOM-DSS treatment to induce tumor growth upon three repetitive DSS treatments mimic chronic colitis. **B.** Colon length, **C.** Tumor number, and **D.** Tumor burden of *Clec9a$^{cre/+}$Bcl10$^{fl/fl}$* mice and control mice after AOM-DSS treatment (Each dot represents a mouse). **E.** Weight curves of *Clec9a$^{cre/+}$Bcl10$^{fl/fl}$* mice (n = 17) and control mice (n = 17) for the three DSS cycles. **E.** Histological scoring of tumor invasiveness (Mice per group: control mice n = 15, *Clec9a$^{cre/+}$Bcl10$^{fl/fl}$* mice n = 11). **G.** Histological quantification of pStat3 and Ki67 in tumor and stroma areas to assess cell proliferation (Each dot represents the mean of one mouse, 3 – 4 areas were analyzed per mouse, per area type). Data from three independent experiments. Bars indicate the mean; error bars indicate SEM. Statistical analyses were done by t-test. * p-value < 0.05, ** p-value < 0.01

Monitoring the mice within each DSS cycle showed no differences in weight loss and recovery. Endpoint analysis of *Clec9a*$^{cre/+}$*BCl10*$^{fl/fl}$ and their controls revealed a similar colon length between the groups. Even though tumor numbers and burden were increased upon AOM-DSS treatment when BCL10 was deleted in cDCs. The histological evolution of colon sections was assessed in collaboration with the Institute of Pathology (TUM). This histological analysis revealed more invasive tumors in *Clec9a*$^{cre/+}$*BCl10*$^{fl/fl}$ mice. However, this aggravated tumor development was not due to elevated proliferation within the epithelium, determined by the histological staining and quantification of pSTAT3 and Ki67 in stromal and tumor cells.

3.4.2 Immune profiling of the intestinal compartment affected by CAC from *Clec9a*^{cre}*BCl10*^{flox} mice after AOM-DSS

To uncover the cause for the increased tumor development in *Clec9a*$^{cre/+}$*BCl10*$^{fl/fl}$ mice upon AOM-DSS challenge, in-depth immune phenotyping was performed in the colon and CO LN with a focus on cDCs and T cells. This analysis should allow the detection of a failure in anti-tumor immunity induced by the loss of BCL10 in cDCs.

Before this, several organs not directly affected by the AOM-DSS treatment were examined for signs of inflammation, determined by the infiltration of monocytes and neutrophils of the respective organ. Further, the cDC compartment was analyzed in those organs to check for systemic changes in the cDC compartment when BCL10 is absent in cDCs during chronic colitis followed by tumor development. Therefore, the spleen and the intestinal compartment upstream of the colon, including SI LP, SI LN, and the PPs of *Clec9a*$^{cre/+}$*BCl10*$^{fl/fl}$ mice and control mice were analyzed. However, no difference could be observed for monocytes or neutrophils, neither for total cDCs nor the cDC subsets (Data not shown).

3.4.2.1 Profiling of the cDC compartment in the colonic compartment of *Clec9a*$^{cre/+}$*Bcl10*$^{fl/fl}$ mice after AOM-DSS

For the analysis of the colonic compartment, first, the proportion of immune cells localized in the remaining non-tumorigenic CO LP was determined, and similar cell counts were measured in *Clec9a*$^{cre/+}$*BCl10*$^{fl/fl}$ mice compared to control mice (Figure 37). Monocytes and Neutrophils were detected, and similar frequencies of both cell populations indicated an equal level of inflammation in the CO LP after AOM-DSS treatment. As in steady state and acute inflammation, BCL10 deletion in cDCs did not alter their occurrence in the CO LP after the AOM-DSS challenge. Similar frequencies of total cDCs and cDC1, DP cDC2, SP cDC2, and DN DC subsets were detected. Further, macrophages were detected in equal amounts in the CO LP of *Clec9a*$^{cre/+}$*BCl10*$^{fl/fl}$ and control mice.

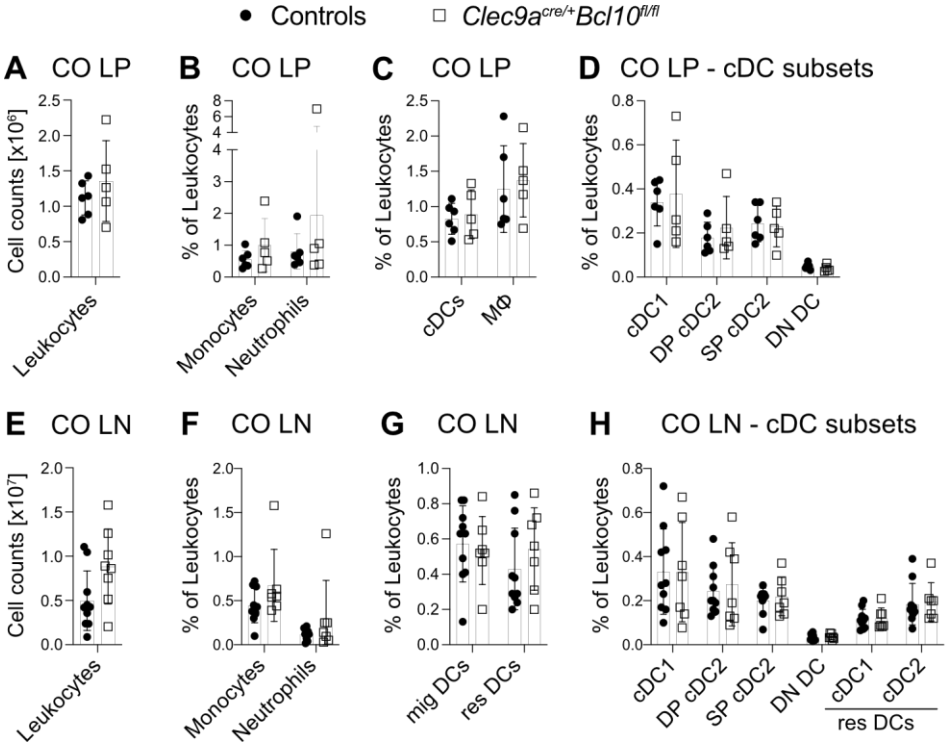

Figure 37 Equal frequencies of myeloid cell populations in the colonic compartment of *Clec9a$^{cre/+}$Bcl10$^{fl/fl}$* and control mice after AOM-DSS.

A. Cell counts of CD45.2$^+$ live leukocytes in the CO LP. **B.** Frequency out of leukocytes of Monocytes and Neutrophils, **C.** cDCs and Macrophages, and **D.** cDC1, SP cDC2, DN DC and DP cDC2 in the CO LP of *Clec9a$^{cre/+}$Bcl10$^{fl/fl}$* mice and their controls after AOM-DSS treatment. **E.** Cell counts of live leukocytes in the CO LN. **F.** Frequency out of leukocytes of monocytes and neutrophils, **G.** resident and migratory cDCs and **H.** the subsets cDC1, DP cDC2, SP cDC2, DN DC (mig cDCs) and cDC1 and cDC2 (res cDCs) in the CO LN of *Clec9a$^{cre/+}$Bcl10$^{fl/fl}$* mice and their controls after AOM-DSS treatment. Each dot represents a mouse. Data of one (CO LP) or two (CO LN) independent experiments. Bars indicate mean, error bars indicate SEM. Statistical analyses were done by t-test.

In line with the increased cellularity of the CO LN of *Clec9a$^{cre/+}$Bcl10$^{fl/fl}$* mice during acute colitis, the same trend was noted after AOM-DSS. Even though a specific cell population accounting for this increase could not be identified with the selected parameters for analysis. Monocytes and neutrophils, total resident and migratory cDCs, and the respective cDC1 and cDC2 subsets were detected in similar frequencies in *Clec9a$^{cre/+}$Bcl10$^{fl/fl}$* and control mice.

To complete the analysis of the cDC compartment at the site of cancer development, tumors were dissected from the remaining CO LP. Immune cells infiltrating the tumor and contributing to the TME were isolated and analyzed for different myeloid cell types (Figure 38). Leukocytes were identified like in other peripheral organs as CD45.2$^+$ live cells. Neutrophils were identified as Ly6G$^+$CD11b$^+$, and from Ly6G negative fraction, the expression of Ly6C and CD11b determined monocytes. It must be considered that MDSCs express similar markers and contribute to both populations. MHCII$^+$CD11c$^+$ cells

were gated and further dissected into cDCs and macrophages through the expression of CD64 by the latter one. The cDC population was further subdivided into the classical intestinal subsets cDC1, SP cDC2, DP cDC2, and the DN DC population.

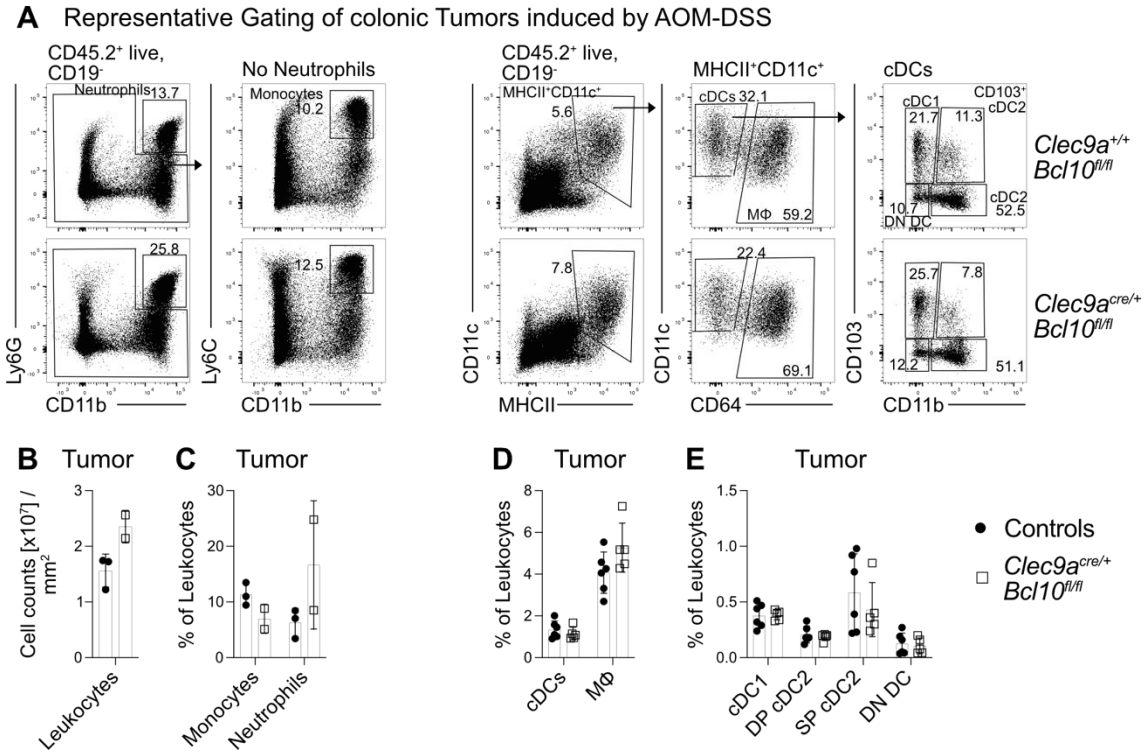

Figure 38 Identification of myeloid cells in colonic tumors after AOM-DSS and their frequencies.

A. Representative gating strategy to identify myeloid cells in AOM-DSS induced colonic tumors in *Clec9a*$^{+/+}$*Bcl10*$^{fl/fl}$ (top) and *Clec9a*$^{cre/+}$*Bcl10*$^{fl/fl}$ mice (bottom) mice. Neutrophils were identified as Ly6G$^+$CD11b$^+$ cells from CD45.2$^+$ live leukocytes and further exclusion of B cells (Gate on CD19$^-$ population). Ly6C$^+$CD11b$^+$ monocytes were gated on Ly6G$^-$ fraction. In parallel MHCII$^+$CD11c$^+$, identified from CD45.2$^+$ live, CD19$^-$ cells, were segregated into cDCs and CD64$^+$ Macrophages (MΦ). CDCs were further subdivided by CD103 and CD11b into cDC1, CD103$^+$ cDC2 (DP cDC2), CD103$^-$ cDC2 (SP cDC2) and DN DCs. **B.** Cell counts of live CD45.2$^+$ leukocytes in the tumor. **F.** Frequency out of leukocytes of Monocytes and Neutrophils, **G.** cDCs and Macrophages, and **H.** the subsets cDC1, DP cDC2, SP cDC2, and DN DC in the colonic tumors of *Clec9a*$^{cre/+}$*Bcl10*$^{fl/fl}$ mice and their controls after AOM-DSS treatment. Each dot represents a mouse. Data of one experiment. Bars indicate mean, error bars indicate SEM. Statistical analyses were done by t-test.

Assessing the overall immune cell infiltration by cell counting and normalization based on the tumor burden revealed increased amounts of immune cells within the tumors of *Clec9a*$^{cre/+}$*Bcl10*$^{fl/fl}$ mice. However, only a tiny fraction of mice were used for this measurement; hence, the other mice were used to perform single-cell RNA sequencing of tumor-derived cDCs and T cells. The same applies to the analysis of monocytes and neutrophils, even though a trend towards decreased neutrophils was observed in *Clec9a*$^{cre/+}$*Bcl10*$^{fl/fl}$ mice, whereby the frequency of monocytes spread throughout the group.

Analysis of total cDCs and macrophages revealed no difference in their frequency. In addition, cDC1, DP cDC2, SP cDC2, and DN DCs were found in similar frequency in the tumors of *Clec9a*$^{cre/+}$*Bcl10*$^{fl/fl}$ and control mice.

In summary, the deletion of BCL10 in cDCs did not affect the occurrence of cDC1s and the different cDC2 subsets in the colonic compartment during CAC.

3.4.2.2 Multiparameter spectral analysis of T cells from the tumor environment of *Clec9a*$^{cre/+}$*Bcl10*$^{fl/fl}$ mice after AOM-DSS

The primary function of cDCs is the activation of T cells, and the kind of T cell response highly influences tumor growth. Therefore, a multi-parameter spectral analysis profiled intra-tumoral T cells and T cells from surrounding non-tumorous CO LP and the CO LN.

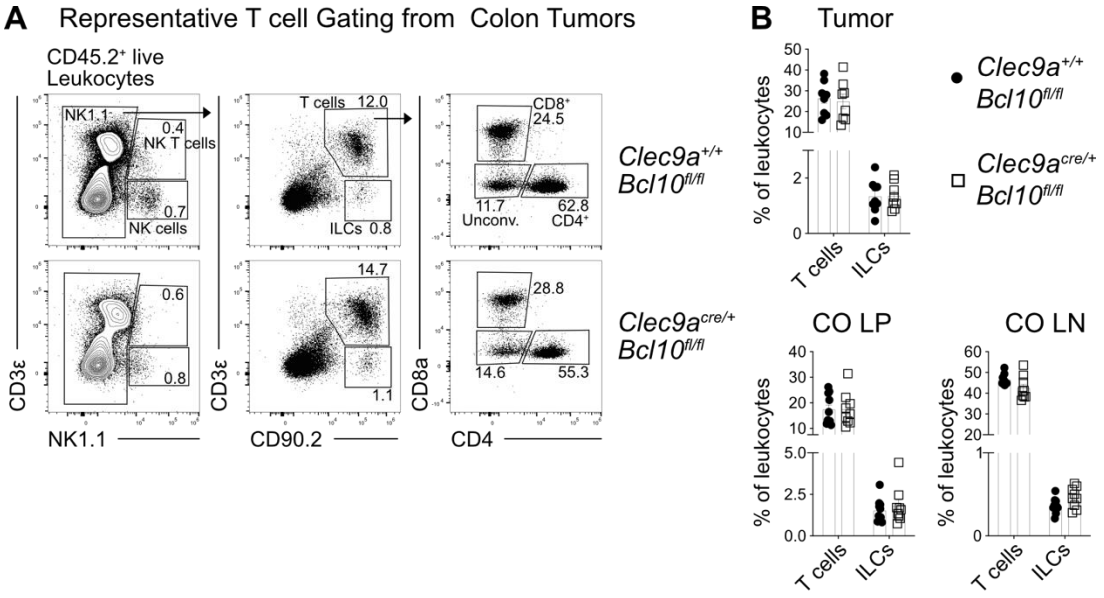

Figure 39 Identification of ILCs and T cells in colonic tumors after AOM-DSS and their frequencies.

A. Representative gating strategy to identify ILCs and T cells in AOM-DSS induced colonic tumors in *Clec9a*$^{+/+}$*Bcl10*$^{fl/fl}$ (top) and *Clec9a*$^{cre/+}$*Bcl10*$^{fl/fl}$ mice (bottom) mice. Before T cell identification NK1.1 positive NK T cells (NK1.1$^+$CD3ε$^+$) and NK cells (NK1.1$^+$CD3ε$^-$) were excluded from CD45.2$^+$ live leukocytes. From NK1.1 negative fraction, T cells were identified as CD3ε$^+$CD90.2$^+$ double positive cells and further subdivided by CD4 and CD8a. CD3ε$^-$CD90.2$^+$ were classified as ILCs. **B**. Frequency of T cells and ILCs in the tumor, the CO LP, and the CO LN of *Clec9a*$^{cre/+}$*Bcl10*$^{fl/fl}$ mice and their controls after AOM-DSS treatment. Each dot represents a mouse. Data of two independent experiments. Bars indicate mean, error bars indicate SEM. Statistical analyses were done by t-test.

The overall presence of T cells and ILCs was determined in the tumor, CO LP, and CO LN. In doing so, a similar gating strategy was used for all three organs (Figure 39). First, NK1.1 expressing NK cells and NK1.1$^+$CD3ε$^+$ NK T cells were gated on CD45.2$^+$ live leukocytes. T cells were identified within the NK1.1 negative population as double positive for CD90.2 and CD3ε.

Further, ILCs were detected in the same fraction of cells as CD90.2$^+$ and the lack of CD3ε. Similar frequencies of T cells and ILCs out of total leukocytes could be observed throughout all three organs in *Clec9a*$^{cre/+}$*Bcl10*$^{fl/fl}$ mice compared to control mice.

Comparison of the NK cell gating revealed a shift of this population within the gate in *Clec9a*$^{cre/+}$*Bcl10*$^{fl/fl}$ mice towards lower NK1.1 intensity. This decreased expression of NK1.1 was observed in the tumor, the CO LP, and the CO LN (Figure 40). Determination of the NK cell frequency revealed comparable values for the tumor and the CO LP, whereas NK cell frequency was increased in the CO LN of *Clec9a*$^{cre/+}$*Bcl10*$^{fl/fl}$ mice. Additional activation markers and cytokine production were analyzed because decreased NK1.1 can be a sign of NK cell exhaustion.

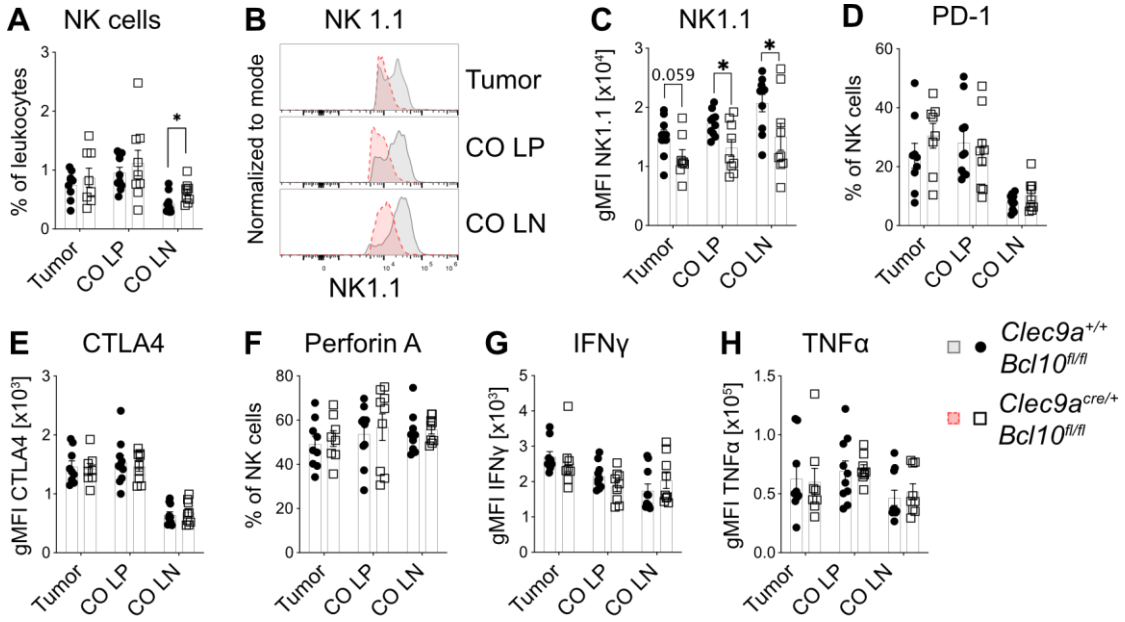

Figure 40 Reduced NK1.1 expression on NK cells from *Clec9a*$^{cre/+}$*Bcl10*$^{fl/fl}$ mice upon AOM-DSS treatment.

A. Frequency out of leukocytes of NK cells in the tumor, CO LP, and CO LN. **B**. Representative histogram overlays and **C.** GMFI of the NK1.1 fluorescent intensity of NK cells from tumor, CO LP, and CO LN of *Clec9a*$^{cre/+}$*Bcl10*$^{fl/fl}$ mice and their controls to compare NK1.1 expression level. **D.** Frequency of PD-1$^+$ NK cells, **E.** GMFI of the CTLA expression on NK cells, **F.** Frequency of Perforin A$^+$ NK cells, **G.** GMFI of the IFNγ expression in NK cells and **H.** GMFI of the TNFα expression in NK cells from the tumor, CO LP and CO LN of *Clec9a*$^{cre/+}$*Bcl10*$^{fl/fl}$ mice and their controls after AOM-DSS treatment. Each dot represents a mouse. Data of two independent experiments. Bars indicate mean, error bars indicate SEM. Statistical analyses were done by t-test. * p-value < 0.05

Similar amounts of PD-1-expressing cells and an equal expression level of CTLA4 were detected in the tumor, CO LP, and CO LN of *Clec9a*$^{cre/+}$*Bcl10*$^{fl/fl}$ mice. Further, no difference was observed in the production of IFNγ or the cytotoxic molecules Perforin A and Granzyme B. Therefore, besides the decreased level of NK1.1, no additional signs of NK cell exhaustion were observed.

Next, the frequency of the classical CD4 and CD8 T cells and the proportion of unconventional T cells were determined. This revealed an equal infiltration of the tumors by all three T cell subsets and similar T cell frequencies within the CO LP of *Clec9a*$^{cre/+}$*Bcl10*$^{fl/fl}$ and control mice. Nevertheless, the CO LN of *Clec9a*$^{cre/+}$*Bcl10*$^{fl/fl}$ mice harbored fewer CD8 T cells, whereas CD4 and unconventional T cells appeared normal.

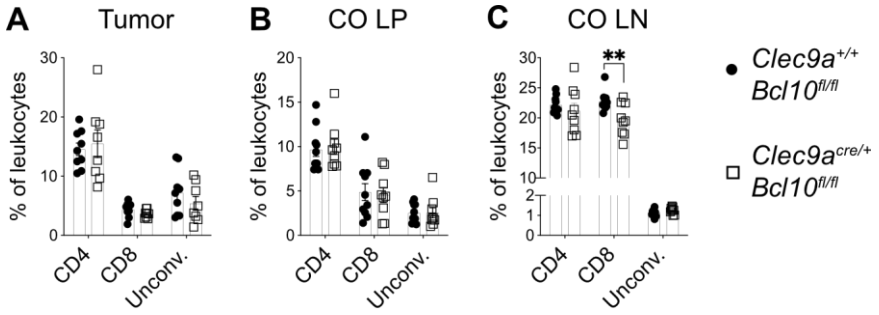

Figure 41 Reduction of CD8 T cells in the CO LN of *Clec9a*$^{cre/+}$*Bcl10*$^{fl/fl}$ mice after AOM-DSS treatment.

Frequency out of leukocytes of CD4, CD8, and unconventional T cells in the **A.** Tumor, **B**. CO LP and **C.** CO LN of *Clec9a*$^{cre/+}$*Bcl10*$^{fl/fl}$ mice and their controls after AOM-DSS treatment. Each dot represents a mouse. Data of two independent experiments. Bars indicate mean, error bars indicate SEM. Statistical analyses were done by t-test. ** p-value < 0.01

For in-depth analysis of T cell phenotype, CD90.2$^+$CD3ε$^+$ T cells from both genotypes were concatenated in a 50:50 ratio and subjected to unbiased clustering (Figure 43). Manually gated Tregs are depicted separately, and the remaining Foxp3 negative CD4 T cells were subdivided into CD44$^-$ and CD44$^+$ fractions. CD8-expressing T cells and unconventional T cells were identified and, like CD4 T cells, segregated into a CD44$^-$ and CD44$^+$ population. This separation by CD44 was done, as each T cell subset formed two distinct clusters, whereby the main feature of this division was the CD44 expression. UMAPs of the tumor, the CO LP, and the CO LN were split based on the genetic background of the cells. Comparing the cluster appearance revealed no significant difference since every cluster was found in both genotypes. Besides the general occurrence of each T cell population, the overall T cell composition was assessed in each profiled organ. Whereas a similar distribution of activated and CD44 negative CD4, CD8, and unconventional T cell and Tregs was found in the CO LP and CO LN, a shift towards increased CD4 T cells was observed in the tumor of *Clec9a*$^{cre/+}$*Bcl10*$^{fl/fl}$ mice whereby unconventional T cells decreased. Further, the proportion of activated CD44$^+$ CD8 T cells was reduced, wherein overall CD8 T cell presence was not altered.

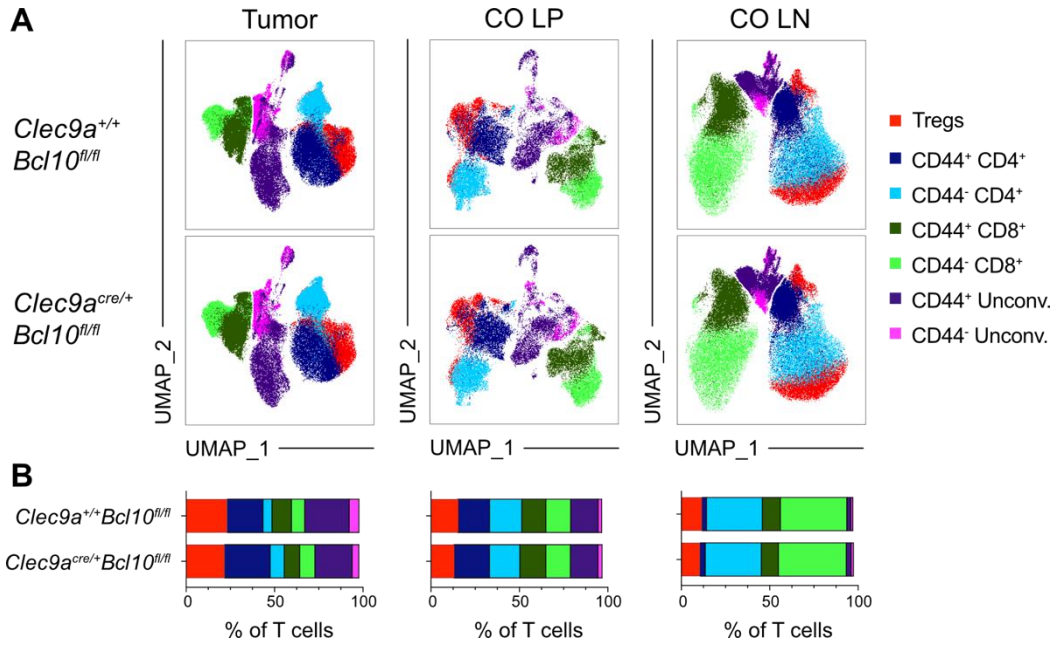

Figure 42 Unbiased clustering of multi-parameter spectral analysis of T cells from tumor, CO LP, and CO LN from *Clec9a$^{cre/+}$Bcl10$^{fl/fl}$* mice after AOM-DSS.
A. UMAP projection of T cells from tumor, CO LP, and CO LN separated by the genotypic background. (*Clec9a$^{+/+}$Bcl10$^{fl/fl}$* (top) and *Clec9a$^{cre/+}$Bcl10$^{fl/fl}$* mice (bottom)) **B.** Cluster distribution within total T cells of tumor, CO LP, and CO LN from *Clec9a$^{+/+}$Bcl10$^{fl/fl}$* and *Clec9a$^{cre/+}$Bcl10$^{fl/fl}$* mice.

Next, each cluster was compared between the genotypes for the expression of the activation markers CD69, CD44, and CD25. In addition, the expression pattern of PD-1 and CTLA4 was assessed, markers known to be expressed on exhausted or pro-tumorigenic T cells (Figure 43). No significant alterations were observed in the T cells from CO LP and CO LN (data not shown). Further on, expression of CD69 and CD44 appeared in a similar intensity and frequency in CD4, CD8, and unconventional T cell clusters from the *Clec9a$^{cre/+}$Bcl10$^{fl/fl}$* mice tumors. For CD25, a slight increase was observed for activated CD4 T cells but not in other T cell subsets in those mice. Evaluation of PD-1 expression revealed a substantial rise in PD-1 positive CD44$^+$ CD4 T cells in the tumors isolated from *Clec9a$^{cre/+}$Bcl10$^{fl/fl}$* mice.

In contrast, PD-1 level in Tregs appeared slightly diminished, and CTLA4 was significantly less expressed on tumor-derived Tregs from mice with BCL10 deficient cDCs. Within CD8 and unconventional T cells, no drastic differences were observed. Even though, in both CD44$^-$ fractions, PD-1 expressing cells were marginally decreased in tumors originating from *Clec9a$^{cre/+}$Bcl10$^{fl/fl}$* mice. Thus, the distribution of T cell subsets within total T cells and the alterations in PD-1 and CTLA4 expression revealed considerable changes in the CD4 T cell compartment.

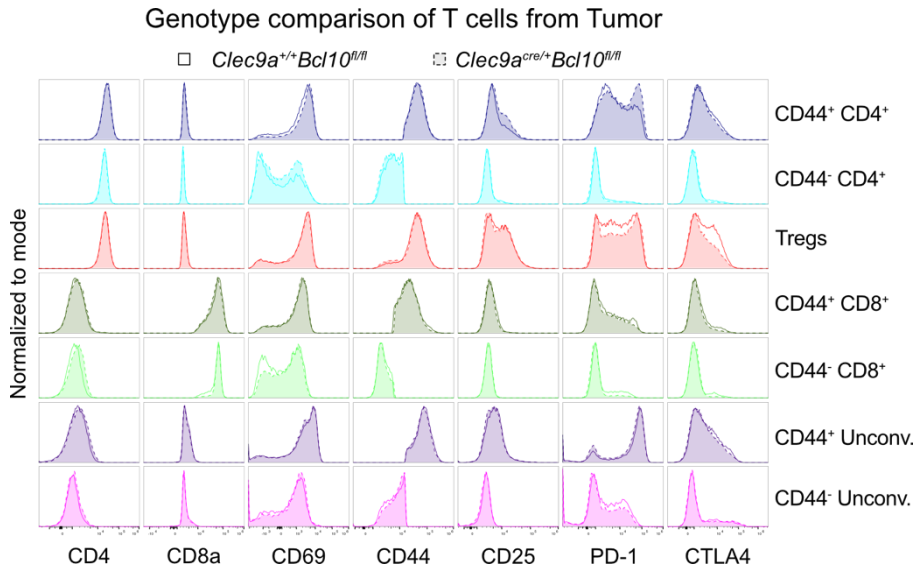

Figure 43 Histogram depiction of surface marker expression by each T cell cluster from the tumor.

Comparison of each identified T cell cluster from the tumors of *Clec9a*$^{+/+}$*Bcl10*$^{fl/fl}$ (line, clear) and *Clec9a*$^{cre/+}$*Bcl10*$^{fl/fl}$ mice (dotted line, filled) for the expression of CD4 and CD8a and different activation markers.

As previously observed in CD4 T cells isolated from the CO LP from steady-state or *Clec9a*$^{cre/+}$*Bcl10*$^{fl/fl}$ mice with acute colitis, CD4 T cells derived from the tumor environment of those mice showed a trend towards decreased Th17-related cytokines, in particular IL-17F and IL-22. However, the decrease was not statistically significant, and unconventional T cells produced the same cytokines in equal amounts. The frequency of CD4 T cells, positive for the anti-inflammatory cytokine IL-10, appeared similar in both groups. Cytotoxic molecules like Granzyme B and Perforin A were produced predominantly by CD8 and unconventional T cells. However, no difference was observed between the T cells of *Clec9a*$^{cre/+}$*Bcl10*$^{fl/fl}$ and control mice. Last, IFNγ production was assessed in all three T cell subsets, and equal frequencies of IFNγ^{+} cells were detected in the tumors of *Clec9a*$^{cre/+}$*Bcl10*$^{fl/fl}$ and control mice (Figure 44).

In addition to cytokine measurement within certain cell types via flow cytometric analysis, the overall cytokine milieu was analyzed through tissue cytokine extraction from tumors. This method revealed comparable levels of TNFα but decreased IFNγ in the colonic tumors of *Clec9a*$^{cre/+}$*Bcl10*$^{fl/fl}$ mice. As the detected IFNγ in NK and T cells was similar between the genotypes, this overall reduced IFNγ might reflect a reduced presence of T cells. Further, the same trend of less IL-17F and IL-22, found in tumor CD4 T cells, was observed in the total tumor cytokine milieu. Last, the total amount of IL-10 was detected in equal amounts in tumors of *Clec9a*$^{cre/+}$*Bcl10*$^{fl/fl}$ and the control mice.

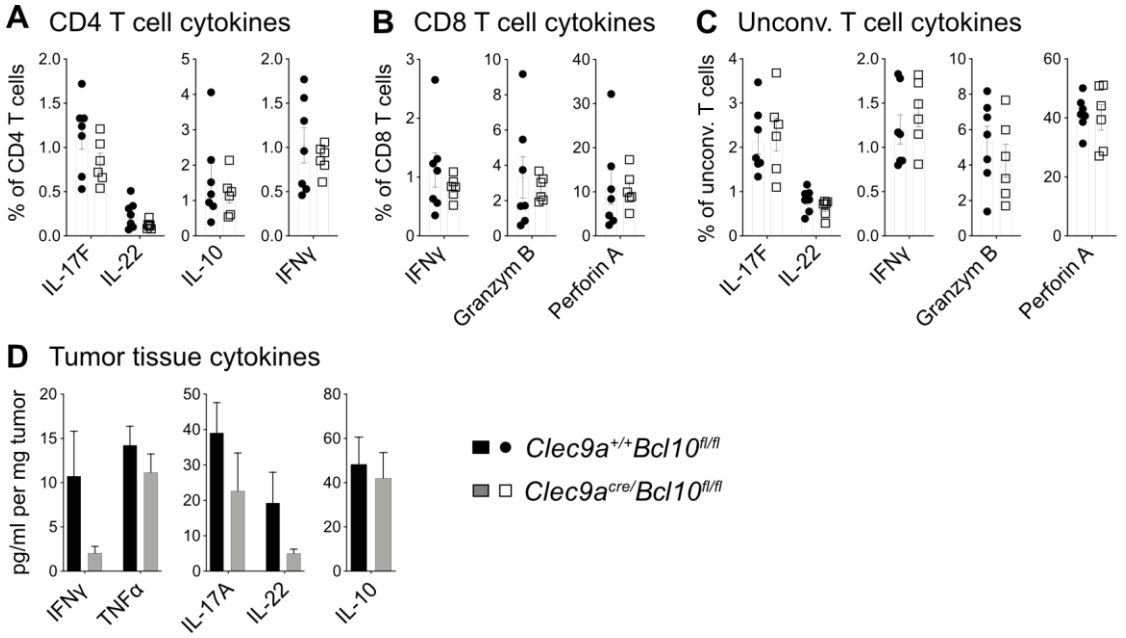

Figure 44 Cytokine expression of the different T cell subsets in Clec9acre/+Bcl10fl/fl mice colonic tumors after AOM-DSS.

Frequency out of the respective T cell subsets **A.** of IL-17F, IL-22, IL-10, and IFNγ expression in CD4 T cells, **B**. of IFNγ, Granzyme B, and Perforin A expression in CD8 T cells, and **C.** of IL-17F, IL-22, IFNγ, Granzyme B and Perforin A expression in unconventional T cells from the tumors of *Clec9a*$^{cre/+}$*Bcl10*$^{fl/fl}$ mice and their controls after AOM-DSS treatment. Each dot represents a mouse. (Representative data of one out of two independent experiments.) **D.** Analysis of IFNγ and TNFα, IL-17F and IL-22 and IL-10 in the tissue cytokine extraction supernatants of tumors (Data from two independent experiments. Mice per group: control mice n = 13, *Clec9a*$^{cre/+}$*Bcl10*$^{fl/fl}$ n = 10). Bars indicate mean, error bars indicate SEM. Statistical analyses were done by t-test.

To conclude findings within the T cells and ILC compartment, decreased expression of NK1.1 was found on NK cells in all three colonic organs (CO LP, CO LN & tumor) of *Clec9a*$^{cre/+}$*Bcl10*$^{fl/fl}$ mice, indicating NK cell exhaustion. Further on, fewer CD8 T cells were detected in the CO LN and fewer activated CD8 T cells in the *Clec9a*$^{cre/+}$*Bcl10*$^{fl/fl}$ mice tumors. Last, a shift towards CD4 T cells and less unconventional T cells were found in the tumor environment, with a lower level of Th17-related cytokines when BCL10 was deleted in cDCs.

3.4.3 scRNA seq of the colon from *Clec9a*^{cre}*BCl10*^{flox} mice after AOM-DSS

AOM-DSS treatment led to increased tumor development in the colon of *Clec9a*$^{cre/+}$*Bcl10*$^{fl/fl}$ mice. Even though the frequency of cDCs with BCL10 deletion was not altered, changes within the T cell compartment could be observed in the tumor. To further dissect the effects of loss of BCL10 in cDCs in a tumor environment, transcriptional profiling was performed on a single cell level. In addition, the T cell and ILC compartment were subjected to similar analysis to gain in-depth information about alterations. For this purpose, leukocytes were isolated from tumors from *Clec9a*$^{cre/+}$*Bcl10*$^{fl/fl}$ and

control mice. First, CD90.2$^+$ were sorted directly from CD45.2$^+$ live leukocytes. From CD90.2 and CD19 double negative cells, MHCII$^+$CD11c$^+$ were selected. Next, CD64 negative cells were identified as cDCs and sorted. Purity for cDCs and CD90.2$^+$ sorted from the tumor of *Clec9a*$^{+/+}$*Bcl10*$^{fl/fl}$ and *Clec9a*$^{cre/+}$*Bcl10*$^{fl/fl}$ after AOM-DSS (Figure 45) was confirmed. After sorting, genotypes were pooled per cell type for further processing and sequencing.

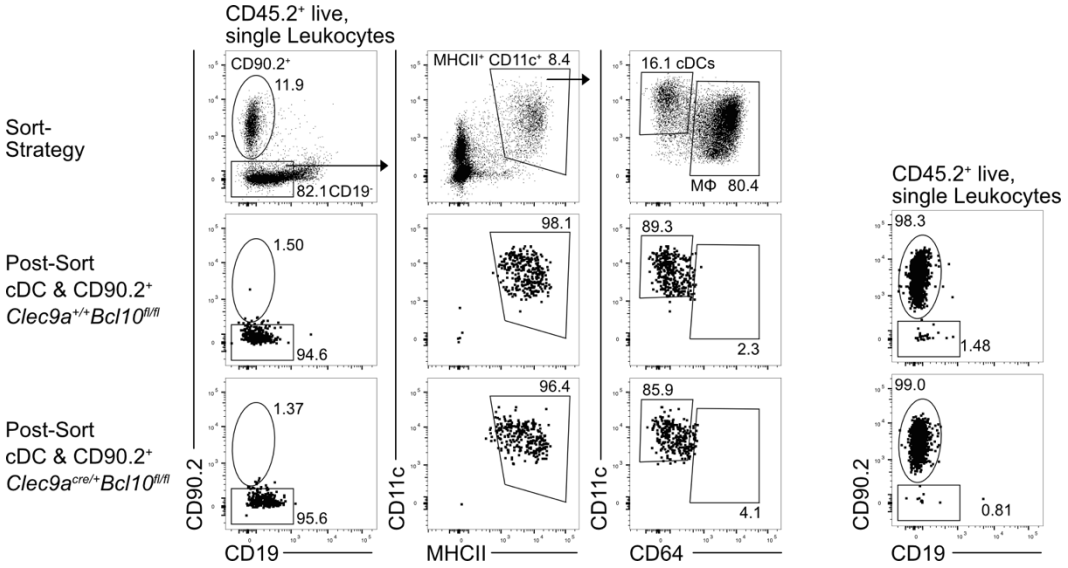

Figure 45 Sort strategy and purity check of cDCs and CD90.2$^+$ isolated from colonic tumors induced by AOM-DSS.

Representative gating to sort cDCs and CD90.2$^+$ cells for scRNA sequencing from the tumors of *Clec9a*$^{cre/+}$*Bcl10*$^{fl/fl}$ mice and their controls after AOM-DSS treatment. CD90.2$^+$ cells were directly identified and sorted from pre-gated CD45.2$^+$ live Leukocytes (Plots on the right). For cDC gating, CD90.2$^+$ and CD19$^+$ B cells were excluded before MHCII$^+$CD11c$^+$ gating. From there, CD64$^+$ macrophages were excluded, and CD64$^-$ cDCs were identified and selected for sorting.

3.4.3.1 Single-cell RNA sequencing of tumor-derived cDCs from *Clec9a*$^{cre/+}$*Bcl10*$^{fl/fl}$ mice

Aligned sequencing data was put through quality control, resulting in 4180 cells with an overall sequencing depth of 15711 reads per cell and an average number of 3285 genes per cell. UMAP approximation of this data set revealed seven clusters upon which one could be identified as highly proliferating cells (Figure 46). In contrast to the previous sequencing of cDCs from CO LP, cDCs derived from the tumors of *Clec9a*$^{cre/+}$*Bcl10*$^{fl/fl}$ cluster together with control cells. Examination of the cluster for the expression of classical cDC genes (*Flt3l, Itgax, Zbtb46*) identified four clusters of cDCs. One cluster showed *Cx3cr1*, *Mafb*, and *Cd63* expression and was classified as a macrophage population. The last cluster consisted of a small fraction of cells positive for *Siglech* and, therefore, identified as pDCs. Two out of four cDC clusters expressed *Irf8*, *Xcr1,* and *Itgae,* allowing their classification as cDC1.

The separation into two clusters was attributed to the increased expression of activation markers (e.g., *Ccr7*, *Ccl22*, *Cd40*, *Cd86*), whereby one of these cDC1 clusters was classified as activated cDC1. Further on, cDC2s were encountered by detecting *Irf4*, *Sirpa*, *Itgam,* and *Cd209a*. The remaining cDC cluster was classified as a migratory DC population marked by high *Ccr7*, *Fscn1,* and *Ccl22*.

Comparison of the occurrence of both genotypes showed an equal distribution within each identified cluster of cells derived from either *Clec9a*$^{+/+}$*Bcl10*$^{fl/fl}$ or *Clec9a*$^{cre/+}$*Bcl10*$^{fl/fl}$ tumor mice.

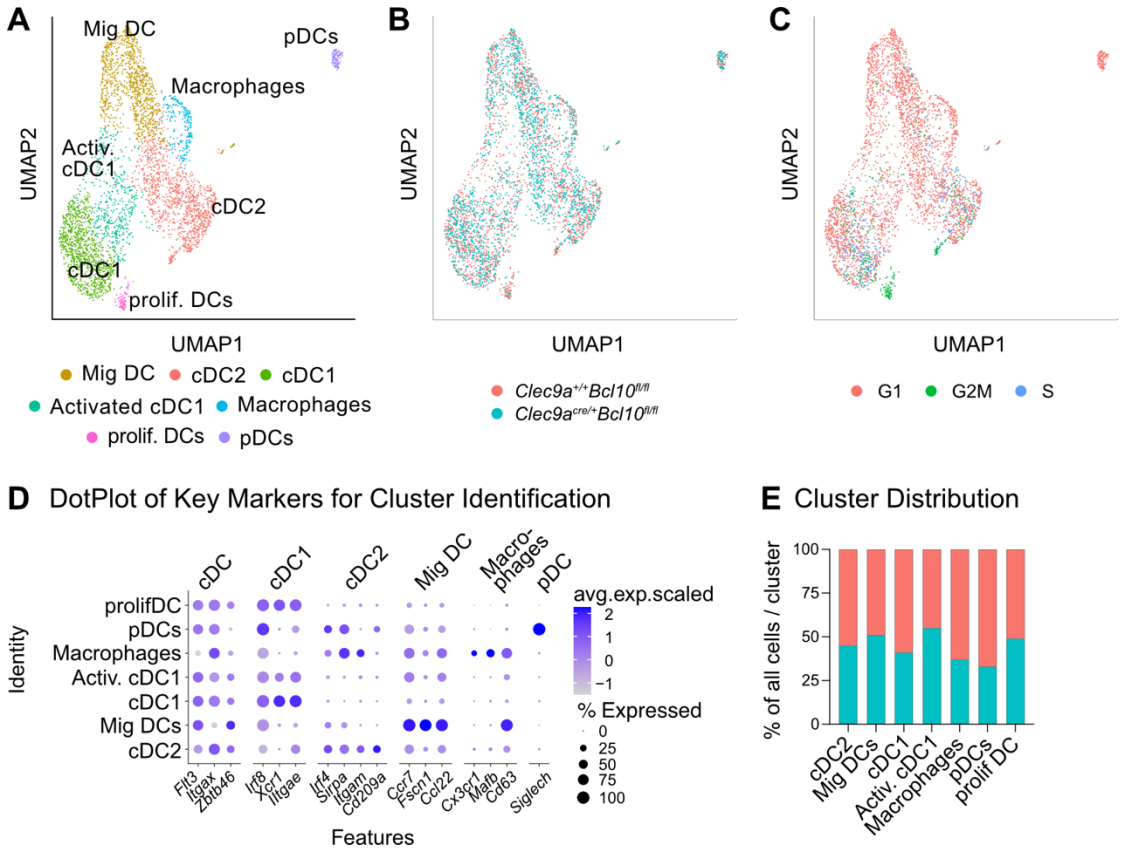

Figure 46 UMAP depiction of tumor cDCs based on their transcriptional profile.
A. Unbiased clustering of colonic tumor MHCII^{+}CD11c^{+}CD64^{-} cDCs resulted in seven clusters. **B.** cDCs from different genetic background overlap in UMAP depiction. **C.** Highly proliferating cells (G2M phase) form a separate cluster. **D.** Dot plot shows cluster identification based on cell-specific genes. **E.** Genotype distribution within every cDC and other clusters.

Having identified several cDC clusters, the transcriptional level of classical activation markers was compared between *Clec9a*$^{cre/+}$*Bcl10*$^{fl/fl}$ derived cells and their controls (Figure 47). Within the cDC1s, no *Cd40* expression could be detected in both genotypes, whereas a decreased level of *Cd40* was detected in the activated cDC1s of *Clec9a*$^{cre/+}$*Bcl10*$^{fl/fl}$ mice. Less *Cd40* could also be observed for cDC2 and migratory DCs. Latter ones showed a reduction in *Cd86* as well. No differences could be detected in the expression levels of *Cd80* and *Cd274*, encoding PD-L1, in any of the cDC clusters.

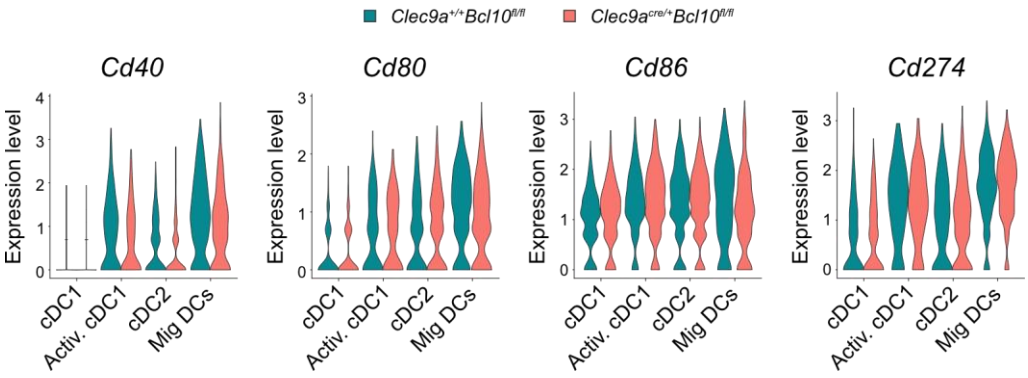

Figure 47 Transcriptional expression level of activation markers by cDCs.
The expression level of *Cd40, Cd80*, *Cd86,* and *Cd274* by cDC1, activated cDC1, cDC2, and migratory DCs cluster derived from the tumors of *Clec9a*$^{+/+}$*Bcl10*$^{fl/fl}$ or *Clec9a*$^{cre/+}$*Bcl10*$^{fl/fl}$ mice.

Based on the previous finding of an altered metabolic state in cDCs upon deletion of BCL10, the same pathways were investigated in the current sequencing data set of tumor-derived cDCs from *Clec9a*$^{cre/+}$*Bcl10*$^{fl/fl}$ mice. However, no changes in the overall expression of genes contributing to OXPHOS were detected. Further, equal levels of ROS response and mTOR signaling were determined within cDC1, activated cDC1, cDc2, and migratory DCs.

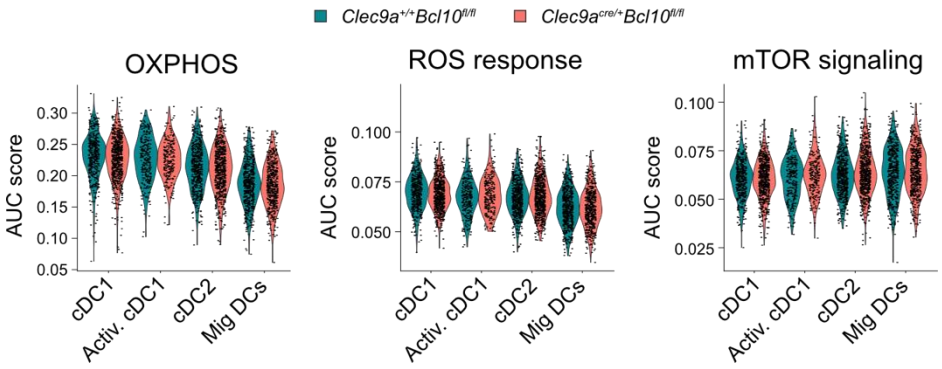

Figure 48 AUC score of metabolic and stress response pathways in different DC clusters.
Analysis of the area under the curve for gene signatures of OXPHOS, ROS response, and mTOR signaling for each (c)DC cluster with the two genotypes obtained from scRNA sequencing of cDCs from colonic tumors.

Next, differential gene expression analysis between cells from *Clec9a*$^{+/+}$*Bcl10*$^{fl/fl}$ *and Clec9a*$^{cre/+}$*Bcl10*$^{fl/fl}$ mice was performed for all identified clusters. Subsequently, genes compiling the heat shock protein 70 (HSP70) complex were the differential expressed genes with the highest negative $\log_2$-foldchange in both the cDC1 and cDC2 clusters (Figure 49). Calculating the average expression of all genes contributing to HSP70 revealed a decreased level in cDC1s and cDC2s.

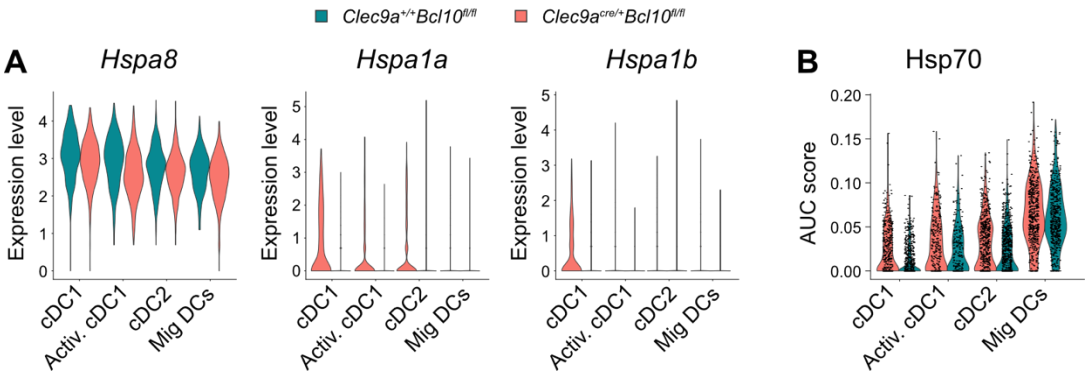

Figure 49 Decreased transcriptional level of Hsp70 genes in cDCs derived from colonic tumors of *Clec9a$^{cre/+}$Bcl10$^{fl/fl}$* mice.

A. Expression level of *Hspa8*, *Hspa1a* and *Hspa1b* and **B.** AUC score of all Hsp70 contributing genes in the four different DC clusters identified in the UMAP analysis of cDCs from colonic tumors of *Clec9a$^{+/+}$Bcl10$^{fl/fl}$ and Clec9a$^{cre/+}$Bcl10$^{fl/fl}$* mice.

3.4.3.2 Single-cell RNA sequencing of CD90.2^{+} from colonic tumors of *Clec9a$^{cre/+}$Bcl10$^{fl/fl}$* mice

For the CD90.2^{+} cells isolated from the AOM-DSS-induced colon tumors of *Clec9a$^{+/+}$Bcl10$^{fl/fl}$ and Clec9a$^{cre/+}$Bcl10$^{fl/fl}$* mice, 11984 cells were recovered after alignment and downstream quality processing. Within these ~12.000 cells, approximately 2378 genes were detected per cell, and 8181 total transcripts were sequenced per cell. UMAP approximation of these T cells and ILCs led to 17 clusters (Figure 50). Separation based on the genotypic background of the cells showed an overlap of *Clec9a$^{+/+}$Bcl10$^{fl/fl}$ and Clec9a$^{cre/+}$Bcl10$^{fl/fl}$* derived cells for all clusters. Cell cycle regression and projection onto the UMAP identified one cluster as highly proliferating cells. Examination of *Cd3e* expression identified 10 clusters as T cells. Out of these, one cluster expressed high levels of *Sell* (CD62L) together with *Cd4*, *Cd8a,* and *Cd8b*, therefore classified as naïve T cells containing CD4 and CD8 T cells. Three clusters of conventional CD4 T cells were detected and further subdivided into Treg (*Foxp3* & *Ctla4*), Rorγt^{+} Treg (*Foxp3, Rorc* & *Ctla4*), and a CD4 T cell cluster expressing *Gata3* and *Tbc1d4*. Further on, conventional CD8 T cells (*Cd8a* & *Cd8b*) cluster close to other cytotoxic cells, like NK cells (*Klrb1c*, *Klrd1* & *Xcl1*) and NK T cells (*Cd3e*, *Klrd1* & *Xcl1*). An additional *CD8a* expressing cluster was identified as CD8aa IEL. Three clusters of T cells neither expressed *Cd4*, *Cd8a,* or *Cd8b* and were identified as the unconventional T cells known from flow cytometric analysis. All three expressed *Rorc;* however, only the larger clusters were classified as TCRγδ cells, separating due to high *Areg* and *Pdcd1*. The last T cell cluster lacking *Cd4* and *Cd8a/b* expression was DN Th17. Besides the two clusters, consisting of DC (*Itgax*, *Ccr7*) and B cell (*Jchain*) contaminations, one more cluster was identified as ILC2s through the expression of *Gata3*, *Rora,* and the lack of *Cd3e*.

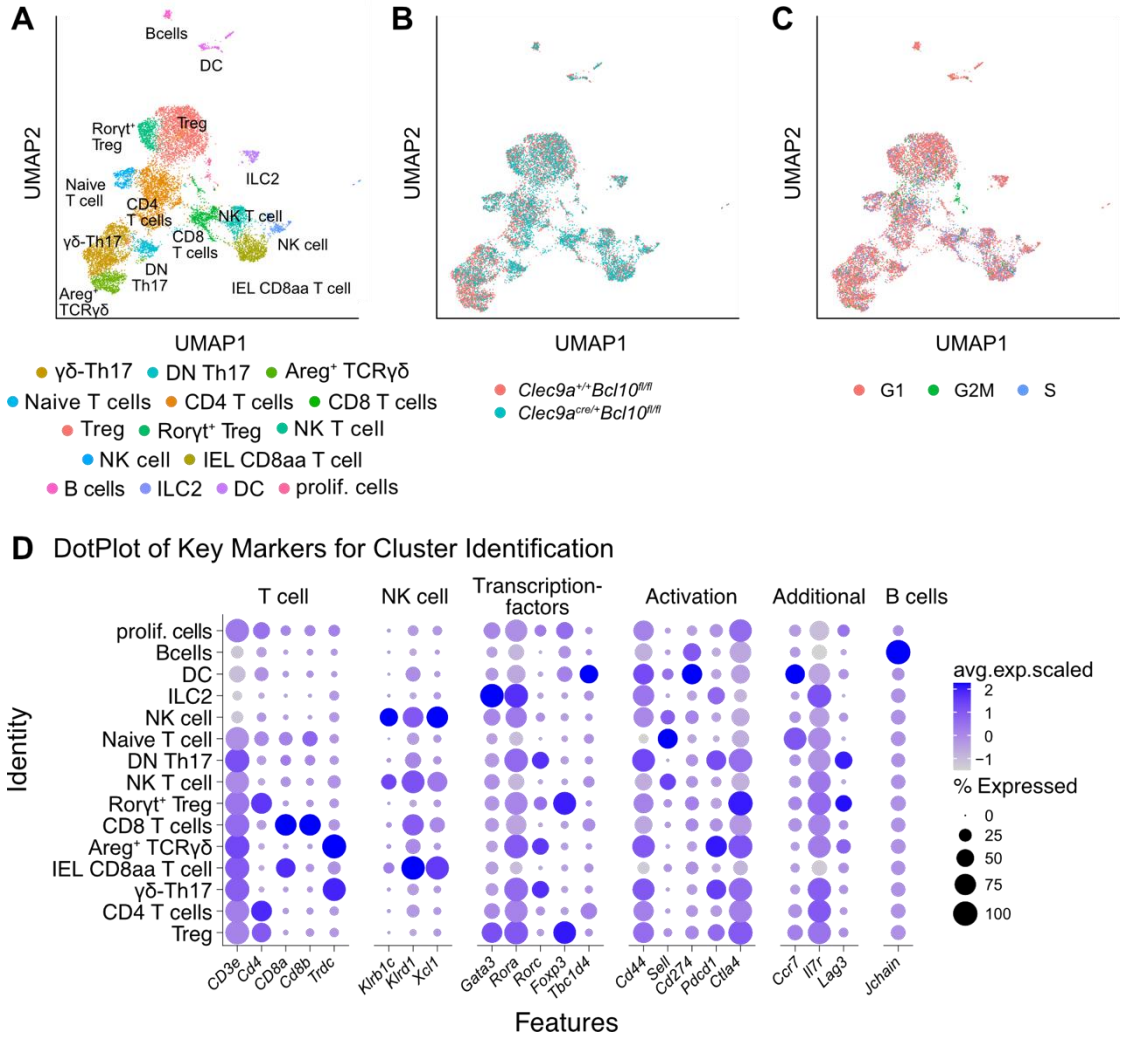

Figure 50 Unbiased clustering of CD90.2⁺ cells from AOM-DSS induced tumors.
A. Unbiased clustering of colonic tumor CD.90.2⁺ cells resulted in 17 clusters. **B.** Cells from different genotypes cluster together. **C.** Highly proliferating cells (G2M phase) form a separate cluster. **D.** Dot plot shows cluster identification based on cell-specific genes like transcription markers.

Next, the frequency of each cluster/cell type out of all sequenced cells was determined. Before doing so, DC and B cell contaminations and the highly proliferating cells were excluded. The distribution of these cells derived from Clec*9a*$^{+/+}$*Bcl10*$^{fl/fl}$ *or* *Clec9a*$^{cre/+}$*Bcl10*$^{fl/fl}$ mice was equal; therefore, the exclusion did not influence further calculations.

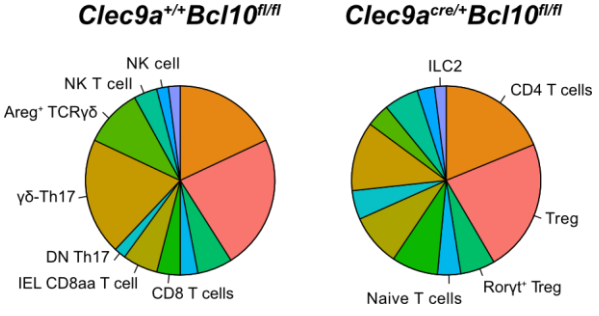

Figure 51 Distribution of clusters within total cells derived from tumors of Clec*9a*$^{+/+}$*Bcl10*$^{fl/fl}$ *or* *Clec9a*$^{cre/+}$*Bcl10*$^{fl/fl}$ mice.
Frequency of each cluster out of all relevant clusters per genotype. (Exclusion of DC and B cell contamination and highly proliferating cells)

All CD4 T cell clusters (CD4 & Treg clusters) showed an equal presence in both genotypes. However, alterations could be observed within the compartment of cytotoxic cells. Whereby the fraction of CD8 T cells and IEL CD8aa T cells was increased in *Clec9a*$^{cre/+}$*Bcl10*$^{fl/fl}$ mice, the proportion of both γδ T cell clusters was diminished. This decrease was already visible in the UMAP projections, as the density of *Clec9a*$^{cre/+}$*Bcl10*$^{fl/fl}$ derived cells was less within the γδ T cell clusters. No significant changes were found for NK (T) cells and ILC2s.

Nevertheless, CD4 T cells were detected in similar frequency in both genotypes. DEG analysis revealed the most significant changes in this cell type. Within this, the pro-inflammatory cytokines *Il17f* and *Il17a* were decreased together with *Il22*. Further, additional markers of Th17 cells like *Batf, Ikzf3,* and *Ccr6* were lower expressed in CD4 T cells isolated from the *Clec9a*$^{cre/+}$*Bcl10*$^{fl/fl}$ mice tumors. Along with this loss of pro-inflammatory Th17 markers, the immuno-suppressive markers *Pdcd1, Cd274,* and *Il10* appeared to be increased, with a significantly higher expression of *Lgals3*. This gene encodes the lectin Galectin-3, described in the literature to suppress cytotoxic CD8 T cells in the anti-tumor response (Kouo et al. 2015).

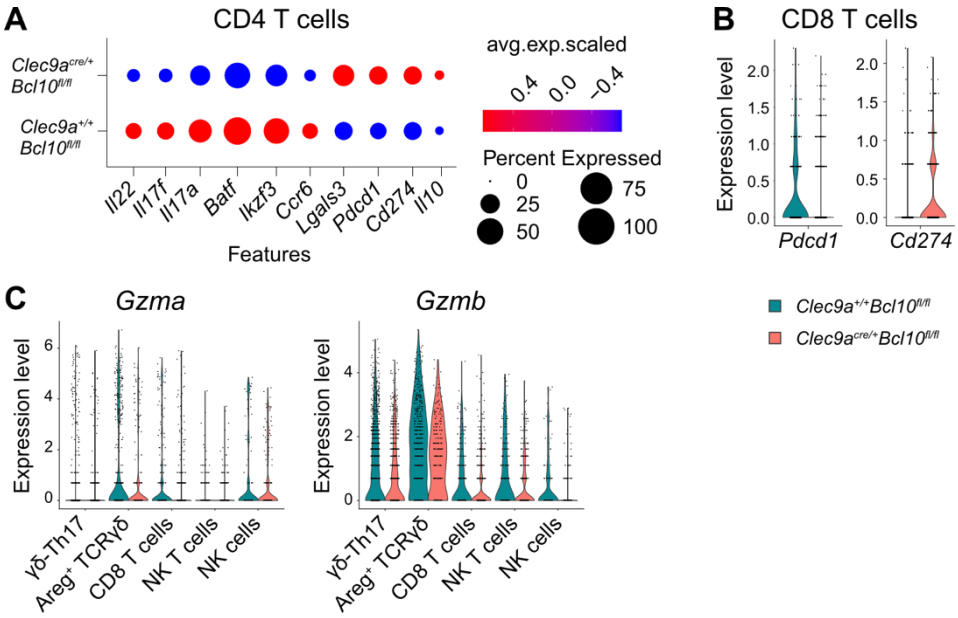

Figure 52 Gene expression comparison within different T cell and NK (T) cell clusters.
A. Differential gene expression of the Th17-related *Il22*, *Il17f*, *Il17a*, *Batf*, *Ikzf3,* and *Ccr6* and the tolerogenic markers *Lgals3*, *Pdcd1*, *Cd274,* and *Il10* within CD4 T cell cluster between-*Clec9a*$^{+/+}$*Bcl10*$^{fl/fl}$ and *Clec9a*$^{cre/+}$*Bcl10*$^{fl/fl}$ derived cells. **B.** Expression level of Pdcd1 and Cd274 in CD8 T cell cluster separated by genotype origin. **C.** Comparison of the transcriptional level of *Gzma* and *Gzmb* in different clusters between cells originated from *Clec9a*$^{+/+}$*Bcl10*$^{fl/fl}$ or *Clec9a*$^{cre/+}$*Bcl10*$^{fl/fl}$.

Even though the DEG analysis did not reveal significant alterations between CD8 T cells from *Clec9a*$^{+/+}$*Bcl10*$^{fl/fl}$ and *Clec9a*$^{cre/+}$*Bcl10*$^{fl/fl}$ mice, less *Pdcd1* expression was found in CD8 T cells from *Clec9a*$^{cre/+}$*Bcl10*$^{fl/fl}$ mice, whereas *Cd274* was increased.

Last, the expression of genes encoding cytotoxic molecules was assessed in several cell types known to harbor cytotoxic functions. In doing so, less *Gzma* and *Gzmb* expression was detected in the γδ T cell clusters, CD8 T cells, and NK and NK T cells. Indicating a loss of cytotoxicity within the tumor T cell compartment in parallel to a shift towards a more immuno-suppressive, less inflammatory CD4 T cell population, leading to increased tumor growth in *Clec9a*$^{cre/+}$*Bcl10*$^{fl/fl}$ mice.

3.5 In-vitro T cell Assays to assess T cell activation capacity of colonic cDCs from *Clec9a*$^{cre/+}$*Bcl10*$^{fl/fl}$ mice

To investigate if intestinal cDCs from Clec*9a*$^{cre/+}$*Bcl10*$^{fl/fl}$ mice have a defect in activating and polarizing T cells, in vitro co-cultures were performed with cDCs sorted from the CO LP of *Clec9a*$^{+/+}$*Bcl10*$^{fl/fl}$ and *Clec9a*$^{cre/+}$*Bcl10*$^{fl/fl}$ mice. Representative sorting strategy and purity check are depicted in Figure 53.

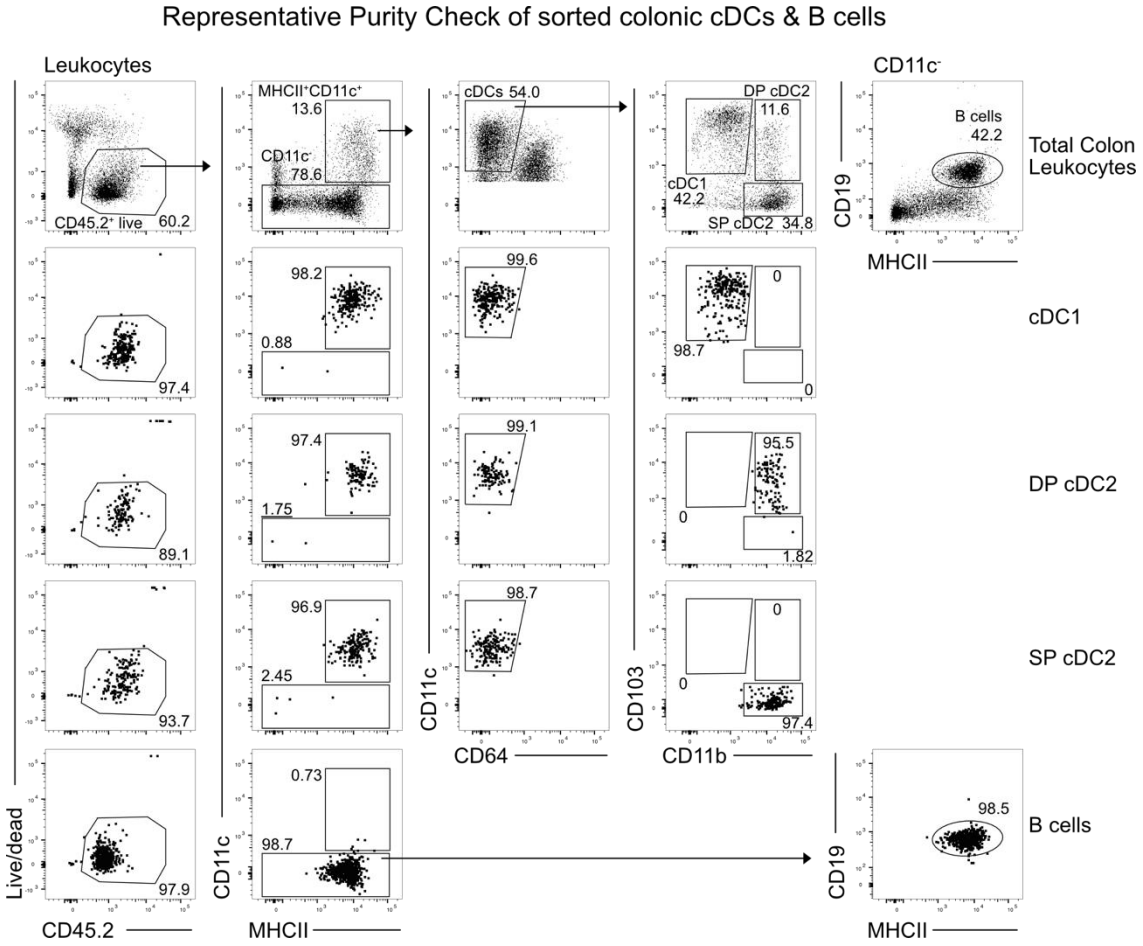

Figure 53 Sorting strategy and purity check of cDCs and B cells from the CO LP.
Representative gating strategy to sort three cDC subsets and B cells from the CO LP (Top). Leukocytes were identified as CD45.2+ live cells. Next, CD11c+MHCII+ cells were gated, and cDCs were further identified as CD64- population. The three cDC subsets were sorted and purity was assessed cDC1 (2nd row), DP cDC2 (3rd row), and SP cDC2 (4th row) were selected for sorting. From the CD11c negative fraction, B cells were identified as CD19^{+}MHCII^{+} cells (Purity check: bottom).

As previously described, within the MHCII$^+$CD11c$^+$ population, cDCs were segregated from macrophages by CD64 and further subdivided into CD103$^+$ cDC1, CD103$^+$ CD11b$^+$ cDC2, and CD103$^-$ cDC2. In parallel, CD19$^+$MHCII$^+$ B cells were selected for sorting. Sorted APCs were co-cultured in different DC : T cell ratios in the presence of OVA protein with either CD4 or CD8 T cells.

3.5.1 In-vitro T cell Assay to address the capacity of colonic, BCL10-deficient cDCs to activate and polarize CD4 T cells

The capacity of BCL10 deficient cDCs to activate and polarize CTV labeled CD4 T cells was determined in the first step through the amount of activated and proliferated T cells (CD90.1$^+$ CD4$^+$ TCR Vα2$^+$) identified based on the diluted CTV signal (Figure 54). Within these CTV-negative T cells, the expression of Foxp3 was analyzed to identify Tregs. In parallel, the production of TNFα and IFNγ was determined.

To investigate the capacity of colonic cDCs from *Clec9a$^{cre/+}$Bcl10$^{fl/fl}$* mice to induce Tregs, cell counts of proliferated T cells (CTV$^-$) and frequency of Foxp3$^+$ cells were determined after co-culturing cDC1, DP cDC2, and SP cDC2 with CD4 T cells under Treg polarizing conditions. In doing so, no differences in total proliferated T cells nor the presence of Tregs were observed when comparing BCL10 deficient cDCs to control cells.

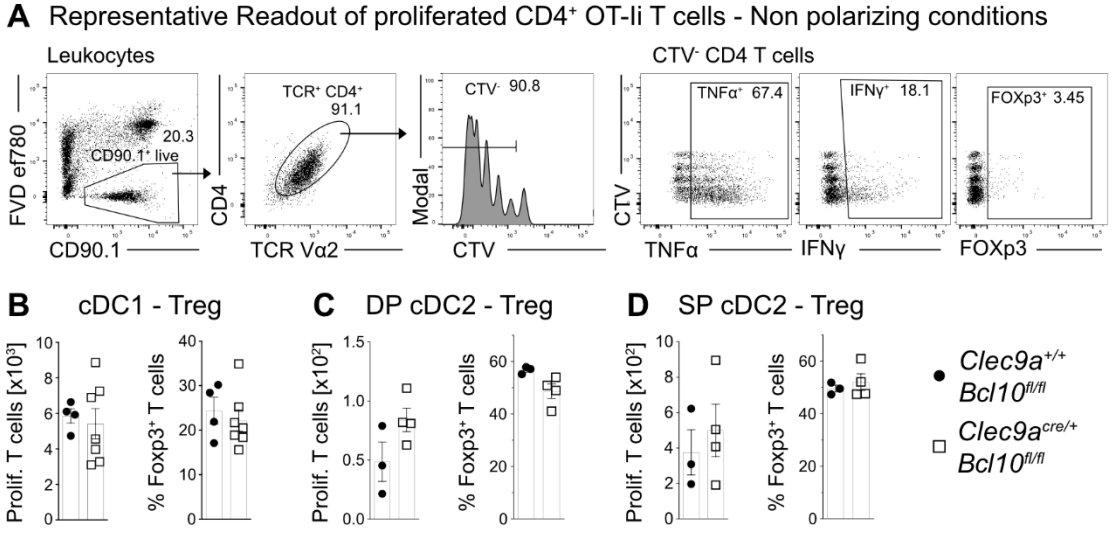

Figure 54 CD4 T cell activation by colonic cDC subsets under Treg polarizing conditions. **A.** Representative gating to analyze proliferated CD4 T cells in the presence of colonic cDCs without polarizing conditions (Th0). T cells were identified as CD90.1$^+$ live cells and further gating on CD4 and TCR Vα2. Proliferated cells were selected based on their CTV expression. Within proliferated (CTV$^-$) cells, TNFα and IFNγ expressing cells were gated. And Tregs were identified as Foxp3$^+$. **B.** Cell counts of proliferated (CTV$^-$) T cells and frequency of Foxp3$^+$ cells within the proliferated T cells after co-culture of OT-II cells in the presence of cDC1, DP cDC2 or cDC2 from *Clec9a$^{cre/+}$Bcl10$^{fl/fl}$* CO LP or their controls, under Treg polarizing conditions. Data of two independent experiments. Each dot represents a mouse. Bars indicate mean, and error bars indicate SEM. Statistical analyses were done by t-test.

Further on, CD4 T cell proliferation was examined in the presence of PRR stimuli. As BCL10 is in the signaling cascade downstream of Dectin-1, Zymosan was added to activate cDCs. However, as Zymosan is recognized by the TLR2, too, a second stimulus was the depleted Zymosan, specifically detected by Dectin-1. In addition, one condition without polarizing conditions and any stimulus (Th0) was analyzed.

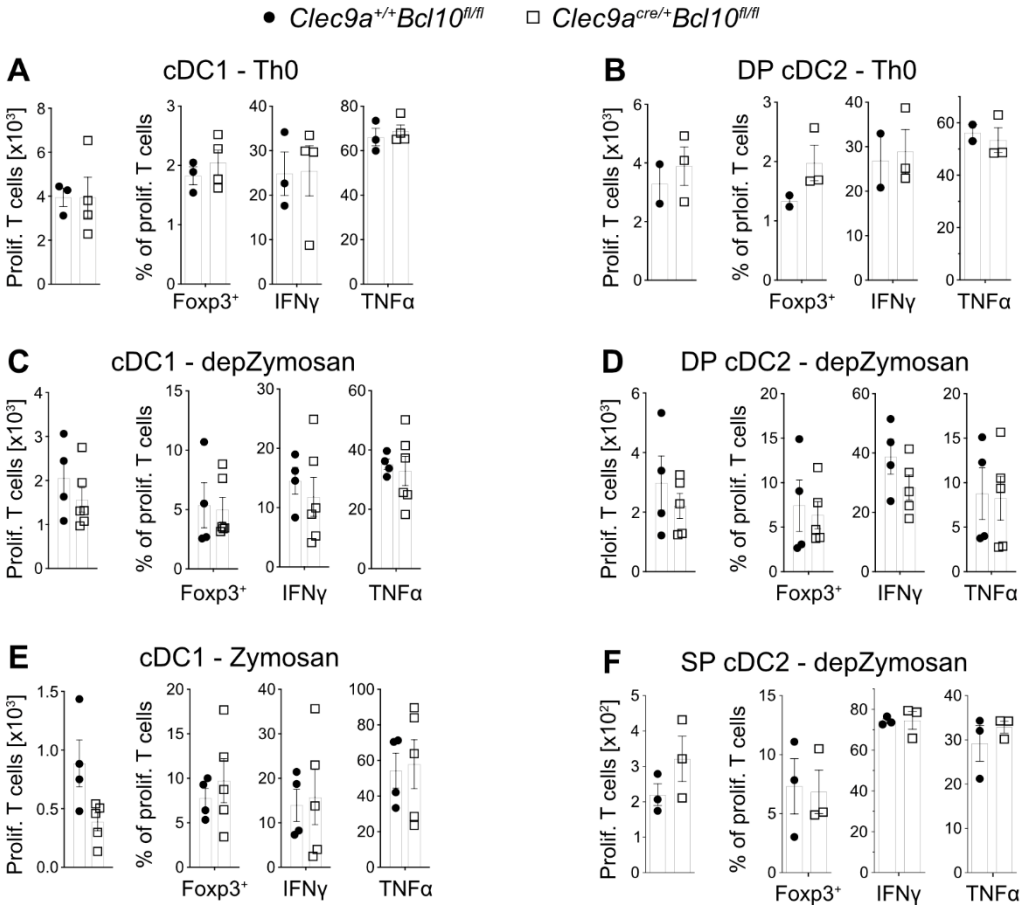

Figure 55 Proliferation and activation of CD4 T cell by colonic cDC subsets in the presence of Dectin-1 antagonists.

Cell counts of CTV$^-$ T cells and frequency of FOXp3$^+$, IFNγ$^+$, and TNFα$^+$ cells within the CTV negative cells after co-culture of OT-II cells in the presence of **A.** cDC1 or **B.** DP cDC2 without polarizing conditions. Cell counts of proliferated (CTV$^-$) T cells and frequency of Foxp3$^+$, IFNγ$^+$, and TNFα$^+$ T cells after co-culture with **C.** cDC1 and depleted Zymosan, **D.** DP cDC2 and depleted Zymosan, **E.** cDC1 and Zymosan and **F.** SP cDC2 and depleted Zymosan. APCs were isolated from the CO LP of *Clec9a*$^{cre/+}$*Bcl10*$^{fl/fl}$ or controls mice. Data of two independent experiments. Each dot represents a mouse. Bars indicate mean, and error bars indicate SEM. Statistical analyses were done by t-test.

Th0 conditions led to similar T cell proliferation and cytokine production for cDC1 and DP cDC2 from *Clec9a*$^{cre/+}$*Bcl10*$^{fl/fl}$ and control mice. Stimulation of cDC1, DP cDC2, or SP cD2 with depleted Zymosan induced less T cell proliferation and a large spread of the data points. However, comparing BCL10 deficient cDCs to sufficient ones revealed no differences for CTV$^-$ cell counts, Treg (Foxp3$^+$) frequency, or the production of IFNγ

and TNFα. Due to the limited cell number of both cDC2s in the CO LP, only cDC1 capacity to activate T cells was investigated in the presence of total Zymosan. As a result, a trend towards less proliferated T cells was found for cDC1s from *Clec9a*$^{cre/+}$*Bcl10*$^{fl/fl}$ mice. However, this decrease was not statistically significant, and no additional changes were found concerning Foxp3, IFNγ, and TNFα expression frequency.

Analysis of Th17 polarization failed within the flow cytometric examination as no significant IL-17A signal could be observed. Therefore, the supernatants of each condition were analyzed for several Th cytokines, including IL-17A, IL-17F, and IL-22. No significant differences were observed for the produced levels of all three Th17-related cytokines if CD4 T cells were activated and polarized by cDC1 under Th0 conditions. Also, activating cDC1s through Dectin-1 by depleted Zymosan or Dectin-1 and TLR3 by Zymosan did not induce significant changes in the production of IL-17A, IL-17F or IL-22 when BCL10 deficient cDC1s were compared to their controls.

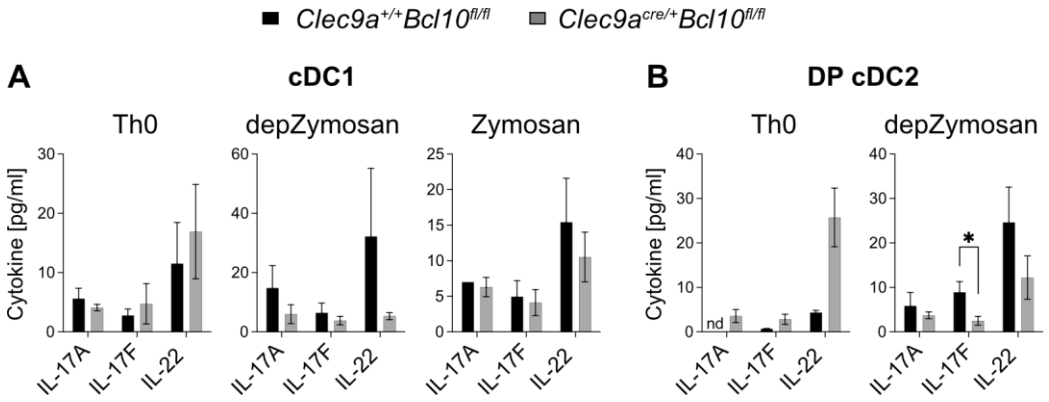

Figure 56 Secreted Th17 cytokines from in-vitro CD4 T cell assays.
IL-17A, IL-17F, and IL-22 secured by CD4 T cells activated bc colonic cDCs from *Clec9a*$^{cre/+}$*Bcl10*$^{fl/fl}$ mice or their controls **A.** T cells activated by cDC1 in the presence of no-stimulus (Th0; $n_{CX} = 3$, $n_{KO} = 3$), depleted Zymosan ($n_{CX} = 4$, $n_{KO} = 6$) or Zymosan ($n_{CX} = 4$, $n_{KO} = 5$) or **B.** DP cDC2 activated T cells without additional stimuli (Th0; $n_{CX} = 2$, $n_{KO} = 3$) or in the presence of depleted Zymosan ($n_{CX} = 4$, $n_{KO} = 5$). Data of two independent experiments. Each dot represents a mouse. Bars indicate mean, and error bars indicate SEM. Statistical analyses were done by t-test. * p-value < 0.05

No significant differences could be observed in the presence of DP cDC2 without further PRR stimuli for the secreted Th17 cytokines. However, IL-17A was not detected if CD4 T cells were activated by control DP cDC2 and measured IL-17F were lower than the levels induced by DP cDC2 from *Clec9a*$^{cre/+}$*Bcl10*$^{fl/fl}$ mice. Therefore, under non-polarizing conditions without PRR antagonists, DP cDC2 induced slightly more Th17 cytokines. However, this observation reversed in the presence of the Dectin-1-specific PAMP, depleted Zymosan. A decreased IL-17A and IL-22 trend was detected, and significantly less IL-17F was measured.

Overall, no significant alterations were detected for the in-vitro activation of naïve CD4 T cells by intestinal cDC1 and the two cDC2 subsets. Nevertheless, the trend towards fewer Th17 cells observed in the CO LP under different conditions could be observed.

3.5.2 In-vitro T cell Assay to address the Capacity of colonic, BCL10-deficient cDC1 to activate CD8 T cells

According to the literature, cDC1s are the main inducers of cytotoxic CD8 T cells. In a first step, this was confirmed for the in-vitro CD8 T cell assay with colonic cDCs. If the antigen had to be ingested and loaded on the MHCI by the cell themselves, B cells failed to induce CD8 T cell activation. Likewise, SP cDC2 and DP cDC2 showed only a minor activation of T cells. Only cDC1s were able to induce extensive proliferation of the CD8 T cells (Data not shown). Having confirmed that only colonic cDC1s can activate CD8 T cells in the presence of OVA protein, in the next step, cDC1s from *Clec9a*$^{cre/+}$*Bcl10*$^{fl/fl}$ and control mice were compared.

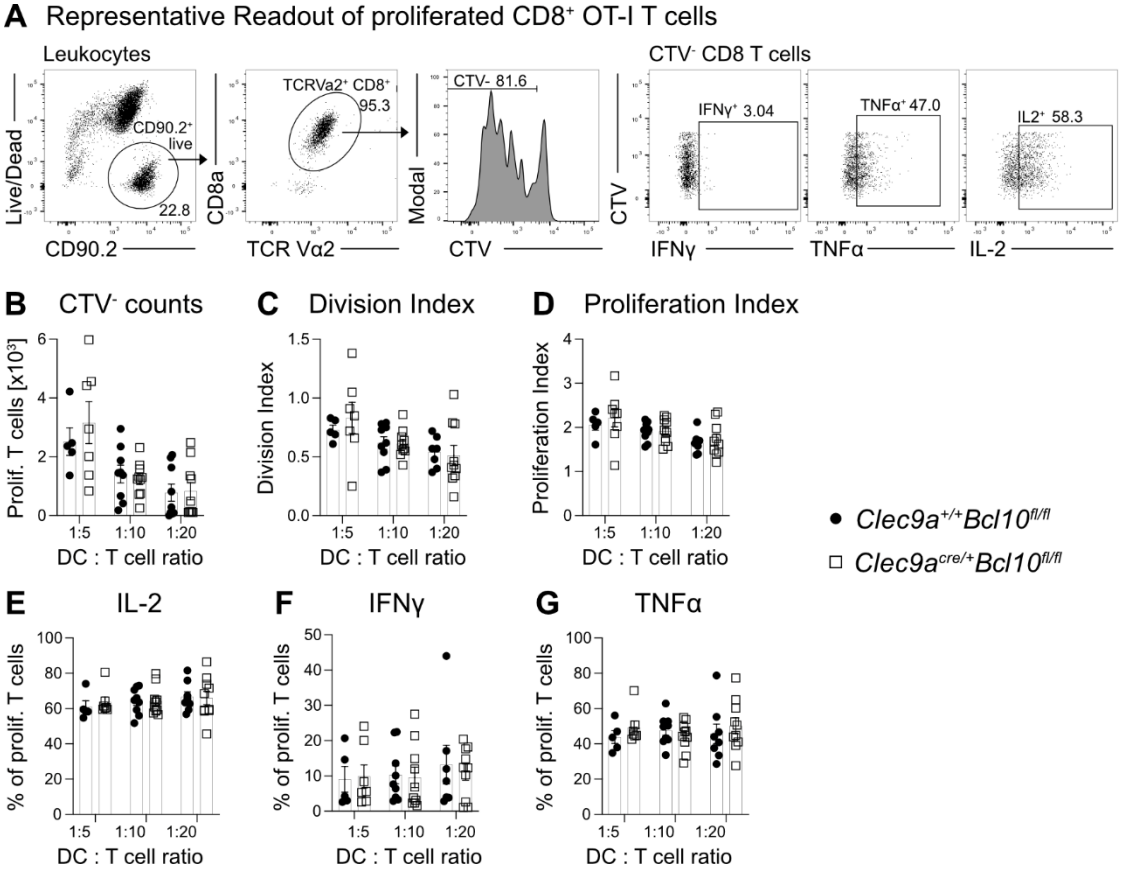

Figure 57 CD8 T cell activation by cDC1s isolated from the CO LP of *Clec9a*$^{cre/+}$*Bcl10*$^{fl/fl}$.
A. Representative gating to analyze proliferated CD8 T cells in the presence of colonic cDC1 and OVA protein. T cells were identified as CD90.2$^+$ live cells and further gating on CD8a and TCR Vα2. Proliferated cells were selected based on their CTV expression. Within proliferated (CTV$^-$) cells IFNγ, TNFα, and IL-2 expressing cells were gated. **B.** Cell counts of proliferated CD8 CTV$^-$ T cells, **C.** Division Index, and **D.** Proliferation index of CD8 T cells after co-culture with Bcl10 deleted cDC1s or control cDC1 at different APC: T cell ratios. **E.** IL-2, **F.** IFNγ, and **G.** TNFα positive proliferate CD8 T cells induced by cDC1 from the CO LP of *Clec9a*$^{cre/+}$*Bcl10*$^{fl/fl}$ or their

controls. Data from three independent experiments. Each dot represents a mouse. Bars indicate mean, and error bars indicate SEM. Statistical analyses were done by t-test.

Activated and proliferated CD8 T cells ($CD90.2^+$ $CD8a^+$ $TCRV\alpha2^+$) were identified as CTV^- and within those cells expressing IFNγ, TNFα, or IL-2 were analyzed. Different cDC versus T cell ratios were used to investigate how efficiently BCL10 deficient cDC1s induce CD8 T cell cells compared to control cDC1s. Nevertheless, the analysis of cell counts of proliferated CD8 T cells showed that neither the division nor proliferation index revealed any defect in cDC1s from *Clec9a*$^{cre/+}$*Bcl10*$^{fl/fl}$ CO LP. Further, the frequencies of T cells expressing IL-2, IFNγ, or TNFα were similar for both genotypes at any cDC: T cell ratio.

Even though no alteration in the capacity to activate CD8 T cells could be observed for BCL10 deficient cDCs in this assay, it must be considered that the processing of cell-associated antigens differs from how OVA-protein is ingested and loaded to MHCI. Therefore, the processing or presentation of tumor-derived antigens in BCL10 deficient cDC1 may still be impaired.

3.6 Flow Cytometric profiling of *Clec9a$^{cre/+}$Syk$^{fl/fl}$* mice

In parallel to the study of BCL10 in intestinal dendritic cells in health and disease, the kinase initiating the activation of the CARD9-BCL10-MALT1 complex was studied, too. Using the combination of Clec9a-driven Cre recombinase together with a floxed *Syk* allele should lead to a cDC-specific deletion of this respective kinase. Deleting SYK in cDCs had no general effect on mouse constitution as *Clec9a$^{cre/+}$Syk$^{fl/fl}$* mice appeared healthy.

3.6.1 Immune profiling of myeloid and lymphoid cells in *Clec9a$^{cre/+}$Syk$^{fl/fl}$*

In the first step, flow cytometric analysis was used to profile the cDC compartment in several organs. With this, developmental effects induced by the deletion of SYK should be assessed. In doing so, *Clec9a$^{cre/+}$Syk$^{fl/fl}$* and control mice's spleen were analyzed combined with the intestinal compartment, including the SI and CO LP and the mLN. Total leukocyte counts were determined for each organ and showed equal amounts of overall immune cells between *Clec9a$^{cre/+}$Syk$^{fl/fl}$* mice compared to their controls (Figure 58). In non-lymphatic organs, leukocytes were identified as CD45.2^{+} cells.

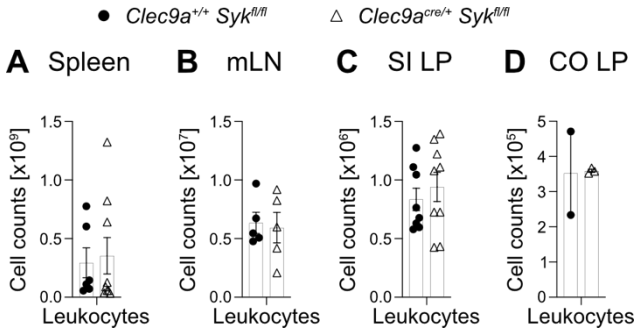

Figure 58 Total leukocyte counts in the Spleen and in intestinal organs.
Leukocyte cell counts isolated from the spleen, mLN, SI LP, and CO LP of *Clec9a$^{cre/+}$Syk$^{fl/fl}$* and control mice. Data from three (Spleen, mLN + SI LP) and one (CO LP) independent experiments. Each dot represents a mouse. Bars indicate mean, and error bars indicate SEM. Statistical analyses were done by t-test.

Next, the frequency of cDCs and other myeloid immune cells was determined (Figure 59). The respective markers and gating strategies to identify macrophages, cDCs, and their organ-specific subsets, as well as monocytes and neutrophils, were described previously. Doing so, monocytes and neutrophils were found in similar frequencies in all analyzed organs.

Analysis of the mLN, consisting of CO LN and SI LN, revealed a normal distribution of total migratory and resident cDCs along with similar frequencies of their respective subsets. Likewise, no differences were found in the occurrence of macrophages, total cDCs, and the cDC subsets in the CO LP of *Clec9a$^{cre/+}$Syk$^{fl/fl}$* mice.

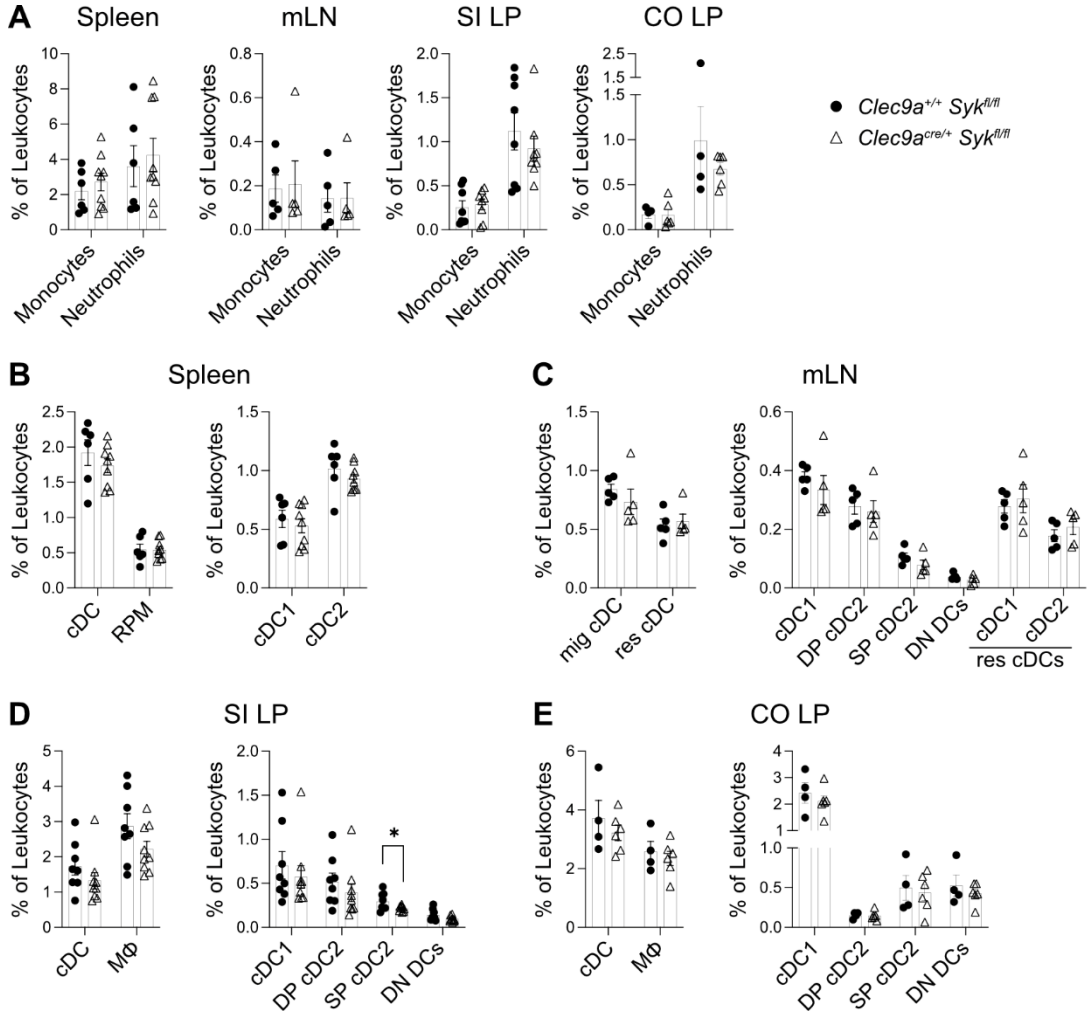

Figure 59 Frequency of several immune cell types in the spleen and three intestinal organs. **A.** Frequency of monocytes and neutrophils in the spleen, mLN, SI LP and CO LP of control mice and *Clec9a*$^{cre/+}$*Syk*$^{fl/fl}$ mice. Frequency of total cDCs, macrophages, the respective organ-specific cDC subsets in the **B.** Spleen, **C.** mLN, **D.** SI LP and **E.** CO LP of *Clec9a*$^{cre/+}$*Syk*$^{fl/fl}$ mice and their controls. Data from three (Spleen & SI LP) and two (mLN & CO LP) independent experiments. Each dot represents a mouse. Bars indicate mean and error bars indicate SEM. Statistical analyses were done by t-test. * p-value < 0.05

A comparison of the frequencies of total cDCs and RPMs showed normal proportions of both immune cell types in the spleen of *Clec9a*$^{cre/+}$*Syk*$^{fl/fl}$ mice. However, a slight trend towards fewer cDC2s could be detected, whereas cDC1s appeared normal. Similar results could be obtained from the SI LP of *Clec9a*$^{cre/+}$*Syk*$^{fl/fl}$ mice. Whereby total cDCs and macrophages already showed a trend towards decreased frequency in Clec*9a*$^{cre/+}$*Syk*$^{fl/fl}$ mice. Within the cDC subsets, a significant decrease of the SP cDC2s was detected with a similar trend for DP cDC2, whereas cDC1 and DN DC were found in equal amounts.

Even though cDC2s were slightly decreased in the spleen and SI LP, the deletion of SYK in cDCs does not significantly affect cDC development within several organs.

3.6.2 In-depth phenotypic profiling of intestinal T cells from *Clec9a$^{cre/+}$Syk$^{fl/fl}$* mice

As it is described in the literature that *CD11c^{cre}Syk^{flox}* mice have a deficiency in intestinal Th17 cells, in-depth flow cytometric analysis was performed to dissect the intestinal T cell compartment of *Clec9a$^{cre/+}$Syk$^{fl/fl}$* (Figure 60). In doing so, T cells were identified according to the gating strategy described in chapter 3.1.2.

The frequency of these cells was compared between *Clec9a$^{cre/+}$Syk$^{fl/fl}$* and control mice (Figure 60). Starting with the mLN, the same frequency of T cells and a normal distribution of CD4, CD8, and unconventional T cells were found. Even though the latter one was nearly absent in the mLN and only a tiny fraction expressed Rorγt^{+} in comparable frequencies in *Clec9a$^{cre/+}$Syk$^{fl/fl}$* and control mice. No differences could be detected in the CD4 T cells for the presence of Th17, Treg, and Rorγt^{+} Tregs.

Further, analysis of the T cells in the SI LP revealed similar frequencies of total T cells and the three subsets identified by CD4 and CD8a. Likewise, the distribution of Th17 and both Treg subsets was comparable between *Clec9a$^{cre/+}$Syk$^{fl/fl}$* and the control mice. However, unconventional Th17 cells were decreased in part of the *Clec9a$^{cre/+}$Syk$^{fl/fl}$* mice. In the PPs, a trend towards increased T cells could be detected, derived by an increase of CD4 and CD8 T cells. However, this increase was not statistically significant, and the control group was relatively small. No alterations were found for the identified subsets of CD4 T cells nor the unconventional Th17 cells.

As the last intestinal organ, the CO LP was analyzed for the presence of total T cells and further subsets. No difference could be observed in the frequency of the total T cell population, neither in one of the three subsets marked by their individual expression pattern of CD4 or CD8. Further, the proportion of Th17, Tregs, and Rorγt^{+} Tregs was assessed, and a slight decrease in both Treg populations could be detected. However, this could be observed only as a trend due to the low number of control mice. In addition, no significant difference was found in the frequency of unconventional Th17 cells between *Clec9a$^{cre/+}$Syk$^{fl/fl}$* and control mice.

Besides the T cells, ILCs and the NK T cells were assessed for their appearance in the intestinal compartment of *Clec9a$^{cre/+}$Syk$^{fl/fl}$* mice; likewise, it was done for *Clec9a$^{cre/+}$Bcl10$^{fl/fl}$* mice. Comparison of the frequency of these cell types in the mLN, SI LP, PPs, and CO LP revealed no alterations in the proportions of each cell type within the respective organ (Data not shown).

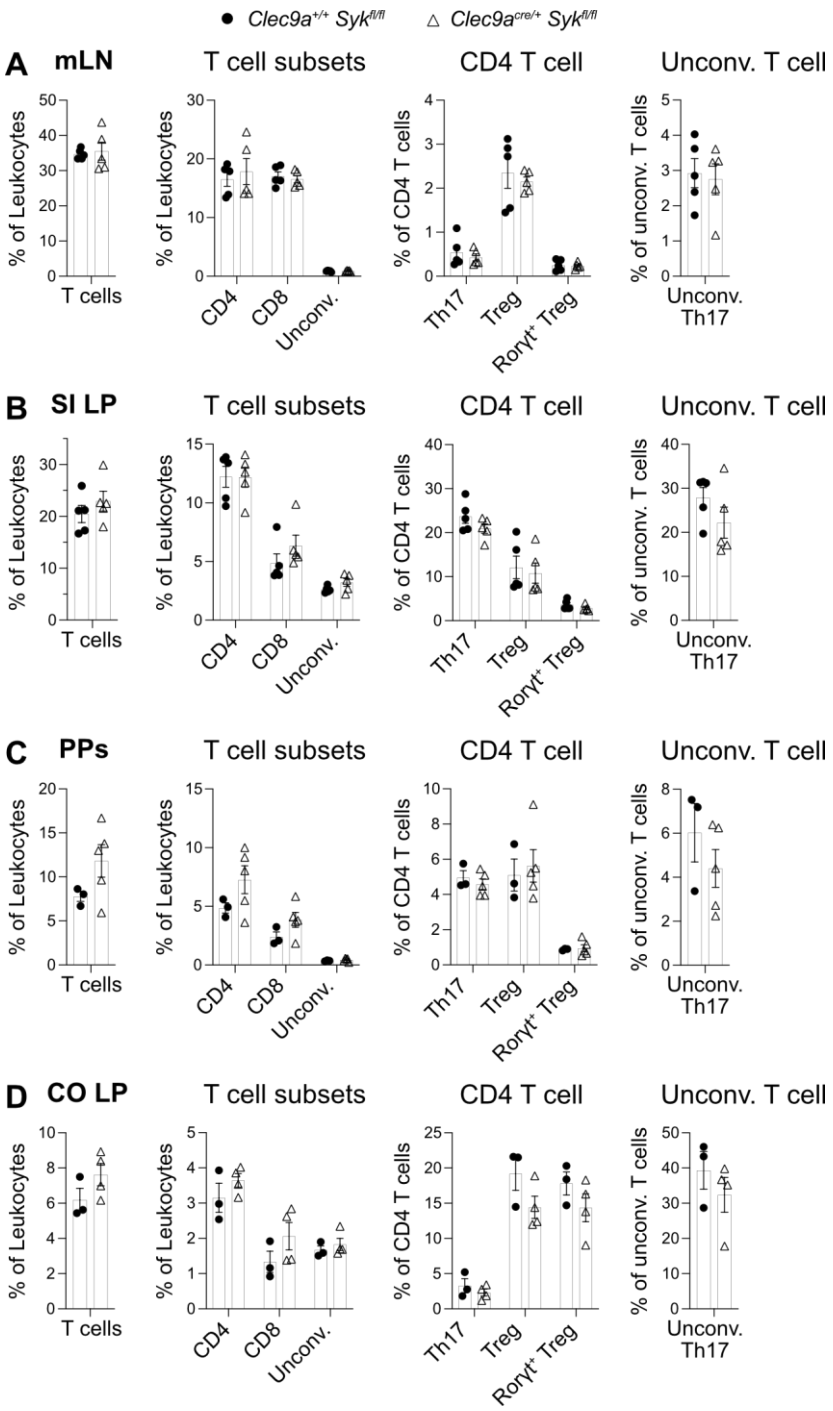

Figure 60 Frequency of T cells and several subsets in four intestinal organs of *Clec9a$^{cre/+}$Syk$^{fl/fl}$* mice.

Frequency of total T cells, the subsets identified by the expression or lack of CD4 and CD8 and their respective subsets in the **A.** mLN, **B.** SI LP, **C.** PPs and **D.** CO LP of *Clec9a$^{cre/+}$Syk$^{fl/fl}$* and control mice. Data from three (SI LP) and two (mLN, PPs & CO LP) independent experiments. Each dot represents a mouse. Bars indicate mean, and error bars indicate SEM Statistical analyses were done by t-test.

Last, T cell's capacity to produce cytokines was analyzed. Overall, cytokine production was low within the CD4 T cells isolated from the mLN. Even though a trend towards a reduction of IL-17A positive CD4 T cells was found in *Clec9a*$^{cre/+}$*Syk*$^{fl/fl}$ mice. For IL-22 and IFNγ, no difference was found. However, the data points spread in both groups and separated based on the experiment. The same applies to the cytokines, especially the IFNγ produced by CD8 and unconventional T cells.

The cytokines produced by T cells derived from the SI LP showed no difference in the percentage of IL-17A, IL-22, and IFNγ expressing CD4 and unconventional T cells. Further, an average frequency of IFNγ producing CD8 T cells was found in the SI LP of *Clec9a*$^{cre/+}$*Syk*$^{fl/fl}$ mice.

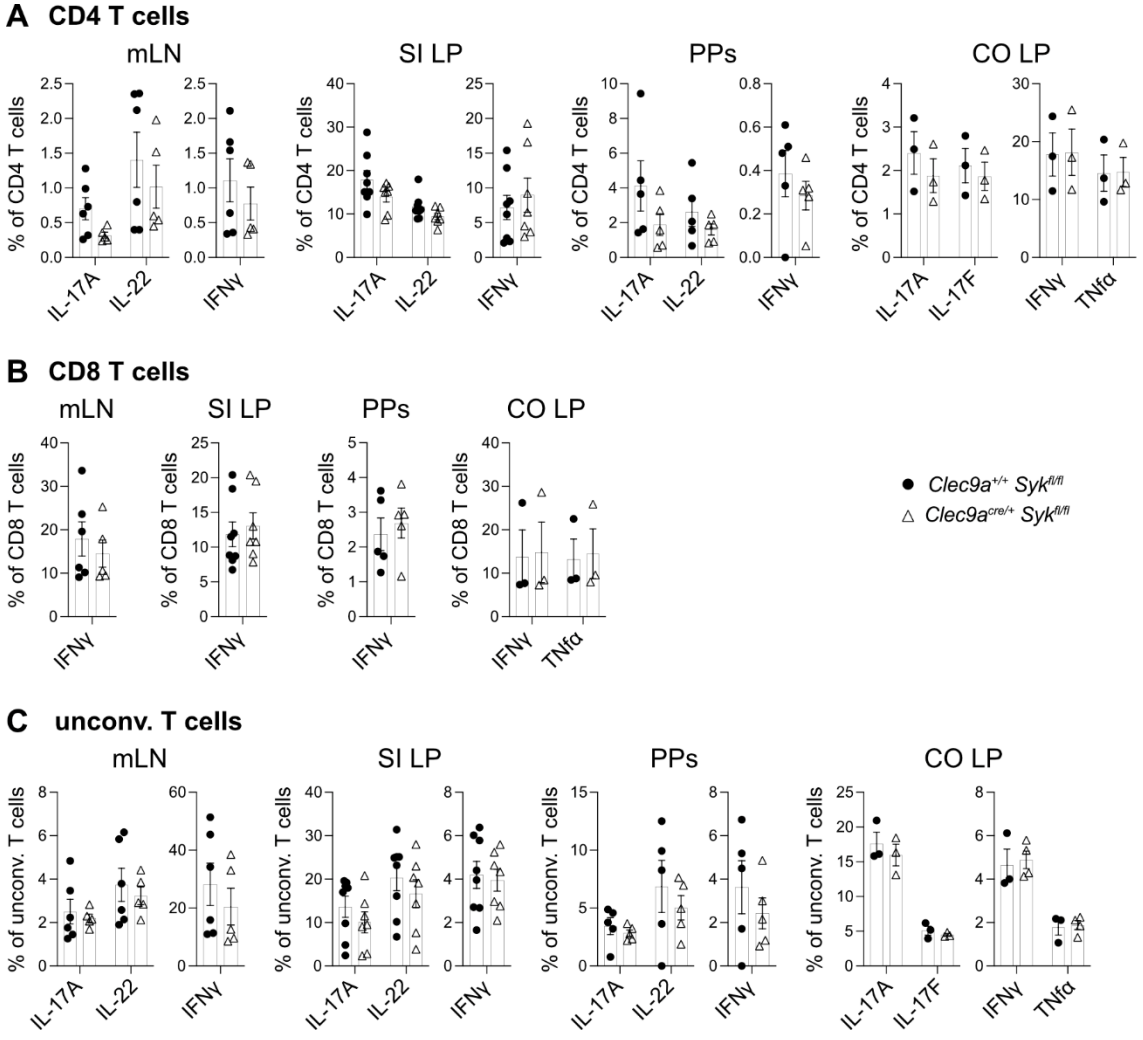

Figure 61 Cytokine production by intestinal T cells from *Clec9a*$^{cre/+}$*Syk*$^{fl/fl}$ mice.
Frequency of **A.** IL-17A, IL-22, and IFNγ and TNFα produced by CD4 T cells, **B.** IFNγ produced by CD8 T cells, and **C.** IL-17A, IL-22, and IFNγ produced by unconventional T cells in the mLN, SI LP, PPs and CO LP from control mice and *Clec9a*$^{cre/+}$*Syk*$^{fl/fl}$ mice. Data from three (SI LP) and two (mLN, PPs & CO LP) independent experiments. Each dot represents a mouse. Bars indicate mean and error bars indicate SEM. Statistical analyses were done by t-test.

Analysis of the CD4 T cells of the PPs revealed a non-significant decrease of IL-17A positive T cells, like the trend observed in the mLN. No additional alterations were found in the IL-22 and IFNγ production of CD4 T cells nor the frequency of IFNγ$^+$ CD8 T cells. Consequent analysis of IL-17A, Il-22, and IFNγ in unconventional T cells showed no difference between the cells derived from the PPs of *Clec9a*$^{cre/+}$*Syk*$^{fl/fl}$ mice or their controls.

Subsequently, the assessment of the cytokine production of colonic T cells revealed no significant differences in CD4 T cells expressing IL-17A or IL-17F nor IFNγ and TNFα, nor in unconventional T cells. Further on, similar values were obtained for the frequency of IFNγ and TNFα positive CD8 T cells. Even though no significant differences could be observed, it must be considered that the groups for the cytokine production by colonic T cells were small.

3.7 Transcriptional profiling of intestinal cDCs and T cells from *Clec9a*$^{cre/+}$*Syk*$^{fl/fl}$ mice under steady-state conditions

Single cell sequencing was performed to assess if loss of SYK in cDCs influences the transcriptional profile of cDCs or T cells. Doing so, cDCs and CD90.2$^+$ cells, including T cells and ILCs, were sorted from the SI LP of *Clec9a*$^{+/+}$*Syk*$^{fl/fl}$ and *Clec9a*$^{cre/+}$*Syk*$^{fl/fl}$. Cells were isolated from the SI LP as a previous publication on mice showed a reduction of Th17 cells in the SI if SYK is deleted in CD11c-expressing cells, including cDCs (Martinez-Lopez et al. 2019). The sorting strategy and the purity checks of sorted cells from both genotypes are depicted in Figure 62.

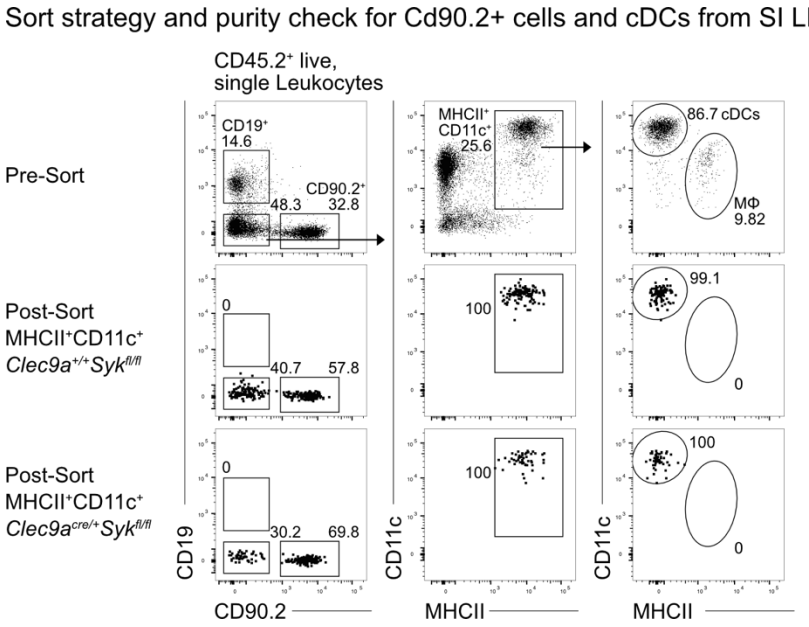

Figure 62 Sort strategy and purity check of cDCs and CD90.2$^+$ cells from the SI LP of *Clec9a*$^{cre/+}$*Syk*$^{fl/fl}$ mice.

Representative gating strategy to identify and sort cDCs and CD90.2$^+$ from the SI LP of *Clec9a*$^{cre/+}$*Syk*$^{fl/fl}$ mice and their controls (top row). CD90.2$^+$ cells were gated directly from live leukocytes. Out of CD90.2$^-$CD19$^-$ cells, MHCII$^+$CD11c$^+$ cells were selected, and cDCs were identified as CD64 negative. CD90.2$^+$ and cDCs were sorted in a 50/50 ratio. Purity was checked for sorted cells from *Clec9a*$^{+/+}$*Syk*$^{fl/fl}$ (controls) and *Clec9a*$^{cre/+}$*Syk*$^{fl/fl}$ mice.

The CD90.2$^+$ cells were gated and selected for sorting out the CD45.2$^+$ live leukocyte population. From the CD90.2 negative cells, CD19-expressing B cells were excluded, and MHCII$^+$CD11c$^+$ cells were determined. Last, intestinal macrophages were separated from the targeted cDC population by the expression of CD64. CD90.2$^+$ cells and cDCs were sorted in a 50/50 ratio, and cells of both genotypes were subjected to single-cell sequencing in separate reactions. Sequencing data from *Clec9a*$^{+/+}$*Syk*$^{fl/fl}$ and *Clec9a*$^{cre/+}$*Syk*$^{fl/fl}$ derived cells were combined in the Cell Ranger Aggregate pipeline, cleaned in the quality control steps, and cDCs were separated from CD90.2$^+$ cells and analyzed separately.

3.7.1 Transcriptional profiling of cDCs from SI LP of *Clec9a*$^{cre/+}$*Syk*$^{fl/fl}$ mice

After quality control and separation of cDCs from the T cells and ILCs, 5493 cells were recovered with an average of 3138 genes detected per cell and a total of 12490 reads per cell. Slightly more cells from *Clec9a*$^{+/+}$*Syk*$^{fl/fl}$ were found with a ratio of 60 to 40. In the next step, unbiased clustering was performed with these cells, resulting in seven individual clusters (Figure 63). Depiction of these clusters based on the genotypic background of the cells revealed that cells derived from different genotypes cluster by cell type. Cell cycle regression identified a small cluster of highly proliferating cells, including different cDCs, and therefore was excluded from further analysis. An additional non-DC cluster was identified as T cells through the high expression of *Cd3e*, excluded from downstream analysis as well. The expression of cDC-specific markers like *Flt3*, *Itgax*, and *Zbtb46* marked the remaining clusters. One of these clusters separated from the others and could be identified as cDC1s (*Irf8*, *Xcr1*, *Itgae*). High levels of *Itgae* were found in another cluster, with *Irf4*, *Sirpa*, and *Itgam*, classifying them as the intestine characteristic CD103$^+$ cDC2 (DP cDC2) subtype. Following the flow cytometric data where DP cDC2s are the primary cDC type in the SI LP, this cluster of DP cDC2s contained the highest number of cells. Two additional clusters of cDC2s were identified, out of which one was marked by the expression of genes upregulated during cell activation (e.g., *Dusp2*, *Nr4a1*, *Nfkbia*). The remaining cluster had a similar signature of cDC2 and activation markers. However, it separated from the other cDC2 clusters through the expression of genes (*Ccr7*, *Fscn1*, *Ccl22*), classifying it as migratory cDCs.

Having identified each cluster, the distribution of the genotypes within the cDC clusters was determined. It revealed a slightly higher occurrence of cells derived from *Clec9a*$^{+/+}$*Syk*$^{fl/fl}$ SI LP in all clusters.

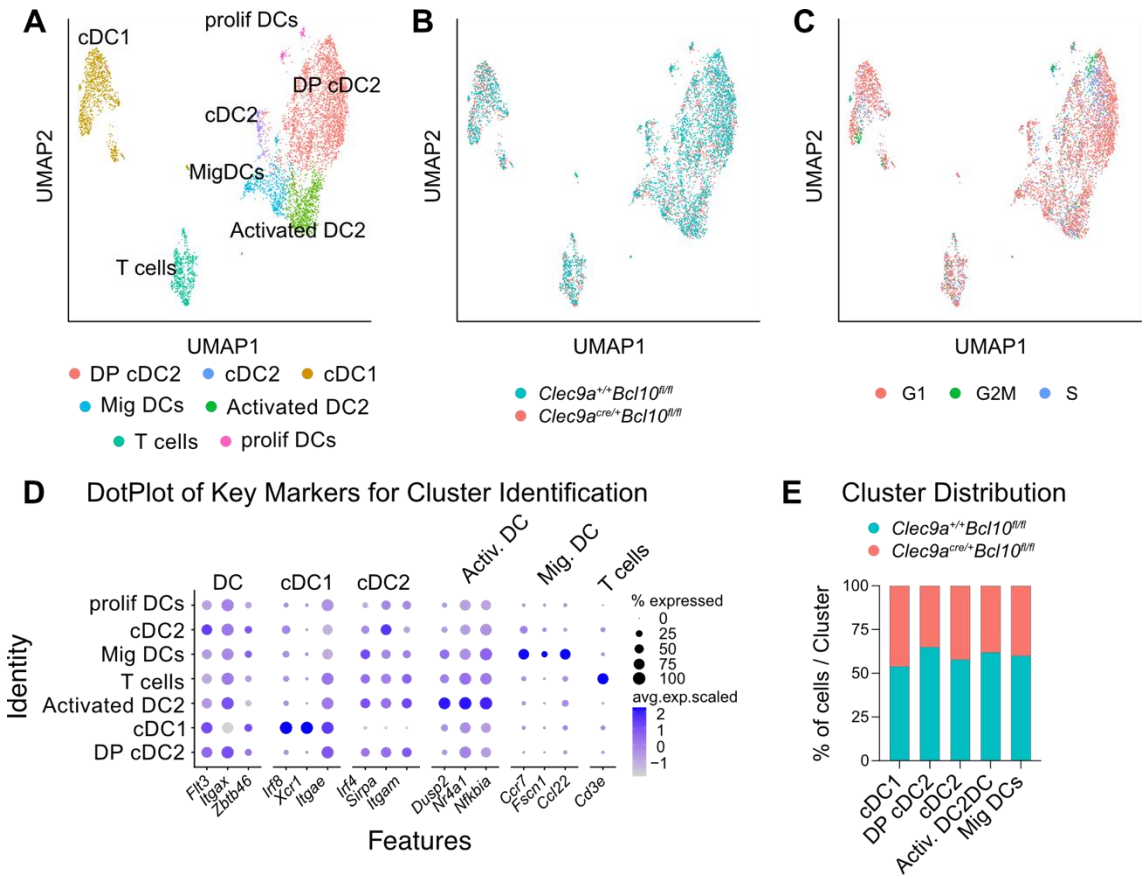

Figure 63 Transcriptional profiling of cDCs from the SI LP of *Clec9a*$^{cre/+}$*Syk*$^{fl/fl}$ mice and their controls.

A. Unbiased clustering of SI LP-derived cDCs resulted in seven clusters. **B.** cDC from different genetic background overlap in the UMAP. **C.** Highly proliferating cells (G2M phase) form a separate cluster. **D.** Dot plot shows cluster identification based on cell-specific genes like transcription markers. **E.** Genotype distribution within every cDC cluster.

The first approach in further analysis of the transcriptome was to assess the presence of the *Syk* mRNA (Figure 64). A comparison between *Clec9a*$^{+/+}$*Syk*$^{fl/fl}$ and *Clec9a*$^{cre/+}$*Syk*$^{fl/fl}$ derived cells revealed no significant decrease within all cDC clusters. However, transcripts were sequenced from the 5' end, and the floxed allele is localized towards the 3' end. The iCre expression was detected only in cDC1s derived from *Clec9a*$^{cre/+}$*Syk*$^{fl/fl}$ SI LP, confirming the genotype. As no difference was seen in the transcript level of *Syk*, the protein expression was assessed through flow cytometric analysis. In doing so, several immune cell populations isolated from the spleen, mLN, and SI LP were analyzed for their expression level of SYK. Gating strategies to identify the organ-specific cDC and macrophage populations were described previously.

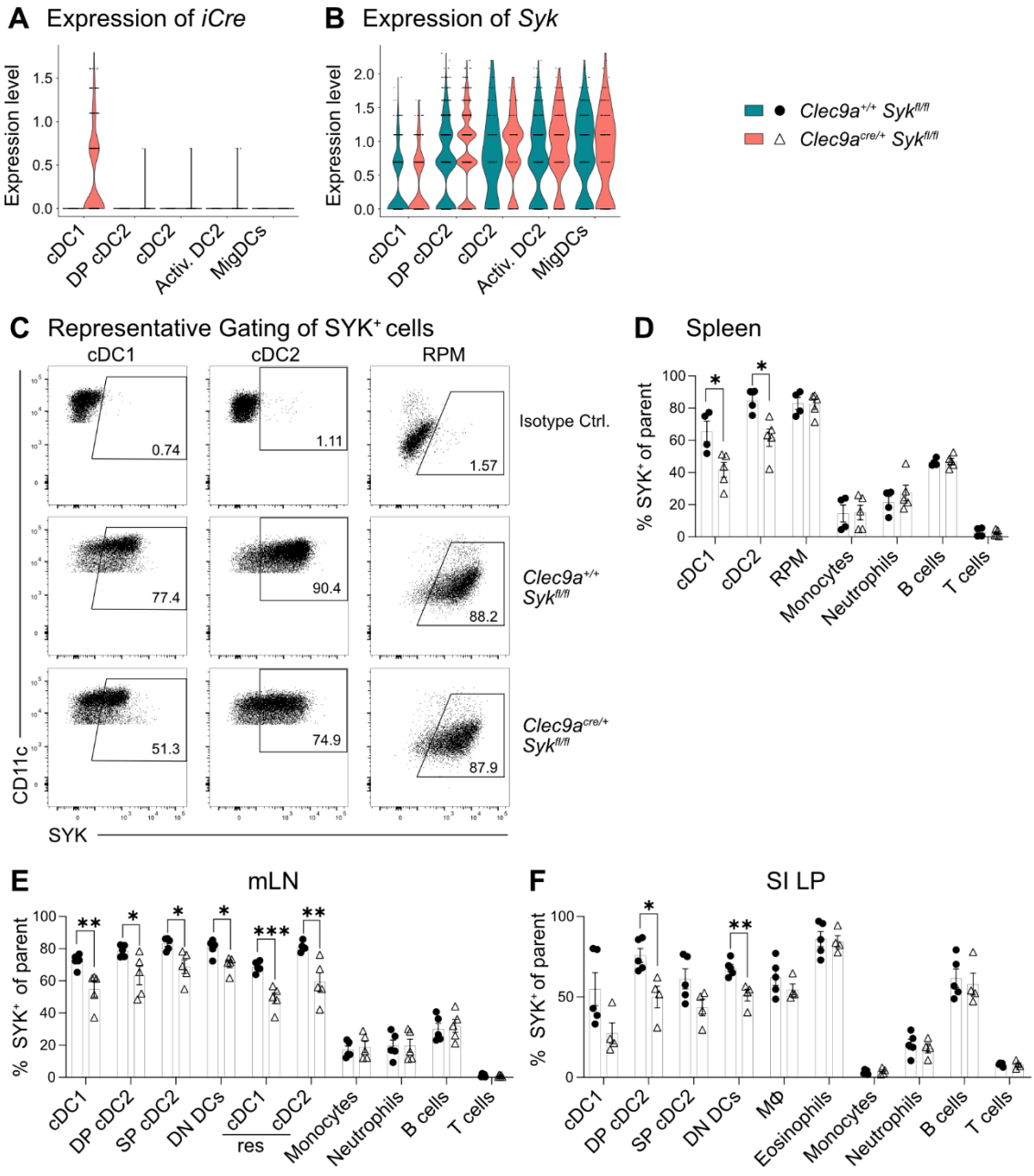

Figure 64 The efficiency of Clec9a-cre-dependent SYK deletion in different cDC subsets. **A.** Transcriptional expression of *iCre* and **B.** *Syk* within the five identified cDC clusters separated by their genetic background. **C.** Representative gating of SYK protein staining in cDC subsets and macrophages from the control spleen and *Clec9a*$^{cre/+}$*Syk*$^{fl/fl}$ mice. Gates were set based on Isotype control staining (top row). **D.** Frequency of SYK-positive cells within the respective immune cell population in the spleen, **E.** the mLN, and **F.** the SI LP of *Clec9a*$^{cre/+}$*Syk*$^{fl/fl}$ mice and their controls. Data from two (D - F) independent experiments. Each dot represents a mouse. Bars indicate mean, and error bars indicate SEM. Statistical analyses were done by t-test. * p-value < 0.05, ** p-value < 0.01, *** p-value < 0.001

Throughout the immune cell types determined in the spleen and investigated from their expression level, only cDC1 and cDC2 significantly reduced their SYK positive fraction. In addition, the fluorescent intensity of the SYK-positive population of cDC1 and cDC2

but not RPMs was decreased, which is already visible within the dot plots. The fluorescent intensity correlates with the protein level present in the cell. Therefore, Syk-expressing cDCs and the SYK protein level within the cDCs are decreased in *Clec9a*$^{cre/+}$*Syk*$^{fl/fl}$ mice. Within the analyzed intestinal organs, a significant reduction of SYK$^+$ cells was determined in all migratory and resident cDC subsets but only in two out of four cDC subsets from the SI LP. However, a clear difference could be observed within cDC1, both cDC2 subsets and DN DCs, even though not all turned significant. No reduction of the SYK-expressing population could be observed in monocytes, neutrophils, or T and B cells, neither in the mLN nor in the SI LP. Further on, SI LP-derived macrophages and eosinophils showed a similar expression level of SYK when *Clec9a*$^{cre/+}$*Syk*$^{fl/fl}$ derived cells were compared to their controls.

In summary, SYK-expressing cells could be reduced within the cDC compartment, but no complete deletion of SYK in any of the cDC subtypes was found, even though the SYK protein level was decreased in the remaining SYK$^+$ cDCs. No reduction of SYK$^+$ was found in any of the other investigated immune cell populations in all three organs.

The transcriptional profile of cDCs from *Clec9a*$^{cre/+}$*Syk*$^{fl/fl}$ SI LP was further dissected by identifying differentially expressed genes across genotypes within each cDC cluster. *Clec7a* turned up as the top differentially expressed gene in the cDC1s, being highly upregulated in cDC1 from *Clec9a*$^{cre/+}$*Syk*$^{fl/fl}$ mice. This phenotype could be confirmed on the protein level by flow cytometry. Compared to their controls, increased Dectin-1 staining was found on cDC1s isolated from the SI LP of *Clec9a*$^{cre/+}$*Syk*$^{fl/fl}$ mice. No transcriptional or protein level difference was observed in any other cDC subset.

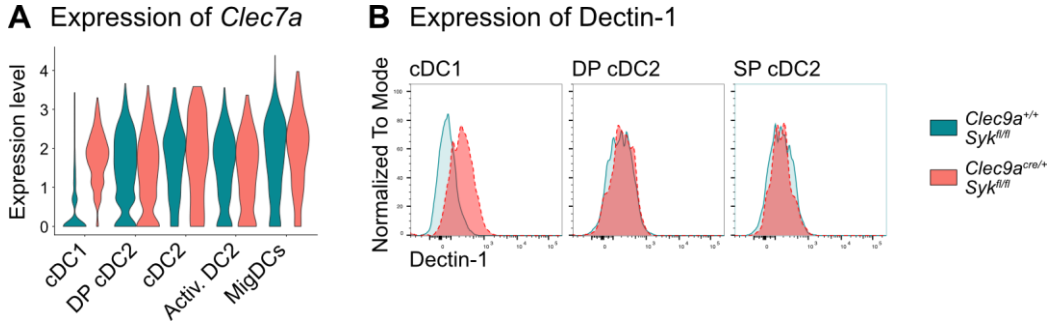

Figure 65 Increased expression of *Clec7a*/Dectin1 upon SYK deletion in cDC1.

A. Transcriptional expression of *Clec7a* in all five cDC clusters, identified in the previously performed unbiased clustering. Clusters are divided based on the genotype of the cells they derived from. **B.** Representative histogram overlays of the flow cytometric analysis of Dectin-1 staining on cDC1, DP, and SP cDC2 isolated from the SI LP of *Clec9a*$^{cre/+}$*Syk*$^{fl/fl}$ mice or their controls.

Further analysis of the DEGs within each cDC cluster using a gene set enrichment analysis revealed an upregulation of IFNγ response (e.g., *Ifngr1, Itgb7, Ciita, Ccl5*) and TNFα signaling via NFκB (e.g., *Zfp36, Pik2, Jun, Fos, Dusp1*) in multiple cDC clusters from

Clec9a$^{cre/+}$*Syk*$^{fl/fl}$ mice. *Nfkb1*, encoding the NFκB subunit p105, is downregulated in cDC1, activated cDC2, and migratory DCs originated from *Clec9a*$^{cre/+}$*Syk*$^{fl/fl}$ mice. The p105 subunit is the precursor of p50, which is generated by co-translational processing.

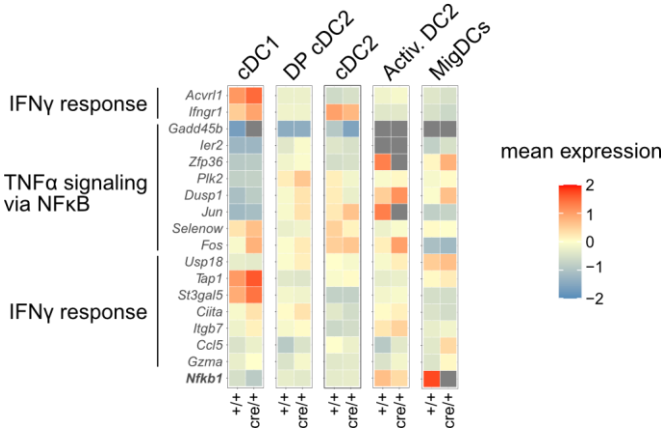

Figure 66 Differentially expressed genes within all five cDC clusters. Heatmap depiction of differentially expressed genes within each cDC cluster between the cells derived from *Clec9a*$^{+/+}$*Syk*$^{fl/fl}$ or *Clec9a*$^{cre/+}$*Syk*$^{fl/fl}$ SI LP. And gene set enrichment analysis of those genes for pathway enrichment.

No additional hits could be identified among the other differentially expressed genes. However, the total number of DEGs did not exceed 50, including up- and downregulated genes, in any of the cDC clusters.

3.7.2 Transcriptional profiling of CD90.2$^+$ from SI LP of *Clec9a*$^{cre/+}$*Syk*$^{fl/fl}$ mice

Separation of CD90.2$^+$ cells from cDCs through their transcriptional profile led to 11953 sequenced cells, with an average read number of 3454 per cell and 1557 different detected genes. The proportion of *Clec9a*$^{+/+}$*Syk*$^{fl/fl}$ and *Clec9a*$^{cre/+}$*Syk*$^{fl/fl}$ derived cells was equal. The unbiased clustering of these cells led to 12 clusters, whereby these cells clustered into two meta-cluster consisting either of conventional T cells (*Thy1.2*, *Cd3e*) or ILCs (*Thy1.2*, no *Cd3e)* together with NK T cells (*Cd3e*, *Klrd1*, *Xcl1*) and DN γδT cells (*Cd3e*, *Trdc*). Cells of different genetic origins cluster together, and cell cycle regression identifies proliferating cells within each cluster (Figure 67).

Within the T cell meta cluster, four CD4 T cell (*Cd4*) clusters could be identified, whereby individual clusters were characterized by the expression of the *Foxp3*, *Rorc,* and high or low *Cd44*, respectively. The expression of these genes and each cluster's top differentially expressed genes allowed their classification as Tregs, Th17, and activated and non-activated CD4 T cells. Further on, two CD8 T cell clusters were detected and separated by the expression of *Trdc* by one of them. The last cluster of this group showed high levels of *Ccr7* and *Sell* and was assigned as migratory (naïve) T cells.

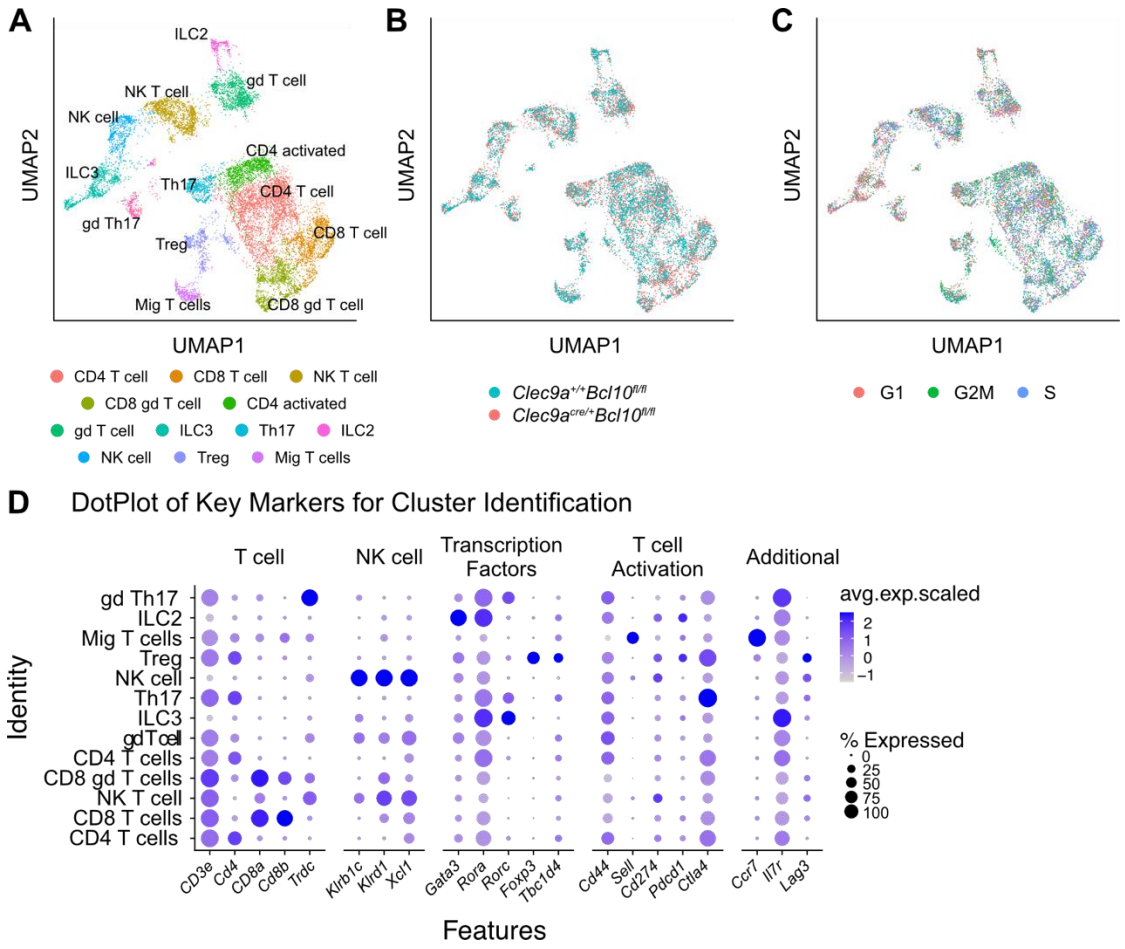

Figure 67 Unbiased clustering of CD90.2$^+$ cells from the SI LP of *Clec9a$^{cre/+}$Syk$^{fl/fl}$* mice.
A. Unbiased clustering of SI LP-derived CD90.2 expressing cells, resulted in 12 clusters. **B.** T cells and ILCs from different genetic background overlap in the UMAP depiction. **C.** Cell cycle does not exceed the clustering based on cell type-specific markers. **D.** Dot plot shows cluster identification based on cell-specific genes like transcription markers.

Besides the CD8 γδ T cells, two additional clusters were marked by the expression of *Trdc*. Within those, one of them expressed, in addition, *Rorc,* leading to the identification of this cluster as unconventional γδ Th17 cells. ILC clusters included NK cells (*Klrb1c*, *Klrd1*, *Xcl1*), ILC2s (*Rora*, *Gata3*), and ILC3s (*Rora*, *Rorc*).

Further, transcriptional differences should be investigated. However, differential gene expression analysis revealed barely any differences between CD90.2$^+$ derived from *Clec9a$^{+/+}$Syk$^{fl/fl}$* and *Clec9a$^{cre/+}$Syk$^{fl/fl}$* SI LP. This might be due to the low sequencing depth of approximately 3500 reads per cell.

3.8 Loss of SYK in cDCs has no impact on acute Colitis

CD11c^{cre}*Syk*^{flox} mice were described to be more susceptible to acute colitis and CAC (Malik et al. 2018). Even though CD11c-cre is often used to target DCs, intestinal macrophages also express high levels of CD11c. Therefore, the *Clec9a*$^{cre/+}$*Syk*$^{fl/fl}$ allows a more specific deletion in cDCs. To investigate if SYK in cDCs protects mice from acute colitis, *Clec9a*$^{cre/+}$*Syk*$^{fl/fl}$ and control mice were treated with DSS-supplemented drinking water to induce colitis. A low concentration of DSS was selected to mimic the colitis, usually caused during the AOM-DSS model, where mice can recover from colitis.

3.8.1 Acute Colitis in *Clec9a*$^{cre/+}$*Syk*$^{fl/fl}$ mice

Challenging *Clec9a*$^{cre/+}$*Syk*$^{fl/fl}$ and their controls to DSS-induced colitis and monitoring them for weight loss and disease activity revealed no significant differences between the groups (Figure 68). However, *Clec9a*$^{cre/+}$*Syk*$^{fl/fl}$ mice showed slightly less weight loss and seemed to start to recover earlier than the control mice.

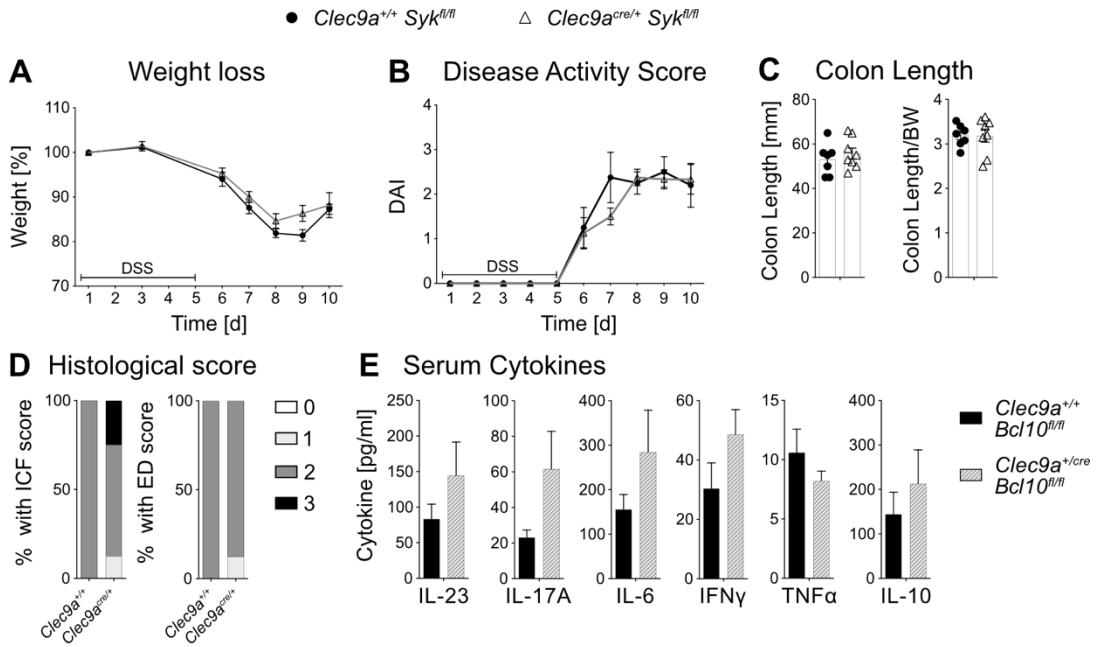

Figure 68 Acute colitis performed with *Clec9a*$^{cre/+}$*Syk*$^{fl/fl}$ mice and their controls.
A. Weight in percent of starting weight and **B.** Disease activity score upon DSS-induced acute colitis in *Clec9a*$^{cre/+}$*Syk*$^{fl/fl}$ and control mice (n per group = 8). **C.** Colon length and colon length/weight ratio at the endpoint analysis. Each dot represents a mouse. **D.** Immune cell infiltration (ICF) and epithelial damage (ED) were determined by histological scoring (n per group = 8). **E.** Levels of the cytokines IL-23, IL-17A, IL-6, IFNγ, TNFα, and IL-10 in the *Clec9a*$^{cre/+}$*Syk*$^{fl/fl}$ mice serum and their controls at the endpoint analysis (n per group = 8). Data from two independent experiments. Bars indicate mean, and error bars indicate SEM. Statistical analyses were done by t-test.

Analysis of the colon length and determination of the colon length/bodyweight ratio showed similar values obtained from both groups. Histological scoring of H&E-stained

colon swiss roles uncovered a relatively increased immune cell infiltration of the colon tissue of *Clec9a*$^{cre/+}$*Syk*$^{fl/fl}$ mice. The detected epithelial damage was scored equally in *Clec9a*$^{cre/+}$*Syk*$^{fl/fl}$ mice and their controls. Last, serum cytokines were measured, and a trend of increased pro-inflammatory cytokines, like IL-23, IL-17A, IL-6, and IFNγ, was detected in the serum of the *Clec9a*$^{cre/+}$*Syk*$^{fl/fl}$ mice. However, none of them significantly increased. No differences could be observed for the anti-inflammatory cytokine IL-10.

3.8.2 Flow cytometric analysis of immune cell compartments in CO LP and CO LN of *Clec9a*$^{cre/+}$*Syk*$^{fl/fl}$ mice with acute colitis.

Even though no significant differences were detected in the clinical scorings of *Clec9a*$^{cre/+}$*Syk*$^{fl/fl}$ mice suffering from acute colitis, the immune cell compartment of the CO LP and the CO LN was investigated. A comparison of the cell counts of total leukocytes showed no difference in the total amount of immune cells in the CO LP or the CO LN (Figure 69). However, cell counts for leukocytes in the CO LP were only obtained from one cohort.

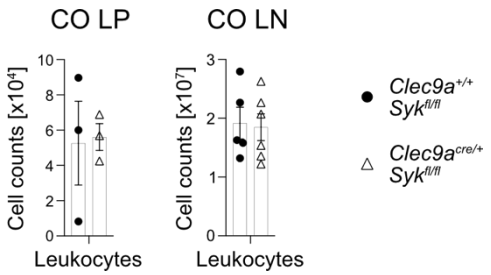

Figure 69 Leukocyte counts in the CO LP and CO LN upon DSS-induced acute colitis.
Cell counts of total leukocytes determined in the CO LP and the CO LN of *Clec9a*$^{cre/+}$*Syk*$^{fl/fl}$ mice and their controls after DSS-induced colitis. Data of one (CO LP) and two (CO LN) independent experiments. Each dot represents a mouse. Bars indicate mean, and error bars indicate SEM. Statistical analyses were done by t-test.

The leukocytes isolated from the CO LP were further dissected for the presence of several immune cell types (Figure 70). Total cDCs and macrophages were identified as previously described (3.1.1), and no difference in their frequency within the CO LP of *Clec9a*$^{cre/+}$*Syk*$^{fl/fl}$ mice was found. Further, cDC1s and both cDC2s subsets and the DN DCs were analyzed for their occurrence, and similar values were obtained. Even though data points were spread within both groups. Determination of eosinophils, monocytes, and neutrophils showed a similar proportion in the CO LP of *Clec9a*$^{cre/+}$*Syk*$^{fl/fl}$ and control mice. Last, B and T cells were identified, and T cells were further subdivided based on their expression of CD4. The CD4 negative fraction contained the CD8 T cells and the unconventional T cells. Similar frequencies of B cells, total T cells, and the subdivided CD4$^+$ and CD4$^-$ T cells were found in the CO LP of *Clec9a*$^{cre/+}$*Syk*$^{fl/fl}$ and control mice.

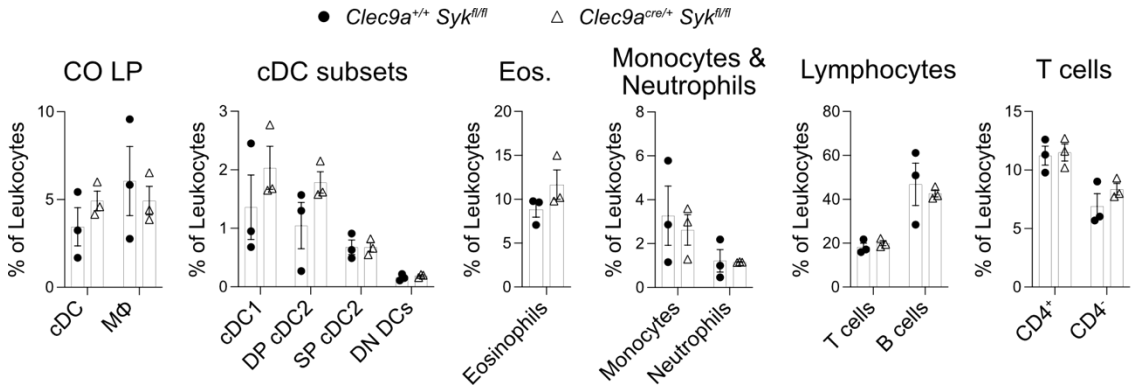

Figure 70 Frequency of cDCs and other myeloid and lymphoid cells in the CO LP of *Clec9a$^{cre/+}$Syk$^{fl/fl}$* mice upon acute colitis.

Frequency of total cDCs and macrophages and the four intestinal cDC subsets in the CO LP of *Clec9a$^{cre/+}$Syk$^{fl/fl}$* mice and their controls after DSS-induced colitis. The frequency of eosinophils, monocytes, and neutrophils as well as T and B cells in those mice is shown. T cells were further divided into CD4$^+$ and CD4$^-$ and analyzed for their frequency. Data of one experiment. Each dot represents a mouse. Bars indicate mean and error bars indicate SEM. Statistical analyses was done by t-test.

For the analysis of the CO LN, the focus was set on the occurrence of T cells and their capacity to produce cytokines. To assess the latter, isolated leukocytes were re-stimulated ex-vivo, which induced massive down-regulation of CD4. Therefore, T cells could only be subdivided based on their expression pattern of CD8a. However, the fraction of unconventional T cells lacking CD4 and CD8a is negligible in the LN, and CD8 negative T cells are predominantly CD4 T cells.

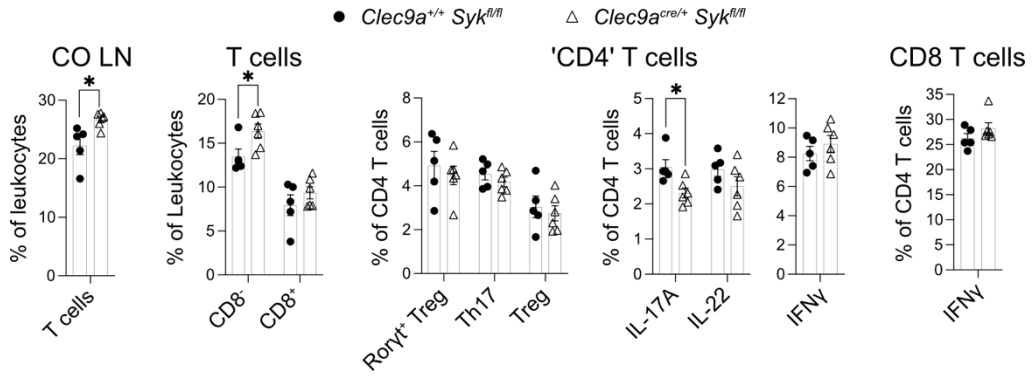

Figure 71 Frequency of T cells and several subsets in the CO LN of *Clec9a$^{cre/+}$Syk$^{fl/fl}$* mice upon acute colitis.

Frequency of total T cells and the two subsets subdivided by CD8a expression *Clec9a$^{cre/+}$Syk$^{fl/fl}$* mice and their controls after DSS-induced colitis. CD8$^-$ cells were analyzed for the frequency of Rorγt$^+$ Tregs, Th17, and Tregs and the production of IL-17A, IL-22, and IFNγ. Further on, the frequency of IFNγ expressing CD8 T cells was analyzed. Data of two independent experiments. Each dot represents a mouse. Bars indicate mean and error bars indicate SEM. Statistical analyses was done by t-test.

In the CO LN of *Clec9a*$^{cre/+}$*Syk*$^{fl/fl}$ mice, an increase of total T cells was observed, caused by a higher frequency of 'CD4' T cells, whereas CD8 T cells were found in similar proportions. Subdividing CD4 T cells by the Foxp3 and Rorγt expression identified Tregs, Th17 cells, and Rorγt^{+} Tregs. All three subsets could be detected in a similar frequency within the CD4 T cells. Measuring the production of IL-17A, IL-22, and IFNγ by CD4 T cells revealed a significant reduction of IL-17A^{+} CD4 T cells, whereby the other two cytokines were produced in similar proportions in CD4 T cells from *Clec9a*$^{cre/+}$*Syk*$^{fl/fl}$ and control mice. Further on, no difference could be found in the capacity of CD8 T cells to produce IFNγ. A similar trend of decreased Th17 and less IL-17A production by CD4 T cells was found in a cohort of 2 vs. 2 mice, which had to be sacrificed on day 8 due to reaching termination criteria (Data not shown).

4. Discussion

4.1 The Role of BCL10 in Intestinal cDCs in Health and Disease

4.1.1 Deletion of BCL10 does not alter cDC development but influences their capacity to polarize CD4 T cells

This study aimed to characterize the role of the signaling cascade of the CBM complex in cDCs in colitis and colitis-associated cancer. First, steady-state profiling was performed to exclude possible pre-dispositions of *Clec9a*$^{cre/+}$*Bcl10*$^{fl/fl}$ mice for later induction of acute and chronic colitis. Doing so, *Clec9a*$^{cre/+}$*Bcl10*$^{fl/fl}$ mice showed an overall normal cDC compartment in the spleen and the SI. However, the frequency of total migratory cDCs in the CO LN from *Clec9a*$^{cre/+}$*Bcl10*$^{fl/fl}$ mice tended to be decreased, caused by a significant decrease in the migratory cDC1 subsets. As migratory cDC1s in the CO LN migrated in a CCR7-dependent manner from the CO LP via the lymphatics into the LN, it may be presumed that cDC1s are increased in CO LP. The decrease could be caused by less migration or, alternatively, decreased overall presence of cDC1s in the colon (Cerovic et al. 2013, Esterházy et al. 2016). Analysis of the CO LP revealed a slight but not statistically significant increase of cDC1s in frequency. Therefore, an overall reduction of cDC1s within the colon does not cause a decrease in migratory cDC1 in its draining LN. Since no differences were found in examining the SI and its draining LN, a defect in the migration of cDC1s is unlikely. CD103^{+} cDC1s migrate upon activation into the colon-draining LN; a difference in activation and, therefore, less migration could explain the reduction migration of cDC1 into the CO LN (Cerovic et al. 2013).

In conclusion, BCL10 is dispensable for the overall development of cDCs and their colonization of the intestinal compartment. Whereas its deletion might alter the activation of colonic cDC1, leading to a reduced migration of cDC1s from the CO LP into the CO LN, where they usually cross-present self-antigens, induce CD8 effector T cells, and polarize CD4 T cells predominately to Th1 and Treg phenotype.

Therefore, the intestinal T cell compartment was investigated to address whether the deletion of BCL10 alters the activation of cDCs and, thus, their primary function to activate and polarize CD4 and CD8 T cells. No differences were found in the overall abundance and activation of CD4, CD8, and unconventional T cells, and further on, regulatory T cells occurred in a similar frequency in the intestines of *Clec9a*$^{cre/+}$*Bcl10*$^{fl/fl}$ and control mice.

Previously, it has been described that recognizing fungal PAMPs by Dectin-1 and Dectin-2 drives the induction of Th17 and Th1 cells (Drummond et al. 2011). However, profiling of the SI LP of *Clec9a*$^{cre/+}$*Bcl10*$^{fl/fl}$ mice revealed no difference in the occurrence of these CD4 T-helper subsets or their capacity to produce specific cytokines. In contrast, Th17 cells were reduced in the CO LP when the signaling cascade downstream of these CLRs was disrupted by deleting BCL10 in cDCs. A possible explanation for why this Th17 reduction can be observed in the colon but not within the SI is the change in the microbiota throughout the intestinal axis. Whereas food-derived antigens imprint the SI microbiota, the colon harbors increased amounts of microbes (Mowat and Agace 2014). This hypothesis is favored because SI-restricted Th17 deficiency in *CD11c*^{cre}*Syk*^{flox} mice was traced back to one specific pathogen activating Mincle but not Dectin-1 or Dectin-2 (Martinez-Lopez et al. 2019). Therefore, this respective pathogen, inducing CBM complex activation, might be absent within the SI luminal content, and alternative microbes are present in the colon. No matter what this Th17 deficiency triggers, this might influence the disease outcome of *Clec9a*$^{cre/+}$*Bcl10*$^{fl/fl}$ mice in colitis and CAC, as it has been shown that the increased susceptibility of CARD9 KO mice is in part mediated by the critical role of CARD9 in inducing adaptive Th17 cell responses (Sokol et al. 2013, Bergmann et al. 2017).

4.1.2 BCL10 deficiency alters the metabolism of cDCs

Profiling of the intestinal cDC and T cell compartment of *Clec9a*$^{cre/+}$*Bcl10*$^{fl/fl}$ mice pointed towards a difference in the activation of cDC1 and revealed a reduction in Th17 cells in the CO LP. However, cDC1s are not described to induce Th17 cells, but cDC2s were shown to induce Th17 cells (Schlitzer et al. 2013, Persson et al. 2013, Satpathy et al. 2013). Leading to the assumption that the deletion of BCL10 in cDCs alters the function of cDC1s and cDC2s. Therefore, transcriptional profiling was performed on colonic cDCs and macrophages to gain insights into the altered processes induced by the lack of BCL10. Unbiased clustering of those cells revealed a separation of all identified cDC clusters, but not macrophages, based on the genetic background of the cells. The most significant separation was observed for cDC1 and, to a lesser extent, in other cDC clusters.

That differential expression of *Bcl10* causes this separation could be excluded as similar transcript levels were detected in all cDC subsets from *Clec9a*$^{+/+}$*Bcl10*$^{fl/fl}$ and *Clec9a*$^{cre/+}$*Bcl10*$^{fl/fl}$ mice. As the sequencing occurred from the 5’ prime end of the mRNA, *Bcl10* transcripts detected in the cDCs from *Clec9a*$^{cre/+}$*Bcl10*$^{fl/fl}$ could lack exon 2 that is excised when the Cre recombinase is active. Therefore, the efficiency of the Cre recombinase under the *Clec9a* promoter was determined and revealed a deletion of the floxed

region in cDC1s and, to a lower extent, in the two intestinal cDC2 subsets. Whereby the DN DCs were unaffected, intestinal macrophages showed a slight reduction of the floxed Bcl10 allele. This different efficiency of the Cre recombinase resembles observations from the *Clec9a*^{cre} Fate mapping model in the lab, where some staining of the intestinal macrophages could also be observed in *Clec9a*$^{cre/+}$*Rosa*^{TOM} but not in *Clec9a*$^{cre/cre}$*Rosa*^{YFP}. Whether this is an effect of background labeling or the hint of a *Clec9a* expression history of some intestinal macrophages is still being investigated. Nonetheless, the slight decrease of *Bcl10* in the intestinal macrophages from *Clec9a*$^{cre/+}$*Bcl10*$^{fl/fl}$ mice presumably is not enough to induce an altered immune response as the single-cell sequencing data set revealed no significant effect on macrophages and transcriptional alterations were predominantly found in cDCs.

Further on, when heterozygous *Clec9a*^{cre} mice were used for fate mapping analysis, cDC2s were not as efficiently labeled with the respective fluorescent reporter as when homozygous *Clec9a*^{cre} mice were used. However, homozygous *Clec9a*^{cre} mice are in parallel knockouts for Clec9a/DNGR1, an essential receptor during cross-presentation of cell-associated antigens. Therefore, *Clec9a*$^{cre/+}$*Bcl10*$^{fl/fl}$ mice had to be used, and less efficient deletion of BCL10 in cDC2s had to be accepted. As currently no antibody is available for flow cytometric application, a comparison of the final protein level in intestinal cDCs was not possible. However, considering the high deletion efficiency of the floxed Bcl10 allele in cDC1 and cDC2, it can be assumed that cDC1s lack a sufficient amount of BCL10, and cDC2s at least should have a significant reduction.

The cluster separation based on the genetic background of the cDCs could be traced back to a reduction of the mitochondrial function depicted by a decreased expression of several genes involved in OXPHOS. That the most significant separation is detected with the cDC1s can be explained by two plausibilities: On the one hand, differentiated cDC1s express *Clec9a* and therefore have the highest deletion of BCL10. Conversely, cDC1s rely the most on OXPHOS, indicated by an increased mitochondrial membrane potential compared to cDC2s (McKenna et al. 2000, Sathaliyawala et al. 2010). Despite their distinct metabolic requirements for development and homeostasis, a common feature of cDCs is the rearrangement of the metabolisms upon activation from OXPHOS towards glycolysis. This glycolytic burst has been attributed to be a conserved response upon PRR activation and further maturation of the immunogenic cDCs (Everts et al. 2014, Thwe et al. 2019). However, transcriptomic profiling revealed only a downregulation of OXPHOS, and no alternative metabolic pathway, like glycolysis or fatty acid oxidation, was upregulated. Speaking against a metabolic switch upon PRR stimulation.

In addition to reduced OXPHOS genes, a downregulation of multiple Rps and Rpl genes, constituting the ribosome, could be detected. It has been shown that the translation level directly correlates with ATP production (Argüello et al. 2020). Therefore, this decreased expression of ribosomal genes encoding the primary translation site could result from decreased OXPHOS in the cDCs.

Furthermore, several MYC target genes were found in the list of downregulated genes in cDC1. Previous studies showed that a reduced MYC expression is associated with the terminal differentiation of several cellular lineages and a reduction of cell growth and proliferation (Carroll, Freie, Mathsyaraja and Eisenman 2018). In addition, another downregulated signaling cascade mediated by mTOR drives metabolic reprogramming, protein synthesis, and transcription downstream of PRRs and growth factor receptors (Sukhbaatar, Hengstschläger and Weichhart 2016). Furthermore, a connection between mTOR and MYC was identified, as the mTOR-driven phosphorylation of 4EBP1/eIF4B enhances the translation of MYC (Pourdehnad et al. 2013, Csibi et al. 2014). This phosphorylation of 4EBP1/ eIF4B promotes the CAP-dependent translation, an additional pathway downregulated in BCL10 deficient cDCs (von der Haar, Gross, Wagner and McCarthy 2004).

MYC-supported transcription has been shown downstream of TCR signaling in Tregs to mediate optimal mitochondrial metabolism for Treg expansion. This pathway is mediated by the protease activity of MALT1 within the CARD11-BCL10-MALT1 signalosome complex in T cells (Rosenbaum et al. 2019, Rosenbaum et al. 2022). It is possible that the CBM complex in cDCs has a similar function, and therefore, the deletion of BCL10 leads to less MALT1 signaling, followed by a reduction of MYC activity. However, in T cells, the activation of ribosomal genes and mitochondrial biogenesis through MYC and mTOR signaling drives T cell expansion (Preston et al. 2015). Whereas differentiated cDCs were described as predominantly post-mitotic (Ginhoux et al. 2009). Nevertheless, it has been shown that increased mTOR signaling leads to cDC1 expansion and might be explained by the activation of the PI3K pathway upon Flt3L binding to its receptor, driving cDC development (McKenna et al. 2000). However, further analysis of their cell cycle through cell cycle regression in the single-cell sequencing dataset combined with flow cytometric analysis of Ki67 levels revealed no difference in proliferation.

Three MYC paralogues have been identified: c-MYC, n-MYC, and l-MYC (He et al. 1998). Whereas c-MYC and n-MYC are involved in embryonic development and later, in general hematopoiesis, l-MYC is exclusively expressed in cDCs. The transition from c-MYC expression in cDC committed precursors to l-MYC in cDCs is driven by IRF8 upregulation, and higher expression can be found in cDC1 than in cDC2 (Kc et al. 2014, Anderson III et al. 2021). L-MYC is not required for cDC development but regulates core

biosynthetic processes, like ribosome synthesis, translation, and cell respiration, imprinting the biological fitness of the cell (Anderson III et al. 2020). Therefore, l-MYC was described as a regulator of the transcriptional program that changes throughout the DC maturation (Anderson III et al. 2020). Further, it has been claimed that l-MYC is suppressed during DC maturation (Ardouin et al. 2016, Manh et al. 2013).

Taken together, it is likely that the deletion of BCL10 leads to an altered early activation or maturation of cDCs. A current model of mTOR signaling in DCs described a rapid activation of mTOR upon PAMP recognition, promoting early pro-inflammatory response. In contrast, mTOR signaling decreases while the DC matures and migrates to the LN DC. During maturation, DCs shut down antigen uptake and optimize antigen processing and presentation (Sukhbaatar, Hengstschläger and Weichhart 2016). In accordance with this model, genes upregulated in BCL10 deficient cDC1 were mapped to antigen presentation pathway and genes constituting MHCII and MHCI, even though no differential expression of classical activation markers was found on the transcript level. This differential expression of MHCI and MHCII transcripts could not be confirmed in protein levels on cDC1 isolated from the CO LP of *Clec9a*$^{cre/+}$*Bcl10*$^{fl/fl}$ mice. However, migratory cDC1s in the CO LN showed increased MHCI and MHCII expression, likely explained by the delay between transcription and translation. Even though it seems like the deletion of BCL10 affects the activation of colonic cDCs, a recent study on the role of CARD9 in neutrophils revealed an increase of apoptotic metabolically stressed neutrophils upon CARD9 deletion (Danne et al. 2022). Additional studies addressing mitochondrial wellness by determining the mitochondrial membrane potential and mitochondrial mass using flow cytometric probes and Annexin staining to detect apoptotic cells should be done on colonic cDCs from *Clec9a*$^{cre/+}$*Bcl10*$^{fl/fl}$ mice. In doing so, it is suggested to restart the metabolic activity of isolated cells for a specific time by incubating them at 37°C as the cells are kept on ice for the whole isolation procedure, which might alter their active metabolism. This might explain why the analysis of the mitochondrial membrane potential with the TMRM probe did not reveal any differences in colonic BCL10-deficient cDCs, as the incubation at 37°C occurred only for a short time.

Flow cytometric analysis was used to investigate whether BCL10 deletion in cDCs leads to an altered activation. However, normal levels of the classical activation markers CD40 and CD86 were found on cDC1 and cDC2s isolated from the CO LP of *Clec9a*$^{cre/+}$*Bcl10*$^{fl/fl}$ mice. As the differential expression of MHCI and MHCII complexes was only seen on migratory cDC1 in the CO LN, the activation status of cDCs isolated from this organ was determined. Nevertheless, a similar expression of CD40 and CD86 was detected on BCL10 deficient and sufficient cDCs. This leads to the assumption that the altered mTOR and MYC activity in colonic cDCs is not caused by an increased activation state. Quite

the opposite might be the case, as a significant increase of PD-L1 could be detected in the colonic CD103$^-$ cDC2 population. Similar trends were observed for CD103$^+$ cDC2s and all migratory cDC subsets within the CO LN.

An increased level of PD-L1 points towards a tolerogenic phenotype of BCL10 deficient cDCs. Additionally, tolerogenic cDCs are described in the literature as marked by maintaining high OXPHOS; other studies reveal that the inhibition of mTOR induces a tolerogenic phenotype in DCs (Wculek et al. 2019b, Shao et al. 2020, Avancini et al. 2023). A more tolerogenic phenotype of cDCs from the CO LP of *Clec9a*$^{cre/+}$*Bcl10*$^{fl/fl}$ mice is underlined by the decrease of the inflammatory Th17 cells even though regulatory T cells did not increase.

4.1.3 Deletion of BCL10 in cDCs has no impact on acute colitis

Having identified a trend towards a tolerogenic phenotype of BCL10 deficient cDCs combined with a reduction of Th17 cells, the next step was to assess how this impacts acute colon inflammation. Even though a similar increased expression of PD-L1 on CO LN-derived cDCs and a reduction in IL-17A-producing CD4 T cells in the CO LP could be found in *Clec9a*$^{cre/+}$*BCl10*$^{fl/fl}$ mice suffering from acute colitis, no differences could be observed in disease severity. This was unexpected, as previous studies showed an increased susceptibility of CARD9 KO mice attributed to reduced Th17 induction (Sokol et al. 2013). However, the overall role of Th17 cells in experimental colitis and human IBD is controversial. In one study, neutralizing IL-17A and IL-17F ameliorated colitis, while others showed that anti-IL17 mAb aggravates colitis (Wedebye Schmidt et al. 2013, Ogawa et al. 2004, Maxwell et al. 2015). Further, it has been demonstrated that the ameliorated T cell-induced colitis in *CD11c*^{cre}*IRF4*^{flox} is mediated by a decrease of Th17 cells (Pool, Rivollier and Agace 2020). However, *CD11c*^{cre}*IRF4*^{flox} mice had no altered disease severity in DSS-induced colitis despite reduced Th17 cells in homeostatic conditions (Welty et al. 2013). Therefore, a reduction in Th17 cells does not necessarily mean an aggravated outcome in colitis. Further, it has been proposed that neutrophils and monocyte-derived cells predominantly mediate DSS-induced colitis. In contrast, T cell-mediated colitis largely depends on LP T cells and the cDC function (Tamoutounour et al. 2012, Mildner, Yona and Jung 2013, Maxwell et al. 2015).

Although the IL-22 production by CD4 T cells was similar between the genotypes, unconventional T cells showed significantly increased production. Previous studies depicted that secreted IL-22 acts on the epithelial cell to induce STAT3 and downstream cell survival and proliferation to induce epithelial restitution (Bergmann et al. 2017, Waldner and Neurath 2015, Frigerio, Lartey, D'Haens and Grootjans 2021, Lamas et al.

2016). Unconventional T cells are predominantly γδ T cells, which develop in the embryonic thymus and migrate to peripheral tissue rather than lymphoid organs. These γδ T cells are critical for intestinal epithelial permeability and barrier integrity as they promote the release of antimicrobial peptides and regulate tight junctions between enterocytes (Mielke et al. 2013, Zheng et al. 2008, Lee, Yang, Racke and Lovett-Racke 2015). Even though their functions are independent of MHC-dependent antigen presentation, it has been shown that cDCs are critical for their activation and expansion (Zheng et al. 2008, Muzaki et al. 2017, Willcox, Mohammed and Willcox 2020). Besides the classical Th17-polarizing cytokines produced by cDCs to enhance IL-17 production by γδ T cells, a study revealed that RA stimulated γδ T cells to produce IL-22 and thereby attenuated DSS-induced acute colitis (Muzaki et al. 2017, Mielke et al. 2013). A primary source of RA in the intestine are cDCs, facilitating tolerance under basal conditions (Guilliams et al. 2010). Considering the increased PD-L1 and the possible tolerogenic phenotype of BCL10 deficient cDCs, it is likely that their production of RA is enhanced and should be investigated.

However, the detected alterations in the T cell compartment of *Clec9a*$^{cre/+}$*BCl10*$^{fl/fl}$ mice had no significant impact on the DSS-induced acute colitis. Nevertheless, these alterations might influence the recovery of mild colitis. This hypothesis is further underlined through the shift towards a tolerogenic phenotype in the cDC compartment, observed in the CO LN of *Clec9a*$^{cre/+}$*BCl10*$^{fl/fl}$ mice, marked by the upregulation of PD-L1 on the surface of several cDC subsets.

4.1.4 Deletion of BCL10 in cDCs aggravates colitis-associated-cancer

In the next step, the *Clec9a*$^{cre/+}$*BCl10*$^{fl/fl}$ mouse model was utilized to study the role of the CBM complex in cDCs during inflammation-driven cancer development. When these mice were subjected to the AOM-DSS model to mimic CAC, increased tumor number, burden, and invasiveness were observed.

Based on weight loss and clinical scores, no significant difference in inflammation was detected in *Clec9a*$^{cre/+}$*BCl10*$^{fl/fl}$ mice compared to their controls. Therefore, increased tumor development is presumably not caused by heightened inflammation, which typically increases the risk of adenoma development (Gatenby et al. 2021). A previous study on *Card9*$^{-/-}$ mice revealed a pivotal role of IL-22, driving epithelial restitution and later fostering tumor development by activating STAT3 in epithelial cells (Bergmann et al. 2017). In line with this, increased IL-22 production by colonic unconventional T cells was observed after acute colitis in *Clec9a*$^{cre/+}$*BCl10*$^{fl/fl}$ mice, suggesting that deletion of BCL10 in cDCs

seems to cause an increase of IL-22 and thereby promotes tumor growth through increased proliferation. However, analysis of pSTAT3 and Ki67 in tumor areas and non-tumor tissue of the colon revealed similar epithelial cell proliferation, ruling out this possibility.

Increased tumor development did not impact surrounding intestinal organs in terms of inflammatory signs, as assessed by the infiltration of monocytes and neutrophils into the respective tissues. However, lymphadenopathy was observed in *Clec9a*$^{cre/+}$*BCl10*$^{fl/fl}$ mice with CAC, similar to acute colitis. This effect was limited to the CO LN and did not affect the other mesenteric lymph nodes draining the small intestine or the spleen, the largest lymphoid organ. Increased cellularity of the CO LN could be a side effect of the increased tumor burden, as it has been described overall cellularity of TDL increases with tumor progression (Roberts et al. 2016).

4.1.5 Loss of BCL10 alters tumorigenic cDCs

Profiling of the cDC1 and cDC2 subsets in the colon, within tumors and non-tumor tissue, and in the colon-draining LN depicted a similar presence of all determined subsets. Therefore, the deletion of BCL10 does not influence the infiltration of cDC1 and cDC2 subsets into the tumor or their migration into the CO LN for T cell priming. Due to the lack of respective analysis, no conclusion can be drawn regarding the activation of BCL10-deficient cDCs in the CO LP or CO LN. Specifically, it could be crucial to investigate whether there is an increased expression of PD-L1 in the lymph node during tumor development, likewise the observations in steady state and upon acute colitis.

Additional transcriptional profiling of cDCs isolated from the *Clec9a*$^{cre/+}$*BCl10*$^{fl/fl}$ mice tumor after AOM-DSS treatment was performed to assess the previous finding of reduced mitochondrial and ribosomal biogenesis, presumably caused by reduced mTOR and MYC signaling. However, inflammation and tumorigenesis abrogated this phenotype, as similar levels of OXPHOS and ribosomal genes could be detected, along with equal levels of MYC target genes.

Nonetheless, a significant reduction in *Cd40* expression was found in activated cDC1s and cDC2s. Other activation markers were expressed equally in activated cDC1s and cDC2s, with only migratory DCs showing reduced levels of CD86. CD40 signaling is known to increase the survival of cDCs and plays a critical role in their activation, antigen presentation, cytokine production, and immune regulatory functions (Gerner, Casey and Mescher 2008). Anti-CD40 treatment has been shown to enhance anti-tumor immunity

during anti-PD-1 treatments (Garris et al. 2018). It is unclear whether the reduced transcript level of CD40 results from decreased activation or reduced presence of pro-inflammatory cytokines. Moreover, the overall presence of IFNγ, a known stimulator of CD40 expression, was reduced in the *Clec9a*$^{cre/+}$*BCl10*$^{fl/fl}$ mice tumor tissue.

In addition to the reduced *Cd40* expression, genes encoding the HSP70 protein complex were decreased significantly in cDCs from *Clec9a*$^{cre/+}$*BCl10*$^{fl/fl}$ mice. HSPs are generally upregulated in cells in response to various forms of stress to prevent cellular damage and increase immunoregulation. The decreased capacity for stress-induced HSP expression has been associated with immune disorders (Wieten et al. 2010). A common form of stress within the tumor microenvironment is oxidative stress (Szatrowski and Nathan 1991). However, the transcriptional levels of genes responding to oxidative stress were expressed at equal levels in BCL10-deficient and sufficient cDCs. Nonetheless, several studies depicted that HIF1α, a transcription factor known to drive Hsp70 gene expression (Tsuchida et al. 2014, Xia et al. 2009), can be induced via mTOR signaling. Even though genes involved in mTOR signaling were not differentially expressed, mTOR activity might be reduced in BCL10 deficient cDCs (Land and Tee 2007, Dodd et al. 2015).

In addition to stress-induced upregulation of HSPs, it has been shown that pro-inflammatory cytokines like IFNγ, TNFα, or IL-1β can increase the levels of HSP70 and HSP90 by enhancing the activity of the Hsp70 and Hsp90 promoters. These effects depend on the STAT-1 transcription factor activation by IFNγ (Stephanou and Latchman 1999). HSP70 plays a vital role in cDCs, modulating their maturation, antigen presentation, and general immune response. HSP70 exhibits chaperone activity, assisting in protein folding and assembly. Furthermore, HSP70 can interact with specific antigens in cDCs to promote their processing and presentation on MHC complexes, thereby facilitating the T cell induction (Figueiredo et al. 2009, Takemoto et al. 2010). Nevertheless, HSP70 can also possess a tolerogenic function, as demonstrated by Hsp70$^{-/-}$ dendritic cells, which showed increased activation that inhibits tumor growth (Giri et al. 2021).

Overall, cDCs from *Clec9a*$^{cre/+}$*BCl10*$^{fl/fl}$ colonic tumors show hints towards an impaired capacity to activate T cells. However, the single-cell sequencing of isolated cDCs may hit only a fraction of tumor-infiltrating cDCs. It has been described that cDCs can upregulate CD64 under inflammatory conditions, which is the case for a colitis-induced tumor setting. These cells were excluded during the sort to perform transcriptional profiling of tumor-infiltrating cDCs.

4.1.6 BCL10 deficient cDCs lead to immuno-suppressive CD4 T cells and less cytotoxicity in colonic tumors

Profiling of T cells and innate lymphoid cells (ILCs) in the organs directly affected by colitis-associated cancer revealed a reduced NK1.1 expression on NK cells throughout the tumors, the surrounding non-tumor CO LP, and the CO LN. Reduced NK1.1 expression is associated with NK cell dysfunction and exhaustion (Li et al. 2022, Ni et al. 2020). However, no additional markers assessed in the spectral analysis nor transcriptomic profiling provided further evidence of NK cell exhaustion in *Clec9a*$^{cre/+}$*BCl10*$^{fl/fl}$ mice after AOM-DSS treatment.

Within the CO LN of tumor-bearing mice, a reduced frequency of CD8 T cells was found in *Clec9a*$^{cre/+}$*BCl10*$^{fl/fl}$ mice. Since similar frequencies of cDC1s were detected in the CO LN of *Clec9a*$^{cre/+}$*BCl10*$^{fl/fl}$ mice, it is more likely that their ability to prime or promote clonal expansion of CD8 T cells was affected. A general defect in CD8 T cell activation by CO LP-derived cDC1s has been ruled out through *in-vitro* proliferation assays. However, it's important to note that the antigen used in this assay was a soluble protein. The uptake and processing of cell-associated antigens, such as tumor-derived antigens, may differ. At this point, it has to be further considered that *Clec9a*, encoding DNGR-1, a mediator of cross-presentation of dead cell-associated antigens, is less expressed in *Clec9a*$^{cre/+}$*BCl10*$^{fl/fl}$ derived cDC1 due to the insertion of Cre in one of the alleles (Canton et al. 2021, Hanč et al. 2015). Whether this affects the protein level and the ability of cDC1s to cross-present should be further investigated. Nevertheless, a recent study suggested a role for DNGR-1 in limiting anti-tumor immunity in a setting where tumor cells overexpress the DC growth factor Flt3L (Cueto et al. 2021).

Analysis of tumor infiltration showed similar frequencies of CD4, CD8, and unconventional T cells among total leukocytes. However, the distribution of these T cell subsets within the T-cell compartment revealed a shift towards CD4 T cells and a reduction of unconventional T cells in *Clec9a*$^{cre/+}$*BCl10*$^{fl/fl}$ mice. This observation was consistent with the single-cell sequencing analysis of CD90.2^{+} cells, where more cells derived from *Clec9a*$^{cre/+}$*BCl10*$^{fl/fl}$ mice were detected in the CD4 clusters. In contrast, their presence within the TCRγδ cluster was significantly reduced. A previous study observed a correlation between the frequency of γδ T cells in tumor tissue and better outcome, underlining the anti-tumorigenic capacity of γδ T cells (Gentles et al. 2015). Further, it has been shown that γδ T cells can enhance the maturation and activation of DCs through the production of IFNγ and TNFα and promote the cytotoxic function of NK cells (Wang et al. 2021, Ni et al. 2012, Devilder et al. 2006, Maniar et al. 2010). Therefore, their reduced presence in the AOM-DSS-induced colonic tumors in *Clec9a*$^{cre/+}$*BCl10*$^{fl/fl}$ mice might lead to increased tumor development.

Within the CD4 T cell subset, a reduction in IL-17F production was observed. Additionally, measurement of IL-17A and IL-17F in tumor tissue revealed a corresponding decrease in Th17 cytokines, consistent with the deficiency of Th17 cells observed in homeostatic conditions and during acute colitis. Several studies have demonstrated the critical role of IL-17 in promoting tumor progression, invasion, and angiogenesis (Nam et al. 2008, Wang et al. 2009, Tartour et al. 1999). On the other hand, Th17-driven inflammation can play a crucial role in anti-tumor immunity as Th17 cells can recruit several immune cell types into the TME, including cytotoxic CD8 T cells, and promote their activation and expansion (Martin-Orozco et al. 2009). Together with the increased PD-1 on the cell surface, the CD4 T cell compartment within the tumors of *Clec9a*$^{cre/+}$*BCl10*$^{fl/fl}$ mice appears more immuno-suppressive and anti-inflammatory than in the control mice.

In contrast, Tregs identified in the spectral analysis of the colonic tumors from *Clec9a*$^{cre/+}$*BCl10*$^{fl/fl}$ mice showed significantly less CTLA4 on their cell surface. The expression of the costimulatory regulator CTLA4 on Tregs *in vivo* directly results from their rapid, constant homeostasis, and CTLA4 negatively regulates steady-state Treg homeostasis (Tang et al. 2008). Nevertheless, the immuno-suppressive phenotype of the CD4 T cells in *Clec9a*$^{cre/+}$*BCl10*$^{fl/fl}$ mice could be observed in the transcriptional profiling of the T cells isolated from the tumor environment after AOM-DSS. Whereas pro-inflammatory, Th17-associated genes were significantly downregulated, tolerogenic markers like PD-1 and PD-L1 were higher expressed. Furthermore, CD4 T cells expressed high levels of *Lgals3*, encoding Galectin-3, which has been described to suppress cytotoxic CD8 T cells in a tumor environment and thereby shape the anti-tumor immunity (Kouo et al. 2015). Furthermore, Galectin-3 has been shown to promote tumor cell survival and proliferation, angiogenesis, and modulate immune responses in the tumor microenvironment. It can inhibit the function of immune cells, such as T cells and NK cells (Farhad, Rolig and Redmond 2018).

In parallel with the increased immuno-suppressive phenotype of the CD4 T cells, single-cell sequencing revealed a reduced expression of granzymes in multiple cytotoxic cell types with *Clec9a*$^{cre/+}$*BCl10*$^{fl/fl}$ genetic background. Even though this could not be detected on a protein level, the reduction in transcript level favors the heightened suppressive function of the CD4 T cell compartment.

Furthermore, CD8 T cells isolated from the colonic tumors of *Clec9a*$^{cre/+}$*BCl10*$^{fl/fl}$ mice showed increased transcriptional expression of PD-L1 and a reduction in PD-1. The differential expression of the latter was already detected at the protein level during the spectral profiling of the tumor T cell compartment. While the primary role of PD-L1 is

often associated with its expression on tumor cells, Tregs, and APCs, recent research has revealed additional roles for PD-L1 on cytotoxic CD8 T cells within the tumor microenvironment. In particular, the upregulation of PD-L1 on CD8 T cells modulated T cell exhaustion. Like its role on other immune cells, PD-L1-expressing CD8 T cells can co-regulate the T cell-mediated immune response and contribute to an immunosuppressive environment (Zheng et al. 2022, Brochez et al. 2018).

In summary, a trend towards increased suppressive function in CD4 T cells was detected, and a reduced presence of the pro-inflammatory cytokines IL-17A and IL-17F. There was also a reduced presence of cytotoxic TCRγδ cells and an increased number of exhausted CD8 T cells. The subject of further research should be whether the latter is caused by the increased immuno-suppressive profile of CD4 T cells or originates in the reduced co-stimulation by cDCs. In particular, the capacity of BCL10 deficient cDC1 and cDC2s to produce the Th17-promoting cytokines IL-6, IL-1β, and IL-23 should be investigated to rule out if a deficiency of those leads to reduced Th17 induction (Heink et al. 2017, Chung et al. 2009, Korn et al. 2007). Furthermore, the capacity of cDCs to secrete the more tolerogenic factors TGFβ and RA should be addressed to clarify if increased production of those induces the tolerogenic T cell compartment (Lee et al. 2015, Guilliams et al. 2010).

4.2 The Role of SYK in Intestinal cDCs in steady state and acute colitis

4.2.1 Deletion of SYK has no impact on cDC development or their function to polarize T cells

In parallel to the studies on *Clec9a*$^{cre/+}$*Bcl10*$^{fl/fl}$ to investigate the role of BCL10, mainly the function of CBM complex in cDCs, *Clec9a*$^{cre/+}$*Syk*$^{fl/fl}$ mice underwent intense profiling for their intestinal cDC and T cell compartment. The SYK kinase is the critical link between surface CLRs Dectin-1, Dectin-2, and Mincle and the downstream initiation of CBM complex formation and activation. Therefore, the deletion of SYK in Clec9a expressing CDPs and in the cDC lineage should abrogate this signaling cascade.

Assessment of the organ-specific cDC populations in the spleen and several intestinal organs revealed no significant difference in the occurrence of cDC1s and cDC2s within each organ. However, a slight reduction of the cDC2 population could be observed in the spleen and the SI LP. Nevertheless, SYK in cDCs appears redundant for their overall development.

A previous study identified that dome-CD11b$^+$ DCs and LysoDCs located in PPs mediate Mincle- and Syk-dependent Th17 differentiation in the SI LP upon commensal bacteria encountering (Martinez-Lopez et al. 2019). Therefore, the T cell compartment of *Clec9a*$^{cre/+}$*Syk*$^{fl/fl}$ mice was investigated for similar alterations. Analysis of mLN, PPs, and the LP from SI and colon revealed identical CD4, CD8, and unconventional T cell frequencies. No alterations regarding the CD4 Th17, Treg, and gut-specific Rorγt$^+$ Treg subsets have been found. Nonetheless, intestinal CD4 T cells showed a trend for a reduced capacity to produce IL-17A if re-stimulated *ex-vivo*. This decrease was not statistically significant but could be observed in all four analyzed intestinal organs. One reason the phenotype observed in *CD11c*^{cre}*Syk*^{flox} mice does not appear in *Clec9a*$^{cre/+}$*Syk*$^{fl/fl}$ mice could be that LysoDCs are monocyte-derived and will not be targeted in the *Clec9a*-driven model. Additionally, SYK deletion might be more efficient in CD11c-driven Cre recombinase, particularly for the cDC2 lineage, as CD11c is constantly expressed in cDCs, whereas the Clec9a-cre model targets the cDC progenitor. From Fate Mapping models, it is already known that labeling is lower in cDC2 despite different ontogeny (Schraml et al. 2013).

Furthermore, microbiota significantly impacts Th17 development, and Martinez-Lopez *et al.* traced the Mincle-Syk-dependent Th17 generation to vancomycin-resistant intestinal bacteria (Martinez-Lopez et al. 2019). It might be possible that the respective microbes leading to the activation of the Mincle-SYK cascade are not present in the microbiota of mice from our facility.

4.2.2 Transcriptomic profiling of intestinal cDCs from *Clec9a*$^{cre/+}$*Syk*$^{fl/fl}$

Even though cDC1 and cDC2 appeared normal in the intestine, transcriptomic profiling was used to clarify whether the function of cDCs was altered. Therefore, cDCs, isolated from SI LP, were subjected to single-cell sequencing. The first approach to analyzing the transcript levels of *Syk* revealed a similar expression in *Clec9a*$^{cre/+}$*Syk*$^{fl/fl}$ derived cDCs and their controls. This was entirely surprising as the deletion of *Syk* should be very efficient in cDC1s as they continue to express *Clec9a*. However, it is unclear if the excision of the floxed exon influences the transcription. As the sequencing occurs from the 5’ prime end of the mRNA, and the floxed exon is more localized towards the 3’ prime end, the selected sequencing method presumably detects Syk mRNA despite the excised floxed exon. As a commercially available antibody is there to detect SYK protein by flow cytometry, cDCs were isolated from different organs, and the SYK protein level was assessed. Even though this method did not allow quantification of the excised exon, cDC1 and cDC2 showed a reduction of SYK expression in terms of SYK$^+$ cells and the level of SYK in the remaining cells. This analysis revealed that the main fraction of cDCs

still expressed SYK at a reduced frequency. This fact might contribute to the previous findings that deleting SYK in cDCs does not induce the Th17 deficiency in the SI LP as published for *CD11*^{cre}*Syk*^{flox}. The remaining amount of SYK protein might still be able to mediate signaling from surface CLRs and activate downstream signaling cascades under homeostatic conditions like control cells. How potent cDCs from *Clec9a*$^{cre/+}$*Syk*$^{fl/fl}$ mice drive an immune response against pathogens targeting PRRs upstream of SYK, like Dectin-1, Dectin-2, or Mincle, might be addressed in *ex-vivo* stimulation assays. This should provide information on whether the remaining SYK protein is sufficient to transmit the receptor's signal entirely or whether this reduction already leads to a defect in the SYK signaling pathway.

Further analysis of the sequencing data set revealed multiple differentially expressed genes in more than one cDC cluster. All these genes could be mapped to the IFNγ response or the TNFα signaling via NF-κB. These pathways were upregulated in cDCs derived from the SI LP of *Clec9a*$^{cre/+}$*Syk*$^{fl/fl}$. However, both signaling pathways were not previously described as connected to SYK kinase. Nevertheless, both TNFα signaling and SYK lead to the activation of MAPK and NF-κB (Maney, Reynolds, Krippner-Heidenreich and Hilkens 2014, Mócsai, Ruland and Tybulewicz 2010).

TNFα and IFNγ signaling in DCs has been described to regulate their maturation and survival. DCs further shape their immune response by influencing their antigen presentation, co-stimulatory molecule expression, and cytokine production, thereby contributing to the coordination of innate and adaptive immune responses (Maney et al. 2014, Pan et al. 2004). Although no maturation and activation markers were found upregulated on the transcriptional level, this should be confirmed on the protein level in the future. Several immune cells such as T cells, ILCs including NK cells, and to a lesser extent, macrophages and DCs can produce TNFα and IFNγ. IFNγ has been addressed in the T cells, and no difference could be observed. Nonetheless, the spread of IFNγ production was relatively high in CD8 and unconventional T cells. Therefore, future investigations should clarify if TNFα and IFNγ levels are increased in the SI LP of *Clec9a*$^{cre/+}$*Syk*$^{fl/fl}$.

4.2.3 Reduced level of SYK in cDCs has no significant impact on acute colitis

During acute and chronic inflammations in patients suffering from IBD, an increased expression of SYK has been found at the sites of the inflammation (Biagioli et al. 2018). As SYK is widely expressed in hematopoietic cells, this could be the consequence of immune cell infiltrations. Some studies started to investigate the role of SYK kinase during acute colitis and found that the abrogation of SYK signaling in all hematopoietic-derived

cells attenuates acute inflammation (Biagioli et al. 2018). However, this study used Syk-deficient radiation chimeras, as full-body knockouts are lethal. These chimeras have been previously described to fail the accumulation of mature B cells and showed impaired development of some thymocytes (Turner et al. 1995).

In contrast, the deletion of SYK in the myeloid branch, in particular in macrophages of the immune system, increased inflammation during chemical-induced colitis (Malik et al. 2018). Reduction of SYK in cDCs in the *Clec9a*$^{cre/+}$*Syk*$^{fl/fl}$ model and subsequent treatment with a low dose of DSS showed no significant influence on disease outcome. Nonetheless, *Clec9a*$^{cre/+}$*Syk*$^{fl/fl}$ started to recover slightly earlier than control mice, even though reduced inflammation was not underlined by serum cytokines or histological analysis of colon tissue at end-point analysis.

Further analysis of the colon-draining LN revealed a reduced capacity of CD4 T cells to produce IL-17A. Unfortunately, data regarding the T cell compartment at the site of inflammation is missing and should be investigated in the future. Furthermore, in-depth phenotyping of the cDC compartment in the CO LP and CO LN should be included. Nonetheless, a reduced presence of IL-17A in LN-derived T cells upon acute inflammation and the trend towards reduced Th17 cells under homeostatic conditions is not unexpected. The activation of the CLRs inducing SYK kinase and further CBM-complex activation has been described to favor Th17 polarization through the production of IL-6, Il-23, and TGFβ (Ruland 2008).

Whether this trend of faster recovery or reduced inflammation, together with the potential reduced Th17 cells, impacts chronic colitis and tumor development is part of future investigations. Previous studies described an anti-tumorigenic role of SYK in *Lysm*-expressing cells. However, this function was predominantly traced back to its role in maintaining microbial homeostasis (Malik et al. 2018).

4.3 The Role of SYK-mediated BCL10 Signaling in Intestinal cDCs

Deletion of BCL10 in cDCs led to a metabolic alteration in colonic cDCs, which can be traced back to reduced BCL10-MALT1 signaling, reducing mTOR and MYC signaling. Whether this signaling occurs in a CARD9-dependent manner is part of future investigations. Furthermore, it is still being determined if the signal that drives this function of BCL10 originates from the SYK kinase. Transcriptional profiling of intestinal cDCs from *Clec9a*$^{cre/+}$*Syk*$^{fl/fl}$ revealed no differences in OXPHOS, mTOR signaling of MYC target gene expression. However, cDCs for this analysis were sorted from the SI LP and not

the CO LP for the cDCs' profiling of *Clec9a*$^{cre/+}$*Bcl10*$^{fl/fl}$. Even though both intestines harbor the same subpopulations of cDCs, the composition shifts from a cDC2 dominant cDC compartment towards a cDC1 overload.

Furthermore, the microbial signals activating the cDCs differ between the two intestinal organs. As a previous study showed that SYK-mediated signaling upon helminth infection induces regulatory DCs that can block T cell-dependent colitis (Hang et al. 2016), it is likely that SYK indeed activates BCL10 to mediate mTOR and MYC signaling. Therefore, additional studies should directly compare cDCs derived from the CO LP of *Clec9a*$^{cre/+}$*Syk*$^{fl/fl}$ and *Clec9a*$^{cre/+}$*Bcl10*$^{fl/fl}$. A further point regarding the microbiome should be considered here, as mice of both genotypes originated from different mouse houses when transcriptional profiling was performed.

However, it must be considered that cDCs from *Clec9a*$^{cre/+}$*Syk*$^{fl/fl}$ retain SYK protein even though its expression is decreased compared to control cells. In particular, detected SYK expression is still relatively high in cDC1 even though this cDC subset expresses Cre recombinase, and a high deletion would be expected. Whether this is a result of the reduced excision efficiency of the Cre recombinase has to be investigated through the quantification of either the floxed allele in the genomic DNA or the presence of the floxed exon in mRNA transcripts, as Cre efficiency depends on the accessibility of the floxed locus (Tian and Zhou 2021, Liu et al. 2013). This is further highlighted by the fact that intestinal macrophages from *Clec9a*$^{cre/+}$*Bcl10*$^{fl/fl}$ mice showed a slight reduction of floxed Bcl10 locus, whereas no reduced SYK protein was observed. However, it might be worse to investigate the protein level of BCL10 in cDCs from *Clec9a*$^{cre/+}$*Bcl10*$^{fl/fl}$ mice to clarify if this small Cre activity in macrophages results in reduced protein levels.

A similarity between BCL10 and SYK deleted/reduced cDC1 was the significant upregulation of *Clec7a*, which could be confirmed through increased Dectin-1 detection on the cell surface. Currently, it is known that Dectin-1 expression can be enhanced upon microbial stimuli either binding directly to Dectin-1 or other PRRs or proinflammatory cytokines like TNFα, IL-1β, or IL-6 (Willment et al. 2003, Ozment-Skelton et al. 2009, Feriotti et al. 2015). As none of these signaling pathways is consistently upregulated in both BCL10 and SYK deficient cDC1, the increased expression of Dectin-1 could be a rescue mechanism of the cell to compensate for the reduced signaling through BCL10 and SYK, respectively. Alternatively, the SYK-BCL10 axis further mediates a feedback loop to regulate Dectin-1 expression.

In summary, it could be shown that the deletion of BCL10, and thereby the disruption of CARD9-BCL10-MALT1 signaling complex, in colonic cDCs altered their metabolism, leading to an increased tumor development upon chronic colitis. If this function of BCL10 depends on CARD9 interaction and requires activation via SYK kinase, is part of future investigations.

References

Abe, K., K. P. Nguyen, S. D. Fine, J.-H. Mo, C. Shen, S. Shenouda, M. Corr, S. Jung, J. Lee & L. Eckmann (2007) Conventional dendritic cells regulate the outcome of colonic inflammation independently of T cells. *Proceedings of the National Academy of Sciences,* 104**,** 17022-17027.

Abraham, C. & J. H. Cho (2009) Mechanisms of disease. *N Engl J Med,* 361**,** 2066-78.

Alberts, B., A. Johnson, J. Lewis & e. al. 2002. *Molecular Biology of the Cell*. New York: Garland Science.

Aliberti, J., O. Schulz, D. J. Pennington, H. Tsujimura, C. Reis e Sousa, K. Ozato & A. Sher (2003) Essential role for ICSBP in the in vivo development of murine CD8α+ dendritic cells. *Blood, The Journal of the American Society of Hematology,* 101**,** 305-310.

Anderson III, D. A., T. L. Murphy, R. N. Eisenman & K. M. Murphy (2020) The MYCL and MXD1 transcription factors regulate the fitness of murine dendritic cells. *Proceedings of the National Academy of Sciences,* 117**,** 4885-4893.

Anderson III, D. A., F. Ou, S. Kim, T. L. Murphy & K. M. Murphy (2021) Transition from cMyc to L-Myc during dendritic cell development coordinated by rising levels of IRF8. *Journal of Experimental Medicine,* 219**,** e20211483.

Ardouin, L., H. Luche, R. Chelbi, S. Carpentier, A. Shawket, F. M. Sanchis, C. Santa Maria, P. Grenot, Y. Alexandre & C. Grégoire (2016) Broad and largely concordant molecular changes characterize tolerogenic and immunogenic dendritic cell maturation in thymus and periphery. *Immunity,* 45**,** 305-318.

Argüello, R. J., A. J. Combes, R. Char, J.-P. Gigan, A. I. Baaziz, E. Bousiquot, V. Camosseto, B. Samad, J. Tsui & P. Yan (2020) SCENITH: a flow cytometry-based method to functionally profile energy metabolism with single-cell resolution. *Cell metabolism,* 32**,** 1063-1075. e7.

Auffray, C., D. K. Fogg, E. Narni-Mancinelli, B. Senechal, C. Trouillet, N. Saederup, J. Leemput, K. Bigot, L. Campisi & M. Abitbol (2009) CX3CR1+ CD115+ CD135+ common macrophage/DC precursors and the role of CX3CR1 in their response to inflammation. *Journal of Experimental Medicine,* 206**,** 595-606.

Avancini, D., A. Testori, L. Fresolone, G. Andolfi, M. Vuono, V. Martinelli, F. R. S. de Sio & S. Gregori (2023) Aryl hydrocarbon receptor activity downstream of IL-10 signaling is required to promote regulatory functions in human dendritic cells. *Cell Reports,* 42.

Bachem, A., E. Hartung, S. Güttler, A. Mora, X. Zhou, A. Hegemann, M. Plantinga, E. Mazzini, P. Stoitzner & S. Gurka (2012) Expression of XCR1 characterizes the Batf3-dependent lineage of dendritic cells capable of antigen cross-presentation. *Frontiers in immunology,* 3**,** 214.

Bain, C., J. Montgomery, C. Scott, J. Kel, M. Girard-Madoux, L. Martens, T. Zangerle-Murray, J. Ober-Blöbaum, D. Lindenbergh-Kortleve & J. Samsom (2017) TGFβR signalling controls CD103+ CD11b+ dendritic cell development in the intestine. *Nature communications,* 8**,** 620.

Bain, C. C., A. Bravo-Blas, C. L. Scott, E. Gomez Perdiguero, F. Geissmann, S. Henri, B. Malissen, L. C. Osborne, D. Artis & A. M. Mowat (2014) Constant replenishment from circulating monocytes maintains the macrophage pool in the intestine of adult mice. *Nature immunology,* 15**,** 929-937.

Bain, C. C. & A. M. Mowat (2014) The monocyte-macrophage axis in the intestine. *Cellular immunology,* 291**,** 41-48.

Barry, K. C., J. Hsu, M. L. Broz, F. J. Cueto, M. Binnewies, A. J. Combes, A. E. Nelson, K. Loo, R. Kumar & M. D. Rosenblum (2018) A natural killer–dendritic cell axis defines checkpoint therapy–responsive tumor microenvironments. *Nature medicine,* 24**,** 1178-1191.

Beaugerie, L. & S. H. Itzkowitz (2015) Cancers complicating inflammatory bowel disease. *New England Journal of Medicine,* 372**,** 1441-1452.

Bergmann, H., S. Roth, K. Pechloff, E. A. Kiss, S. Kuhn, M. Heikenwälder, A. Diefenbach, F. R. Greten & J. Ruland (2017) Card9-dependent IL-1β regulates IL-22 production from group

3 innate lymphoid cells and promotes colitis-associated cancer. *European Journal of Immunology,* 47**,** 1342-1353.

Berndt, B. E., M. Zhang, G.-H. Chen, G. B. Huffnagle & J. Y. Kao (2007) The role of dendritic cells in the development of acute dextran sulfate sodium colitis. *The Journal of Immunology,* 179**,** 6255-6262.

Biagioli, M., A. Mencarelli, A. Carino, S. Cipriani, S. Marchianò, C. Fiorucci, A. Donini, L. Graziosi, F. Baldelli & E. Distrutti (2018) Genetic and pharmacological dissection of the role of spleen tyrosine kinase (Syk) in intestinal inflammation and immune dysfunction in inflammatory bowel diseases. *Inflammatory Bowel Diseases,* 24**,** 123-135.

Binnewies, M., A. M. Mujal, J. L. Pollack, A. J. Combes, E. A. Hardison, K. C. Barry, J. Tsui, M. K. Ruhland, K. Kersten & M. A. Abushawish (2019) Unleashing type-2 dendritic cells to drive protective antitumor CD4+ T cell immunity. *Cell,* 177**,** 556-571. e16.

Bosteels, C., K. Neyt, M. Vanheerswynghels, M. J. van Helden, D. Sichien, N. Debeuf, S. De Prijck, V. Bosteels, N. Vandamme & L. Martens (2020) Inflammatory type 2 cDCs acquire features of cDC1s and macrophages to orchestrate immunity to respiratory virus infection. *Immunity,* 52**,** 1039-1056. e9.

Böttcher, J. P., E. Bonavita, P. Chakravarty, H. Blees, M. Cabeza-Cabrerizo, S. Sammicheli, N. C. Rogers, E. Sahai, S. Zelenay & C. R. e Sousa (2018) NK cells stimulate recruitment of cDC1 into the tumor microenvironment promoting cancer immune control. *Cell,* 172**,** 1022-1037. e14.

Boyle, J. P., R. Parkhouse & T. P. Monie (2014) Insights into the molecular basis of the NOD2 signalling pathway. *Open biology,* 4**,** 140178.

Brochez, L., A. Meireson, I. Chevolet, N. Sundahl, P. Ost & V. Kruse (2018) Challenging PD-L1 expressing cytotoxic T cells as a predictor for response to immunotherapy in melanoma. *Nature communications,* 9**,** 2921.

Brown, G. D., J. A. Willment & L. Whitehead (2018) C-type lectins in immunity and homeostasis. *Nature Reviews Immunology,* 18**,** 374-389.

Broz, M. L., M. Binnewies, B. Boldajipour, A. E. Nelson, J. L. Pollack, D. J. Erle, A. Barczak, M. D. Rosenblum, A. Daud & D. L. Barber (2014) Dissecting the tumor myeloid compartment reveals rare activating antigen-presenting cells critical for T cell immunity. *Cancer cell,* 26**,** 638-652.

Buchele, V., P. Konein, T. Vogler, T. Kunert, K. Enderle, H. Khan, M. Büttner-Herold, C. H. Lehmann, L. Amon & S. Wirtz (2021) Th17 cell-mediated colitis is positively regulated by interferon regulatory factor 4 in a T cell-extrinsic manner. *Frontiers in Immunology,* 11**,** 590893.

Cabeza-Cabrerizo, M., A. Cardoso, C. M. Minutti, M. Pereira da Costa & C. Reis e Sousa (2021) Dendritic cells revisited. *Annual review of immunology,* 39**,** 131-166.

Cabeza-Cabrerizo, M., J. van Blijswijk, S. Wienert, D. Heim, R. P. Jenkins, P. Chakravarty, N. Rogers, B. Frederico, S. Acton & E. Beerling (2019) Tissue clonality of dendritic cell subsets and emergency DCpoiesis revealed by multicolor fate mapping of DC progenitors. *Science immunology,* 4**,** eaaw1941.

Canton, J., H. Blees, C. M. Henry, M. D. Buck, O. Schulz, N. C. Rogers, E. Childs, S. Zelenay, H. Rhys & M.-C. Domart (2021) The receptor DNGR-1 signals for phagosomal rupture to promote cross-presentation of dead-cell-associated antigens. *Nature immunology,* 22**,** 140-153.

Carroll, P. A., B. W. Freie, H. Mathsyaraja & R. N. Eisenman (2018) The MYC transcription factor network: balancing metabolism, proliferation and oncogenesis. *Frontiers of medicine,* 12**,** 412-425.

Caton, M. L., M. R. Smith-Raska & B. Reizis (2007) Notch–RBP-J signaling controls the homeostasis of CD8− dendritic cells in the spleen. *The Journal of experimental medicine,* 204**,** 1653-1664.

Cerovic, V., C. C. Bain, A. M. Mowat & S. W. Milling (2014) Intestinal macrophages and dendritic cells: what's the difference? *Trends in immunology,* 35**,** 270-277.

Cerovic, V., S. Houston, C. Scott, A. Aumeunier, U. Yrlid, A. Mowat & S. Milling (2013) Intestinal CD103− dendritic cells migrate in lymph and prime effector T cells. *Mucosal immunology,* 6**,** 104-113.

Chiossone, L., P.-Y. Dumas, M. Vienne & E. Vivier (2018) Natural killer cells and other innate lymphoid cells in cancer. *Nature Reviews Immunology,* 18**,** 671-688.

Chung, Y., S. H. Chang, G. J. Martinez, X. O. Yang, R. Nurieva, H. S. Kang, L. Ma, S. S. Watowich, A. M. Jetten & Q. Tian (2009) Critical regulation of early Th17 cell differentiation by interleukin-1 signaling. *Immunity,* 30**,** 576-587.

Coombes, J. L., K. R. Siddiqui, C. V. Arancibia-Cárcamo, J. Hall, C.-M. Sun, Y. Belkaid & F. Powrie (2007) A functionally specialized population of mucosal CD103+ DCs induces Foxp3+ regulatory T cells via a TGF-β–and retinoic acid–dependent mechanism. *The Journal of experimental medicine,* 204**,** 1757-1764.

Csibi, A., G. Lee, S.-O. Yoon, H. Tong, D. Ilter, I. Elia, S.-M. Fendt, T. M. Roberts & J. Blenis (2014) The mTORC1/S6K1 pathway regulates glutamine metabolism through the eIF4B-dependent control of c-Myc translation. *Current biology,* 24**,** 2274-2280.

Cueto, F. J., C. Del Fresno, P. Brandi, A. J. Combes, E. Hernández-García, A. R. Sánchez-Paulete, M. Enamorado, C. P. Bromley, M. J. Gomez & R. Conde-Garrosa (2021) DNGR-1 limits Flt3L-mediated antitumor immunity by restraining tumor-infiltrating type I conventional dendritic cells. *Journal for immunotherapy of cancer,* 9.

Danne, C., C. Michaudel, J. Skerniskyte, J. Planchais, A. Magniez, A. Agus, M.-L. Michel, B. Lamas, G. Da Costa & M. Spatz (2022) CARD9 in neutrophils protects from colitis and controls mitochondrial metabolism and cell survival. *Gut*.

Devilder, M.-C., S. Maillet, I. Bouyge-Moreau, E. Donnadieu, M. Bonneville & E. Scotet (2006) Potentiation of antigen-stimulated Vγ9Vδ2 T cell cytokine production by immature dendritic cells (DC) and reciprocal effect on DC maturation. *The Journal of Immunology,* 176**,** 1386-1393.

Dieleman, L. A., B. U. Ridwan, G. S. Tennyson, K. W. Beagley, R. P. Bucy & C. O. Elson (1994) Dextran sulfate sodium-induced colitis occurs in severe combined immunodeficient mice. *Gastroenterology,* 107**,** 1643-1652.

Dinarello, C. A., D. Novick, S. Kim & G. Kaplanski (2013) Interleukin-18 and IL-18 binding protein. *Frontiers in immunology,* 4**,** 289.

Dodd, K. M., J. Yang, M. H. Shen, J. R. Sampson & A. R. Tee (2015) mTORC1 drives HIF-1α and VEGF-A signalling via multiple mechanisms involving 4E-BP1, S6K1 and STAT3. *Oncogene,* 34**,** 2239-2250.

Dolan, B. P., K. D. Gibbs & S. Ostrand-Rosenberg (2006) Dendritic cells cross-dressed with peptide MHC class I complexes prime CD8+ T cells. *The Journal of Immunology,* 177**,** 6018-6024.

dos Anjos Cassado, A. (2017) F4/80 as a major macrophage marker: the case of the peritoneum and spleen. *Macrophages: Origin, functions and biointervention***,** 161-179.

Dress, R. J., C.-A. Dutertre, A. Giladi, A. Schlitzer, I. Low, N. B. Shadan, A. Tay, J. Lum, M. F. B. M. Kairi & Y. Y. Hwang (2019) Plasmacytoid dendritic cells develop from Ly6D+ lymphoid progenitors distinct from the myeloid lineage. *Nature immunology,* 20**,** 852-864.

Drummond, R. A., S. Saijo, Y. Iwakura & G. D. Brown (2011) The role of Syk/CARD9 coupled C-type lectins in antifungal immunity. *European journal of immunology,* 41**,** 276-281.

Drummond, R. A., M. Swamydas, V. Oikonomou, B. Zhai, I. M. Dambuza, B. C. Schaefer, A. C. Bohrer, K. D. Mayer-Barber, S. A. Lira & Y. Iwakura (2019) CARD9+ microglia promote antifungal immunity via IL-1β-and CXCL1-mediated neutrophil recruitment. *Nature immunology,* 20**,** 559-570.

Duong, E., T. B. Fessenden, E. Lutz, T. Dinter, L. Yim, S. Blatt, A. Bhutkar, K. D. Wittrup & S. Spranger (2022) Type I interferon activates MHC class I-dressed CD11b+ conventional dendritic cells to promote protective anti-tumor CD8+ T cell immunity. *Immunity,* 55**,** 308-323. e9.

Edelson, B. T., T. R. Bradstreet, W. KC, K. Hildner, J. W. Herzog, J. Sim, J. H. Russell, T. L. Murphy, E. R. Unanue & K. M. Murphy (2011) Batf3-dependent CD11blow/− peripheral dendritic cells are GM-CSF-independent and are not required for Th cell priming after subcutaneous immunization. *PloS one,* 6**,** e25660.

Edelson, B. T., W. KC, R. Juang, M. Kohyama, L. A. Benoit, P. A. Klekotka, C. Moon, J. C. Albring, W. Ise & D. G. Michael (2010) Peripheral CD103+ dendritic cells form a unified subset developmentally related to CD8α+ conventional dendritic cells. *Journal of Experimental Medicine,* 207**,** 823-836.

Edwards, A. D., D. Chaussabel, S. Tomlinson, O. Schulz, A. Sher & C. Reis e Sousa (2003) Relationships among murine CD11chigh dendritic cell subsets as revealed by baseline gene expression patterns. *The Journal of Immunology,* 171**,** 47-60.

Esterházy, D., M. C. Canesso, L. Mesin, P. A. Muller, T. B. de Castro, A. Lockhart, M. ElJalby, A. M. Faria & D. Mucida (2019) Compartmentalized gut lymph node drainage dictates adaptive immune responses. *Nature,* 569**,** 126-130.

Esterházy, D., J. Loschko, M. London, V. Jove, T. Y. Oliveira & D. Mucida (2016) Classical dendritic cells are required for dietary antigen–mediated induction of peripheral Treg cells and tolerance. *Nature immunology,* 17**,** 545-555.

Everts, B., E. Amiel, S. C.-C. Huang, A. M. Smith, C.-H. Chang, W. Y. Lam, V. Redmann, T. C. Freitas, J. Blagih & G. J. Van Der Windt (2014) TLR-driven early glycolytic reprogramming via the kinases TBK1-IKKε supports the anabolic demands of dendritic cell activation. *Nature immunology,* 15**,** 323-332.

Everts, B., R. Tussiwand, L. Dreesen, K. C. Fairfax, S. C.-C. Huang, A. M. Smith, C. M. O'Neill, W. Y. Lam, B. T. Edelson & J. F. Urban Jr (2016) Migratory CD103+ dendritic cells suppress helminth-driven type 2 immunity through constitutive expression of IL-12. *Journal of Experimental Medicine,* 213**,** 35-51.

Farhad, M., A. S. Rolig & W. L. Redmond (2018) The role of Galectin-3 in modulating tumor growth and immunosuppression within the tumor microenvironment. *Oncoimmunology,* 7**,** e1434467.

Feriotti, C., S. B. Bazan, F. V. Loures, E. F. Araújo, T. A. Costa & V. L. Calich (2015) Expression of dectin-1 and enhanced activation of NALP3 inflammasome are associated with resistance to paracoccidioidomycosis. *Frontiers in microbiology,* 6**,** 913.

Ferlay, J., M. Ervik, F. Lam, M. Colombet, L. Mery, M. Piñeros, A. Znaor, I. Soerjomataram & F. Bray. 2020. Global Cancer Observatory: Cancer Today. International Agency for Research on Cancer.

Ferris, S. T., V. Durai, R. Wu, D. J. Theisen, J. P. Ward, M. D. Bern, J. T. Davidson IV, P. Bagadia, T. Liu & C. G. Briseño (2020) cDC1 prime and are licensed by CD4+ T cells to induce anti-tumour immunity. *Nature,* 584**,** 624-629.

Figueiredo, C., M. Wittmann, D. Wang, R. Dressel, A. Seltsam, R. Blasczyk & B. Eiz-Vesper (2009) Heat shock protein 70 (HSP70) induces cytotoxicity of T-helper cells. *Blood, The Journal of the American Society of Hematology,* 113**,** 3008-3016.

Foster, D. S., R. E. Jones, R. C. Ransom, M. T. Longaker & J. A. Norton (2018) The evolving relationship of wound healing and tumor stroma. *JCI insight,* 3.

Frigerio, S., D. A. Lartey, G. R. D'Haens & J. Grootjans (2021) The role of the immune system in ibd-associated colorectal cancer: From pro to anti-tumorigenic mechanisms. *International Journal of Molecular Sciences,* 22**,** 12739.

Fukata, M. & M. Abreu (2007) TLR4 signalling in the intestine in health and disease. *Biochemical Society Transactions,* 35**,** 1473-1478.

Gabrilovich, D. I. & S. Nagaraj (2009) Myeloid-derived suppressor cells as regulators of the immune system. *Nature reviews immunology,* 9**,** 162-174.

Garrett, W. S., S. Punit, C. A. Gallini, M. Michaud, D. Zhang, K. S. Sigrist, G. M. Lord, J. N. Glickman & L. H. Glimcher (2009) Colitis-associated colorectal cancer driven by T-bet deficiency in dendritic cells. *Cancer cell,* 16**,** 208-219.

Garris, C. S., S. P. Arlauckas, R. H. Kohler, M. P. Trefny, S. Garren, C. Piot, C. Engblom, C. Pfirschke, M. Siwicki & J. Gungabeesoon (2018) Successful anti-PD-1 cancer immunotherapy requires T cell-dendritic cell crosstalk involving the cytokines IFN-γ and IL-12. *Immunity,* 49**,** 1148-1161. e7.

Gatenby, G., T. Glyn, J. Pearson, R. Gearry & T. Eglinton (2021) The long-term incidence of dysplasia and colorectal cancer in a Crohn's colitis population-based cohort. *Colorectal Disease,* 23**,** 2399-2406.

Gentles, A. J., A. M. Newman, C. L. Liu, S. V. Bratman, W. Feng, D. Kim, V. S. Nair, Y. Xu, A. Khuong & C. D. Hoang (2015) The prognostic landscape of genes and infiltrating immune cells across human cancers. *Nature medicine,* 21**,** 938-945.

Gerner, M. Y., K. A. Casey & M. F. Mescher (2008) Defective MHC class II presentation by dendritic cells limits CD4 T cell help for antitumor CD8 T cell responses. *The Journal of Immunology,* 181**,** 155-164.

Ginhoux, F., K. Liu, J. Helft, M. Bogunovic, M. Greter, D. Hashimoto, J. Price, N. Yin, J. Bromberg & S. A. Lira (2009) The origin and development of nonlymphoid tissue CD103+ DCs. *Journal of Experimental Medicine,* 206**,** 3115-3130.

Giri, B., P. Sharma, T. Jain, A. Ferrantella, U. Vaish, S. Mehra, B. Garg, S. Iyer, V. Sethi & Z. Malchiodi (2021) Hsp70 modulates immune response in pancreatic cancer through dendritic cells. *Oncoimmunology,* 10**,** 1976952.

Grajales-Reyes, G. E., A. Iwata, J. Albring, X. Wu, R. Tussiwand, W. Kc, N. M. Kretzer, C. G. Briseño, V. Durai & P. Bagadia (2015) Batf3 maintains autoactivation of Irf8 for commitment of a CD8α+ conventional DC clonogenic progenitor. *Nature immunology,* 16**,** 708-717.

Greter, M., J. Helft, A. Chow, D. Hashimoto, A. Mortha, J. Agudo-Cantero, M. Bogunovic, E. L. Gautier, J. Miller & M. Leboeuf (2012) GM-CSF controls nonlymphoid tissue dendritic cell homeostasis but is dispensable for the differentiation of inflammatory dendritic cells. *Immunity,* 36**,** 1031-1046.

Gross, O., A. Gewies, K. Finger, M. Schäfer, T. Sparwasser, C. Peschel, I. Förster & J. Ruland (2006) Card9 controls a non-TLR signalling pathway for innate anti-fungal immunity. *Nature,* 442**,** 651-656.

Guilliams, M., K. Crozat, S. Henri, S. Tamoutounour, P. Grenot, E. Devilard, B. de Bovis, L. Alexopoulou, M. Dalod & B. Malissen (2010) Skin-draining lymph nodes contain dermis-derived CD103− dendritic cells that constitutively produce retinoic acid and induce Foxp3+ regulatory T cells. *Blood, The Journal of the American Society of Hematology,* 115**,** 1958-1968.

Haas, T., S. Heidegger, A. Wintges, M. Bscheider, S. Bek, J. C. Fischer, G. Eisenkolb, M. Schmickl, S. Spoerl & C. Peschel (2017) Card9 controls Dectin-1-induced T-cell cytotoxicity and tumor growth in mice. *European Journal of Immunology,* 47**,** 872-879.

Hacker, C., R. D. Kirsch, X.-S. Ju, T. Hieronymus, T. C. Gust, C. Kuhl, T. Jorgas, S. M. Kurz, S. Rose-John & Y. Yokota (2003) Transcriptional profiling identifies Id2 function in dendritic cell development. *Nature immunology,* 4**,** 380-386.

Hafemeister, C. & R. Satija (2019) Normalization and variance stabilization of single-cell RNA-seq data using regularized negative binomial regression. *Genome biology,* 20**,** 296.

Hamade, H., J. T. Stamps, D. T. Stamps, S. K. More, L. S. Thomas, A. Y. Blackwood, N. L. Lahcene, S. L. Castanon, B. C. Salumbides & Y. Shimodaira (2022) BATF3 Protects Against Metabolic Syndrome and Maintains Intestinal Epithelial Homeostasis. *Frontiers in Immunology,* 13.

Hanahan, D. & R. A. Weinberg (2011) Hallmarks of cancer: the next generation. *cell,* 144**,** 646-674.

Hanč, P., T. Fujii, S. Iborra, Y. Yamada, J. Huotari, O. Schulz, S. Ahrens, S. Kjær, M. Way & D. Sancho (2015) Structure of the complex of F-actin and DNGR-1, a C-type lectin receptor involved in dendritic cell cross-presentation of dead cell-associated antigens. *Immunity,* 42**,** 839-849.

Hao, Y., S. Hao, E. Andersen-Nissen, W. M. Mauck, S. Zheng, A. Butler, M. J. Lee, A. J. Wilk, C. Darby & M. Zager (2021) Integrated analysis of multimodal single-cell data. *Cell,* 184**,** 3573-3587. e29.

Hartjes, L. & J. Ruland (2019) CARD9 signaling in intestinal immune homeostasis and oncogenesis. *Frontiers in Immunology,* 10**,** 419.

Hawiger, D., K. Inaba, Y. Dorsett, M. Guo, K. Mahnke, M. Rivera, J. V. Ravetch, R. M. Steinman & M. C. Nussenzweig (2001) Dendritic cells induce peripheral T cell unresponsiveness under steady state conditions in vivo. *The Journal of experimental medicine,* 194**,** 769-780.

He, T.-C., A. B. Sparks, C. Rago, H. Hermeking, L. Zawel, L. T. Da Costa, P. J. Morin, B. Vogelstein & K. W. Kinzler (1998) Identification of c-MYC as a target of the APC pathway. *Science,* 281**,** 1509-1512.

Heink, S., N. Yogev, C. Garbers, M. Herwerth, L. Aly, C. Gasperi, V. Husterer, A. L. Croxford, K. Möller-Hackbarth & H. S. Bartsch (2017) Trans-presentation of IL-6 by dendritic cells is required for the priming of pathogenic TH17 cells. *Nature immunology,* 18**,** 74-85.

Helft, J., J. Böttcher, P. Chakravarty, S. Zelenay, J. Huotari, B. U. Schraml, D. Goubau & C. R. e Sousa (2015) GM-CSF mouse bone marrow cultures comprise a heterogeneous population of CD11c+ MHCII+ macrophages and dendritic cells. *Immunity,* 42**,** 1197-1211.

Herman, J. S. & D. Grün (2018) FateID infers cell fate bias in multipotent progenitors from single-cell RNA-seq data. *Nature methods,* 15**,** 379-386.

Hildner, K., B. T. Edelson, W. E. Purtha, M. Diamond, H. Matsushita, M. Kohyama, B. Calderon, B. U. Schraml, E. R. Unanue & M. S. Diamond (2008) Batf3 deficiency reveals a critical role for CD8α+ dendritic cells in cytotoxic T cell immunity. *Science,* 322**,** 1097-1100.

Iborra, S., M. Martínez-López, S. C. Khouili, M. Enamorado, F. J. Cueto, R. Conde-Garrosa, C. Del Fresno & D. Sancho (2016) Optimal generation of tissue-resident but not circulating memory T cells during viral infection requires crosspriming by DNGR-1+ dendritic cells. *Immunity,* 45**,** 847-860.

Ignacio, A., C. N. S. Breda & N. O. S. Camara (2017) Innate lymphoid cells in tissue homeostasis and diseases. *World journal of hepatology,* 9**,** 979.

Iwanowycz, S., S. Ngoi, Y. Li, M. Hill, C. Koivisto, M. Parrish, B. Guo, Z. Li & B. Liu (2021) Type 2 dendritic cells mediate control of cytotoxic T cell resistant tumors. *JCI insight,* 6.

Iwasaki, A. & R. Medzhitov (2010) Regulation of adaptive immunity by the innate immune system. *science,* 327**,** 291-295.

Jaensson-Gyllenbäck, E., K. Kotarsky, F. Zapata, E. Persson, T. Gundersen, R. Blomhoff & W. Agace (2011) Bile retinoids imprint intestinal CD103+ dendritic cells with the ability to generate gut-tropic T cells. *Mucosal immunology,* 4**,** 438-447.

Jess, T., M. Frisch & J. Simonsen (2013) Trends in overall and cause-specific mortality among patients with inflammatory bowel disease from 1982 to 2010. *Clinical Gastroenterology and Hepatology,* 11**,** 43-48.

Joeris, T., C. Gomez-Casado, P. Holmkvist, S. J. Tavernier, A. Silva-Sanchez, L. Klotz, T. D. Randall, A. M. Mowat, K. Kotarsky & B. Malissen (2021) Intestinal cDC1 drive cross-tolerance to epithelial-derived antigen via induction of FoxP3+ CD8+ Tregs. *Science immunology,* 6**,** eabd3774.

Joeris, T., K. Müller-Luda, W. W. Agace & A. M. Mowat (2017) Diversity and functions of intestinal mononuclear phagocytes. *Mucosal immunology,* 10**,** 845-864.

Johnson, C. M., C. Wei, J. E. Ensor, D. J. Smolenski, C. I. Amos, B. Levin & D. A. Berry (2013) Meta-analyses of colorectal cancer risk factors. *Cancer causes & control,* 24**,** 1207-1222.

Kc, W., A. T. Satpathy, A. S. Rapaport, C. G. Briseño, X. Wu, J. C. Albring, E. V. Russler-Germain, N. M. Kretzer, V. Durai & S. P. Persaud (2014) L-Myc expression by dendritic cells is required for optimal T-cell priming. *Nature,* 507**,** 243-247.

Keller, D., A. Windsor, R. Cohen & M. Chand (2019) Colorectal cancer in inflammatory bowel disease: review of the evidence. *Techniques in coloproctology,* 23**,** 3-13.

Kingston, D., M. A. Schmid, N. Onai, A. Obata-Onai, D. Baumjohann & M. G. Manz (2009) The concerted action of GM-CSF and Flt3-ligand on in vivo dendritic cell homeostasis. *Blood, The Journal of the American Society of Hematology,* 114**,** 835-843.

Korn, T., E. Bettelli, W. Gao, A. Awasthi, A. Jäger, T. B. Strom, M. Oukka & V. K. Kuchroo (2007) IL-21 initiates an alternative pathway to induce proinflammatory TH17 cells. *Nature,* 448**,** 484-487.

Kouo, T., L. Huang, A. B. Pucsek, M. Cao, S. Solt, T. Armstrong & E. Jaffee (2015) Galectin-3 Shapes Antitumor Immune Responses by Suppressing CD8+ T Cells via LAG-3 and Inhibiting Expansion of Plasmacytoid Dendritic CellsGalectin-3 Regulates CD8+ T Cells via LAG-3 and pDCs. *Cancer immunology research,* 3**,** 412-423.

Kühl, A. A., N. N. Pawlowski, K. Grollich, C. Loddenkemper, M. Zeitz & J. C. Hoffmann (2007) Aggravation of intestinal inflammation by depletion/deficiency of γδ T cells in different types of IBD animal models. *Journal of leukocyte biology,* 81**,** 168-175.

Kumar, H., T. Kawai & S. Akira (2011) Pathogen recognition by the innate immune system. *International reviews of immunology,* 30**,** 16-34.

Lai, J., S. Mardiana, I. G. House, K. Sek, M. A. Henderson, L. Giuffrida, A. X. Chen, K. L. Todd, E. V. Petley & J. D. Chan (2020) Adoptive cellular therapy with T cells expressing the dendritic cell growth factor Flt3L drives epitope spreading and antitumor immunity. *Nature immunology,* 21**,** 914-926.

Lamas, B., M. L. Richard, V. Leducq, H.-P. Pham, M.-L. Michel, G. Da Costa, C. Bridonneau, S. Jegou, T. W. Hoffmann & J. M. Natividad (2016) CARD9 impacts colitis by altering gut microbiota metabolism of tryptophan into aryl hydrocarbon receptor ligands. *Nature medicine,* 22**,** 598-605.

Land, S. C. & A. R. Tee (2007) Hypoxia-inducible factor 1α is regulated by the mammalian target of rapamycin (mTOR) via an mTOR signaling motif. *Journal of Biological Chemistry,* 282**,** 20534-20543.

Lee, P. W., Y. Yang, M. K. Racke & A. E. Lovett-Racke (2015) Analysis of TGF-β1 and TGF-β3 as regulators of encephalitogenic Th17 cells: Implications for multiple sclerosis. *Brain, behavior, and immunity,* 46**,** 44-49.

LeibundGut-Landmann, S., F. Osorio, G. D. Brown & C. Reis e Sousa (2008) Stimulation of dendritic cells via the dectin-1/Syk pathway allows priming of cytotoxic T-cell responses. *Blood, The Journal of the American Society of Hematology,* 112**,** 4971-4980.

Lewis, K. L., M. L. Caton, M. Bogunovic, M. Greter, L. T. Grajkowska, D. Ng, A. Klinakis, I. F. Charo, S. Jung & J. L. Gommerman (2011) Notch2 receptor signaling controls functional differentiation of dendritic cells in the spleen and intestine. *Immunity,* 35**,** 780-791.

Li, X., M. Chen, Y. Wan, L. Zhong, X. Han, X. Chen, F. Xiao, J. Liu, Y. Zhang & D. Zhu (2022) Single-cell transcriptome profiling reveals the key role of ZNF683 in natural killer cell exhaustion in multiple myeloma. *Clinical and Translational Medicine,* 12**,** e1065.

Liu, J., S. G. Willet, E. D. Bankaitis, Y. Xu, C. V. Wright & G. Gu (2013) Non-parallel recombination limits Cre-LoxP-based reporters as precise indicators of conditional genetic manipulation. *genesis,* 51**,** 436-442.

Liu, K., G. D. Victora, T. A. Schwickert, P. Guermonprez, M. M. Meredith, K. Yao, F.-F. Chu, G. J. Randolph, A. Y. Rudensky & M. Nussenzweig (2009) In vivo analysis of dendritic cell development and homeostasis. *Science,* 324**,** 392-397.

Liu, K., C. Waskow, X. Liu, K. Yao, J. Hoh & M. Nussenzweig (2007) Origin of dendritic cells in peripheral lymphoid organs of mice. *Nature immunology,* 8**,** 578-583.

Lowe, E. L., T. R. Crother, S. Rabizadeh, B. Hu, H. Wang, S. Chen, K. Shimada, M. H. Wong, K. S. Michelsen & M. Arditi (2010) Toll-like receptor 2 signaling protects mice from tumor development in a mouse model of colitis-induced cancer. *PloS one,* 5**,** e13027.

Luda, K. M., T. Joeris, E. K. Persson, A. Rivollier, M. Demiri, K. M. Sitnik, L. Pool, J. B. Holm, F. Melo-Gonzalez & L. Richter (2016) IRF8 transcription-factor-dependent classical dendritic cells are essential for intestinal T cell homeostasis. *Immunity,* 44**,** 860-874.

MacNabb, B. W., S. Tumuluru, X. Chen, J. Godfrey, D. N. Kasal, J. Yu, M. L. Jongsma, R. M. Spaapen, D. E. Kline & J. Kline (2022) Dendritic cells can prime anti-tumor CD8+ T cell responses through major histocompatibility complex cross-dressing. *Immunity,* 55**,** 982-997. e8.

Maier, B., A. M. Leader, S. T. Chen, N. Tung, C. Chang, J. LeBerichel, A. Chudnovskiy, S. Maskey, L. Walker & J. P. Finnigan (2020) A conserved dendritic-cell regulatory program limits antitumour immunity. *Nature,* 580**,** 257-262.

Malik, A., D. Sharma, R. S. Malireddi, C. S. Guy, T.-C. Chang, S. R. Olsen, G. Neale, P. Vogel & T.-D. Kanneganti (2018) SYK-CARD9 signaling axis promotes gut fungi-mediated inflammasome activation to restrict colitis and colon cancer. *Immunity,* 49**,** 515-530. e5.

Maney, N. J., G. Reynolds, A. Krippner-Heidenreich & C. M. Hilkens (2014) Dendritic cell maturation and survival are differentially regulated by TNFR1 and TNFR2. *The Journal of Immunology,* 193**,** 4914-4923.

Manh, T. P. V., Y. Alexandre, T. Baranek, K. Crozat & M. Dalod (2013) Plasmacytoid, conventional, and monocyte-derived dendritic cells undergo a profound and convergent genetic reprogramming during their maturation. *European journal of immunology,* 43**,** 1706-1715.

Maniar, A., X. Zhang, W. Lin, B. R. Gastman, C. D. Pauza, S. E. Strome & A. I. Chapoval (2010) Human γδ T lymphocytes induce robust NK cell–mediated antitumor cytotoxicity through CD137 engagement. *Blood, The Journal of the American Society of Hematology,* 116**,** 1726-1733.

Maraskovsky, E., K. Brasel, M. Teepe, E. R. Roux, S. D. Lyman, K. Shortman & H. J. McKenna (1996) Dramatic increase in the numbers of functionally mature dendritic cells in Flt3 ligand-treated mice: multiple dendritic cell subpopulations identified. *The Journal of experimental medicine,* 184**,** 1953-1962.

Martin-Orozco, N., P. Muranski, Y. Chung, X. O. Yang, T. Yamazaki, S. Lu, P. Hwu, N. P. Restifo, W. W. Overwijk & C. Dong (2009) T helper 17 cells promote cytotoxic T cell activation in tumor immunity. *Immunity,* 31**,** 787-798.

Martinez-Lopez, M., S. Iborra, R. Conde-Garrosa, A. Mastrangelo, C. Danne, E. R. Mann, D. M. Reid, V. Gaboriau-Routhiau, M. Chaparro & M. P. Lorenzo (2019) Microbiota sensing by Mincle-Syk axis in dendritic cells regulates interleukin-17 and-22 production and promotes intestinal barrier integrity. *Immunity,* 50**,** 446-461. e9.

Mattar, M. C., D. Lough, M. J. Pishvaian & A. Charabaty (2011) Current management of inflammatory bowel disease and colorectal cancer. *Gastrointestinal cancer research: GCR,* 4**,** 53.

Maxwell, J. R., Y. Zhang, W. A. Brown, C. L. Smith, F. R. Byrne, M. Fiorino, E. Stevens, J. Bigler, J. A. Davis & J. B. Rottman (2015) Differential roles for interleukin-23 and interleukin-17 in intestinal immunoregulation. *Immunity,* 43**,** 739-750.

Mayer, J. U., M. Demiri, W. W. Agace, A. S. MacDonald, M. Svensson-Frej & S. W. Milling (2017) Different populations of CD11b+ dendritic cells drive Th2 responses in the small intestine and colon. *Nature communications,* 8**,** 15820.

McKenna, H. J., K. L. Stocking, R. E. Miller, K. Brasel, T. De Smedt, E. Maraskovsky, C. R. Maliszewski, D. H. Lynch, J. Smith & B. Pulendran (2000) Mice lacking flt3 ligand have deficient hematopoiesis affecting hematopoietic progenitor cells, dendritic cells, and natural killer cells. *Blood, The Journal of the American Society of Hematology,* 95**,** 3489-3497.

Medzhitov, R. & C. Janeway Jr (2000) Innate immune recognition: mechanisms and pathways. *Immunological reviews,* 173**,** 89-97.

Menezes, S., D. Melandri, G. Anselmi, T. Perchet, J. Loschko, J. Dubrot, R. Patel, E. L. Gautier, S. Hugues & M. P. Longhi (2016) The heterogeneity of Ly6Chi monocytes controls their

differentiation into iNOS+ macrophages or monocyte-derived dendritic cells. *Immunity,* 45**,** 1205-1218.

Merad, M., P. Sathe, J. Helft, J. Miller & A. Mortha (2013) The dendritic cell lineage: ontogeny and function of dendritic cells and their subsets in the steady state and the inflamed setting. *Annual review of immunology,* 31**,** 563-604.

Mielke, L. A., S. A. Jones, M. Raverdeau, R. Higgs, A. Stefanska, J. R. Groom, A. Misiak, L. S. Dungan, C. E. Sutton & G. Streubel (2013) Retinoic acid expression associates with enhanced IL-22 production by γδ T cells and innate lymphoid cells and attenuation of intestinal inflammation. *Journal of Experimental Medicine,* 210**,** 1117-1124.

Mikucki, M., D. Fisher, J. Matsuzaki, J. Skitzki, N. Gaulin, J. Muhitch, A. Ku, J. Frelinger, K. Odunsi & T. Gajewski (2015) Non-redundant requirement for CXCR3 signalling during tumoricidal T-cell trafficking across tumour vascular checkpoints. *Nature communications,* 6**,** 7458.

Mildner, A., S. Yona & S. Jung (2013) A close encounter of the third kind: monocyte-derived cells. *Advances in immunology,* 120**,** 69-103.

Miller, J. C., B. D. Brown, T. Shay, E. L. Gautier, V. Jojic, A. Cohain, G. Pandey, M. Leboeuf, K. G. Elpek & J. Helft (2012) Deciphering the transcriptional network of the dendritic cell lineage. *Nature immunology,* 13**,** 888-899.

Mittal, D., D. Vijayan, E. M. Putz, A. R. Aguilera, K. A. Markey, J. Straube, S. Kazakoff, S. L. Nutt, K. Takeda & G. R. Hill (2017) Interleukin-12 from CD103+ Batf3-dependent dendritic cells required for NK-cell suppression of metastasis. *Cancer immunology research,* 5**,** 1098-1108.

Mócsai, A., J. Ruland & V. L. Tybulewicz (2010) The SYK tyrosine kinase: a crucial player in diverse biological functions. *Nature Reviews Immunology,* 10**,** 387-402.

Moreira, T. G., D. Mangani, L. M. Cox, J. Leibowitz, E. L. Lobo, M. A. Oliveira, C. D. Gauthier, B. N. Nakagaki, V. Willocq & A. Song (2021) PD-L1+ and XCR1+ dendritic cells are region-specific regulators of gut homeostasis. *Nature Communications,* 12**,** 4907.

Mowat, A. M. & W. W. Agace (2014) Regional specialization within the intestinal immune system. *Nature Reviews Immunology,* 14**,** 667-685.

Murphy, K. M., P. Travers & M. Walport. 2014. *Janeway Immunologie*. Springer Berlin Heidelberg.

Murphy, T. L., G. E. Grajales-Reyes, X. Wu, R. Tussiwand, C. G. Briseño, A. Iwata, N. M. Kretzer, V. Durai & K. M. Murphy (2016) Transcriptional control of dendritic cell development. *Annual review of immunology,* 34**,** 93-119.

Murphy, T. L. & K. M. Murphy (2022) Dendritic cells in cancer immunology. *Cellular & Molecular Immunology,* 19**,** 3-13.

Murwanti, R., K. Denda-Nagai, D. Sugiura, K. Mogushi, S. J. Gendler & T. Irimura (2023) Prevention of Inflammation-Driven Colon Carcinogenesis in Human MUC1 Transgenic Mice by Vaccination with MUC1 DNA and Dendritic Cells. *Cancers,* 15**,** 1920.

Muzaki, A. R. B. M., I. Soncin, Y. A. Setiagani, J. Sheng, P. Tetlak, K. Karjalainen & C. Ruedl (2017) Long-lived innate IL-17–producing γ/δ T cells modulate antimicrobial epithelial host defense in the colon. *The Journal of Immunology,* 199**,** 3691-3699.

Muzaki, A. R. B. M., P. Tetlak, J. Sheng, S. Loh, Y. A. Setiagani, M. Poidinger, F. Zolezzi, K. Karjalainen & C. Ruedl (2016) Intestinal CD103+ CD11b− dendritic cells restrain colitis via IFN-γ-induced anti-inflammatory response in epithelial cells. *Mucosal immunology,* 9**,** 336-351.

Nam, J.-S., M. Terabe, M.-J. Kang, H. Chae, N. Voong, Y.-a. Yang, A. Laurence, A. Michalowska, M. Mamura & S. Lonning (2008) Transforming growth factor β subverts the immune system into directly promoting tumor growth through interleukin-17. *Cancer research,* 68**,** 3915-3923.

Ni, J., X. Wang, A. Stojanovic, Q. Zhang, M. Wincher, L. Bühler, A. Arnold, M. P. Correia, M. Winkler & P.-S. Koch (2020) Single-cell RNA sequencing of tumor-infiltrating NK cells reveals that inhibition of transcription factor HIF-1α unleashes NK cell activity. *Immunity,* 52**,** 1075-1087. e8.

Ni, M., D. Martire, E. Scotet, M. Bonneville, F. Sanchez & V. Lafont (2012) Full restoration of Brucella-infected dendritic cell functionality through Vγ9Vδ2 T helper type 1 crosstalk.

Niu, C., H. Jin, M. Li, J. Xu, D. Xu, J. Hu, H. He, W. Li & J. Cui (2015) In vitro analysis of the proliferative capacity and cytotoxic effects of ex vivo induced natural killer cells, cytokine-induced killer cells, and gamma-delta T cells. *BMC immunology,* 16**,** 1-10.

Ogawa, A., A. Andoh, Y. Araki, T. Bamba & Y. Fujiyama (2004) Neutralization of interleukin-17 aggravates dextran sulfate sodium-induced colitis in mice. *Clinical immunology,* 110**,** 55-62.

Ohta, T., M. Sugiyama, H. Hemmi, C. Yamazaki, S. Okura, I. Sasaki, Y. Fukuda, T. Orimo, K. J. Ishii & K. Hoshino (2016) Crucial roles of XCR1-expressing dendritic cells and the XCR1-XCL1 chemokine axis in intestinal immune homeostasis. *Scientific reports,* 6**,** 23505.

Ozment-Skelton, T. R., E. A. Defluiter, T. Ha, C. Li, B. M. Graves, D. A. Ferguson Jr, J. B. Schweitzer, J. Preizsner, G. D. Brown & S. Gordon (2009) Leukocyte Dectin-1 expression is differentially regulated in fungal versus polymicrobial sepsis. *Critical care medicine,* 37**,** 1038.

Pakalniškytė, D. & B. U. Schraml (2017) Tissue-specific diversity and functions of conventional dendritic cells. *Advances in Immunology,* 134**,** 89-135.

Pan, J., M. Zhang, J. Wang, Q. Wang, D. Xia, W. Sun, L. Zhang, H. Yu, Y. Liu & X. Cao (2004) Interferon-γ is an autocrine mediator for dendritic cell maturation. *Immunology letters,* 94**,** 141-151.

Paul, W. E. (2011) Bridging innate and adaptive immunity. *Cell,* 147**,** 1212-1215.

Persson, E. K., H. Uronen-Hansson, M. Semmrich, A. Rivollier, K. Hägerbrand, J. Marsal, S. Gudjonsson, U. Håkansson, B. Reizis & K. Kotarsky (2013) IRF4 transcription-factor-dependent CD103+ CD11b+ dendritic cells drive mucosal T helper 17 cell differentiation. *Immunity,* 38**,** 958-969.

Pool, L. (2018) Intestinal classical Dendritic cells in T cell induced colitis and colitis associated colorectal cancer.

Pool, L., A. Rivollier & W. W. Agace (2020) Deletion of IRF4 in Dendritic Cells Leads to Delayed Onset of T Cell–Dependent Colitis. *The Journal of Immunology,* 204**,** 1047-1055.

Pourdehnad, M., M. L. Truitt, I. N. Siddiqi, G. S. Ducker, K. M. Shokat & D. Ruggero (2013) Myc and mTOR converge on a common node in protein synthesis control that confers synthetic lethality in Myc-driven cancers. *Proceedings of the National Academy of Sciences,* 110**,** 11988-11993.

Preston, G. C., L. V. Sinclair, A. Kaskar, J. L. Hukelmann, M. N. Navarro, I. Ferrero, H. R. MacDonald, V. H. Cowling & D. A. Cantrell (2015) Single cell tuning of Myc expression by antigen receptor signal strength and interleukin-2 in T lymphocytes. *The EMBO journal,* 34**,** 2008-2024.

Rivollier, A., J. He, A. Kole, V. Valatas & B. L. Kelsall (2012) Inflammation switches the differentiation program of Ly6Chi monocytes from antiinflammatory macrophages to inflammatory dendritic cells in the colon. *Journal of Experimental Medicine,* 209**,** 139-155.

Roberts, E. W., M. L. Broz, M. Binnewies, M. B. Headley, A. E. Nelson, D. M. Wolf, T. Kaisho, D. Bogunovic, N. Bhardwaj & M. F. Krummel (2016) Critical role for CD103+/CD141+ dendritic cells bearing CCR7 for tumor antigen trafficking and priming of T cell immunity in melanoma. *Cancer cell,* 30**,** 324-336.

Rodrigues, P. F., L. Alberti-Servera, A. Eremin, G. E. Grajales-Reyes, R. Ivanek & R. Tussiwand (2018) Distinct progenitor lineages contribute to the heterogeneity of plasmacytoid dendritic cells. *Nature immunology,* 19**,** 711-722.

Rodrigues, P. F., A. Kouklas, G. Cvijetic, N. Bouladoux, M. Mitrovic, J. V. Desai, D. S. Lima-Junior, M. S. Lionakis, Y. Belkaid & R. Ivanek (2023) pDC-like cells are pre-DC2 and require KLF4 to control homeostatic CD4 T cells. *Science Immunology,* 8**,** eadd4132.

Rosenbaum, M., A. Gewies, K. Pechloff, C. Heuser, T. Engleitner, T. Gehring, L. Hartjes, S. Krebs, D. Krappmann & M. Kriegsmann (2019) Bcl10-controlled Malt1 paracaspase

activity is key for the immune suppressive function of regulatory T cells. *Nature communications,* 10**,** 2352.

Rosenbaum, M., T. Schnalzger, T. Engleitner, C. Weiß, R. Mishra, C. Mibus, T. Mitterer, R. Rad & J. Ruland (2022) MALT1 protease function in regulatory T cells induces MYC activity to promote mitochondrial function and cellular expansion. *European journal of immunology,* 52**,** 85-95.

Roth, S. & J. Ruland (2013) Caspase recruitment domain-containing protein 9 signaling in innate immunity and inflammation. *Trends in immunology,* 34**,** 243-250.

Rowshanravan, B., N. Halliday & D. M. Sansom (2018) CTLA-4: a moving target in immunotherapy. *Blood, The Journal of the American Society of Hematology,* 131**,** 58-67.

Ruhland, M. K., E. W. Roberts, E. Cai, A. M. Mujal, K. Marchuk, C. Beppler, D. Nam, N. K. Serwas, M. Binnewies & M. F. Krummel (2020) Visualizing synaptic transfer of tumor antigens among dendritic cells. *Cancer cell,* 37**,** 786-799. e5.

Ruland, J. (2008) CARD9 signaling in the innate immune response. *Annals of the New York Academy of Sciences,* 1143**,** 35-44.

Rustgi, A. K. (2007) The genetics of hereditary colon cancer. *Genes & development,* 21**,** 2525-2538.

Saijo, K., C. Schmedt, I.-h. Su, H. Karasuyama, C. A. Lowell, M. Reth, T. Adachi, A. Patke, A. Santana & A. Tarakhovsky (2003) Essential role of Src-family protein tyrosine kinases in NF-κB activation during B cell development. *Nature immunology,* 4**,** 274-279.

Salmon, H., J. Idoyaga, A. Rahman, M. Leboeuf, R. Remark, S. Jordan, M. Casanova-Acebes, M. Khudoynazarova, J. Agudo & N. Tung (2016) Expansion and activation of CD103+ dendritic cell progenitors at the tumor site enhances tumor responses to therapeutic PD-L1 and BRAF inhibition. *Immunity,* 44**,** 924-938.

Salvermoser, J., J. Van Blijswijk, N. E. Papaioannou, S. Rambichler, M. Pasztoi, D. Pakalniškytė, N. C. Rogers, S. J. Keppler, T. Straub & C. Reis e Sousa (2018) Clec9a-mediated ablation of conventional dendritic cells suggests a lymphoid path to generating dendritic cells in vivo. *Frontiers in immunology,* 9**,** 699.

Sánchez-Paulete, A. R., F. J. Cueto, M. Martínez-López, S. Labiano, A. Morales-Kastresana, M. E. Rodríguez-Ruiz, M. Jure-Kunkel, A. Azpilikueta, M. A. Aznar & J. I. Quetglas (2016) Cancer Immunotherapy with Immunomodulatory Anti-CD137 and Anti–PD-1 Monoclonal Antibodies Requires BATF3-Dependent Dendritic CellsCross-Priming and Immunomodulatory mAbs. *Cancer discovery,* 6**,** 71-79.

Sathaliyawala, T., W. E. O'Gorman, M. Greter, M. Bogunovic, V. Konjufca, Z. E. Hou, G. P. Nolan, M. J. Miller, M. Merad & B. Reizis (2010) Mammalian target of rapamycin controls dendritic cell development downstream of Flt3 ligand signaling. *Immunity,* 33**,** 597-606.

Satpathy, A. T., C. G. Briseño, J. S. Lee, D. Ng, N. A. Manieri, W. Kc, X. Wu, S. R. Thomas, W.-L. Lee & M. Turkoz (2013) Notch2-dependent classical dendritic cells orchestrate intestinal immunity to attaching-and-effacing bacterial pathogens. *Nature immunology,* 14**,** 937-948.

Schlitzer, A., N. McGovern, P. Teo, T. Zelante, K. Atarashi, D. Low, A. W. Ho, P. See, A. Shin & P. S. Wasan (2013) IRF4 transcription factor-dependent CD11b+ dendritic cells in human and mouse control mucosal IL-17 cytokine responses. *Immunity,* 38**,** 970-983.

Schlitzer, A., V. Sivakamasundari, J. Chen, H. R. B. Sumatoh, J. Schreuder, J. Lum, B. Malleret, S. Zhang, A. Larbi & F. Zolezzi (2015) Identification of cDC1-and cDC2-committed DC progenitors reveals early lineage priming at the common DC progenitor stage in the bone marrow. *Nature immunology,* 16**,** 718-728.

Schraml, B. U. & C. R. e Sousa (2015) Defining dendritic cells. *Current opinion in immunology,* 32**,** 13-20.

Schraml, B. U., J. Van Blijswijk, S. Zelenay, P. G. Whitney, A. Filby, S. E. Acton, N. C. Rogers, N. Moncaut, J. J. Carvajal & C. R. e Sousa (2013) Genetic tracing via DNGR-1 expression history defines dendritic cells as a hematopoietic lineage. *Cell,* 154**,** 843-858.

Scott, C. L., C. C. Bain, P. B. Wright, D. Sichien, K. Kotarsky, E. K. Persson, K. Luda, M. Guilliams, B. N. Lambrecht & W. W. Agace (2015) CCR2+ CD103− intestinal dendritic cells develop from DC-committed precursors and induce interleukin-17 production by T cells. *Mucosal immunology,* 8**,** 327-339.

Scott, C. L., B. Soen, L. Martens, N. Skrypek, W. Saelens, J. Taminau, G. Blancke, G. Van Isterdael, D. Huylebroeck & J. Haigh (2016) The transcription factor Zeb2 regulates development of conventional and plasmacytoid DCs by repressing Id2. *Journal of Experimental Medicine,* 213**,** 897-911.

Shao, S., D. Cui, C. Ma, P. Chen, B. Zhou, R. Tao & J. Wang (2020) Transcriptome profiling of tolerogenic dendritic cells conditioned with dual mTOR kinase inhibitor, AZD8055. *International Immunopharmacology,* 81**,** 106241.

Shaw, T. N., S. A. Houston, K. Wemyss, H. M. Bridgeman, T. A. Barbera, T. Zangerle-Murray, P. Strangward, A. J. Ridley, P. Wang & S. Tamoutounour (2018) Tissue-resident macrophages in the intestine are long lived and defined by Tim-4 and CD4 expression. *Journal of Experimental Medicine,* 215**,** 1507-1518.

Siegmund, B., F. Rieder, S. Albrich, K. Wolf, C. Bidlingmaier, G. S. Firestein, D. Boyle, H.-A. Lehr, F. Loher & G. Hartmann (2001) Adenosine kinase inhibitor GP515 improves experimental colitis in mice. *Journal of Pharmacology and Experimental Therapeutics,* 296**,** 99-105.

Sokol, H., K. L. Conway, M. Zhang, M. Choi, B. Morin, Z. Cao, E. J. Villablanca, C. Li, C. Wijmenga & S. H. Yun (2013) Card9 mediates intestinal epithelial cell restitution, T-helper 17 responses, and control of bacterial infection in mice. *Gastroenterology,* 145**,** 591-601. e3.

Spranger, S., D. Dai, B. Horton & T. F. Gajewski (2017) Tumor-residing Batf3 dendritic cells are required for effector T cell trafficking and adoptive T cell therapy. *Cancer cell,* 31**,** 711-723. e4.

Stagg, A. J. (2018) Intestinal dendritic cells in health and gut inflammation. *Frontiers in immunology,* 9**,** 2883.

Steinman, R. M. & Z. A. Cohn (1973) Identification of a novel cell type in peripheral lymphoid organs of mice: I. Morphology, quantitation, tissue distribution. *The Journal of experimental medicine,* 137**,** 1142-1162.

Steinman, R. M., B. Gutchinov, M. D. Witmer & M. C. Nussenzweig (1983) Dendritic cells are the principal stimulators of the primary mixed leukocyte reaction in mice. *The Journal of experimental medicine,* 157**,** 613-627.

Stephanou, A. & D. S. Latchman (1999) Transcriptional regulation of the heat shock protein genes by STAT family transcription factors. *Gene Expression The Journal of Liver Research,* 7**,** 311-319.

Strasser, D., K. Neumann, H. Bergmann, M. J. Marakalala, R. Guler, A. Rojowska, K.-P. Hopfner, F. Brombacher, H. Urlaub & G. Baier (2012) Syk kinase-coupled C-type lectin receptors engage protein kinase C-δ to elicit Card9 adaptor-mediated innate immunity. *Immunity,* 36**,** 32-42.

Stuart, T., A. Butler, P. Hoffman, C. Hafemeister, E. Papalexi, W. M. Mauck, Y. Hao, M. Stoeckius, P. Smibert & R. Satija (2019) Comprehensive integration of single-cell data. *Cell,* 177**,** 1888-1902. e21.

Sukhbaatar, N., M. Hengstschläger & T. Weichhart (2016) mTOR-mediated regulation of dendritic cell differentiation and function. *Trends in immunology,* 37**,** 778-789.

Sulczewski, F. B., R. A. Maqueda-Alfaro, M. Alcántara-Hernández, O. A. Perez, S. Saravanan, T. J. Yun, D. Seong, R. Arroyo Hornero, H. M. Raquer-McKay & E. Esteva (2023) Transitional dendritic cells are distinct from conventional DC2 precursors and mediate proinflammatory antiviral responses. *Nature Immunology***,** 1-16.

Sun, C.-M., J. A. Hall, R. B. Blank, N. Bouladoux, M. Oukka, J. R. Mora & Y. Belkaid (2007) Small intestine lamina propria dendritic cells promote de novo generation of Foxp3 T reg cells via retinoic acid. *The Journal of experimental medicine,* 204**,** 1775-1785.

Szatrowski, T. P. & C. F. Nathan (1991) Production of large amounts of hydrogen peroxide by human tumor cells. *Cancer research,* 51**,** 794-798.

Szlosarek, P. W. & F. R. Balkwill (2003) Tumour necrosis factor α: a potential target for the therapy of solid tumours. *The lancet oncology,* 4**,** 565-573.

Takemoto, S., M. Nishikawa, X. Guan, Y. Ohno, T. Yata & Y. Takakura (2010) Enhanced generation of cytotoxic T lymphocytes by heat shock protein 70 fusion proteins harboring both CD8+ T cell and CD4+ T cell epitopes. *Molecular pharmaceutics,* 7**,** 1715-1723.

Tamoutounour, S., S. Henri, H. Lelouard, B. de Bovis, C. de Haar, C. J. van der Woude, A. M. Woltman, Y. Reyal, D. Bonnet & D. Sichien (2012) CD 64 distinguishes macrophages from dendritic cells in the gut and reveals the T h1-inducing role of mesenteric lymph node macrophages during colitis. *European journal of immunology,* 42**,** 3150-3166.

Tang, A. L., J. R. Teijaro, M. N. Njau, S. S. Chandran, A. Azimzadeh, S. G. Nadler, D. M. Rothstein & D. L. Farber (2008) CTLA4 expression is an indicator and regulator of steady-state CD4+ FoxP3+ T cell homeostasis. *The Journal of Immunology,* 181**,** 1806-1813.

Tartour, E., F. Fossiez, I. Joyeux, A. Galinha, A. Gey, E. Claret, X. Sastre-Garau, J. Couturier, V. Mosseri & V. Vives (1999) Interleukin 17, a T-cell-derived cytokine, promotes tumorigenicity of human cervical tumors in nude mice. *Cancer research,* 59**,** 3698-3704.

Theisen, D. J., J. T. Davidson IV, C. G. Briseño, M. Gargaro, E. J. Lauron, Q. Wang, P. Desai, V. Durai, P. Bagadia & J. R. Brickner (2018) WDFY4 is required for cross-presentation in response to viral and tumor antigens. *Science,* 362**,** 694-699.

Thompson, E. D., H. L. Enriquez, Y.-X. Fu & V. H. Engelhard (2010) Tumor masses support naive T cell infiltration, activation, and differentiation into effectors. *Journal of Experimental Medicine,* 207**,** 1791-1804.

Thwe, P. M., D. I. Fritz, J. P. Snyder, P. R. Smith, K. D. Curtis, A. O'Donnell, N. A. Galasso, L. A. Sepaniac, B. J. Adamik & L. R. Hoyt (2019) Syk-dependent glycolytic reprogramming in dendritic cells regulates IL-1β production to β-glucan ligands in a TLR-independent manner. *Journal of leukocyte biology,* 106**,** 1325-1335.

Tian, X. & B. Zhou (2021) Strategies for site-specific recombination with high efficiency and precise spatiotemporal resolution. *Journal of Biological Chemistry,* 296.

Tsuchida, S., Y. Arai, K. A. Takahashi, T. Kishida, R. Terauchi, K. Honjo, S. Nakagawa, H. Inoue, K. Ikoma & K. Ueshima (2014) HIF-1α-induced HSP70 regulates anabolic responses in articular chondrocytes under hypoxic conditions. *Journal of Orthopaedic Research,* 32**,** 975-980.

Tsuchiya, T., S. Fukuda, H. Hamada, A. Nakamura, Y. Kohama, H. Ishikawa, K. Tsujikawa & H. Yamamoto (2003) Role of γδT cells in the inflammatory response of experimental colitis mice. *The Journal of Immunology,* 171**,** 5507-5513.

Turner, M., P. Joseph Mee, P. S. Costello, O. Williams, A. A. Price, L. P. Duddy, M. T. Furlong, R. L. Geahlen & V. L. Tybulewicz (1995) Perinatal lethality and blocked B-cell development in mice lacking the tyrosine kinase Syk. *Nature,* 378**,** 298-302.

Turvey, S. E. & D. H. Broide (2010) Innate immunity. *Journal of Allergy and Clinical Immunology,* 125**,** S24-S32.

Tussiwand, R., B. Everts, G. Grajales-Reyes, N. Kretzer, A. Iwata, J. Bagaitkar, X. Wu, R. Wong, D. Anderson & T. Murphy (2015) Klf4 expression in conventional dendritic cells is required for T helper 2 cell responses. *Immunity,* 42**,** 916-928.

Tussiwand, R., W.-L. Lee, T. L. Murphy, M. Mashayekhi, W. Kc, J. C. Albring, A. T. Satpathy, J. A. Rotondo, B. T. Edelson & N. M. Kretzer (2012) Compensatory dendritic cell development mediated by BATF–IRF interactions. *Nature,* 490**,** 502-507.

Ugur, M., R. J. Labios, C. Fenton, K. Knöpper, K. Jobin, F. Imdahl, G. Golda, K. Hoh, A. Grafen & T. Kaisho (2023) Lymph node medulla regulates the spatiotemporal unfolding of resident dendritic cell networks. *Immunity,* 56**,** 1778-1793. e10.

Uronis, J. M., M. Mühlbauer, H. H. Herfarth, T. C. Rubinas, G. S. Jones & C. Jobin (2009) Modulation of the intestinal microbiota alters colitis-associated colorectal cancer susceptibility. *PloS one,* 4**,** e6026.

Van Acker, H. H., S. Anguille, V. F. Van Tendeloo & E. Lion (2015) Empowering gamma delta T cells with antitumor immunity by dendritic cell-based immunotherapy. *Oncoimmunology,* 4**,** e1021538.

von der Haar, T., J. D. Gross, G. Wagner & J. E. McCarthy (2004) The mRNA cap-binding protein eIF4E in post-transcriptional gene expression. *Nature structural & molecular biology,* 11**,** 503-511.

Vornholz, L. & J. Ruland (2020) Physiological and pathological functions of CARD9 signaling in the innate immune system. *C-Type Lectins in Immune Homeostasis***,** 177-203.

Vremec, D., J. Pooley, H. Hochrein, L. Wu & K. Shortman (2000) CD4 and CD8 expression by dendritic cell subtypes in mouse thymus and spleen. *The Journal of Immunology,* 164**,** 2978-2986.

Waldner, M. J. & M. F. Neurath (2015) Mechanisms of immune signaling in colitis-associated cancer. *Cellular and molecular gastroenterology and hepatology,* 1**,** 6-16.

Wang, B., Q. Tian, D. Guo, W. Lin, X. Xie & H. Bi (2021) Activated γδ T cells promote dendritic cell maturation and exacerbate the development of experimental autoimmune uveitis (EAU) in mice. *Immunological Investigations,* 50**,** 164-183.

Wang, L., T. Yi, M. Kortylewski, D. M. Pardoll, D. Zeng & H. Yu (2009) IL-17 can promote tumor growth through an IL-6–Stat3 signaling pathway. *Journal of experimental medicine,* 206**,** 1457-1464.

Wang, T., C. Fan, A. Yao, X. Xu, G. Zheng, Y. You, C. Jiang, X. Zhao, Y. Hou & M.-C. Hung (2018) The adaptor protein CARD9 protects against colon cancer by restricting mycobiota-mediated expansion of myeloid-derived suppressor cells. *Immunity,* 49**,** 504-514. e4.

Waskow, C., K. Liu, G. Darrasse-Jèze, P. Guermonprez, F. Ginhoux, M. Merad, T. Shengelia, K. Yao & M. Nussenzweig (2008) The receptor tyrosine kinase Flt3 is required for dendritic cell development in peripheral lymphoid tissues. *Nature immunology,* 9**,** 676-683.

Wculek, S. K., J. Amores-Iniesta, R. Conde-Garrosa, S. C. Khouili, I. Melero & D. Sancho (2019a) Effective cancer immunotherapy by natural mouse conventional type-1 dendritic cells bearing dead tumor antigen. *Journal for immunotherapy of cancer,* 7**,** 1-16.

Wculek, S. K., S. C. Khouili, E. Priego, I. Heras-Murillo & D. Sancho (2019b) Metabolic control of dendritic cell functions: digesting information. *Frontiers in immunology,* 10**,** 775.

Wedebye Schmidt, E. G., H. L. Larsen, N. N. Kristensen, S. S. Poulsen, A. M. Lynge Pedersen, M. H. Claesson & A. E. Pedersen (2013) TH17 cell induction and effects of IL-17A and IL-17F blockade in experimental colitis. *Inflammatory bowel diseases,* 19**,** 1567-1576.

Welty, N. E., C. Staley, N. Ghilardi, M. J. Sadowsky, B. Z. Igyártó & D. H. Kaplan (2013) Intestinal lamina propria dendritic cells maintain T cell homeostasis but do not affect commensalism. *Journal of Experimental Medicine,* 210**,** 2011-2024.

Wendel, M., I. E. Galani, E. Suri-Payer & A. Cerwenka (2008) Natural killer cell accumulation in tumors is dependent on IFN-γ and CXCR3 ligands. *Cancer research,* 68**,** 8437-8445.

Wieten, L., R. van der Zee, R. Goedemans, J. Sijtsma, M. Serafini, N. H. Lubsen, W. van Eden & F. Broere (2010) Hsp70 expression and induction as a readout for detection of immune modulatory components in food. *Cell Stress and Chaperones,* 15**,** 25-37.

Willcox, C. R., F. Mohammed & B. E. Willcox (2020) The distinct MHC-unrestricted immunobiology of innate-like and adaptive-like human γδ T cell subsets—Nature's CAR-T cells. *Immunological Reviews,* 298**,** 25-46.

Willment, J. A., H.-H. Lin, D. M. Reid, P. R. Taylor, D. L. Williams, S. Y. Wong, S. Gordon & G. D. Brown (2003) Dectin-1 expression and function are enhanced on alternatively activated and GM-CSF-treated macrophages and are negatively regulated by IL-10, dexamethasone, and lipopolysaccharide. *The Journal of immunology,* 171**,** 4569-4573.

Worthington, J. J., B. I. Czajkowska, A. C. Melton & M. A. Travis (2011) Intestinal dendritic cells specialize to activate transforming growth factor-β and induce Foxp3+ regulatory T cells via integrin αvβ8. *Gastroenterology,* 141**,** 1802-1812.

Wu, R., R. A. Ohara, S. Jo, T.-T. Liu, S. T. Ferris, F. Ou, S. Kim, D. J. Theisen, D. A. Anderson III & B. W. Wong (2022) Mechanisms of CD40-dependent cDC1 licensing beyond costimulation. *Nature Immunology***,** 1-15.

Xia, L.-M., D.-A. Tian, Q. Zhang, W. Yan, Q. Zhu, M. Luo, Z.-Z. Zhou, Y. Tang, Q.-L. Zhang & W. Wang (2009) Hypoxia induces heat shock protein HSP70-2 expression in a HIF-1 dependent manner. *Zhonghua gan zang bing za zhi= Zhonghua ganzangbing zazhi= Chinese journal of hepatology,* 17**,** 207-212.

Zhang, X., M. Artola-Boran, A. Fallegger, I. C. Arnold, A. Weber, S. Reuter, C. Taube & A. Müller (2020) IRF4 expression is required for the immunoregulatory activity of conventional type 2 dendritic cells in settings of chronic bacterial infection and cancer. *The Journal of Immunology,* 205**,** 1933-1943.

Zheng, Y., L. Han, Z. Chen, Y. Li, B. Zhou, R. Hu, S. Chen, H. Xiao, Y. Ma & G. Xie (2022) PD-L1+ CD8+ T cells enrichment in lung cancer exerted regulatory function and tumor-promoting tolerance. *Iscience,* 25**,** 103785.

Zheng, Y., P. A. Valdez, D. M. Danilenko, Y. Hu, S. M. Sa, Q. Gong, A. R. Abbas, Z. Modrusan, N. Ghilardi & F. J. De Sauvage (2008) Interleukin-22 mediates early host defense against attaching and effacing bacterial pathogens. *Nature medicine,* 14**,** 282-289.

Zhernakova, A., E. M. Festen, L. Franke, G. Trynka, C. C. van Diemen, A. J. Monsuur, M. Bevova, R. M. Nijmeijer, R. van't Slot & R. Heijmans (2008) Genetic analysis of innate immunity in Crohn's disease and ulcerative colitis identifies two susceptibility loci harboring CARD9 and IL18RAP. *The American Journal of Human Genetics,* 82**,** 1202-1210.

Ziegler-Heitbrock, L., T. Ohteki, F. Ginhoux, K. Shortman & H. Spits (2023) Reclassifying plasmacytoid dendritic cells as innate lymphocytes. *Nature Reviews Immunology,* 23**,** 1-2.

Appendix / List of publications

Papaioannou, N. E., Salei, N., Rambichler, S., Ravi, K., Popovic, J., Küntzel, V., ... & Schraml, B. U. (2021). Environmental signals rather than layered ontogeny imprint the function of type 2 conventional dendritic cells in young and adult mice. *Nature Communications*, *12*(1), 464.

Salei, N., Ji, X., Pakalniškytė, D., Kuentzel, V., Rambichler, S., Li, N., ... & Schraml, B. U. (2021). Selective depletion of a CD64-expressing phagocyte subset mediates protection against toxic kidney injury and failure. *Proceedings of the National Academy of Sciences*, *118*(39), e2022311118.

Acknowledgements

First, I would like to thank Prof. Dr. Barbara Schraml-Schotta for the opportunity to work in her group and for her supervision, guidance, and support during my project.

Furthermore, I want to thank my thesis advisory committee, Prof. Dr. Anne Krug and Prof. Dr. Jürgen Ruland, for their constructive suggestions on my project.

Mainly, I would like to thank Theresa Schnalzger from the Ruland Lab for their excellent collaboration, great teamwork, and enjoyable late-night experiments.

Thank you to all group and institute members, especially Stephan Rambichler, Johanna Salvermoser, and Nikolaos Papaioannou, for their help and for making our lab a fun place to work in.

I also would like to thank the organizers of the SFB 914 and associated IRTG 914 and the SFB 1335 for financial support and excellent seminars, courses, and retreats. In particular, I would like to thank Dr. Verena Kochan for all her help, mental support, and her excellent coordination of the Program.

Finally, I would like to thank my husband Oliver, my family, and my friends for their great support during my Thesis.

Affidavit

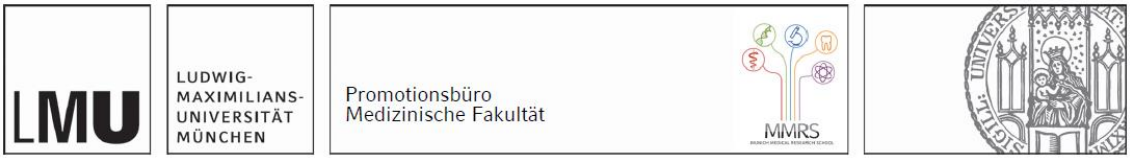

Affidavit

Küntzel, Vanessa
Surname, first name

Street

Zip code, town, country

I hereby declare, that the submitted thesis entitled:

The anti-tumorigenic role of CARD9 signaling cascade in conventional dendritic cells in colitis-associated colon cancer

……

is my own work. I have only used the sources indicated and have not made unauthorised use of services of a third party. Where the work of others has been quoted or reproduced, the source is always given.

I further declare that the dissertation presented here has not been submitted in the same or similar form to any other institution for the purpose of obtaining an academic degree.

Munich, 29.04.2024
place, date

Vanessa Küntzel
Signature doctoral candidate

Confirmation of congruency

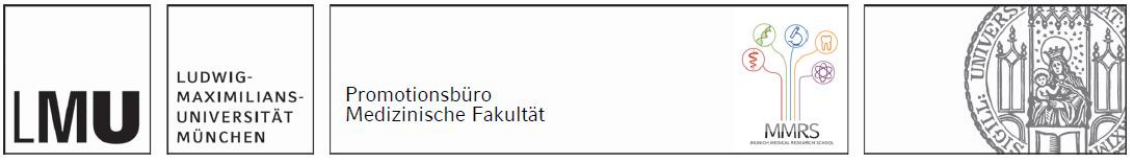

Confirmation of congruency between printed and electronic version of the doctoral thesis

Küntzel, Vanessa
Surname, first name

Street

Zip code, town, country

I hereby declare, that the submitted thesis entitled:
The anti-tumorigenic role of CARD9 signaling cascade in conventional dendritic cells in colitis-associated colon cancer
……

is congruent with the printed version both in content and format.

Munich, 29.04.2024
place, date

Vanessa Küntzel
Signature doctoral candidate